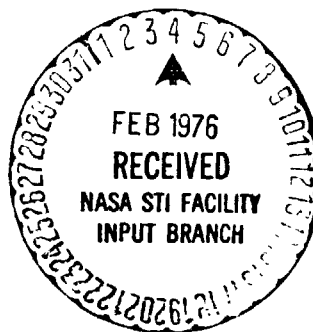


NASA TECHNICAL MEMORANDUM

NASA TM X - 64975



THE EFFECTS OF SOLID ROCKET MOTOR EFFLUENTS ON SELECTED SURFACES AND SOLID PARTICLE SIZE, DISTRIBUTION, AND COMPOSITION FOR SIMULATED SHUTTLE BOOSTER SEPARATION MOTORS

By David W. Jex, Roger C. Linton, Willa M. Russell,
John J. Trenkle, and Donald R. Wilkes
Space Sciences Laboratory

January 12, 1976

NASA

*George C. Marshall Space Flight Center
Marshall Space Flight Center, Alabama*

(NASA-TM-X-64975) THE EFFECTS OF SOLID
ROCKET MOTOR EFFLUENTS ON SELECTED SURFACES
AND SOLID PARTICLE SIZE, DISTRIBUTION, AND
COMPOSITION FOR SIMULATED SHUTTLE BOOSTER
SEPARATION MOTORS (NASA) 218 p HC \$7.75

N76-16169
THRU
N76-16172
Unclas
G3/2J J9945

TECHNICAL REPORT STANDARD TITLE PAGE

1. REPORT NO. NASA TM X-64975		2. GOVERNMENT ACCESSION NO.		3. RECIPIENT'S CATALOG NO.	
4. TITLE AND SUBTITLE The Effects of Solid Rocket Motor Effluents on Selected Surfaces and Solid Particle Size, Distribution, and Composition for Simulated Shuttle Booster Separation Motors				5. REPORT DATE January 12, 1976	
				6. PERFORMING ORGANIZATION CODE	
7. AUTHOR(S) David W. Jex, Roger C. Linton, Willa M. Russell, John J. Trenkle, and Donald R. Wilkes				8. PERFORMING ORGANIZATION REPORT #	
9. PERFORMING ORGANIZATION NAME AND ADDRESS George C. Marshall Space Flight Center Marshall Space Flight Center, Alabama 35812				10. WORK UNIT NO.	
				11. CONTRACT OR GRANT NO.	
				13. TYPE OF REPORT & PERIOD COVERED Technical Memorandum	
12. SPONSORING AGENCY NAME AND ADDRESS National Aeronautics and Space Administration Washington, D. C. 20546				14. SPONSORING AGENCY CODE	
15. SUPPLEMENTARY NOTES Prepared by Space Sciences Laboratory, Science and Engineering					
16. ABSTRACT A series of three tests was conducted using solid rocket propellants to determine the effects a solid rocket plume would have on thermal protective surfaces (TPS). The surfaces tested were those which are baselined for the Shuttle vehicle. The propellants used were to simulate the separation solid rocket motors (SSRM) that separate the solid rocket boosters (SRB) from the Shuttle launch vehicle. This report presents conclusions of two bodies of data obtained by the Space Sciences Laboratory of Marshall Space Flight Center. The bodies of data are (1) the optical effects of the plume environment on spacecraft related surfaces and (2) the solid particle size, distribution, and composition at TPS sample locations.					
17. KEY WORDS			18. DISTRIBUTION STATEMENT <i>David W. Jex</i> Unclassified -- Unlimited		
19. SECURITY CLASSIF. (of this report) Unclassified		20. SECURITY CLASSIF. (of this page) Unclassified		21. NO. OF PAGES 219	22. PRICE NTIS

TABLE OF CONTENTS

	Page
INTRODUCTION	1
SUMMARY	5
Data Concerning Solid Particle Size, Distribution, and Composition	5
Data Concerning the Optical Effects of the Generated Plume Environment on Spacecraft-Related Surfaces	10
SECTION I. THE PLUME IMPINGEMENT TEST PROGRAM AT AEDC UTILIZING THE S-II ULLAGE MOTORS	12 -1
A. Introduction	12
B. Particle Size Analysis	12
C. Chemical Analysis of Solid Rocket Effluents	47
D. Contamination Considerations	56
SECTION II. THE SMALL MOTOR PLUME/MATERIAL IMPINGE- MENT TEST PROGRAM AT MSFC UTILIZING NINE DIFFERENT PROPELLANT FORMULATIONS	96 -2
A. Introduction	96
B. Solid Particle Collection	99
C. Particle Size Analysis	108
D. Holographic Analysis of Small Motor Plumes	124
E. Solid Rocket Motor Contamination of Shuttle Windshield Samples	138
SECTION III. THE LARGE MOTOR PLUME/MATERIAL IMPINGE- MENT TEST PROGRAM AT AEDC UTILIZING THE FOUR SELECTED PROPELLANTS FROM THE SMALL MOTOR TESTS AT MSFC	152 -3
A. Introduction	152
B. Solid Particle Collection Technique	155
C. Particle Size Distribution	162
D. Particle Compositional Analysis	174
E. Effects on Shuttle Windshields	181
APPENDIX: DEFINITION OF ACRONYMS	204

LIST OF ILLUSTRATIONS

Figure	Title	Page
1.	Space Shuttle with Proposed separation system in operation	2
I-1.	Mounting arrangement for quartz disks	14
I-2.	Bracket 2; vertical height, 3.05 m (10 ft); radial distance, 76.2 cm (30 in.)	15
I-3.	Bracket 3; vertical height, 3.05 m (10 ft); radial distance, 96.5 cm (38 in.)	16
I-4.	Bracket 4; vertical height, 3.05 m (10 ft); radial distance, 127 cm (50 in.)	17
I-5.	Bracket 5; vertical height, 3.05 m (10 ft); radial distance, 157.5 cm (62 in.)	18
I-6.	Bracket 7; vertical height, 3.05 m (10 ft); radial distance, 254 cm (100 in.)	19
I-7.	Bracket 11; vertical height, 6.1 m (20 ft); radial distance, 139.7 cm (55 in.)	20
I-8.	Bracket 12; vertical height, 6.1 m (20 ft); radial distance, 139.7 cm (55 in.)	21
I-9.	Bracket 13; vertical height, 6.1 m (20 ft); radial distance, 165.1 cm (65 in.)	22
I-10.	Particle size distribution, bracket 2, firing 1	24
I-11.	Particle size distribution, bracket 3, firing 1	25
I-12.	Particle size distribution, bracket 4, firing 1	26
I-13.	Particle size distribution, bracket 5, firing 1	27
I-14.	Particle size distribution, bracket 6, firing 2	28

LIST OF ILLUSTRATIONS (Continued)

Figure	Title	Page
I-15.	Particle size distribution, bracket 7, firing 1	29
I-16.	Particle size distribution, bracket 8, firing 2	30
I-17.	Particle size distribution, bracket 9, firing 2	31
I-18.	Particle size distribution, bracket 11, firing 1	32
I-19.	Particle size distribution, bracket 12, firing 1	33
I-20.	Particle size distribution, bracket 13, firing 1	34
I-21.	Particle size distribution, bracket 14, firing 1	35
I-22.	Particle size distribution, bracket 15, firing 1	36
I-23.	Bracket 8, 1000X magnification	39
I-24.	Bracket 15, 1000X magnification	40
I-25.	Bracket 8, 3000X magnification	41
I-26.	Bracket 8, 3000X magnification	42
I-27.	Bracket 8, 3000X magnification	43
I-28.	Bracket 8, 10 000X magnification	44
I-29.	Bracket 15, 1000X magnification	45
I-30.	Bracket 15, 3000X magnification	46
I-31.	G. L. C. scan of benzene extract	50
I-32.	Ultraviolet spectra of cyclohexane extract	51
I-33.	Infrared spectra of benzene extract	52
I-34.	Construction of simulated Shuttle bay and vent	58

LIST OF ILLUSTRATIONS (Continued)

Figure	Title	Page
I-35.	Box orientation and vent direction on test firings 1 and 2	59
I-36.	Box orientation and vent direction on test firing 3	60
I-37.	Mass deposition on QCM No. 1	62
I-38.	Mass deposition on QCM No. 2	62
I-39.	Temperature shift on QCM No. 1	63
I-40.	Temperature shift on QCM No. 2	63
I-41.	Solid particles found on adhesive surface of QCM	65
I-42.	Transmissometer after firing 3	67
I-43.	Transmittance of clean Shuttle windshield	68
I-44.	Transmissometer windshield sample, firing 2, deflector plate	69
I-45.	Transmissometer windshield sample, firing 3	71
I-46.	Windshield sample No. 3, aluminum	72
I-47.	Windshield sample location photographed after firing 3	73
I-48.	Passive optical sample test bed	74
I-49.	Optical effects of Shuttle rocket firing tests 2 and 3 on passive platinum samples	76
I-50.	Optical effects of Shuttle rocket firing tests 2 and 3 on passive gold sample	77
I-51.	Simplified heat-balance description	79
I-52.	Specular versus diffuse surface	81

LIST OF ILLUSTRATIONS (Continued)

Figure	Title	Page
I-53.	Spectroreflectometer schematic, Beckman DK2A	83
I-54.	S13G sample 001	87
I-55.	S13G sample 002	87
I-56.	S13G sample 003	88
I-57.	S13G sample 004	88
I-58.	S13G sample 005	89
I-59.	Silver-teflon sample 1	89
I-60.	Silver-teflon sample 2	90
I-61.	Z-93 sample 101	90
I-62.	Z-93 sample 103	91
I-63.	Z-93 sample 106	91
I-64.	Z-93 sample 107	92
I-65.	Z-93 sample 108	92
I-66.	Platinum mirror sample 201	93
I-67.	Platinum mirror sample 202	93
I-68.	Platinum mirror sample 203	94
I-69.	Platinum mirror sample 204	94
I-70.	Platinum mirror sample 205	95
II-1.	Active experiments flow chart	100
II-2.	Particle collector/calibration box	103

LIST OF ILLUSTRATIONS (Continued)

Figure	Title	Page
II-3.	Particle collection screen assembly schematic	104
II-4.	Filter assembly	105
II-5.	Particle size distribution, filter S/N 003, propellant 3, firing 21, 38.1 cm (15 in.)	110
II-6.	Particle size distribution, filter S/N 005, propellant 3, firing 21, 38.1 cm (15 in.)	111
II-7.	Particle size distribution, filter S/N 006, propellant 3, firing 21, 12.7 cm (5 in.)	112
II-8.	Particle size distribution, filter S/N 010, propellant 3, firing 21, 12.7 cm (5 in.)	113
II-9.	Particle size distribution, filter S/N 001, propellant 3, firing 10, 38.1 cm (15 in.)	114
II-10.	Particle size distribution, filter S/N 002, propellant 3, firing 10, 38.1 cm (15 in.)	115
II-11.	Filter S/N 003, propellant 3, firing 21, 38.1 cm (15 in.) . . .	116
II-12.	Filter S/N 005, propellant 3, firing 21, 38.1 cm (15 in.) . . .	117
II-13.	Filter S/N 006, propellant 3, firing 21, 12.7 cm (5 in.) . . .	118
II-14.	Filter S/N 010, propellant 3, firing 21, 12.7 cm (5 in.) . . .	119
II-15.	Filter S/N 001, propellant 3, firing 10, 38.1 cm (15 in.) . . .	120
II-16.	Filter S/N 002, propellant 3, firing 10, 38.1 cm (15 in.) . . .	121
II-17.	Filter 003, 1000X magnification	125
II-18.	Filter 003, 3000X magnification	126
II-19.	Filter 005, sample A, 3000X magnification	127

LIST OF ILLUSTRATIONS (Continued)

Figure	Title	Page
II-20.	Filter 005, sample B, 1000X magnification	128
II-21.	Filter 005, sample B, 3000X magnification	129
II-22.	Filter 006, 3000X magnification	130
II-23.	Filter 010, 3000X magnification	131
II-24.	Filter 010, 10 000X magnification	132
II-25.	Filter 001, 3000X magnification	133
II-26.	Filter 002, 3000X magnification	134
II-27.	Filter 002, 3000X magnification	135
II-28.	Filter 002, 1000X magnification	136
II-29.	In-line holographic layout	137
II-30.	Transmittance loss for propellant type 7	144
II-31.	Transmittance loss for propellant type 3	145
II-32.	Transmittance loss for propellant type 5	146
II-33.	Image clarity photographs (propellant 7, April 18, 1974, test firing 1)	147
II-34.	Image clarity photographs (propellant 8, April 23, 1974, test firing 4)	149
II-35.	Image clarity photographs (propellant 3, May 1, 1974, test firing 12)	150
II-36.	Transmittance of clean Shuttle windshield samples	151
III-1.	Large motor impingement test arrangement	154
III-2.	Filter assembly	156

LIST OF ILLUSTRATIONS (Continued)

Figure	Title	Page
III-3.	Particle collector screen unit installed	157
III-4.	Dual motor firings — mass collected by filters	160
III-5.	Dual motor firings — mass collected by elbows	161
III-6.	Particle size sampling locations	163
III-7.	Features on the front surface of a portion of filter 26 mesh	179
III-8.	Features on the back surface of a portion of filter 26 mesh	180
III-9.	Photographs of areas examined by electron microprobe	182
III-10.	Orientation for optical data	186
III-11.	Transmittance of clean shuttle windshield	188
III-12.	Shuttle windshield contamination	189
III-13.	Shuttle windshield effects of AEDC rocket firings, dual 1 . . .	190
III-14.	Shuttle windshield effects of AEDC rocket firings, dual 6 . . .	191
III-15.	Sample end of transmissometer after firing on September 24, 1974	192
III-16.	Passive sample prior to firing	193
III-17.	Sample shown in Figure III-16 after dual 1 firing	194
III-18.	Sample used in Figure III-17 photographed at 45 degree angle	195
III-19.	Sample used in Figure III-17 photographed at 80 degree angle	196

LIST OF ILLUSTRATIONS (Concluded)

Figure	Title	Page
III-20.	Sample before firing of single 6	198
III-21.	Sample after firing of single 6	199
III-22.	Sample after dual 6 firing	200
III-23.	Sample using type 3 propellant	201
III-24.	Sample after dual 3 firing	202
III-25.	Sample after dual 3 firing oriented -90 degrees	203

LIST OF TABLES

Table	Title	Page
1.	Summary of Compositional Analysis Using X-Ray Diffraction, Electron Microprobe, and Wet Chemistry	7
I-1.	Primary Groups of Experiments and Related Information . . .	13
I-2.	The Percentage of Particles Between Selected Size Ranges of Firing 1	37
I-3.	The Percentage of Particles Between Selected Size Ranges of Firing 2	38
I-4.	Liquid Samples	48
I-5.	Solid Samples	49
I-6.	Aluminum and Iron Testing Procedures	53
I-7.	Tabulated Results of 2.54 cm (1 in.) Diameter Samples . . .	84
I-8.	Sample Locations	95
II-1.	Composition Propellant Formulations	98
II-2.	Double-Base Propellant Formulation	99
II-3.	Test Firing Data	101
II-4.	Windtek Filters — Total Mass Collected	106
II-5.	Particle Collection Boxes — Total Mass Collected	107
II-6.	Percentage of Particles in Selected Size Ranges for Each Filter	123
II-7.	Percentage of Aluminum in Rocket Effluents	124
II-8.	Test Firing History and Corresponding Transmissometer Data	140

LIST OF TABLES (Concluded)

Table	Title	Page
II-9.	Transmissometer Results of Shuttle Windshield Samples . . .	141
II-10.	Propellants Ordered From Least Transmission Loss to Most Transmission Loss	142
III-1.	Propellant Formulations for Tests	153
III-2.	Mass Collected by Particle Collector System Components . . .	158
III-3.	Summary of Compositional Analysis Using X-Ray Diffraction, Electron Microprobe and Wet Chemistry	175
III-4.	Composition of Exhaust Particles	177
III-5.	Electron Microprobe Analysis of Solid Rocket Motor Effluents	183
III-6.	Analysis of Rocket Effluents	184

TECHNICAL MEMORANDUM X-64975

THE EFFECTS OF SOLID ROCKET MOTOR EFFLUENTS ON
SELECTED SURFACES AND SOLID PARTICLE SIZE,
DISTRIBUTION, AND COMPOSITION FOR SIMULATED
SHUTTLE BOOSTER SEPARATION MOTORS

INTRODUCTION

The baseline configuration for the Shuttle launch vehicle has four basic components:

1. The orbiter.
2. The external tank (ET).
3. Two solid rocket boosters (SRE).
4. Sixteen separation solid rocket motors (SSRM).

These components are illustrated in Figure 1, a design of the Shuttle that has since undergone some revision.

The 16 SSRM's are grouped in 4 batteries of 4 each. One battery of four is located on the fore end of each SRB, and one battery of four is located on the aft end of each SRB. (This is also illustrated in Figure 1.) Therefore, there are eight SSRM's per SRB.

These eight SSRM's provide the required force to separate each SRB from the orbiter-external tank system after they have provided the necessary boost to the launch vehicle. Each SSRM develops 10 430 kg (23 000 lb) of thrust for 2 seconds.

Analysis indicated that a portion of the plumes from the forward separation motors would impinge on the orbiter and ET, while a portion of the plumes from the aft separation motors would impinge on the orbiter body flap and Space Shuttle main engine (SSME) nozzle.

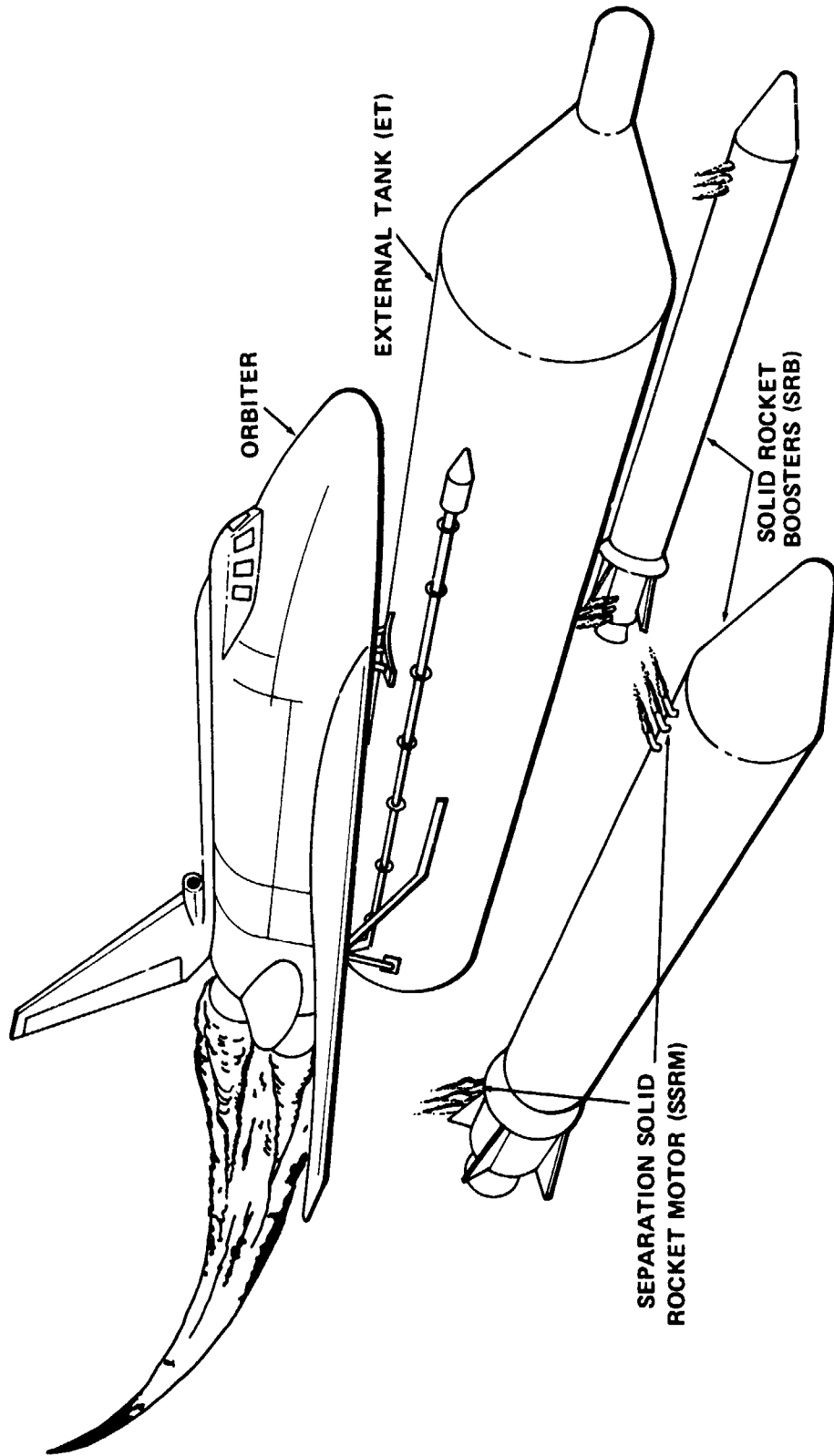


Figure 1. Space Shuttle with proposed separation system in operation.

A plume impingement test program utilizing S-II ullage motors was initiated by NASA-Johnson Space Center (JSC) and supported by NASA-Marshall Space Flight Center (MSFC) and Rockwell International Corp. to obtain a gross assessment of orbiter and ET material degradation resulting from SSRM plume exposure. These test firings were conducted in November 1973 at Arnold Engineering Development Center (AEDC) in the J-4 high altitude test facility. The orbiter thermal protective surface (TPS) materials experienced unacceptable damage at several test locations.

Concurrent with the S-II motor tests, activities were initiated to evaluate:¹

- a. Alternate SSRM orientations and thrust levels to eliminate SSRM plume impingement or reduce SSRM impingement to an acceptable level.
- b. Identify candidate SSRM propellants that minimize orbiter TPS material erosion and contamination.

In support of item a, two candidate SSRM configurations were selected for continued study:¹

1. An orthogonal SSRM system incorporating two pairs of 10 250 kg (22 600 lb) thrust motors at each end of the SRB. This arrangement causes a minimum plume impingement environment on the orbiter nose.
2. An inline SSRM system incorporating four 5440 kg (12 000 lb) thrust motors at each end of the SRB. This system results in lower system weight and cost but causes a more severe plume impingement environment relative to the orthogonal system.

In support of item b, the small motor plume/material impingement test series was conducted during April and May 1974 at the MSFC test position 112 altitude test facility. The test motors produced approximately 230 kg (500 lb) of thrust. The relative effect of the plumes from nine different propellant formulations on orbiter TPS materials [high temperature reusable surface insulation (HRSI) and reinforced carbon-carbon (RCC)] was evaluated (see footnote 1).

These nine propellants permitted the relative effects of metallic exhaust products and high and low combustion temperatures, relative to position of the TPS specimens in the plume, to be determined. Four of these propellant formulations were selected for the large motor plume/material impingement

1. For details and results, contact Ivy Fossler at JSC.

test program conducted during July, August, and September 1974 at AEDC in the J-4 high altitude test facility.

In summary, there have been three test programs conducted to evaluate plume impingement effects on TPS materials:

1. The plume impingement test program at AEDC utilizing the S-II ullage motors (November 1973).
2. The small motor plume/material impingement test program at MSFC utilizing nine different propellant formulations (April and May 1974).
3. The large motor plume/material impingement test program at AEDC utilizing the four selected propellants from the small motor tests (July, August, and September 1974).

The objectives in each test were to:

1. Determine the vulnerability of orbiter and ET materials located at various positions within the exhaust plumes.
2. Determine the effects of a single SSRM plume and/or dual SSRM plumes on these materials.
3. Define the SSRM plume environment at the specimen locations.

This document describes the techniques used, data obtained, and conclusions of the analyzed data from experiments conducted by the Space Sciences Laboratory of MSFC to support test objective 3.

SUMMARY

Two basic bodies of data were obtained from the three test series of solid rocket motors. The three test series are described in detail in the Introduction. The two bodies of data resulted from experiments assembled, conducted, and analyzed by personnel from the Space Sciences Laboratory (NASA/MSFC) and the Rockwell International Corp. These two bodies of data are:

1. Data concerning solid particle size, distribution, and composition.
2. Data concerning the optical effects of the generated plume environment on spacecraft-related surfaces.

Data Concerning Solid Particle Size, Distribution, and Composition

To investigate the source of damage to surfaces caused by rocket plume impingement, the size, composition, volume density, flux rate, etc., of constituent plume particles must be found.

While such characterization is ideally approached by a defined general model for firings under various conditions, at the present time different schools of thought and different theoretical models exist.

The test series described in this paper were not concerned with verifying, modifying, or even supporting any of the proposed theoretical models, but rather with answering the question: What environment of solid particles did the exposed thermal protective surfaces experience?

For this reason, the collection techniques were designed to see the entire environment of solid particles that the TPS materials would see. There were no covers on the TPS material to prevent the impact of solid particles that might originate from the ignitor; therefore, there were no covers for the collectors. There were no cutoff valves on the TPS materials to prevent solid particles generated in the tail-off phase from impacting the surfaces; therefore, there were no cutoff valves used on the collectors.

It is, then, quite safe to assume that the solid particles collected and analyzed are representative of those that impacted the TPS materials. These particles are not necessarily representative of solid particles predicted from an idealized theoretical model based on any one or several single factors, rather they represent the integrated effects of all conditions that occurred in these specific tests.

There are five conclusions reached from examination of the data:

1. There was entrainment of solid particles from a source outside the rocket motor propellant and its system of combustion components.

Supporting Evidence — A significant and comparable percentage of iron was detected in all analyses performed on the collected samples of rocket motor firings using propellants 1, 3, and 5 (none of which contain iron as an element of the formulation, see Table II-1). Table 1 shows the summary of the collected samples.

Possible Sources other than the propellant include the motor nozzle (stainless steel), the collector assembly (stainless steel), and the rusty debris of the chamber.

Considering the first possibility, is it probable that small bits of iron from the motor nozzle were introduced into the plume flow, thereby resulting in iron being present? If this were the case, there should be evidence of chromium (Cr) and nickel (Ni) in significant amounts. In examining Table 1, it is seen that the amount of chromium is low and there is little or no nickel. It is concluded, therefore, that the nozzle does not contribute a significant amount of solid particles to the plume and that stainless steel particles are not present.

Considering the second possibility, it is a fact that one of the products of solid propellant combustion is hydrochloric acid (HCl) and that HCl will react with stainless steel, leaving iron as a reaction residual. As pointed out in section III, the time from firing to final collection of the solid particle sample was approximately 1 hour; the amount of iron from this process over this time would have to be small. Table 1, however, shows rather large amounts of iron were present. It is suggested that the HCl and collector assembly reaction could not account for the amount of iron present.

TABLE 1. SUMMARY OF COMPOSITIONAL ANALYSIS USING X-RAY DIFFRACTION, ELECTRON MICROPROBE, AND WET CHEMISTRY (ALL NUMBERS ARE PERCENTAGE BY WEIGHT)

Test Firing No.	Walter C. McCrone, Inc. ^c X-Ray Diffraction and Electron Microprobe				Section III Athens College Wet Chemistry				MSFC Electron Microprobe (Aluminum Stub Used)				Section II Athens College Wet Chemistry									
	5	4	3	6S	5	4	3	6S	5	7	2	10	12	19	4							
Propellant Type ^a	1D	6D	6S	6S	1D	6D	6S	6S	1D	6D	3D	3S	5S	8S								
Sample Location ^b	UL'75	UL'75	UL'75	UL'75	UL'75	UL'73	UL'73	UL'73	UL'75	UL'73	UL'73	UL'31	UL'92	UL'92	UL'37							
Al	1.5	0.75	-	1.5	3.2	2.6	5.5	1.0	7.9	21.4	27.8	32.0	15.3	1.9	3.0	3.6	3.1	6.8	2.5			
Si	2.5	3.5	0.25	1.5	3.0	13.0	-	-	-	-	5.0	4.2	10.3	-	-	-	-	-	-			
P	2.5	1.5	0.75	2.5	-	-	-	-	-	-	3.7	1.6	-	-	-	-	-	-	-			
S	-	1.5	-	-	-	-	-	-	-	-	0.4	0.9	0.1	-	-	-	-	-	-			
Cl	5.5	4.0	0.25	-	-	-	-	-	-	-	0.4	4.5	0.4	-	-	-	-	-	-			
K	1.5	-	-	1.5	-	-	-	-	-	-	1.0	0.3	0.6	-	-	-	-	-	-			
Ca	-	-	-	0.3	4.0	-	-	-	-	-	1.4	-	1.2	-	-	-	-	-	-			
Cr	6.5	7.5	0.75	6.5	-	-	-	-	-	-	4.3	4.9	0.7	-	-	-	-	-	-			
Mn	-	-	-	1.6	-	-	-	-	-	-	1.4	1.0	1.0	-	-	-	-	-	-			
Fe	42.5	40.0	50	35	50	15.5	12.7	6.3	17.3	14.5	31.6	71.4	51.3	47.7	65.9	2.5	8.1	6.7	5.5	6.5	5.7	
Ni	-	-	-	-	-	-	-	-	-	-	0.9	0.1	0.3	-	-	-	-	-	-	-	-	-
Cu	-	0.35	-	-	-	-	-	-	-	-	0.5	0.5	0.3	-	-	-	-	-	-	-	-	-
Burned on Ignition					49	56	28	16	5	7				76	81	78	96	43	47			

a. Propellant Type: The numerical designation corresponding to Table III-1 will be followed by a D (dual) or S (single) describing the number of motors with that propellant type fired.

b. Sample Location: UL = upper level; LL = lower level; UL' = any level translated to upper level.

c. The midpoint was used for the percentages of Walter C. McCrone data.

ORIGINAL PAGE IS
OF POOR QUALITY

The possibility exists that the combination of these two factors contributes to the results of the data; however, after observing the films of the motor firings and the data presented in this report, it is believed that the debris of the chamber is the major contributor.

In the films of the motor firing, the circulation and recirculation of material is obvious, especially at the edges of the plume flow and again at the interfaces of the sample holders. In the test at MSFC, flakes of debris were seen floating past the window of the chamber through which the pictures were being taken. This coupled with the electron microscope photographs in Sections II and III of particles collected supports the conclusion that entrainment of solid particles from a source outside the rocket motor propellant and its system of combustion components does occur and is significant. The electron microscope pictures show irregular particles instead of smooth spherical or elliptical particles that would be present if the particles originated from the combustion and flow processes.

Compare also the amount of iron for motor 6 (which contains 1 percent Fe_2O_3) to the amounts for motors 1, 3, and 5. A general relationship of comparable amounts is evident even though the propellant for motor 6 contains iron and those for 1, 3, and 5 do not.

Another observation is that the single motor firings of motor 6 have more iron than the double motor firings. If the hypothesis that the iron comes from the propellant and motor components were correct, then the double motor firings should have more than the single motor firings. Instead the reverse is true.

2. Particle sizes between 1 and 10 μm peak at 2 to 3 μm .

Supporting Evidence — All the size distribution plots of Sections I, II, and III show a peak at positions between 2 and 3 μm . There are peaks located at other positions in some of the plots, but these peaks shift and disappear from firing to firing. It is possible that the peaks that shift and disappear are characteristic of the propellant and/or motor parameters, but in all cases the major peak appears between 2 and 3 μm .

3. Solid particles are not a result of solidification.

Supporting Evidence — In every photograph it is striking to observe the irregular shapes of the particles collected. Even small particles do not exhibit the spherical or even elliptical shapes that would be characteristic of molten material solidification in a flow field. The sides and edges of many of the

particles are smooth, indicating they have been subjected to high temperatures. Some of those adhering to the collector mesh show they had a molten layer at the time of impact, but even then the shape is irregular.

4. The flux of particles is concentrated on the outer edge of the plume cone.

Supporting Evidence — All the graphs in Section III show more of each size of particle at upper level locations 75 and 110 (which are the outer edges of the plume cone at those locations) than at other locations.

The total mass collected by filters in Section III increases from location 0 to location 110 and then decreases, showing a total mass concentration at the 75 to 110 locations.

5. The form of the mathematical model that would describe the relationship between the number of particles and the diameter at any one location is of the form

$$y = ae^{-b(x-c)^2} + \frac{d}{x} \cos \left[\frac{4\pi}{3} (x - 2.5) \right] + e$$

Supporting Evidence — All of the plots of the number of particles versus the diameter in Sections I, II, and III have the shape of this equation, and a curve of the form $y = ae^{-b(x-c)^2}$ can be found to fit the general shape of the plots.

There are cyclic peaks superimposed on all of the general curves. Therefore, to be totally accurate, the addition of a cosine function and constant is necessary to produce the cyclic peaks and move the resulting curve up and down. This will give a general curve that will fit the data in any graph, including the peaks which are cyclic in nature.

In the equation $y = ae^{-b(x-c)^2}$ for the general shape, a is the maximum value of the highest peak, b is the rate of increase and decrease of the curve on either side of the highest peak, c is the diameter of the particles where the curve reaches a maximum, x is the diameter of the particle in microns, and y is the number of particles.

All the plots show the curve maximum (c) occurring between 2 and 3 μm . Using regression analysis it is possible to generate an equation for the number of particles as a function of the diameter for a given location and motor. These can be compared to one another and other locations. However, this analysis is beyond the scope of this paper. The data are presented, and the interested individual can perform the comparison.

These are the five conclusions reached by examination of the data obtained from the three test series. The data of each test series are presented as subsequent sections in this document.

Data Concerning the Optical Effects of the Generated Plume Environment on Spacecraft-Related Surfaces

The optical effects of contamination of optical surfaces because of solid rocket motor (SRM) plume impingement were investigated during the SRM tests at AEDC and MSFC in 1973-1974. During the initial firings at AEDC a scaled, simulated Shuttle cargo bay was placed in the J-4 chamber at various locations; inside were active and passive optical contamination monitors. Results of these tests indicate, but do not prove, that the contamination hazard to cargo bay optics would be minimal. The remaining optical surface of concern is then the Shuttle windshield.

This windshield is subject to loss of transmission and optical viewing quality because of impingement and deposition of SRM plume constituents. Results of deployment of both active and passive windshield contamination monitors in the firings show the optical effects to be highly dependent on rocket motor composition and configuration of the various propellant formulations. Windshield optical degradation was generally less for motor types 1, 3, and 6. For any firing of one or more of these type motors, a 30 percent loss of transmission in the visible may be expected with some blurring of image quality because of scattering.

The deposition is a combination of particulates matrixed in a corrosive thin film. The particulate components generally have the greater effect on image quality as gauged from analyses of photographs.

In general, for the latter three types of propellant formulations tested (1, 3, and 6), the degradation of windshield viewing quality is serious but not such as to produce opacity. The data in the following sections show the relative losses in transmissivity, and several photographs are included to provide a comparison of resolution of viewing between a clean Shuttle windshield and one exposed to SRM plume deposits.

N76-16170

SECTION I. THE PLUME IMPINGEMENT TEST PROGRAM
AT AEDC UTILIZING THE S-11 ULLAGE MOTORS
(NOVEMBER 1973)

A. Introduction

The Space Sciences Laboratory (SSL) at MSFC assisted in this test series under a Task Agreement.

A task team was assembled from two separate divisions of SSL and several experiments were proposed by this group. David W. Jex served as the task team leader.

The proposed experiments were broken into two primary groups. These two groups were: (1) those experiments that would help define some of the parameters that characterize the plume and (2) those experiments that would enable evaluation of some of the contamination effects of the plume environment on various items of interest. Table I-1 shows these primary experiment groups and the respective experiments conducted. Also included in Table I-1 are the experimenters, the items investigated, and the purpose of the investigation.

The details of each experiment are included in the subsections that follow.

B. Particle Size Analysis

Willa M. Russell, Jim Bozeman, and Dan Gates

Quartz disks of 2.54 cm (1 in.) diameter were mounted on the back of a 1.27 cm (0.5 in.) thick aluminum plate in the configuration shown in Figure I-1. After each firing, the exposed quartz samples were removed and each disk was placed in its own covered container immediately upon its removal from the holder. Each of the samples was photographed upon receipt at the laboratory for analysis. Copies of these photographs are shown in Figures I-2 through I-9. The caption on each gives its location in the plume by bracket number as well as vertical height above the nozzle of the engine and radial distance from the central axis of the plume. The frosting and decomposition of the disks is quite noticeable in the square area centrally located on each disk. This particular square pattern is a result of the mounting arrangement used for the samples.

TABLE I-1. PRIMARY GROUPS OF EXPERIMENTS AND RELATED INFORMATION

Primary Groups	Experiments	Experimenters	Item Investigated	Purpose of Investigation
Characteristics of the Plume	OMNICON System and Scanning Electron Microscope	Willa Russell Jim Bozeman Dan Gates	Solid Particles in the Plume	Determine the size distribution of solid particles in the plume.
	Wet Chemistry	Ronald McNutt (Athens College)	Solid Particles in the Plume	Determine the percentage of aluminum, iron, and hydrocarbons in samples of solid particles collected from the plume.
Contamination Effects of the Plume Environment	Quartz Crystal Microbalances (QCM)	Daniel Nisen Thomas Edwards David Jex	Simulated Shuttle Bay	Determine the amount of solid particle contamination that might be expected to enter the Shuttle bay.
	Transmissometer and Passive Ultraviolet (UV) Optical Samples	Roger Linton Coy Mattox	Shuttle Windshield and Optical Surfaces	Determine the contamination effect of the plume on Shuttle windshield material and other optical surfaces.
	Beckman DK-2A Spectrometer and Lyons Model 25B-6 Emissometer	John Trenkle Donald Wilkes	Si3G, Silver Teflon, and Z93 Surfaces	Determine the contamination of the plume on typical spacecraft surfaces.

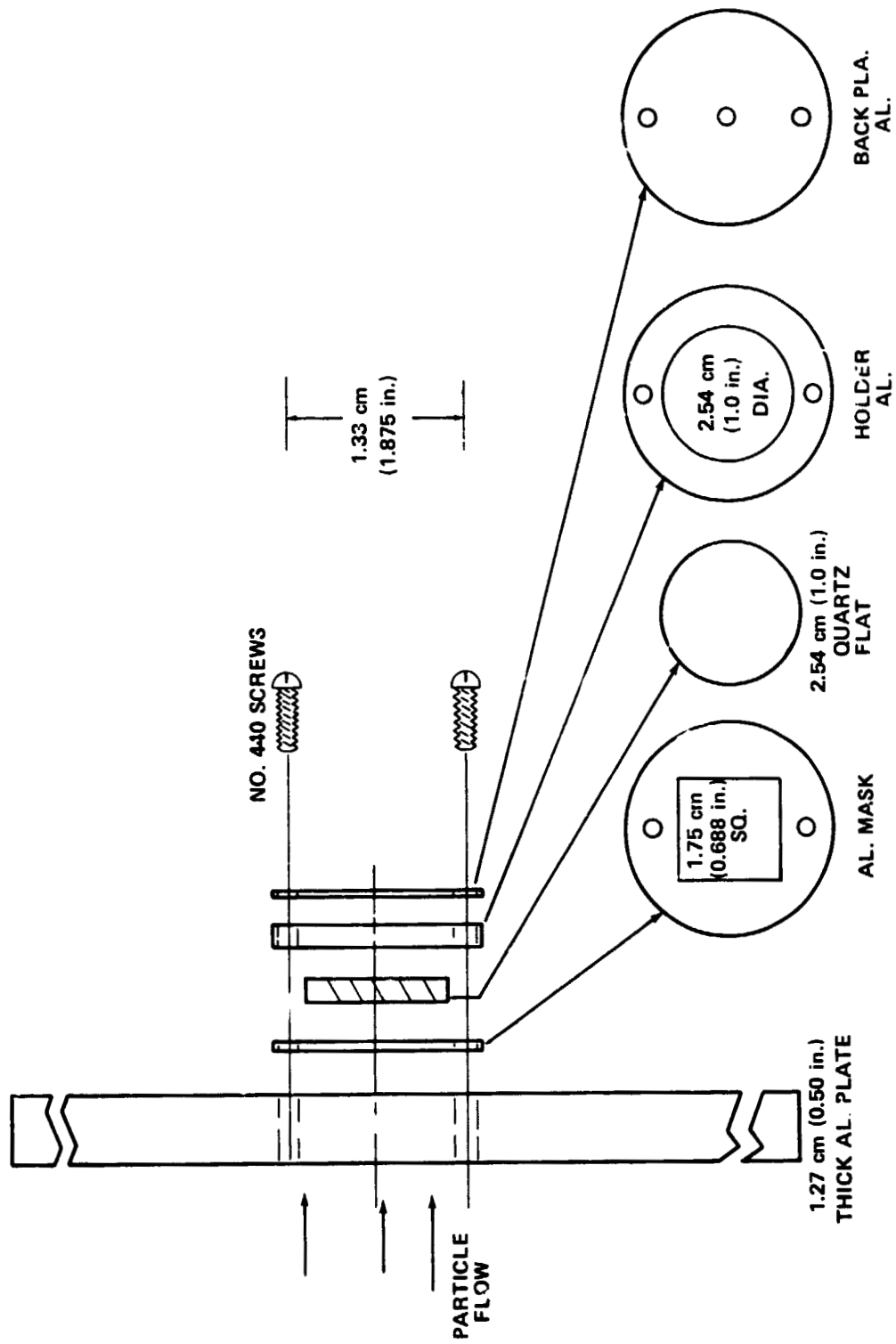


Figure I-1. Mounting arrangement for quartz disks.

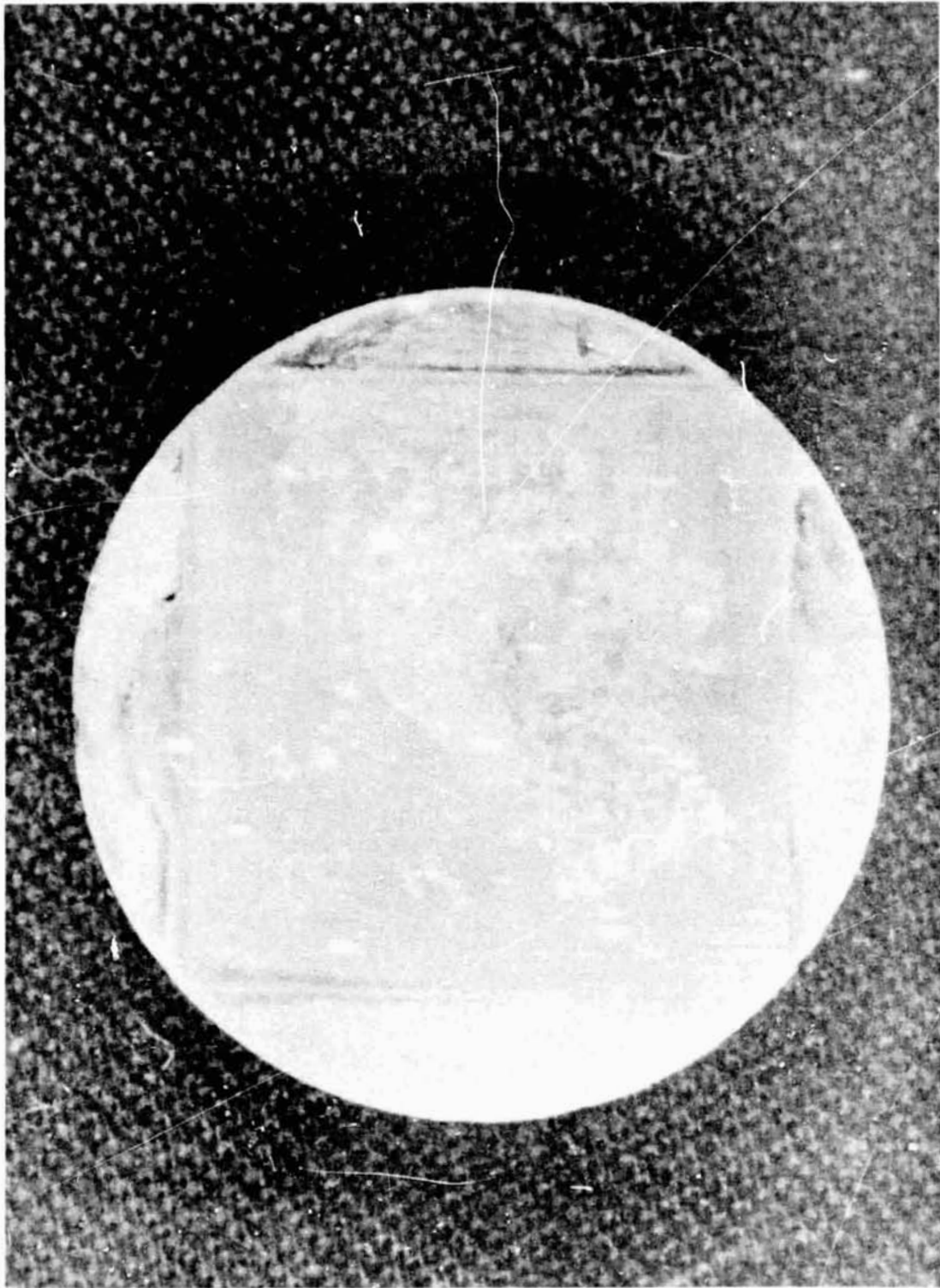


Figure I-2. Bracket 2; vertical height, 3.05 m (10 ft); radial distance, 76.2 cm (30 in.).

**ORIGINAL PAGE IS
OF POOR QUALITY**

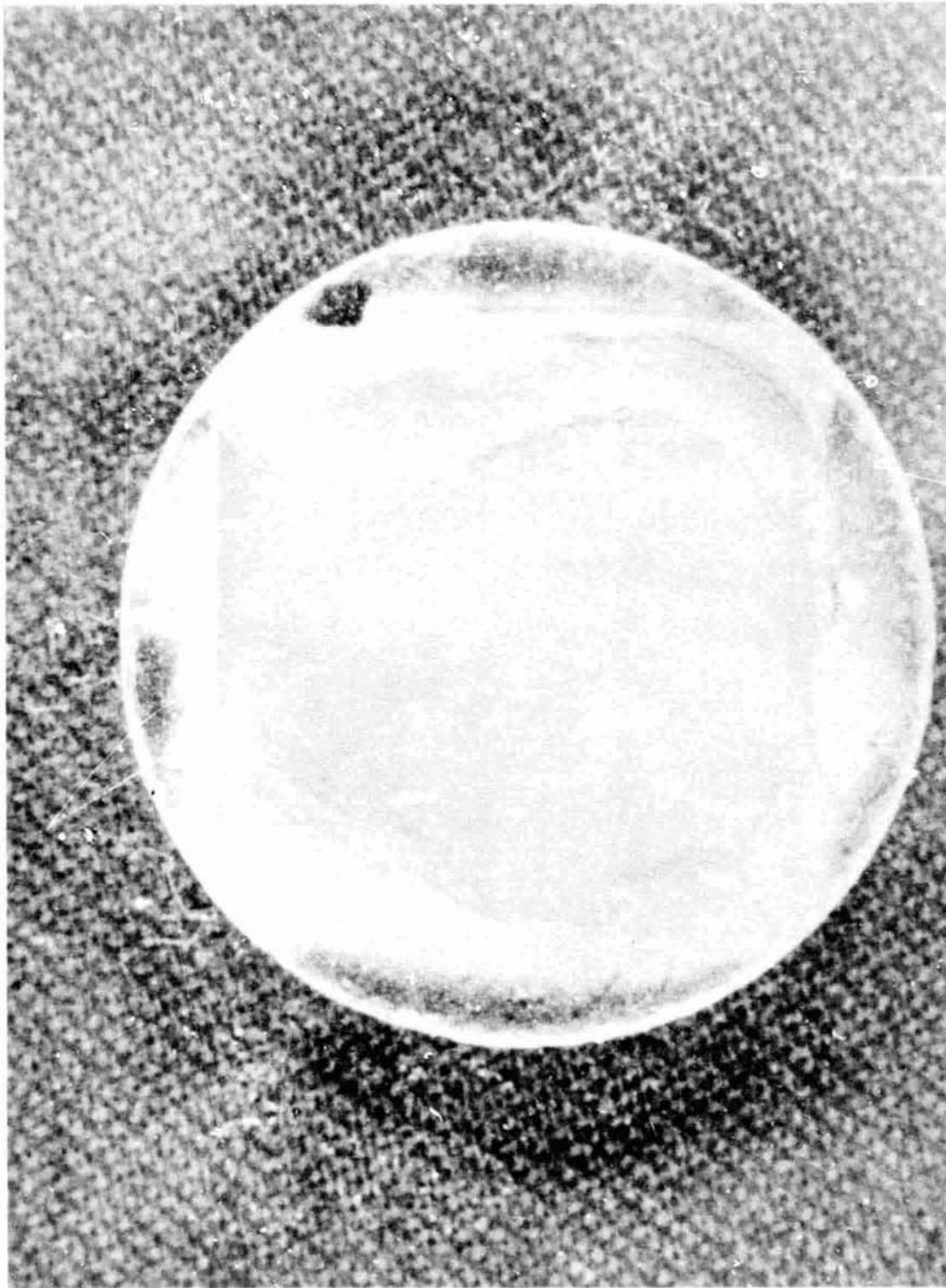


Figure I-3. Bracket 3; vertical height, 3.05 m (10 ft); radial distance, 96.5 cm (38 in.).

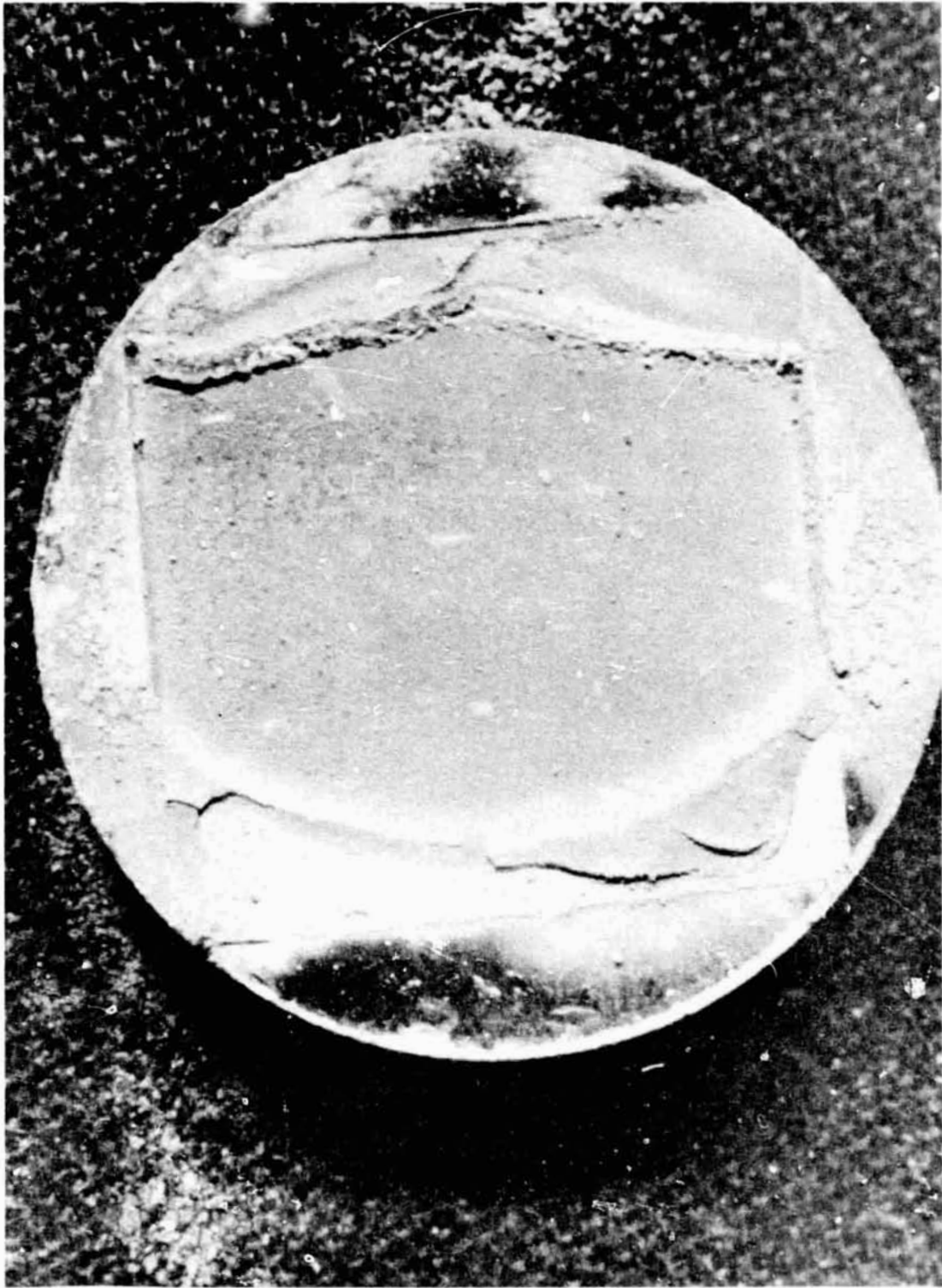


Figure I-4. Bracket 4; vertical height, 3.05 m (10 ft); radial distance, 127 cm (50 in.).

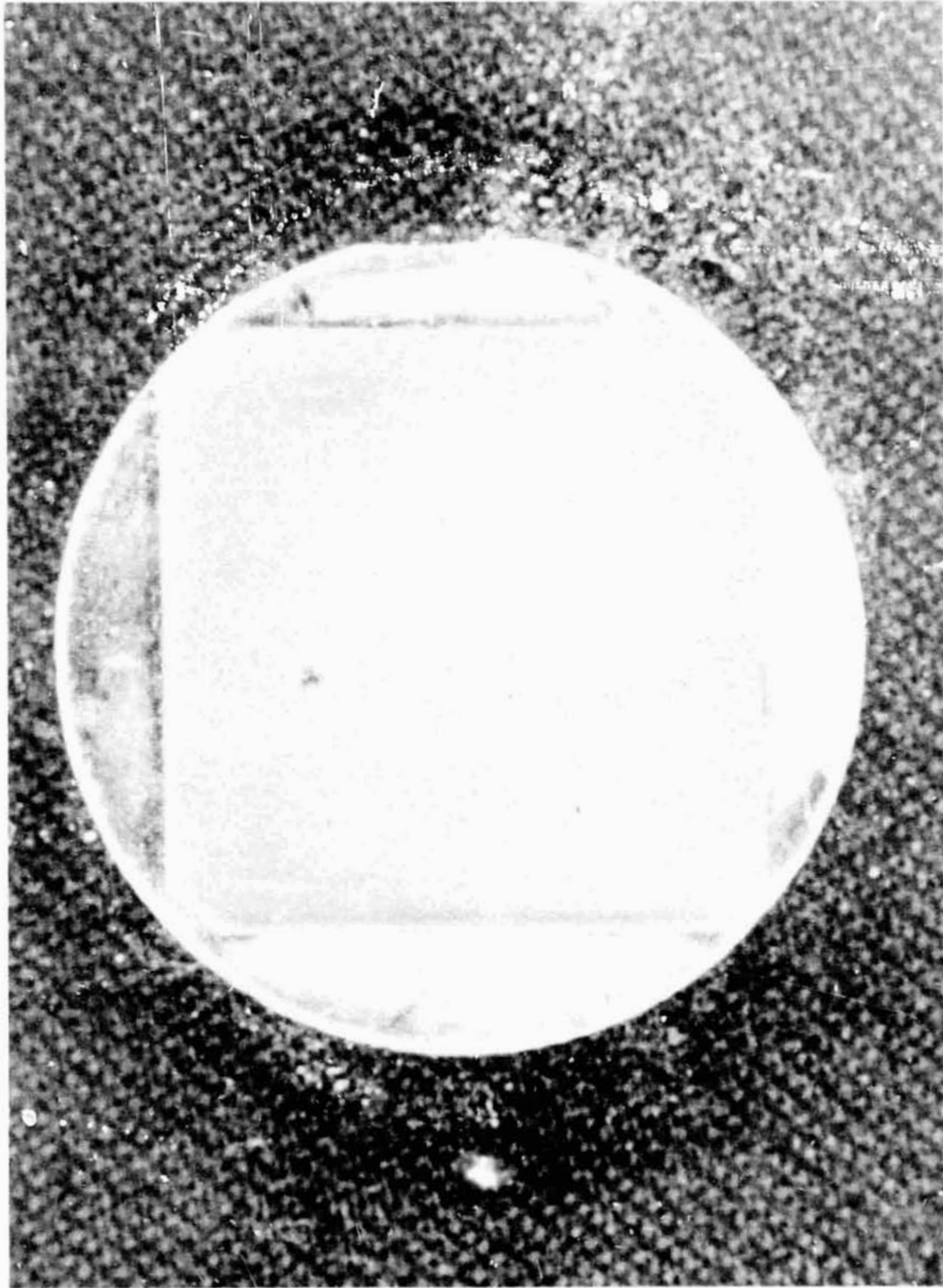


Figure I-5. Bracket 5; vertical height, 3.05 m (10 ft); radial distance, 157.5 cm (62 in.).

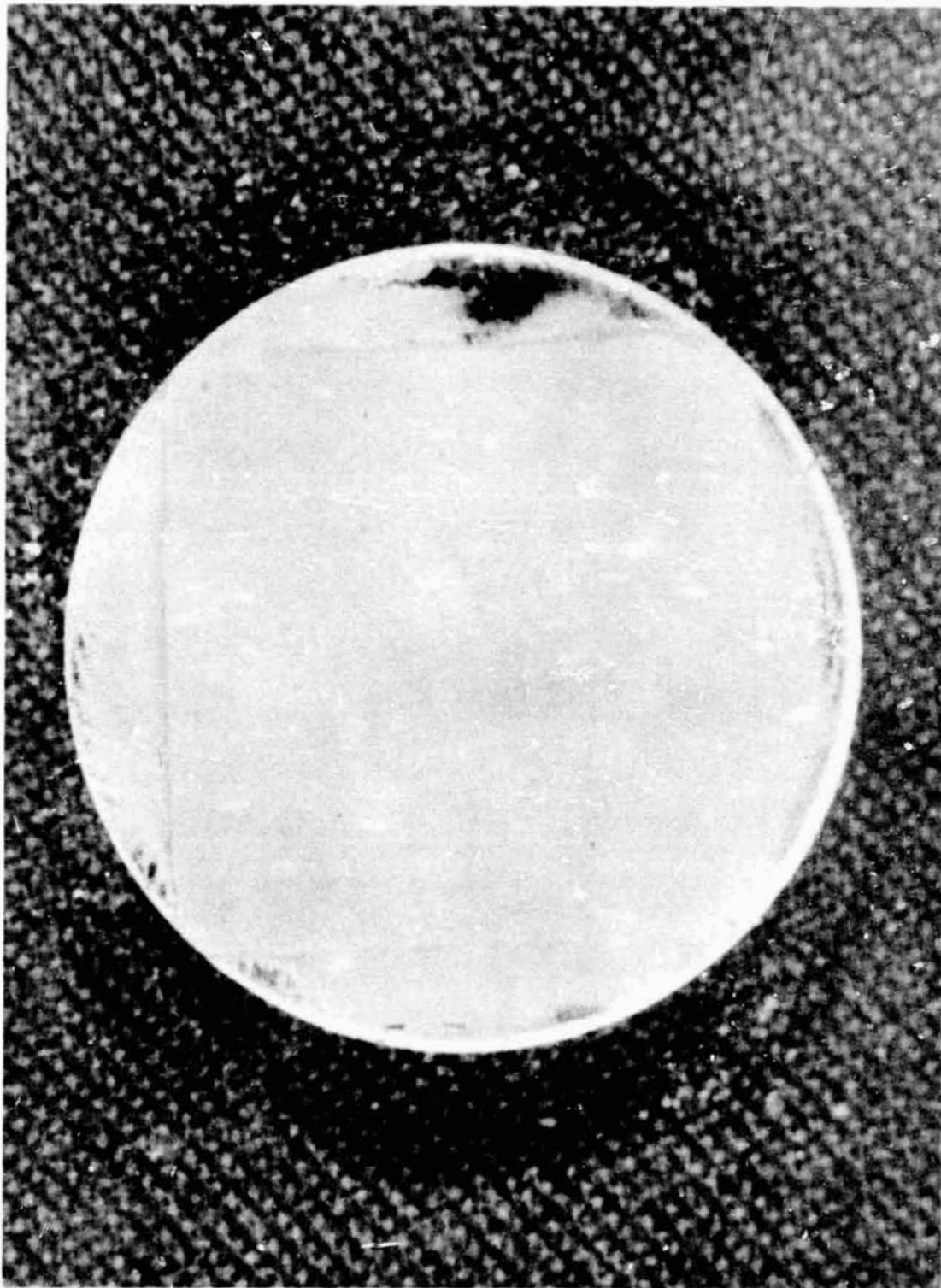


Figure I-6. Bracket 7; vertical height, 3.05 m (10 ft); radial distance, 254 cm (100 in.).

**ORIGINAL PAGE IS
OF POOR QUALITY**

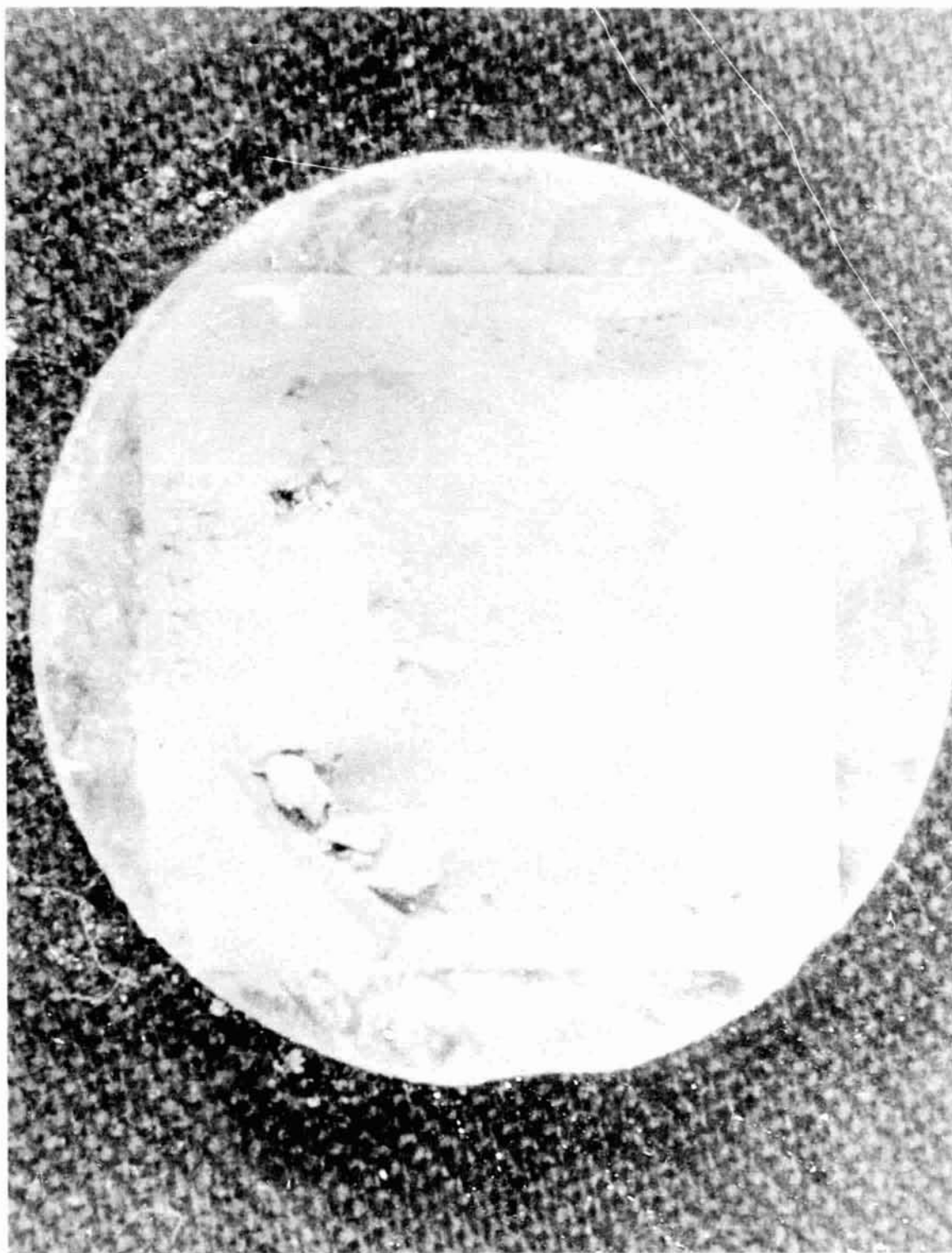


Figure I-7. Bracket 11; vertical height, 6.1 m (20 ft); radial distance, 139.7 cm (55 in.).

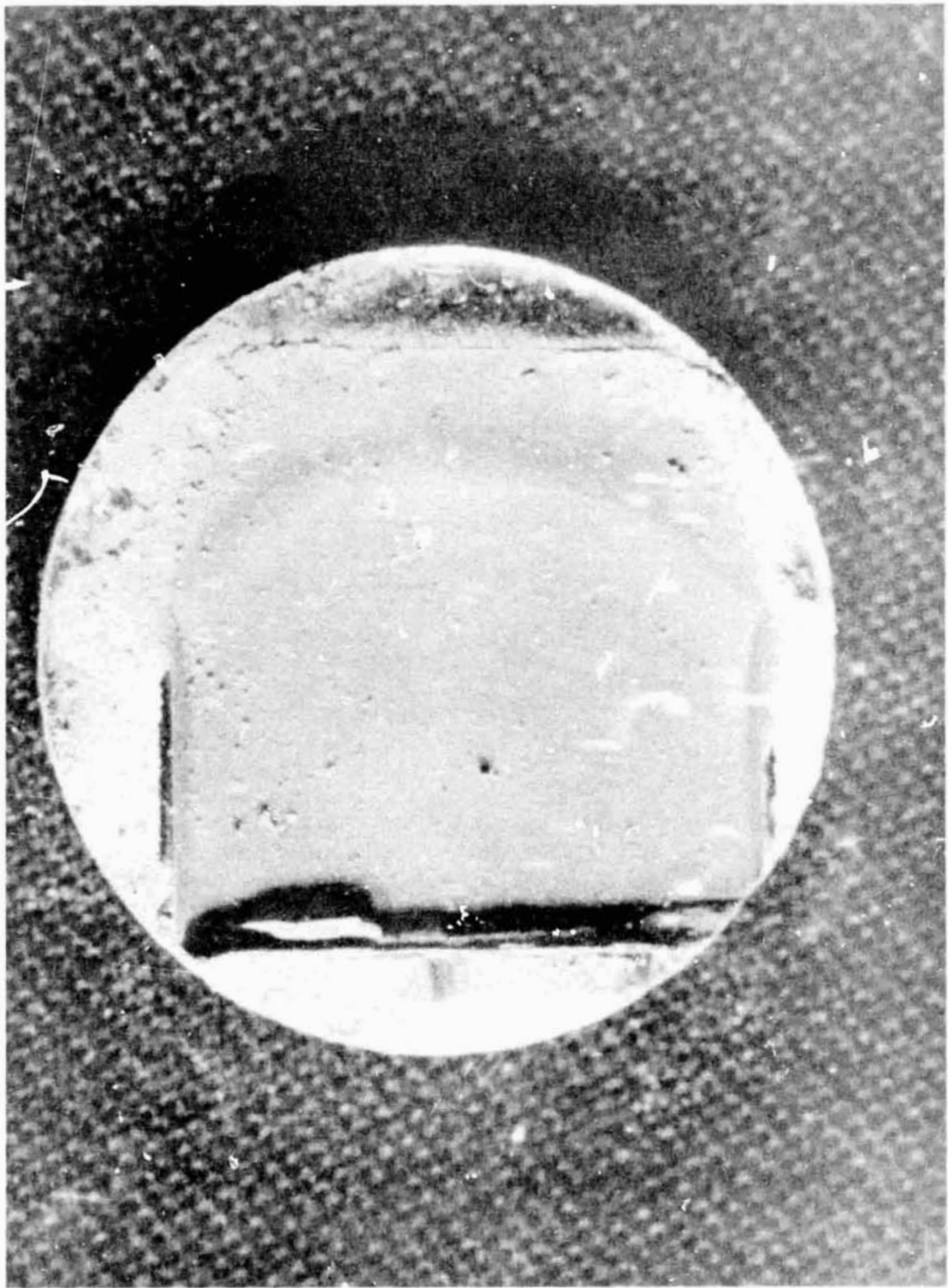


Figure I-8. Bracket 12; vertical height, 6.1 m (20 ft); radial distance, 139.7 cm (55 in.).

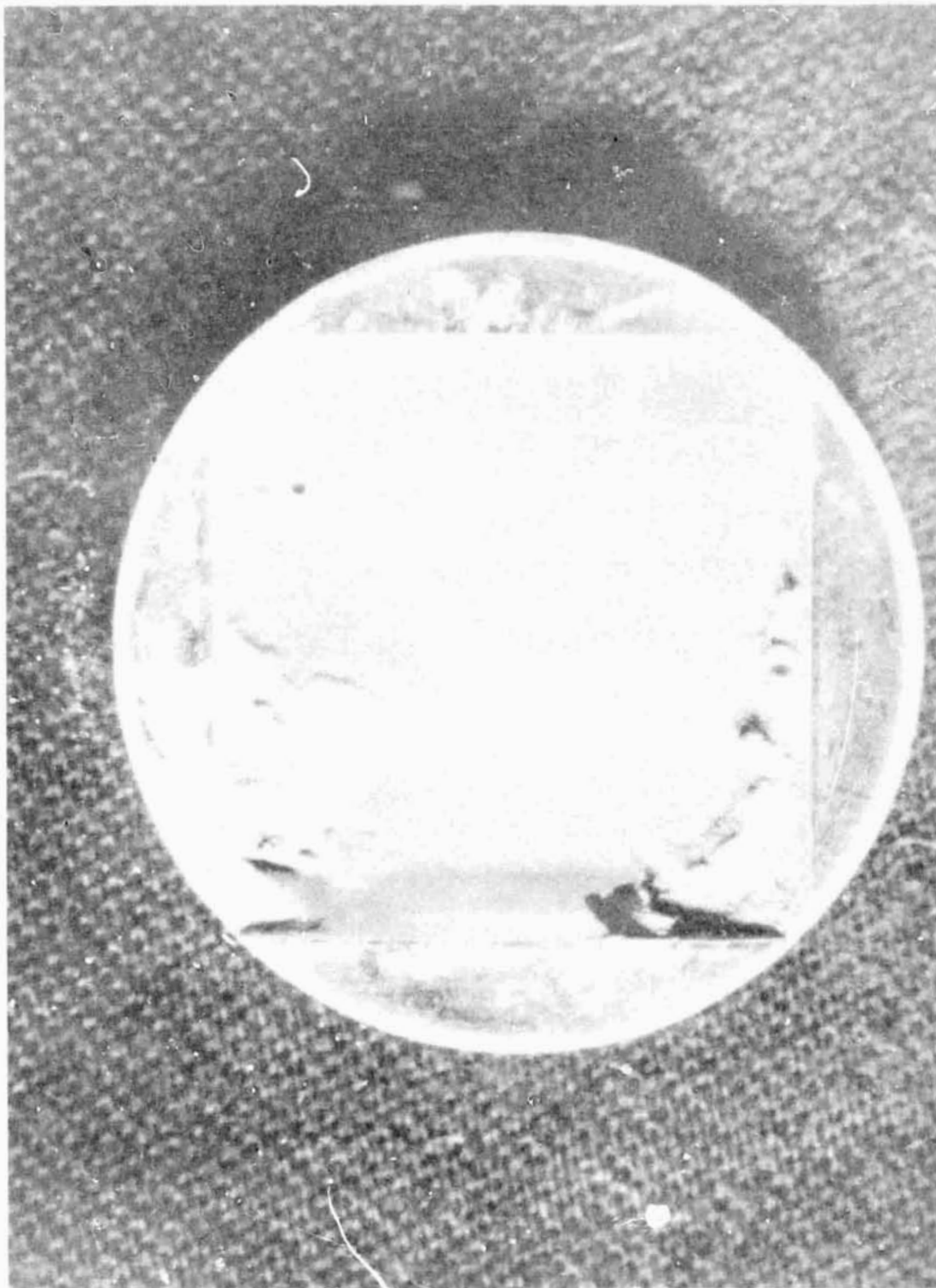


Figure I-9. Bracket 13, vertical height, 6.1 m (20 ft); radial distance, 165.1 cm (65 in.).

Each test flat and the interior of its container, which contained material collected in the recesses of the disk, were then rinsed with ethyl alcohol and the liquid with suspended particles was drained off and stored in a separate closed bottle supplied for each sample. The liquid was shaken to obtain a homogeneous mix; then, assuming one drop of liquid would be the same as any other drop in relation to distribution of particle size, a couple of drops of the liquid were placed on a glass flat for analyzing under a microscope in the OMNICON system.

The automated transmissive light microscope scanned an area of approximately 5000 by 5000 μm at a total magnification of 400X. The software in the processing unit prevented overlapping of fields in the counting procedure. The processor counted the number of features present in the field of view having a maximum horizontal chord greater than a preset value specified by the operator. The feature counts were made using consecutively higher preset values for the horizontal chord from 2 to 100 μm : in steps of 0.5 μm from 2 μm to 10 μm ; a step of 40 μm from 10 μm to 50 μm ; and a step of 50 μm from 50 μm to 100 μm . The processor then calculated the differences in number of features from one size setting to the next to determine the total number of features with horizontal chords in that size range. Since the maximum horizontal chord measurement is dependent on orientation of the features in the field of view and since the measuring disk was placed randomly on the microscope stage, measurements were made three separate times on each slide and the resulting counts were averaged. With this procedure we hoped to minimize the orientation factor. Histogram plots of the averages for each sample are given in Figures I-10 through I-22.

Using the average distributions, the percentages of particles detected in the indicated size ranges for the two firings in which we participated were calculated. These results are given in Table I-2 and Table I-3.

Next, samples of the suspension from bracket 8 and bracket 15 were placed on platforms and scanned under a Scanning Electron Microscope to determine if features counted were actually discrete particles or flocculates/agglomerates. The photographs are shown in Figures I-23 through I-30. The numbers beneath selected features signify the measurement of their horizontal chord in microns (μm). The indentions observed in the background are milling imperfections on the surface of the platform.

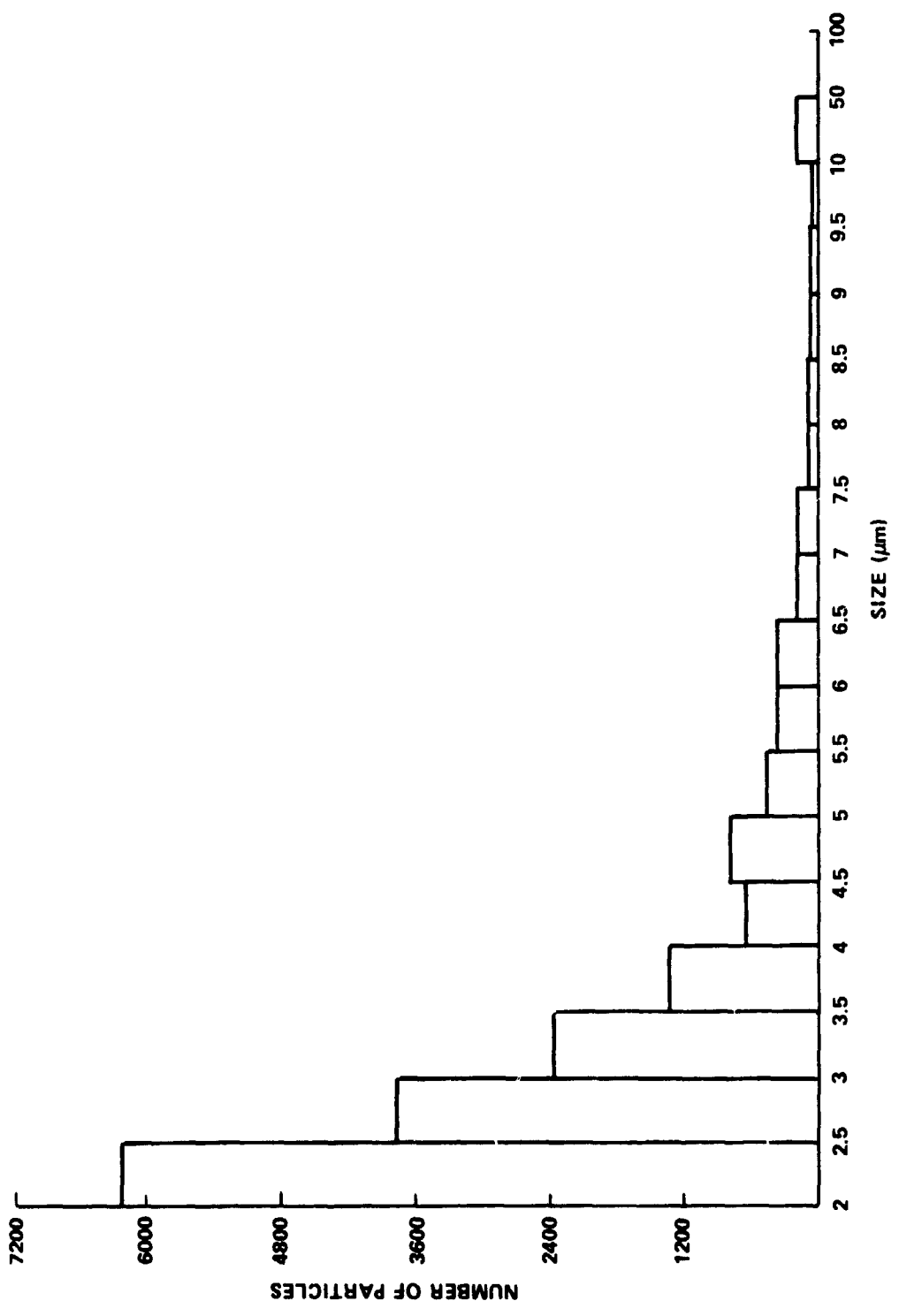


Figure I-10. Particle size distribution, bracket 2, firing 1.

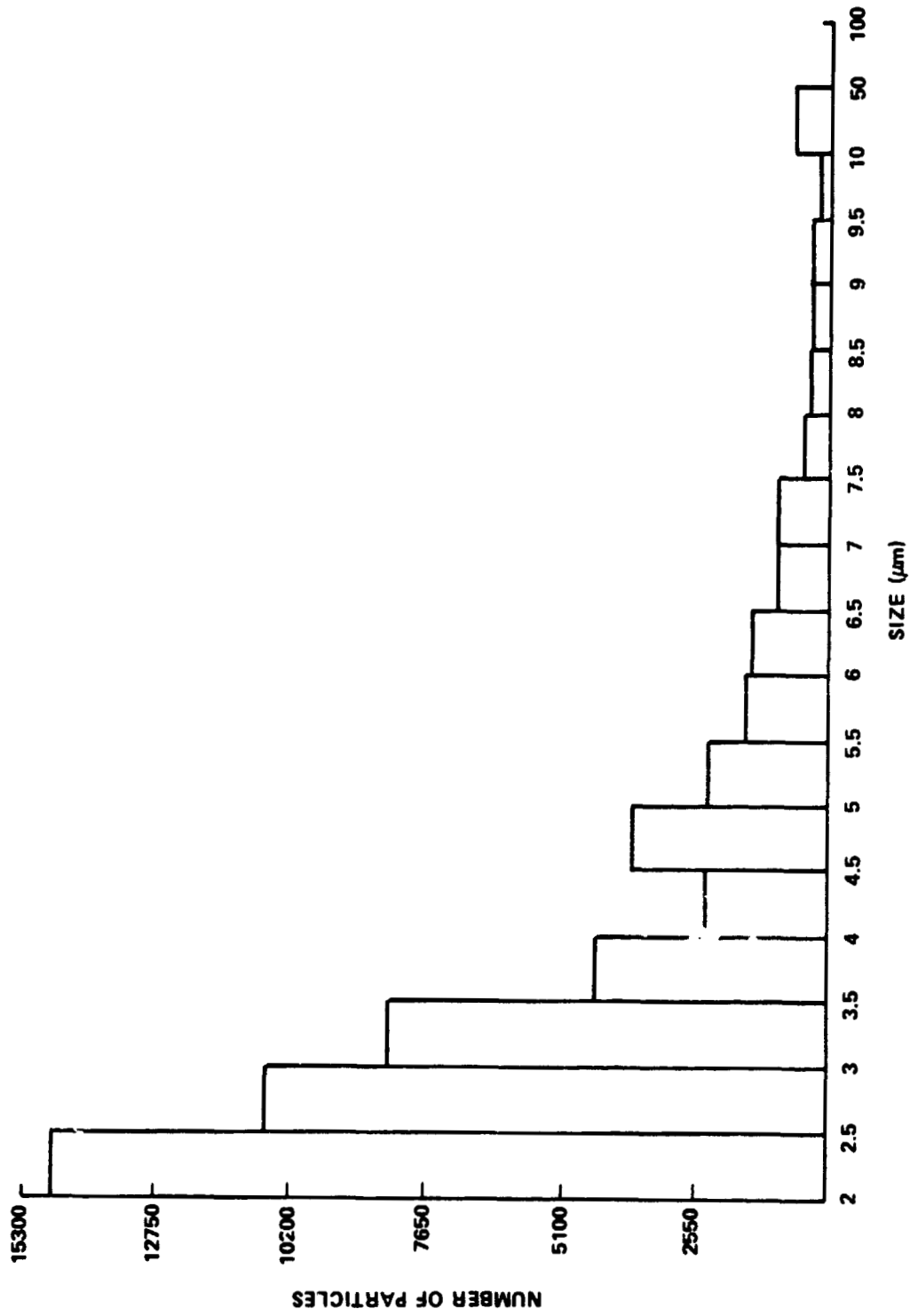


Figure I-11. Particle size distribution, bracket 3, firing 1.

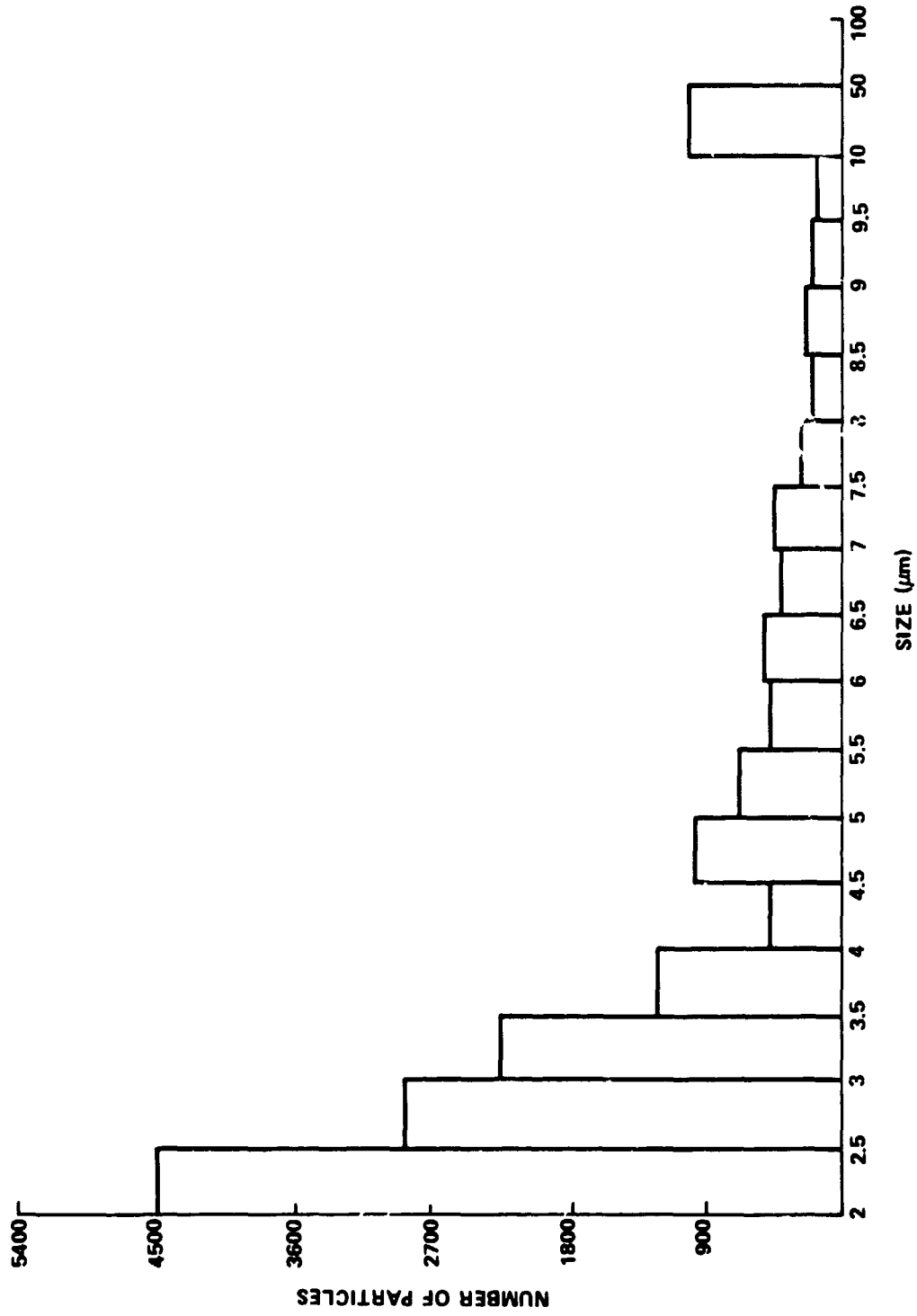


Figure I-12. Particle size distribution, bracket 4, firing 1.

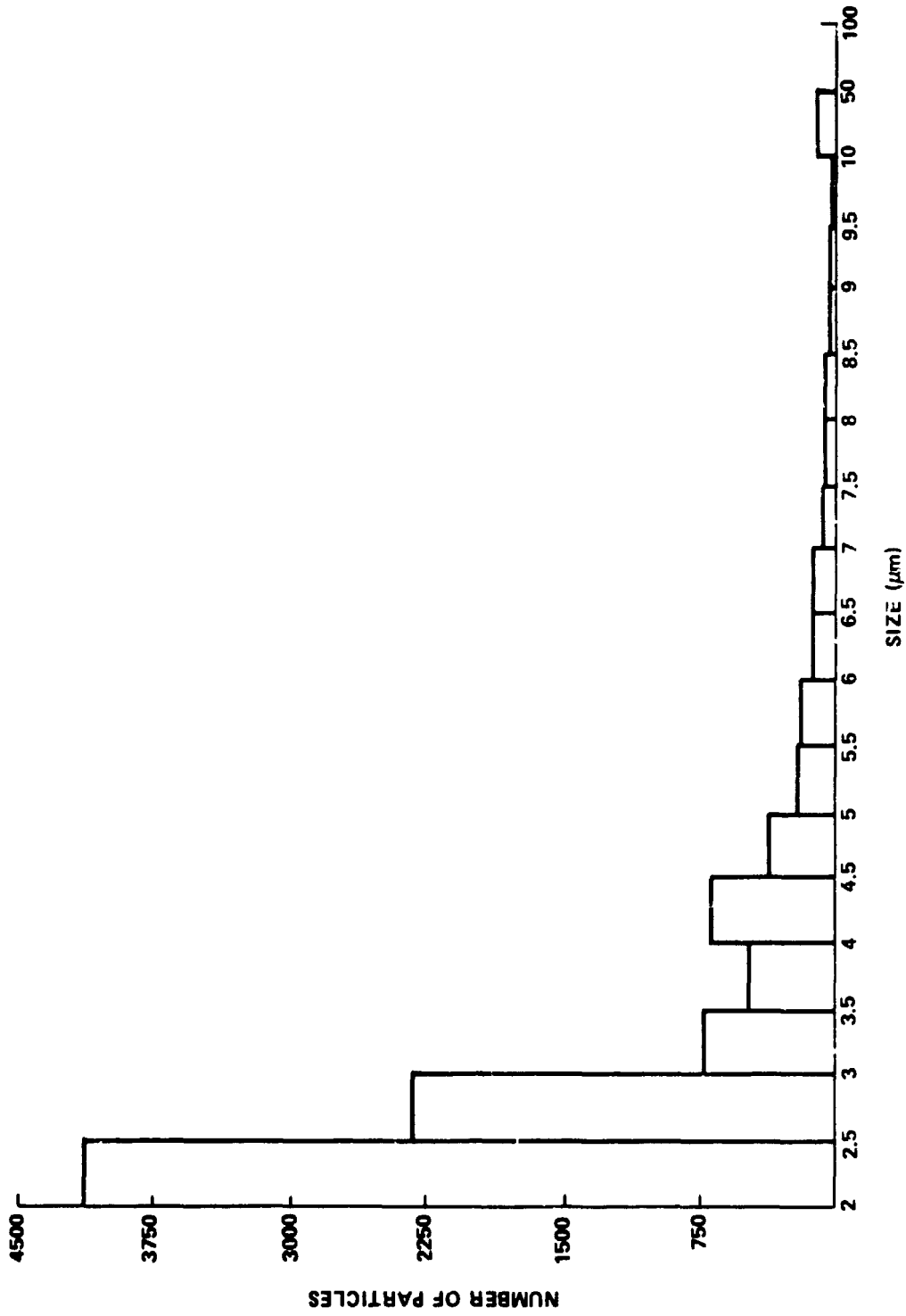


Figure I-13. Particle size distribution, bracket 5, firing 1.

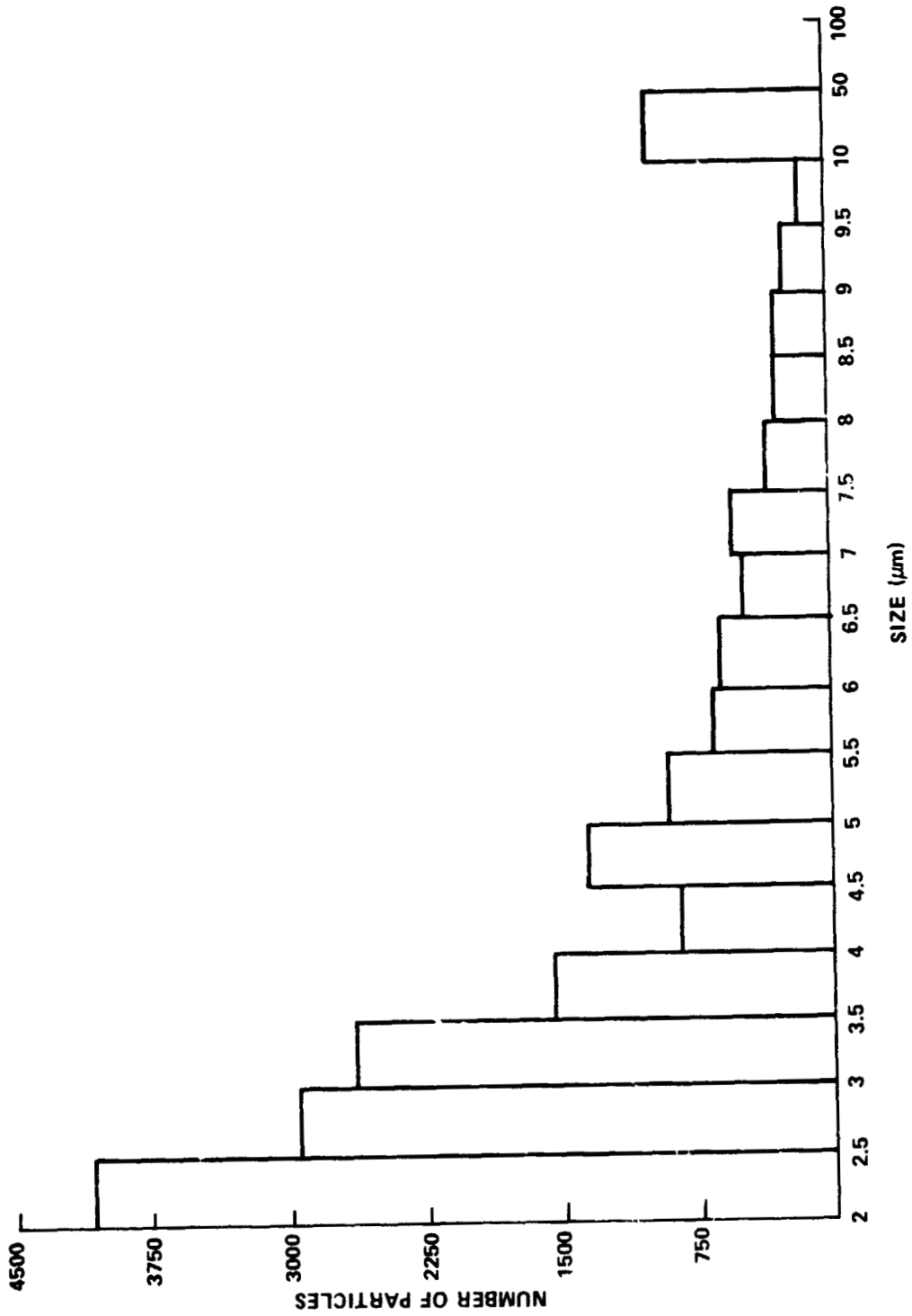


Figure I-14. Particle size distribution, bracket 6, firing 2.

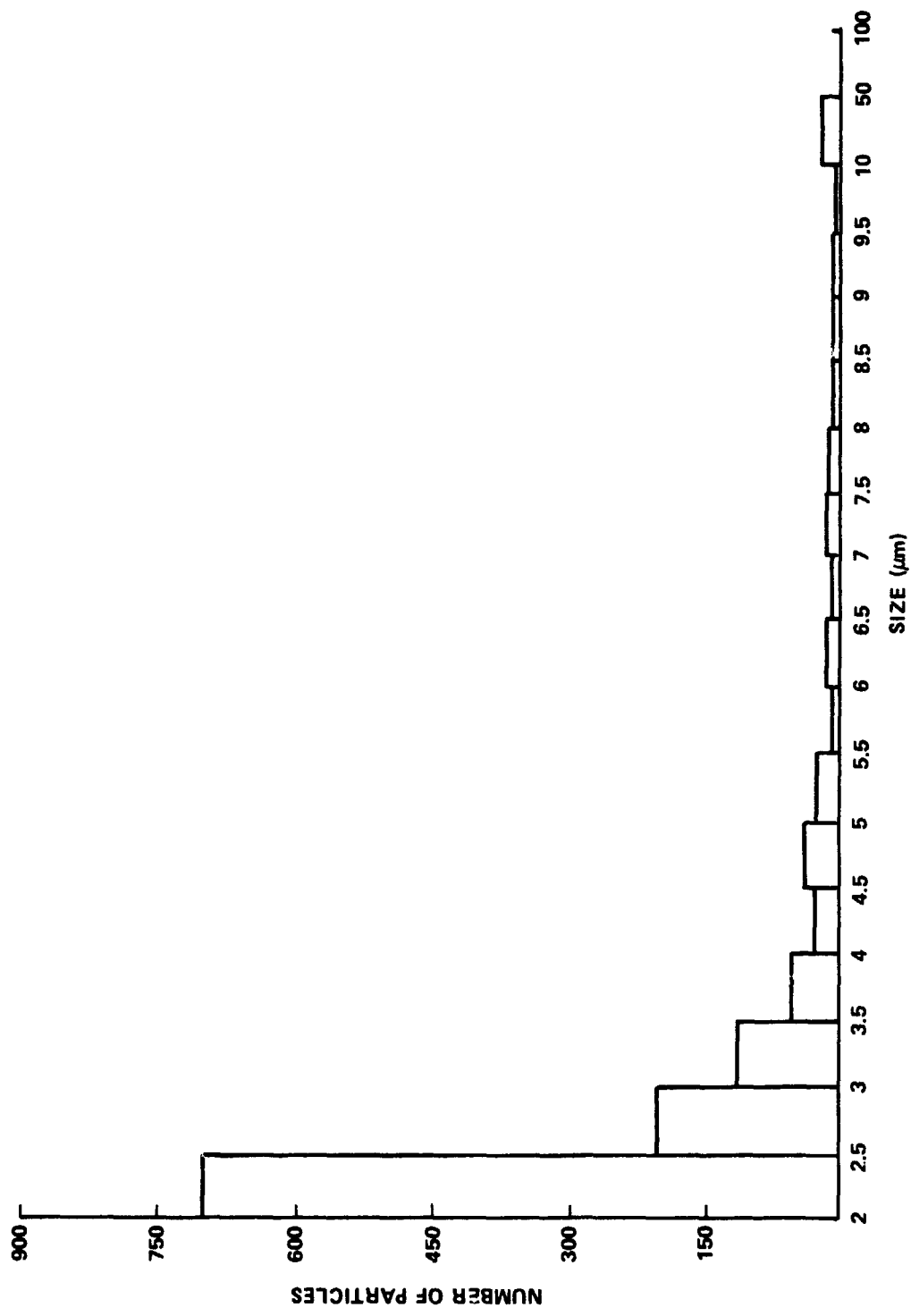


Figure I-15. Particle size distribution, bracket 7, firing 1.

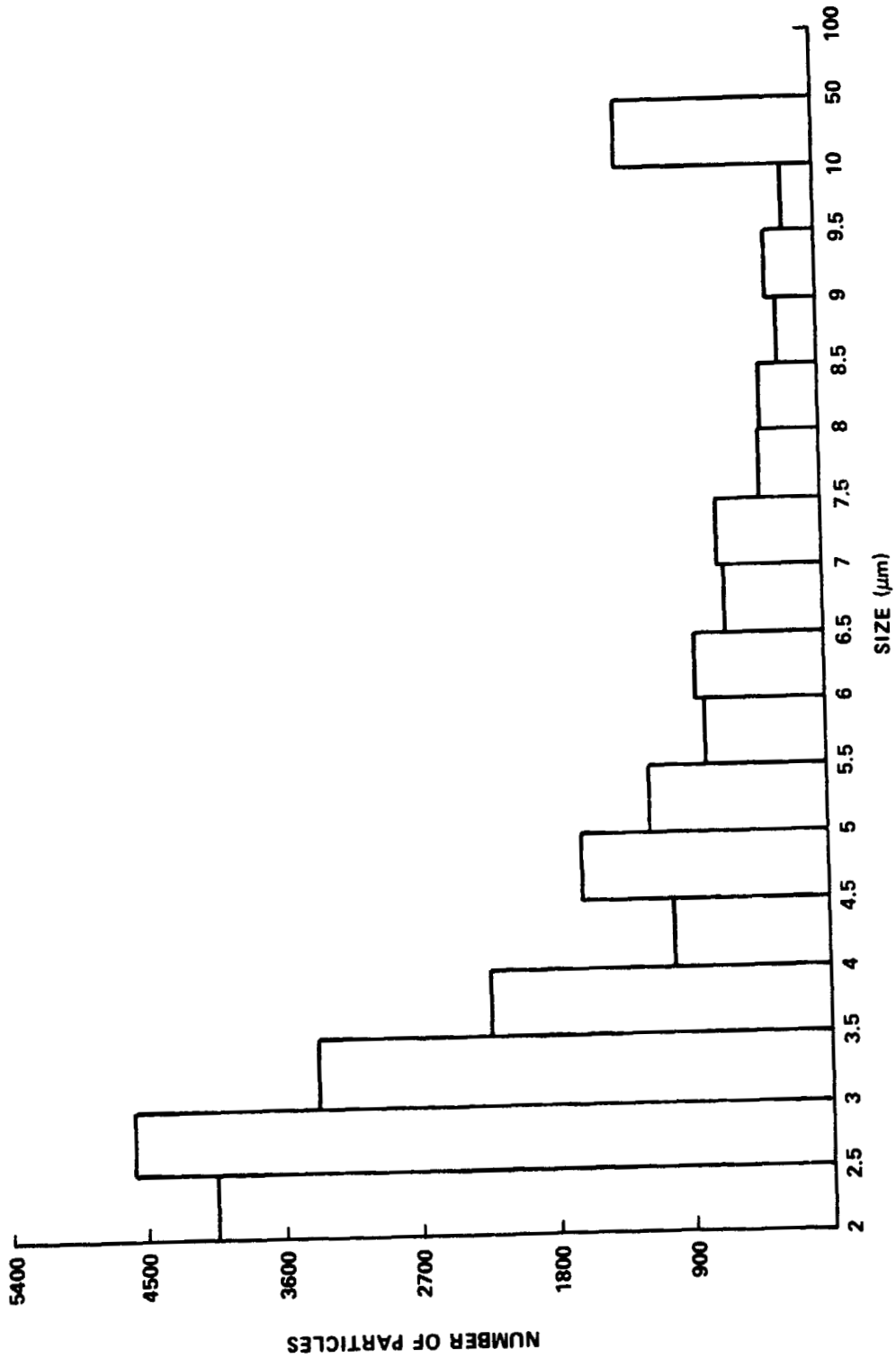


Figure 1-16. Particle size distribution, bracket 8, firing 2.

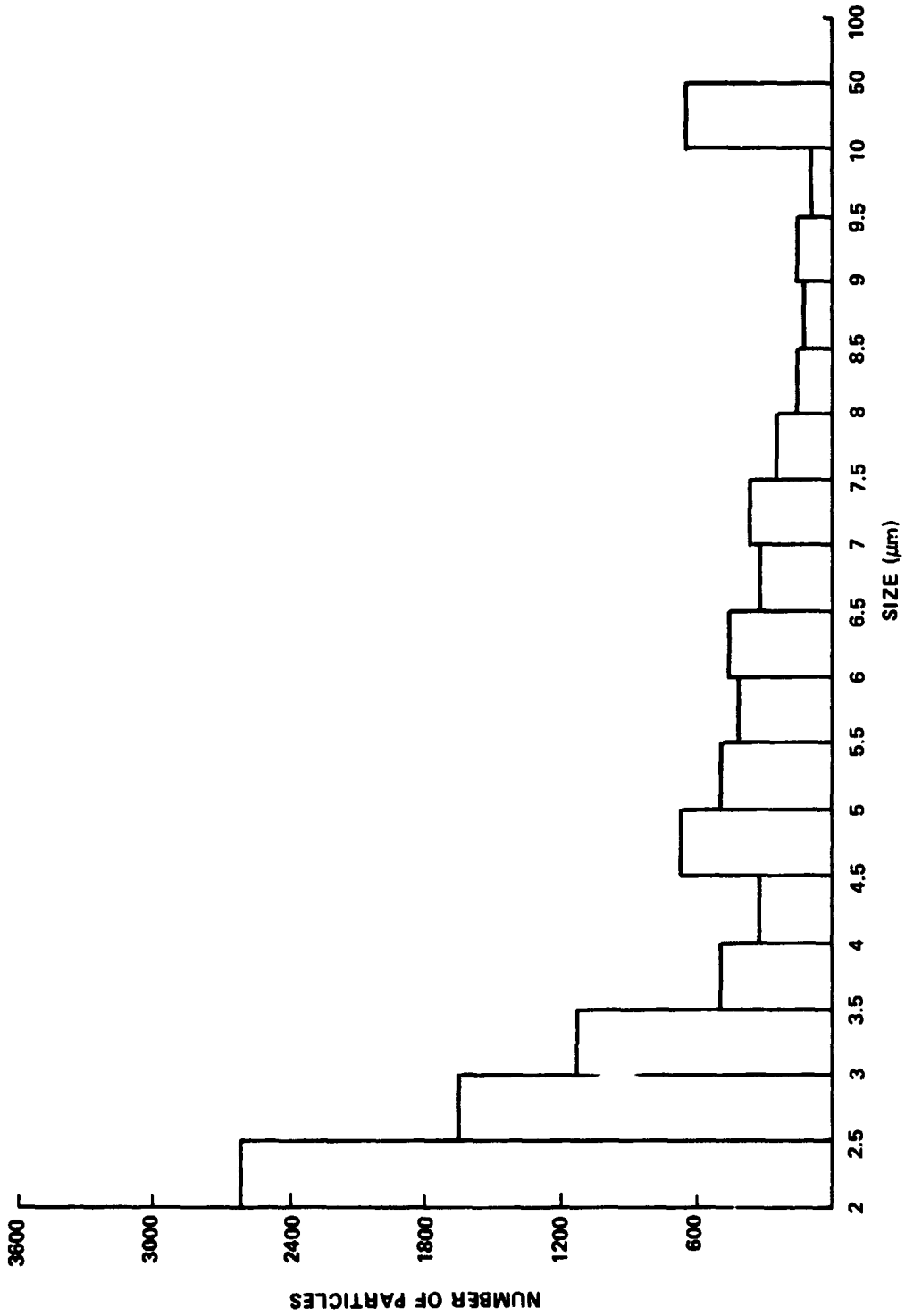


Figure I-17. Particle size distribution, bracket 9, firing 2.

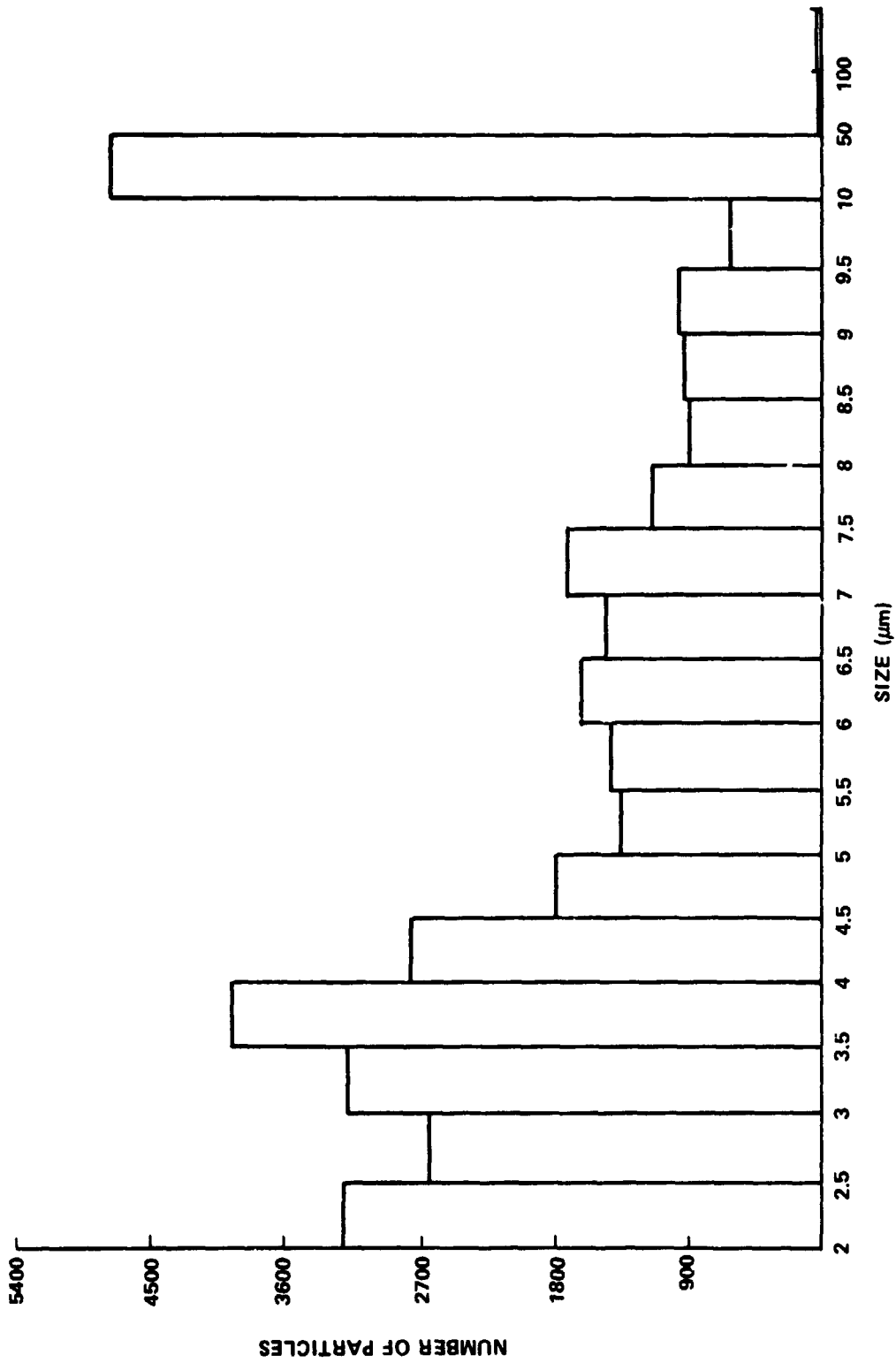


Figure I-18. Particle size distribution, bracket 11, firing 1.

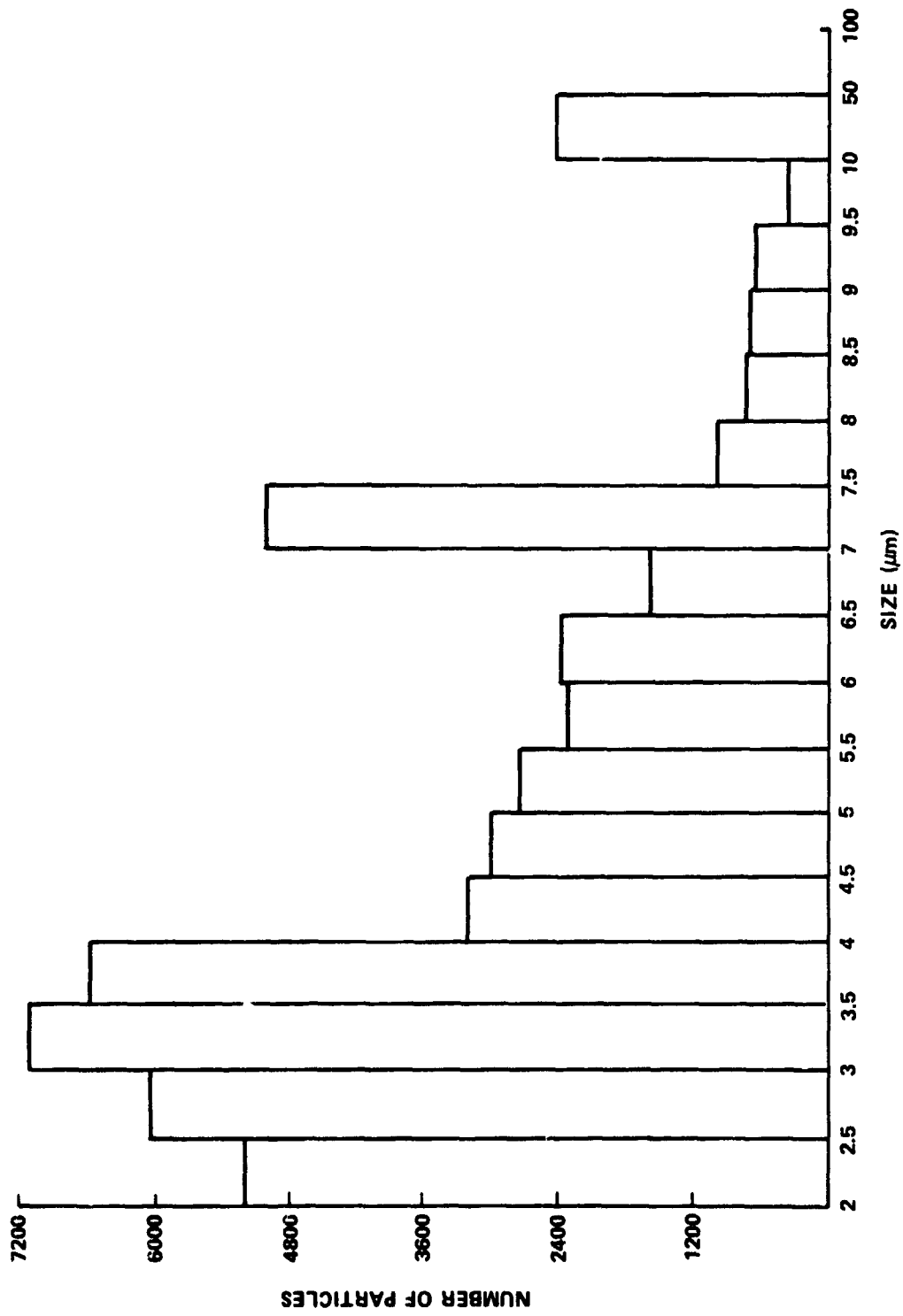


Figure I-19. Particle size distribution, bracket 12, firing 1.

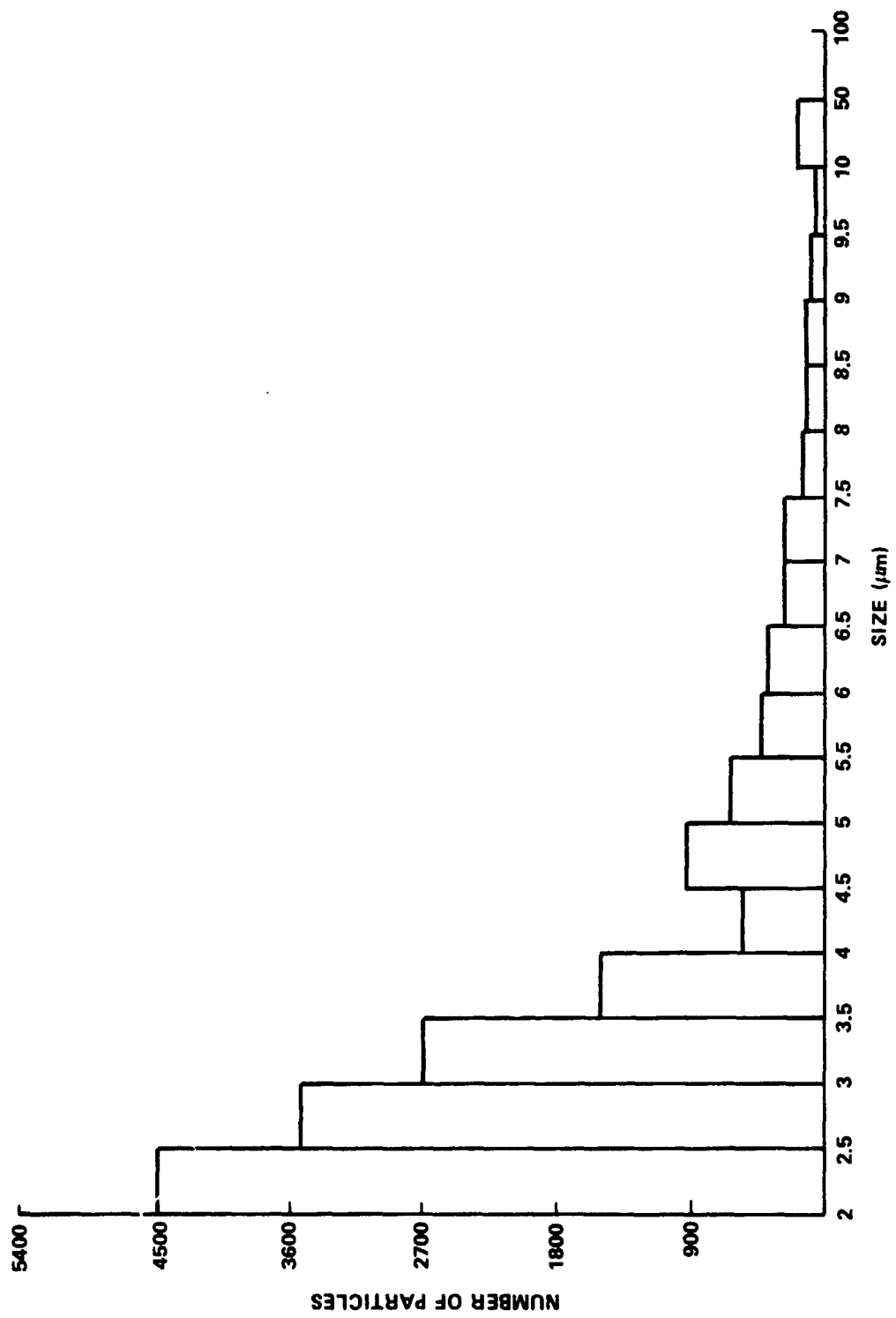


Figure I-20. Particle size distribution, bracket 13, firing 1.

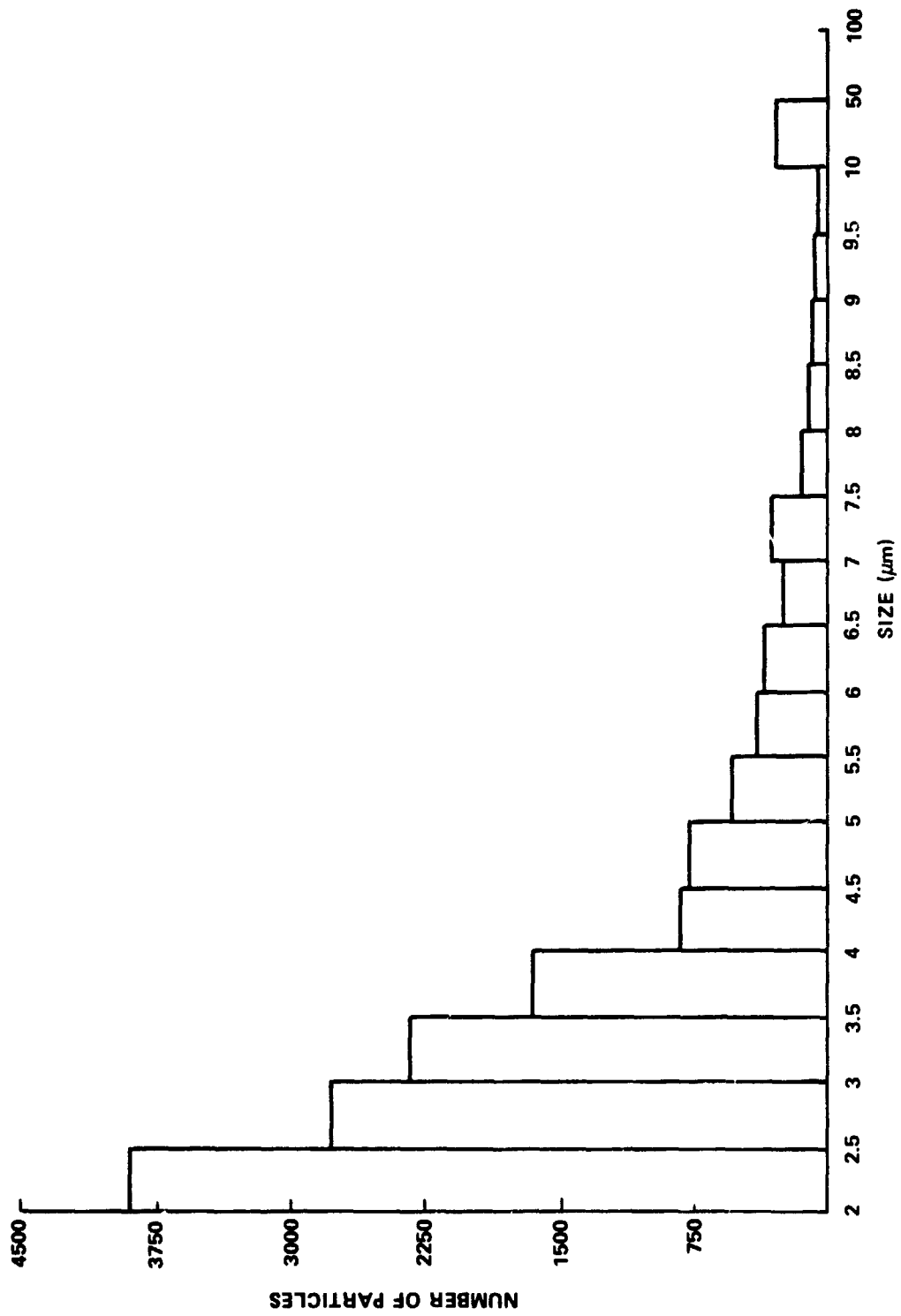


Figure I-21. Particle size distribution, bracket 14, firing 1.

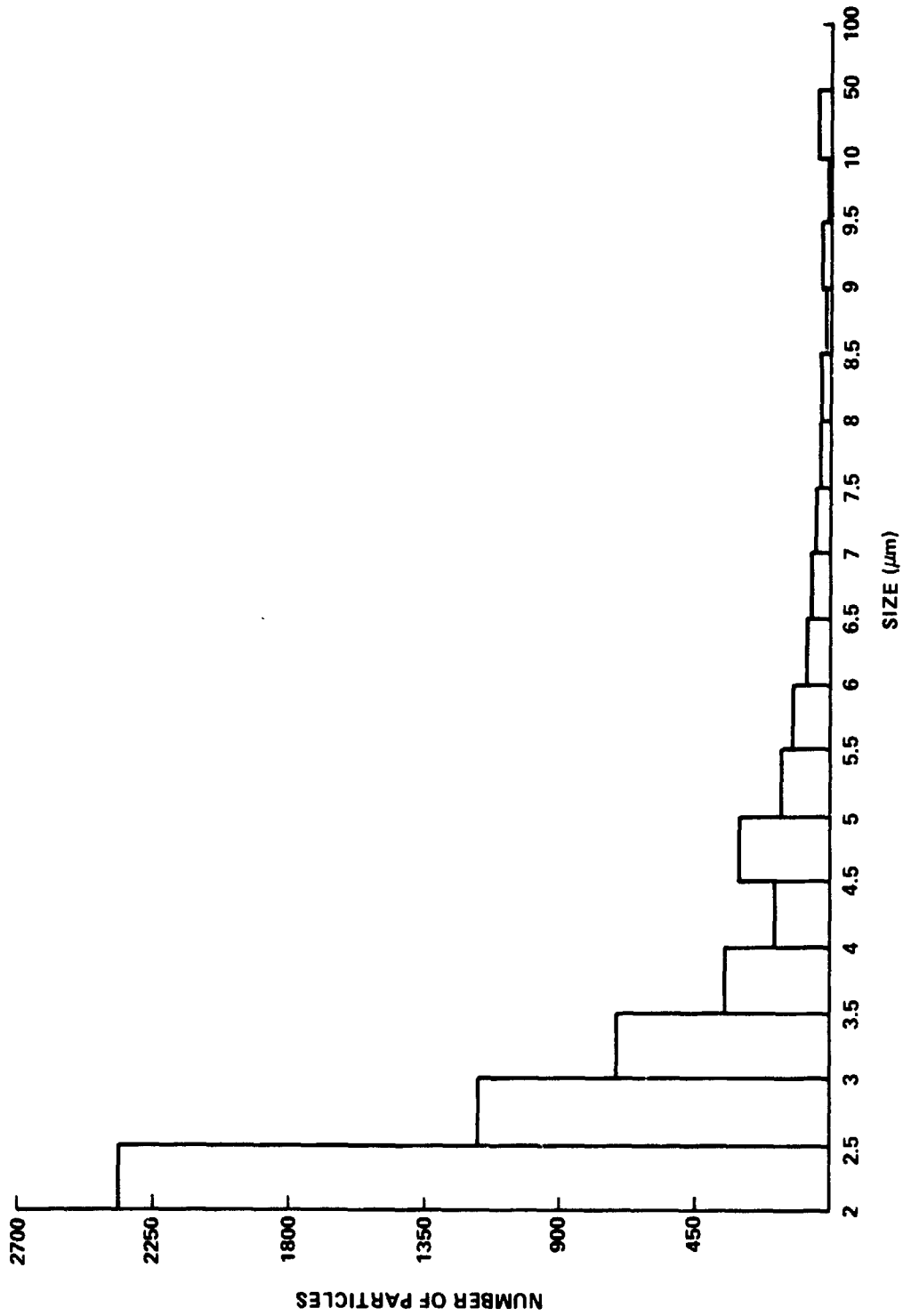


Figure I-22. Particle size distribution, bracket 15, firing 1.

TABLE I-2. THE PERCENTAGE OF PARTICLES BETWEEN SELECTED SIZE RANGES OF FIRING 1

Particles Size Range (μm)	Percentage of Total Particles Counted for Each Bracket ^a														
	2	3	4	5	7	11	12	13	14	15					
2.1 to 2.5	36	27	27	38	56	9	11	28	26	43					
2.6 to 3.0	22	20	17	21	16	8	13	22	18	21					
3.1 to 3.5	14	15	13	12	9	9	15	17	16	13					
3.6 to 4.0	8	8	7	7	4	11	14	9	11	6					
4.1 to 4.5	4	4	3	4	2	8	7	3	5	3					
4.6 to 5.0	5	7	6	6	3	5	6	6	5	5					
5.1 to 5.5	3	4	4	3	2	4	6	4	4	3					
5.6 to 6.0	2	3	3	2	0.6	4	5	3	3	2					
6.1 to 6.5	2	3	3	1	1	5	5	2	2	1					
6.6 to 7.0	1	2	2	1	0.8	4	3	2	2	1					
7.1 to 7.5	1	2	2	1	1	5	10	2	2	0.7					
7.6 to 8.0	0.5	0.9	2	0.5	0.5	3	2	0.8	1	0.3					
8.1 to 8.5	0.5	0.7	1	0.4	0.4	2	2	0.6	0.7	0.3					
8.6 to 9.0	0.3	0.6	1	0.4	0.4	2	2	0.6	0.7	0.2					
9.1 to 9.5	0.3	0.6	1	0.3	0.4	2	1	0.5	0.6	0.3					
9.6 to 10.0	0.1	0.3	0.8	0.2	0.3	2	0.8	0.3	0.4	0.1					
10.1 to 50	0.8	1	6	0.8	2	1	5	1	2	0.6					
50.1 to 100	0	0	0	0	0	0	0	0	0	0					
Over 100	0	0	0	0	0	0	0	0	0	0					

a. Total percentage for individual brackets may equal more than 100 because of roundoff error.

TABLE I-3. THE PERCENTAGE OF PARTICLES BETWEEN
SELECTED SIZE RANGES OF FIRING 2

Particles Size Ranges (μm)	Percentage of Total Particles Counted for Each Bracket ^a		
	6	8	9
2.1 to 2.5	22	21	25
2.6 to 3.0	16	23	16
3.1 to 3.5	14	17	11
3.6 to 4.0	8	11	5
4.1 to 4.5	4	5	3
4.6 to 5.0	7	8	6
5.1 to 5.5	5	6	5
5.6 to 6.0	3	4	4
6.1 to 6.5	3	4	4
6.6 to 7.0	2	3	3
7.1 to 7.5	3	3	3
7.6 to 8.0	2	2	2
8.1 to 8.5	1	2	2
8.6 to 9.0	1	1	1
9.1 to 9.5	1	2	2
9.6 to 10	0.7	1	0.8
10.1 to 50	5	6	6
50.1 to 100	0	0	0
Over 100	0	0	0

a. Total percentage for individual brackets may equal more than 100 because of roundoff error.



**ORIGINAL PAGE IS
OF POOR QUALITY**

Figure I-23. Bracket 8, 1000X magnification.

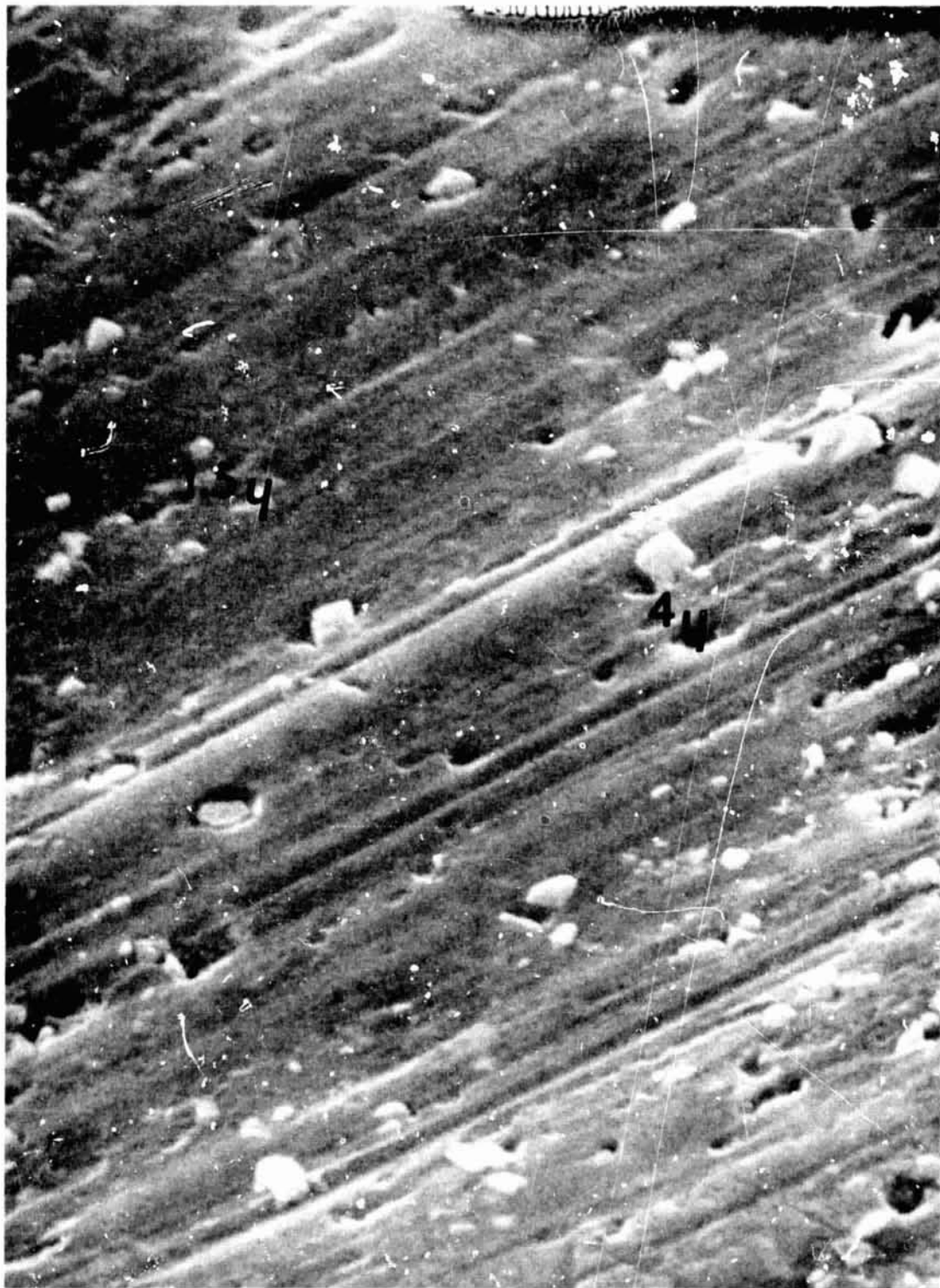
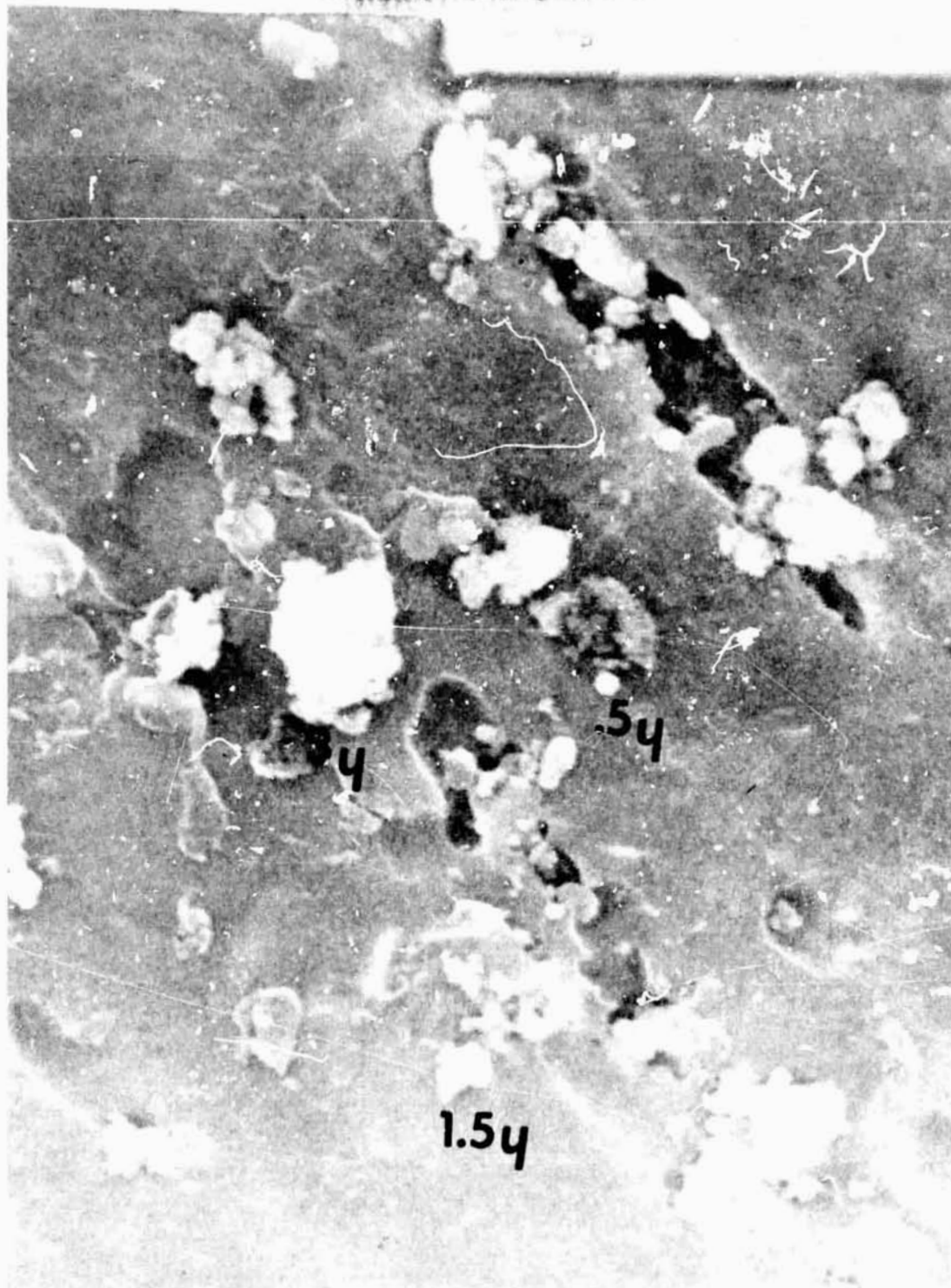


Figure I-24. Bracket 15, 1000X magnification.



**ORIGINAL PAGE IS
OF POOR QUALITY**

Figure I-25. Bracket 8, 3000X magnification.

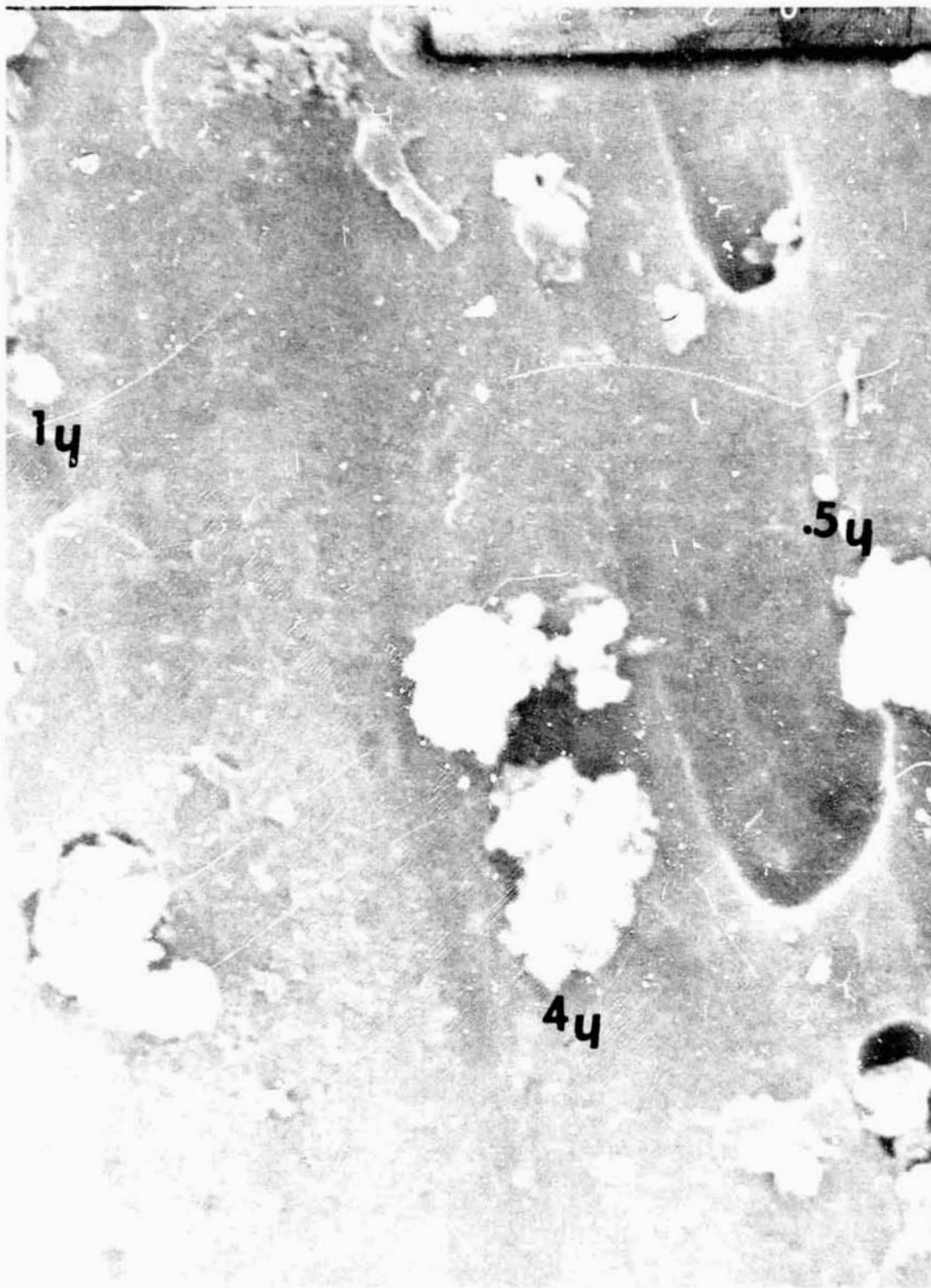


Figure I-26. Bracket 8, 3000X magnification.



ORIGINAL PAGE IS
OF POOR QUALITY

Figure I-27. Bracket 8, 3000X magnification.

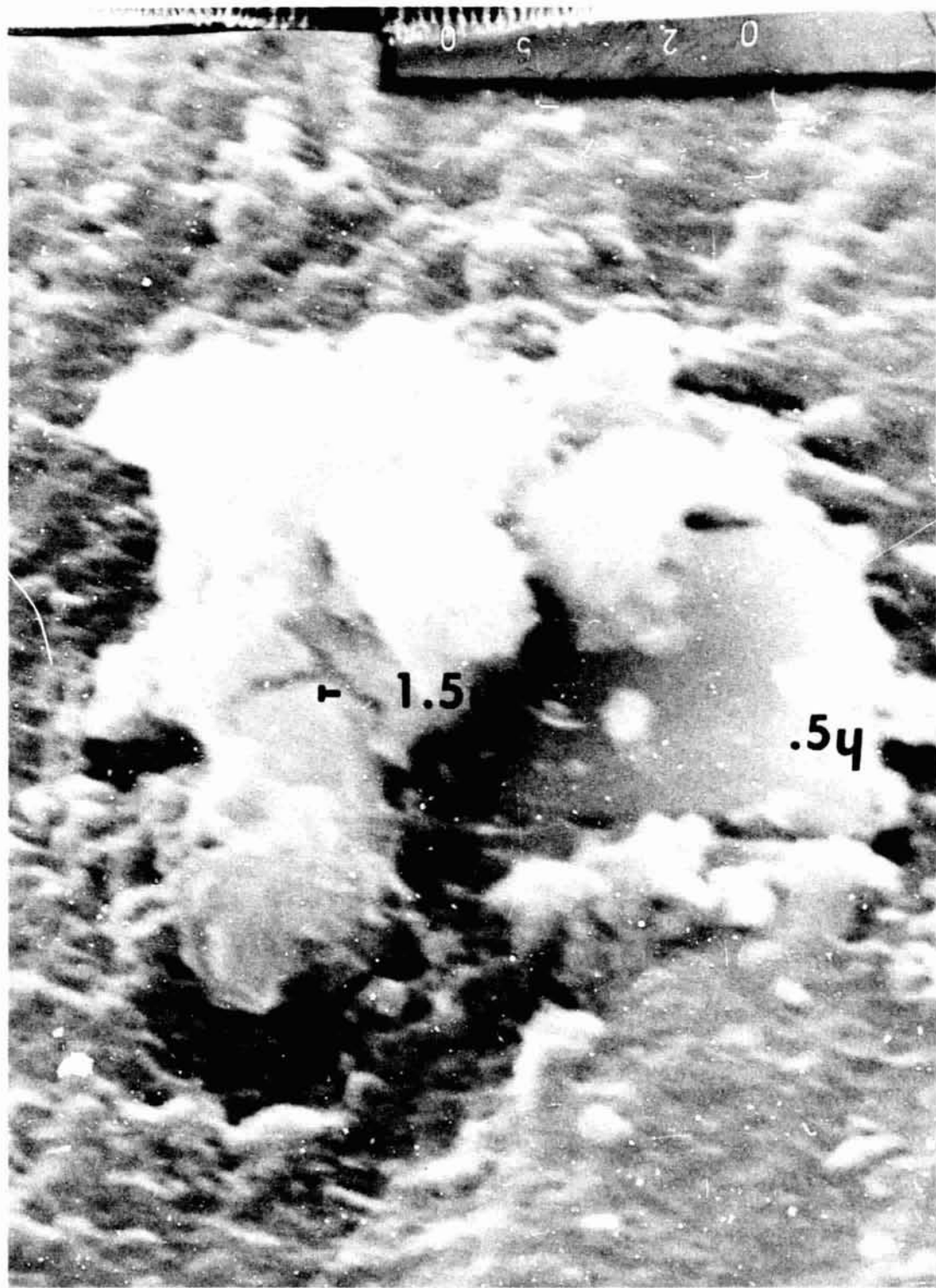
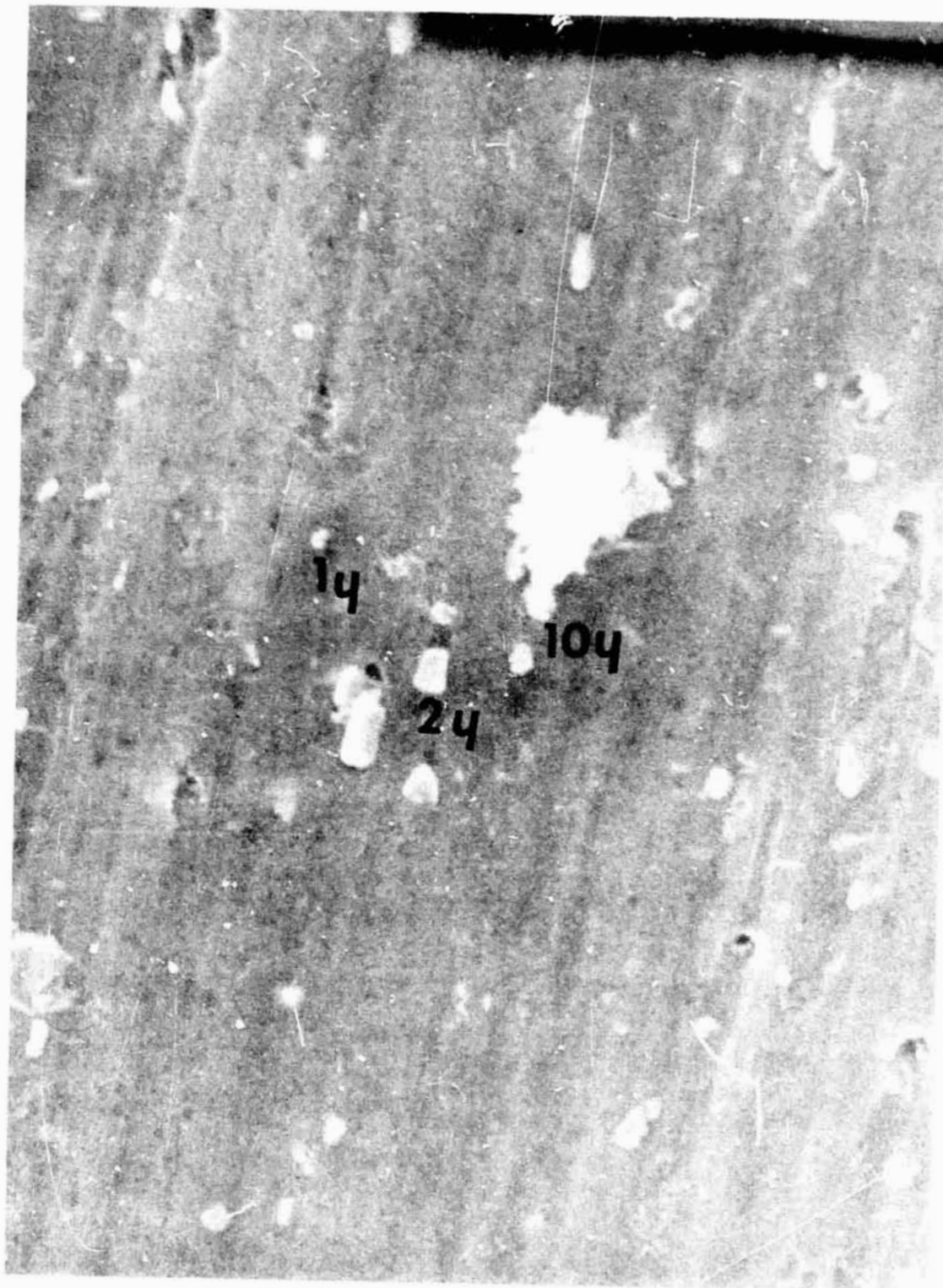


Figure I-28. Bracket 8, 10 000X magnification.



**ORIGINAL PAGE IS
OF POOR QUALITY**

Figure I-29. Bracket 15, 1000X magnification.

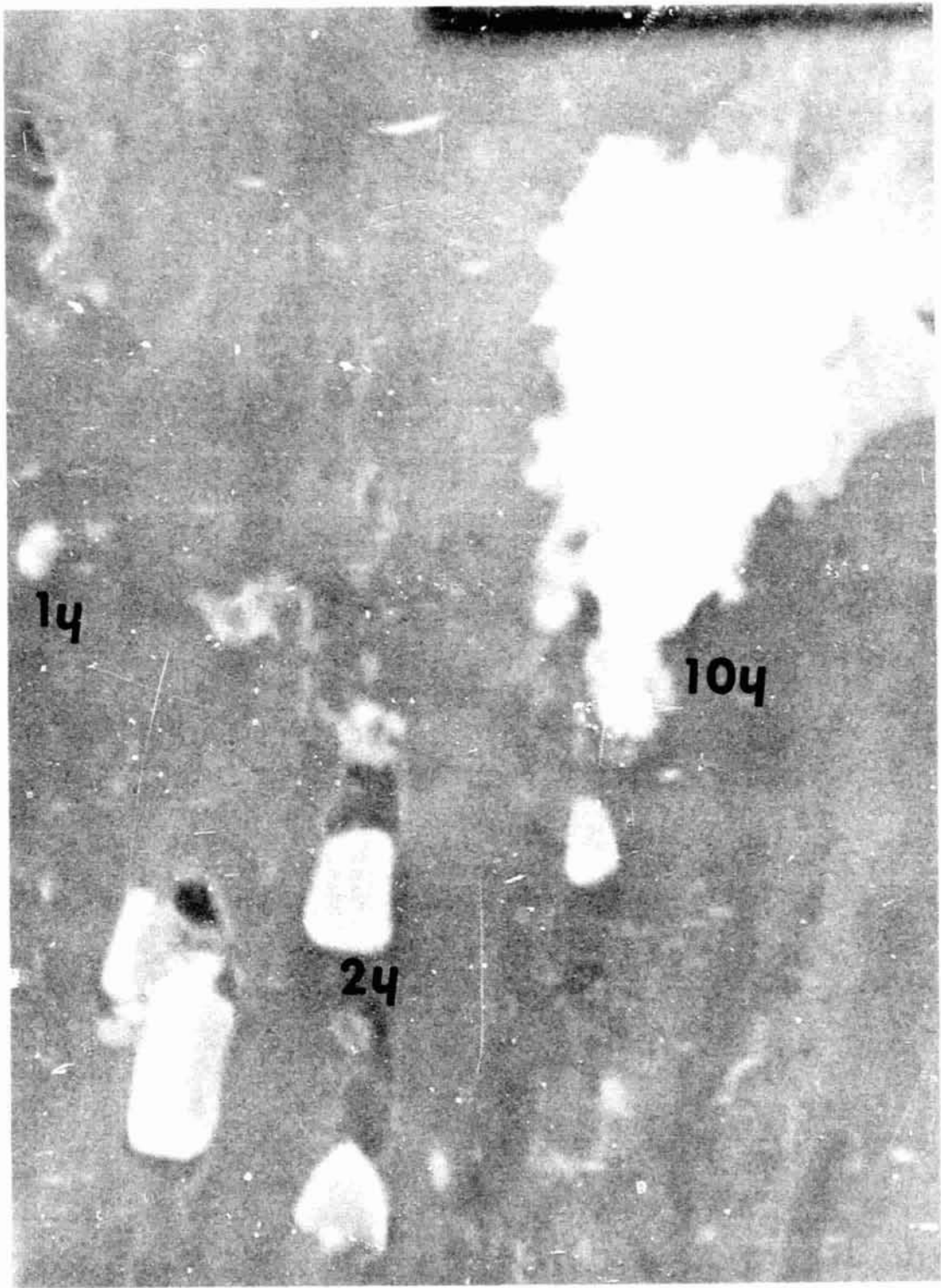


Figure I-30. Bracket 15, 3000X magnification.

C. Chemical Analysis of Solid Rocket Effluents

Ronald C. McNutt
Athens College
Athens, Alabama

Twenty-three samples of rocket effluents were obtained from Willa Russell of Space Sciences Laboratory to be analyzed for iron, aluminum, and organic material. The samples had been deposited onto small pieces of circular quartz by rocket exhausts.

The samples listed in Table I-4 were obtained as alcohol slurries. The samples listed in Table I-5 were received as deposits on quartz and were subsequently washed off the quartz surface to form a slurry in alcohol similar to the Table I-4 samples.

The alcohol slurries were evaporated to dryness, leaving the original sample free of alcohol. These dry samples were then weighed. This weight was the basis for all percentage calculations. The dry samples in crucibles were placed in a muffle furnace for about 1.5 hours at 800° C. This served to ignite and remove the organic material. The samples were then reweighed, and the weight loss was determined. This weight loss is, of course, indicative of the amount of carbonaceous material (hydrocarbons, etc.) present. The residue from ignition containing inorganic materials was then processed for the determination of iron and aluminum content.

The analyses were performed using standard colorimetric techniques, with a Delta Scientific Model 260 colorimeter (Table I-6). The results are summarized in Tables I-4 and I-5.

Two samples not subjected to ignition experimentation were selected in an attempt to obtain some information on organic materials present. Ten milliliters of this material were injected into a gas chromatograph. Figure I-31 shows that at least five different components other than benzene were present in the sample. Sample No. 9 was extracted with cyclohexane. The extract was examined for ultraviolet absorption. Figure I-32 shows the observed ultraviolet spectra. The cyclohexane was then evaporated from the sample and the infrared spectra were obtained (Fig. I-33) on the residue. There appear to be only C-H vibrations and a definite indication of unsaturation. In summary, the ultraviolet absorption indicates that some of the unsaturated components may be carbonyl compounds. The bulk of the organic material is probably various hydrocarbons with some indication of the presence of unsaturation.

TABLE I-4. LIQUID SAMPLES^a

Bracket	Weight of Dried Sample (mg)	Weight of Ashed Sample (mg)	Ignition Weight Loss (mg)	Percent of Weight Loss	Amount of Iron (mg)	Percent of Iron	Amount of Aluminum	Percent of Aluminum
2	1.7	1.7	0.0	0	0.044	2.59	0.050	2.94
3	48.4	47.7	0.7	1.45	0.550	1.14	0.398	0.82
5	3.5	2.9	0.6	17.14	0.072	2.06	0.098	2.80
6	1.5	1.2	0.3	20.00	0.053	3.54	0.043	2.87
7	1.0	0.8	0.2	20.00	0.039	3.90	0.024	2.40
8	20.7	19.8	0.9	4.35	0.110	0.53	0.600	2.90
9	No Weights Were Taken				0.188		0.630	
11	6.1	4.2	1.9	31.15	0.107	1.75	0.164	2.70
12	26.7	26.2	0.5	1.87	0.351	1.32	0.885	3.32
13	94.1	80.8	13.3	14.13	1.045	1.11	1.692	1.80
14	3.7	2.9	0.8	21.62	0.053	1.43	0.087	2.35

a. In general, reliability of these results is accurate to two significant figures.

TABLE I-5. SOLID SAMPLES^a

Bracket	Weight of Dried Sample (mg)	Weight of Ashed Sample (mg)	Ignition Weight Loss (mg)	Percent Weight Loss	Amount of Iron (mg)	Percent of Iron	Amount of Aluminum (mg)	Percent of Aluminum
2	5.1	2.4	2.7	53.94	0.085	1.67	0.100	1.96
4	16.9	16.2	0.7	4.14	0.100	0.59	0.275	1.63
5	1.6	1.6	0	0	0.035	2.19	0.025	1.56
6	2.9	2.8	0.1	3.45	0.015	5.17	0.130	4.48
7	0.4	0.1	0.3	75.00	0.025	6.25	0.038	9.50
11	4.6	3.8	0.8	1.74	0.060	1.30	0.245	5.33
12	7.1	5.8	1.3	18.31	0.050	0.70	0.195	2.75
13	4.4	3.6	0.8	18.18	0.070	1.59	0.140	3.18
14	2.2	0.6	1.6	72.73	0.010	0.46	0.048	2.18
15	1.2	1.0	0.2	16.67	0.008	0.67	0.036	3.00

a. In general, reliability of these results is accurate to two significant figures.

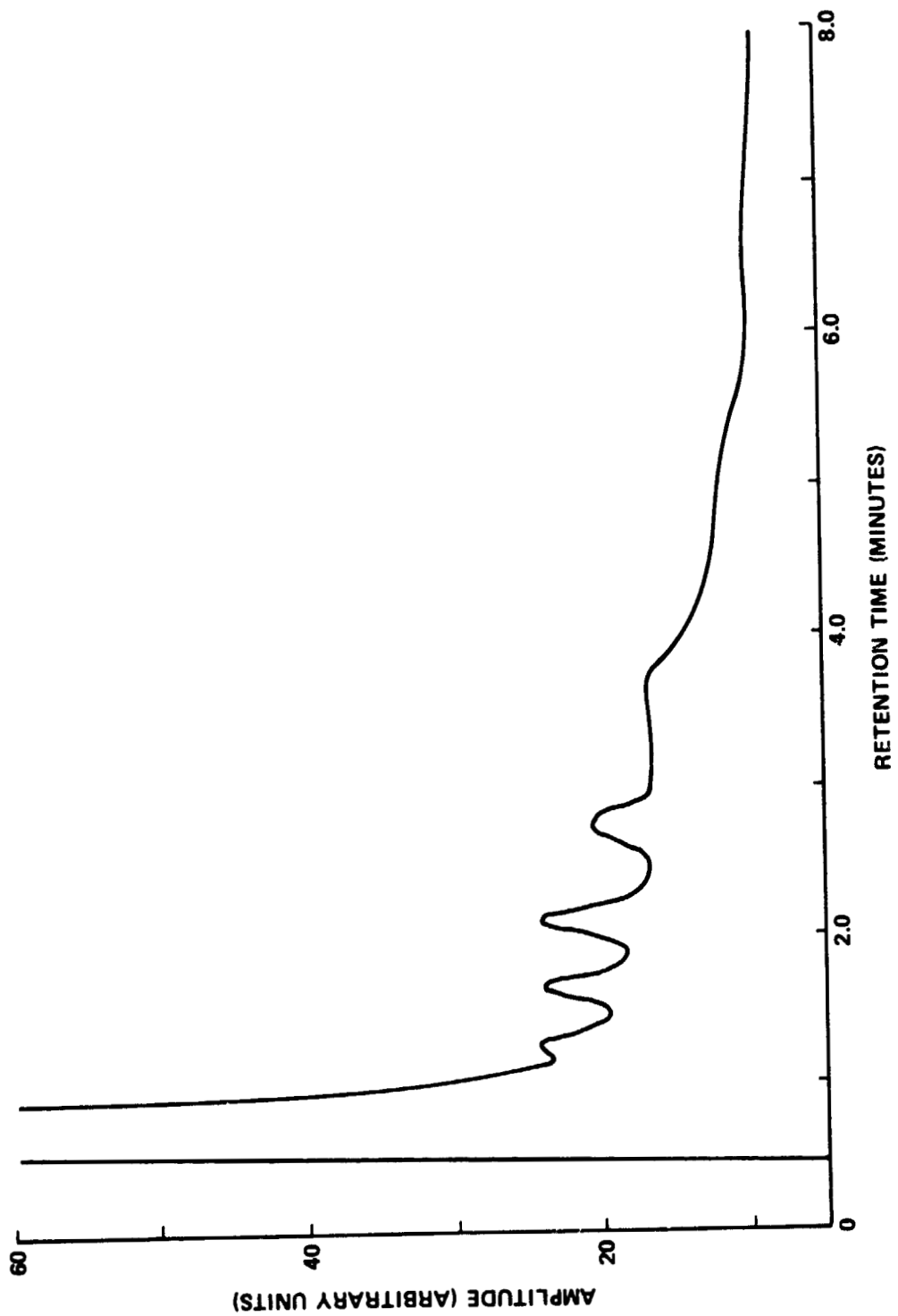


Figure I-31. G. L. C. scan of benzene extract.

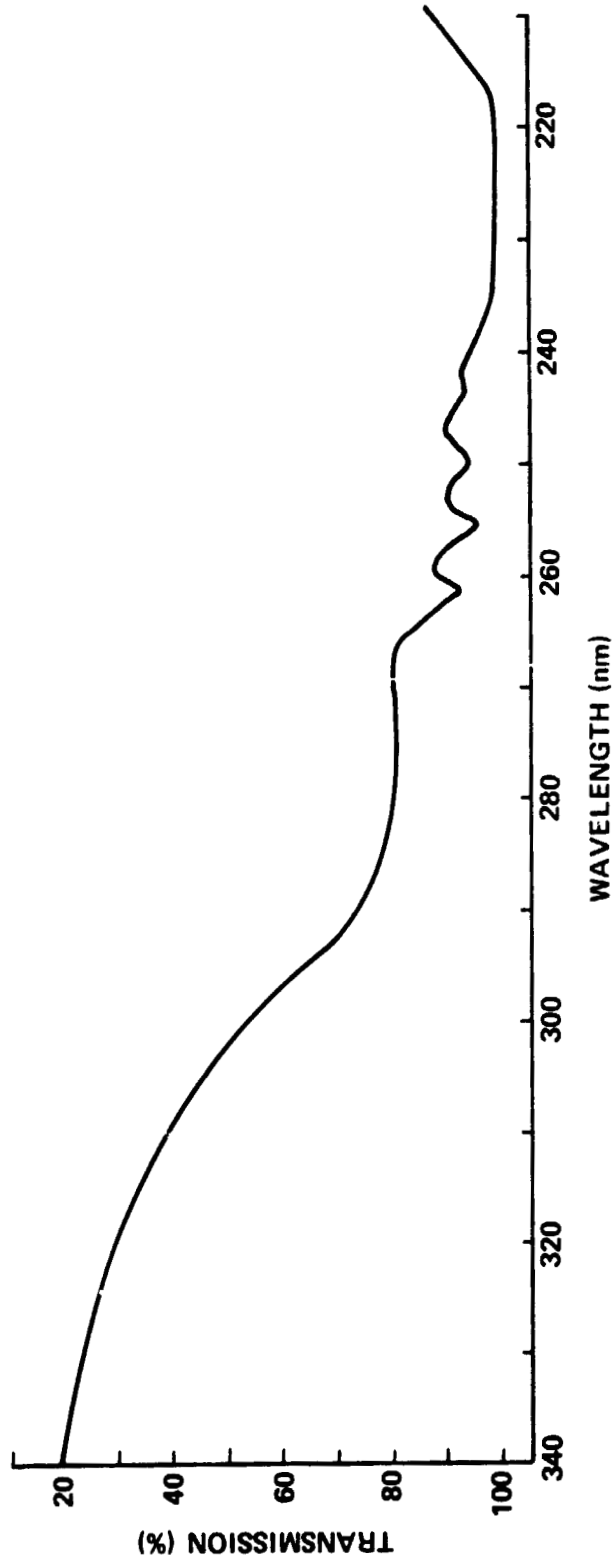


Figure I-32. Ultraviolet spectra of cyclohexane extract.

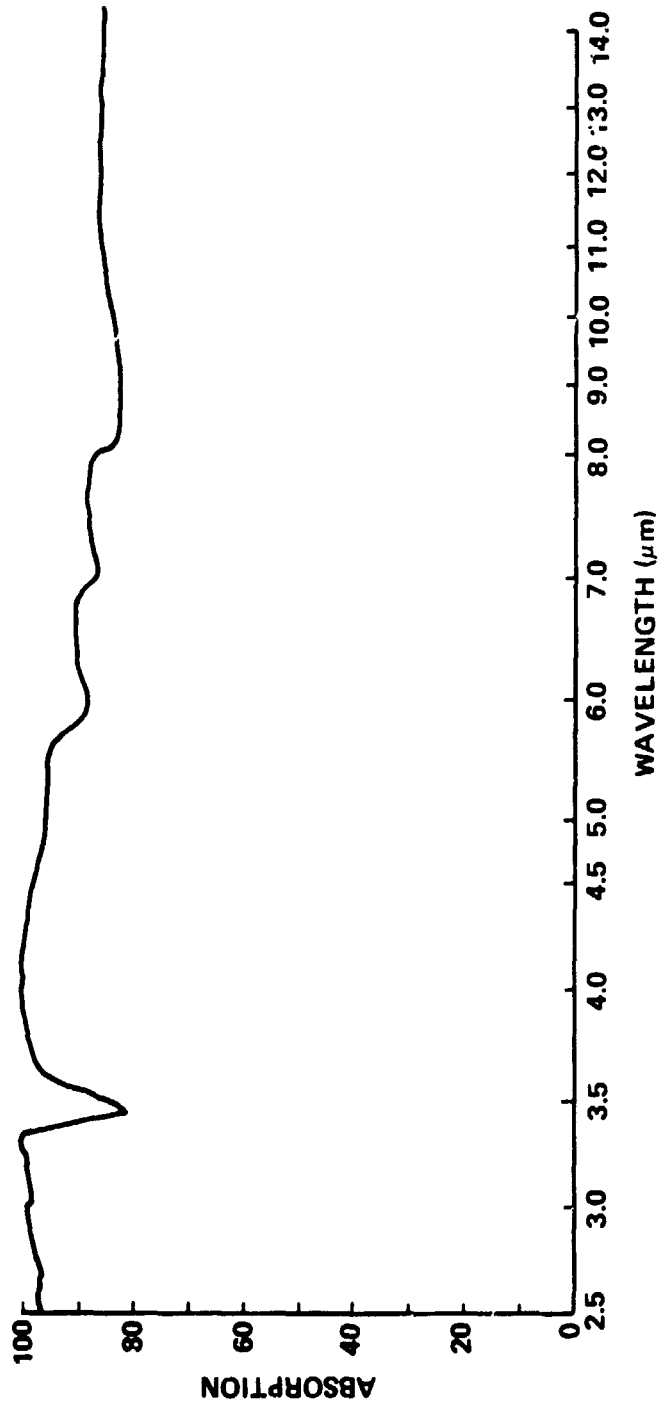


Figure I-33. Infrared spectra of benzene extract.

TABLE I-6. ALUMINUM AND IRON TESTING PROCEDURES

Test No. 260-31 — ALUMINUM

The reagents and accessories required are as follows:

R-183 Citric Acid Solution

R-144 Aluminon Buffer Solution

R-145 Potassium Cyanide, 1%. Stable Form

2 105-A Flasks, Erlenmeyer, 125 ml

1 103-A Cylinder, Graduated, 50 ml

2 126-A Pipettes, Mohr Measuring, 1 ml

1 109-A Pipette, Dropping, 1 ml

1. Using a No. 103-A 50 ml graduated cylinder, measure 50 ml of sample into a No. 105-A 125 ml Erlenmeyer flask.
2. Rinse the cylinder with aluminum-free distilled water, and prepare a reagent blank by measuring 50 ml of aluminum-free distilled water into a second 125 ml Erlenmeyer flask. (See Note B.)
3. Using the 1 ml dropping pipette, add to each flask 1 ml of freshly prepared No. R-145 potassium cyanide, 1%, and mix. Caution! POISON. (See Note A for preparation and stability of solution.)
4. Add to each flask 1 ml of No. R-144 aluminon buffer solution and mix. Note the time and let stand for exactly 30 minutes.
5. Turn on the instrument and rotate the filter selector to No. 520.
6. Fill one No. 260-T square 26 mm test cell with the reagent blank. Fill a second test cell with the treated sample.
7. Insert the test cell containing the blank into the analyzer, making certain that one of the frosted sides faces the front. Adjust the meter needle to a reading of 100.
8. Replace the blank with the test cell containing the treated sample and read the meter.
9. Refer to the graph for aluminum to convert the meter reading to parts per million aluminum. The Model 260 water analyzer is calibrated from 0 to 1.0 ppm aluminum. If necessary expand the range as described in the introduction.

Note A — To prepare potassium cyanide, 1%, add 100 ml of distilled water to the 4 oz bottle containing the 1 gm of potassium cyanide. Replace the cap and shake until dissolved. Record the date of preparation on the label and discard the unused portion after 2 weeks.

WARNING — This solution is poisonous, use the No. 109-A 1 ml dropping pipette for measuring.

TABLE I-6. (Continued)

Note B — If the sample is colored or turbid, prepare a blank by using 50 ml of the sample instead of distilled water in the procedure given above, except in step 3 omit the No. R-145 potassium cyanide, 1%, and substitute 1 ml of No. R-183 citric acid solution. Substitute this sample blank for the reagent blank in step 5. If the sample blank is so highly colored or turbid that the instrument cannot be set to 100, then use distilled water as a blank in step 7 and read both the sample blank and the unknown. Convert the meter readings to ppm and subtract the value (in ppm) of the sample blank from the value (in ppm) of the unknown. The difference is the true concentration of unknown in the sample.

Test No. 260-14 — IRON

The reagents and accessories required are as follows:

- R-101 Ammonium Acetate Buffer
- R-39 Hydrochloric Acid, Concentrated
- R-100 Hydroxylamine Reagent
- R-63 Iron Reagent Powder
- R-102 Phenanthroline, 0.1%
- 2 103-A Cylinder, Graduated, 50 ml
- 2 105-A Flask, Erlenmeyer, 125 ml
- 2 107-A Flask, Volumetric, 50 ml
- 2 110-A Pipette, Mohr Measuring, 5 ml in 1/10 ml
- 112-A Scoop

Procedure A — Rapid dry powder method for dissolved iron, in waters that are free of organic or other interferences.

1. Measure, with a No. 103-A 50 ml graduated cylinder, 25 ml of filtered sample and pour into a No. 105-A 125 ml Erlenmeyer flask.
2. Add one No. 112-A scoop (approximately 380 mg) of No. R-63 iron reagent powder and mix. Let stand for 5 minutes.
3. Turn on the analyzer and rotate filter selector to No. 520.
4. Fill one No. 260-T square 26 mm test cell with the untreated filtered sample, for use as a blank. Fill a second test cell with the treated sample.
5. Insert the test cell containing the blank into the analyzer, making certain that one of the frosted sides faces the front. Adjust the meter needle to 100. (See Note B.)

TABLE I-6. (Continued)

6. Replace the blank with the test cell containing the treated sample, and read the meter.
7. Refer to the graph for iron to convert the meter reading to ppm of iron (Fe).

Procedure B — This is based on the standard A. P. H. A. method, 12th edition, using phenanthroline, where the sample is treated to remove interfering substances. The same calibration graph is used for both procedures.

1. (a) For total iron, mix the sample thoroughly and measure 50 ml of mixed sample into a 125 ml Erlenmeyer flask.
(b) For dissolved iron, allow the sample to settle, decant the supernatant, and filter, discarding the first 25 ml of filtrate. Measure 50 ml into a 125 ml Erlenmeyer flask.
2. Simultaneously prepare a reagent blank by adding 50 ml of distilled water to a second 125 ml Erlenmeyer flask. (See Note C.)
3. To each flask, add 2 ml of No. R-39 hydrochloric acid, concentrated, and 1 ml of no. R-100 hydroxylamine reagent.
4. Heat both flasks to boiling on a hot plate and reduce the volume to approximately 20 ml. (See Note A.)
5. Cool to room temperature and transfer each to No. 107-A 50 ml volumetric flasks.
6. To each, add 10 ml of No. R-101 ammonium acetate buffer and 3 ml of No. R-102 phenanthroline, 0.1%.
7. Dilute each flask to volume with distilled water and mix. Let stand for 5 minutes.
8. Continue as directed in Procedure A, beginning with step 3.
9. The Model 260 water analyzer is calibrated from 0 to 5 ppm iron. If necessary expand the range. The results are reported in ppm iron, either total or dissolved. Total iron is obtained with a mixed, unfiltered sample. Use of a filtered sample gives results in terms of dissolved iron only.

Note A — If the sample contains much color or organic matter, evaporate a 50 ml sample, gently ash the residue, and redissolve in 2 ml of No. R-39 hydrochloric acid, concentrated. Add 1 ml of No. R-100 hydroxylamine reagent, and 5 ml of distilled water. Proceed with step 5.

TABLE I-6. (Concluded)

Note B — If the sample blank is so highly colored or turbid that the instrument cannot be set to 100, then use distilled water as a blank in step 5 and read both the sample blank and the unknown. Convert the meter readings to ppm and subtract the value (in ppm) of the sample blank from the value (in ppm) of the unknown. The difference is the true concentration of unknown in the sample.

Note C — If the sample is colored or turbid, prepare a blank by using 50 ml of sample instead of distilled water in the procedure given above, substitute distilled water for reagents in step 6. Use the sample blank instead of the reagent blank in step 4.

If the sample blank is so highly colored or turbid that the instrument cannot be set to 100, then use distilled water as a blank in step 5 and read both the sample blank and the unknown. Convert the meter readings to ppm and subtract the value (in ppm) of the sample blank from the value (in ppm) of the unknown. The difference is the true concentration of unknown in the sample.

Note D — Estimating Ferrous and Ferric Iron. The procedures given above convert all the iron in the sample to the ferrous (Fe^{++}) form before the color reaction with phenanthroline. The quantity of ferric iron (Fe^{+++}) present may be estimated by adding 1 ml No. R-39 hydrochloric acid, concentrated, to 50 ml of sample in an Erlenmeyer flask, mixing and proceeding at once to step 6 in Procedure B. Continue without delay to step 8 of Procedure B. Convert the reading obtained to ppm iron from the graph, and multiply by 1.2. The value obtained will be close to the quantity of ferrous iron originally present. Subtracting this from the total iron (determined as described in Procedure B) will give the quantity of iron originally present in the ferric form.

D. Contamination Considerations

1. Construction, Orientation, and Position of Simulated Shuttle Bay — David W. Jex

A simulated bay vent was built to obtain data concerning the amount of contamination that might be expected to enter the Shuttle bay. The modeled configuration was supplied by Rockwell International. Because of the time

constraint, only approximately 25 percent (336 channels) of one full vent could be constructed. A diagram of the box is shown in Figure I-34. Two quartz crystal microbalance (QCM) units were to be placed inside the box for measurement of the ingested contamination together with some optical surfaces.

During firing 1, no measurements with the QCM's could be made because all of the available instrumentation lines were being used for calorimeters, thermocouples, and pitot tubes. However, the vent box was placed in the chamber oriented such that the vent openings were facing the angled deflector cone. It was located 24 m (8 ft) below the rim of the motor nozzle and at a 24 m (8 ft) radial distance from the plume centerline. A diagram of the box orientation with respect to the plume flow and the direction that the vent channels were facing is shown in Figure I-35 as an arrow labeled 1.

After the firing, the box was opened and a visibly large amount of solid particulate material covered the bottom. After viewing the movie of the firing, it was evident that this material had entered the box because of the deflected flow field; i. e., as the plume expanded and encountered the stand holding the samples at the 3 m (10 ft) level, some of it was deflected so that it turned and flowed down the deflector cone. The angled deflector cone would continue to turn the flow so that it would be traveling directly into the venting channels. Dirt and flaking paint were abundant on the deflector cone prior to the firing and could be significant contributors to the contaminants that entered the box. Therefore, there was no analysis of the debris for this firing because it was felt such an analysis would not be representative of contamination that could be expected to enter the bay.

For the second firing the box was placed in the same location as the first firing, but turned 180 degrees so that the vent channels were directed toward an area where there was no direct flow. The QCM's were not used during this firing because of malfunctions in the wiring circuit. The orientation and direction that the vent channels were facing is shown in Figure I-35 as an arrow labeled 2.

For the third firing the box was moved out to a radial distance approximately 635 cm (250 in.) from the centerline of the plume and approximately 823 cm (324 in.) above the rim of the nozzle. Again the vent channels were directed toward an area where there was no direct flow. A diagram of the box orientation with respect to the motor and plume is shown in Figure I-36. The catwalk grating on which the box sat should have provided turbulent flow conditions at the mouth of the vent channels.

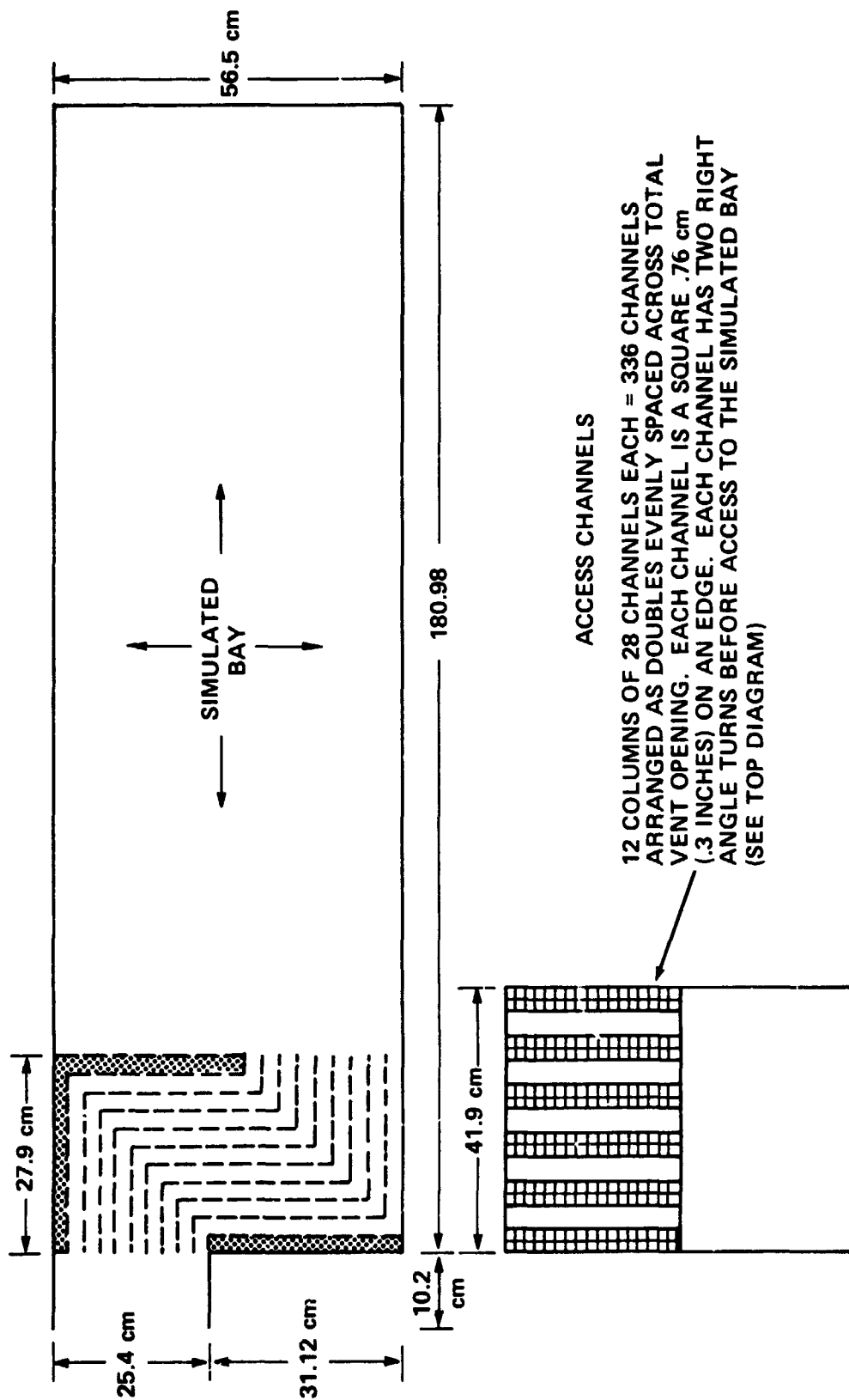


Figure I-34. Construction of simulated Shuttle bay and vent.

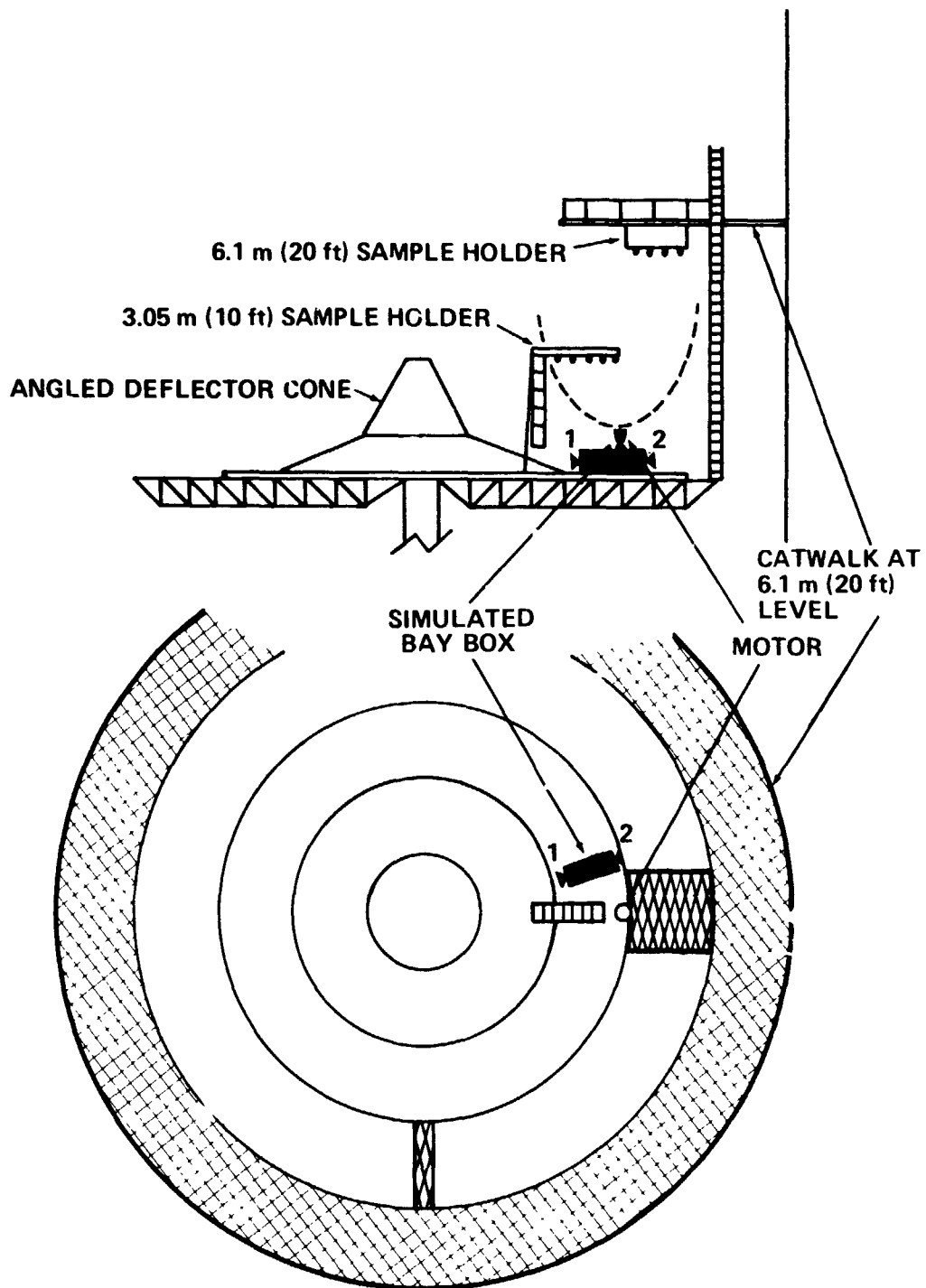


Figure I-35. Box orientation and vent direction on test firings 1 and 2.

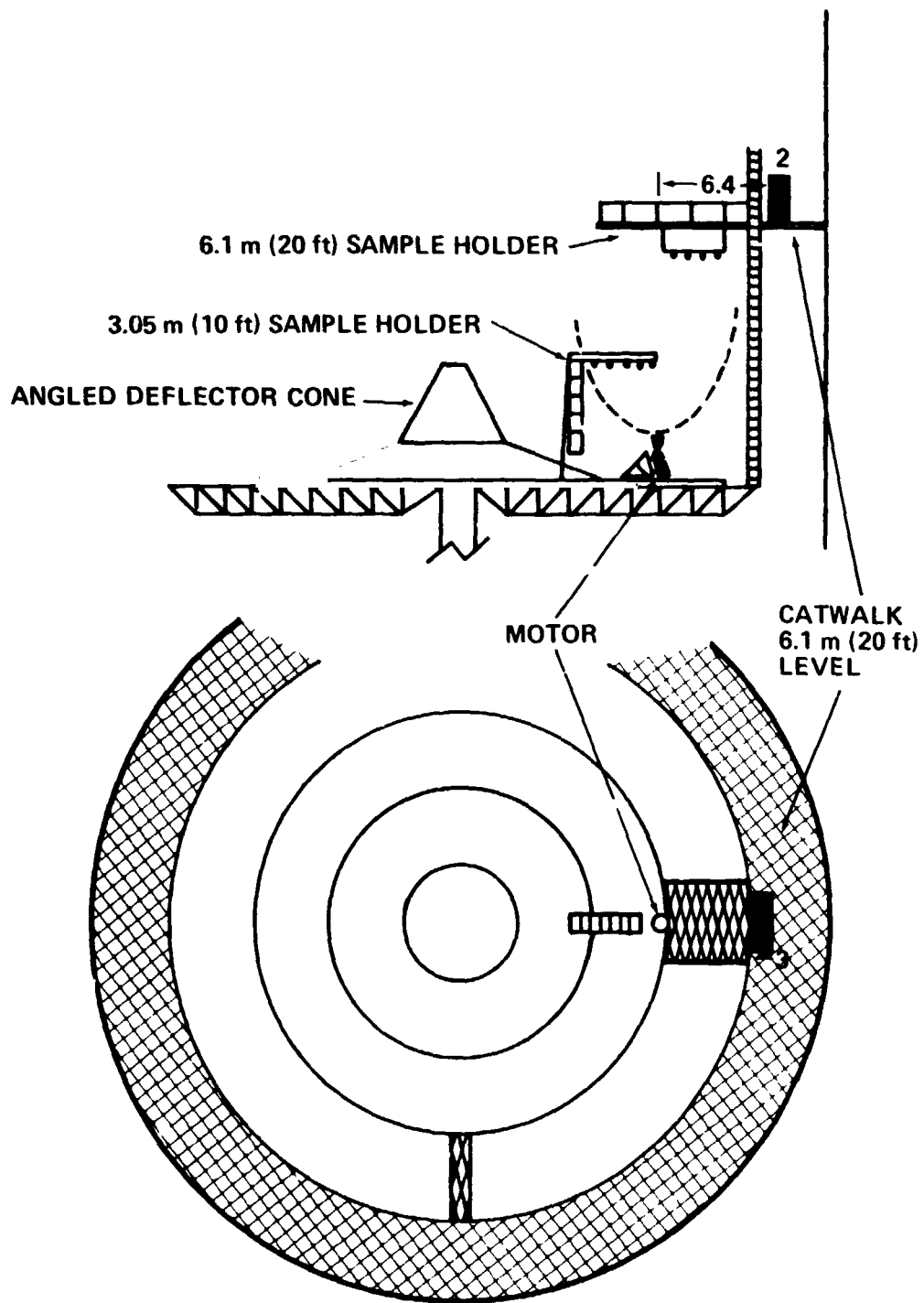


Figure I-36. Box orientation and vent direction on test firing 3.

The information which refers to the simulated Shuttle bay in subsections 2, 3, and 4 that follow is from this configuration. The data are for approximately 25 percent of one full vent and one motor firing. Since there are more than 14 full vents and 4 motors fired during separation, it cannot be concluded that there is no contamination problem with the present proposed venting system for the Shuttle vehicle without further information and/or data. However, the probability of a contamination problem is low.

2. Quartz Crystal Microbalance Measurements -- Daniel B. Nisen, David W. Jex, and Thomas R. Edwards

The QCM is basically an active device in which particulates or molecules come in contact with the surface of a thin quartz disc (about 1.2 cm in diameter and 0.015 cm thick). This disc is part of a high frequency oscillator circuit whose frequency (nominally 10 MHz) is controlled by the crystal. In this particular application, a thin coat of adhesive was bonded to the front and back of each crystal to maintain balance. When solid particulates come in contact with the front surface, they adhere to the adhesive and are "trapped." Mass added to the crystal by this captive process causes a decrease in the resonant frequency, the change being proportional to the amount of mass added. Placed in proximity to the sensing crystal, but not being exposed to any impacting mass, is an identical reference crystal controlling the frequency of another circuit at a slightly higher frequency than that of the sensing oscillator.

The beat frequency between the two oscillators (of the order of 2 kHz) is the signal monitored to determine the mass change. This signal will, of course, vary whenever a Δf is experienced on either crystal. A change in temperature will cause a change in the beat frequency as well as the mass being accumulated. For this reason the temperatures of the crystals are monitored along with the beat frequency.

Two QCM's were placed inside a simulated bay box. One faced the venting channels and was designated No. 1. The other faced in the opposite direction and was designated No. 2. Figures I-37 through I-40 show the plots of mass deposition on QCM No. 1, mass deposition on QCM No. 2, temperature shift on QCM No. 1, and temperature shift on QCM No. 2, respectively. These figures were generated by Hugh Zeanah, under the direction of Dr. Thomas Edwards, from a copy of the data tape made by AEDC during firing 3. It will be noted that identical events are recorded by the mass deposition signal on both QCM's, whereas the temperature shift was not the same. It is also noted that there is an uncertainty associated with the value recorded. This is evidenced by the width of the line. Using the minimum value of this uncertainty (the top edge of the line), we can trace the event in time. Correlating the event with the temperature shift on QCM No. 1, we find that the times, slopes, and deltas (amount of variation) are almost identical. Note, however, that the temperature level never really returns to the original value, whereas the mass deposition not only returns to its original level but increases beyond it.

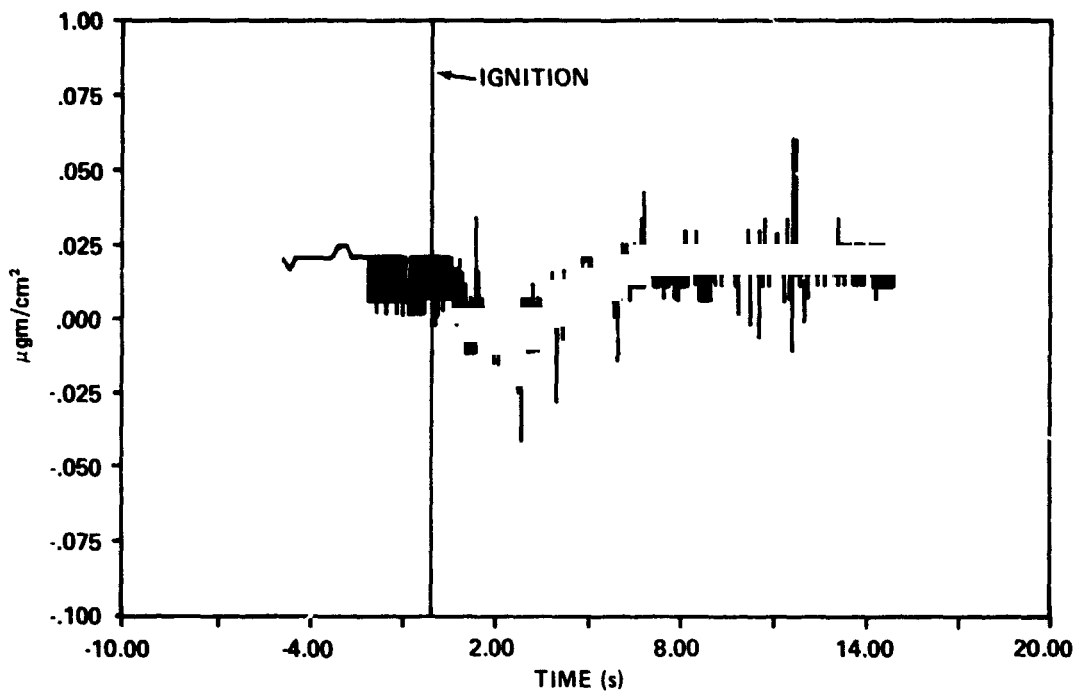


Figure I-37. Mass deposition on QCM No. 1.

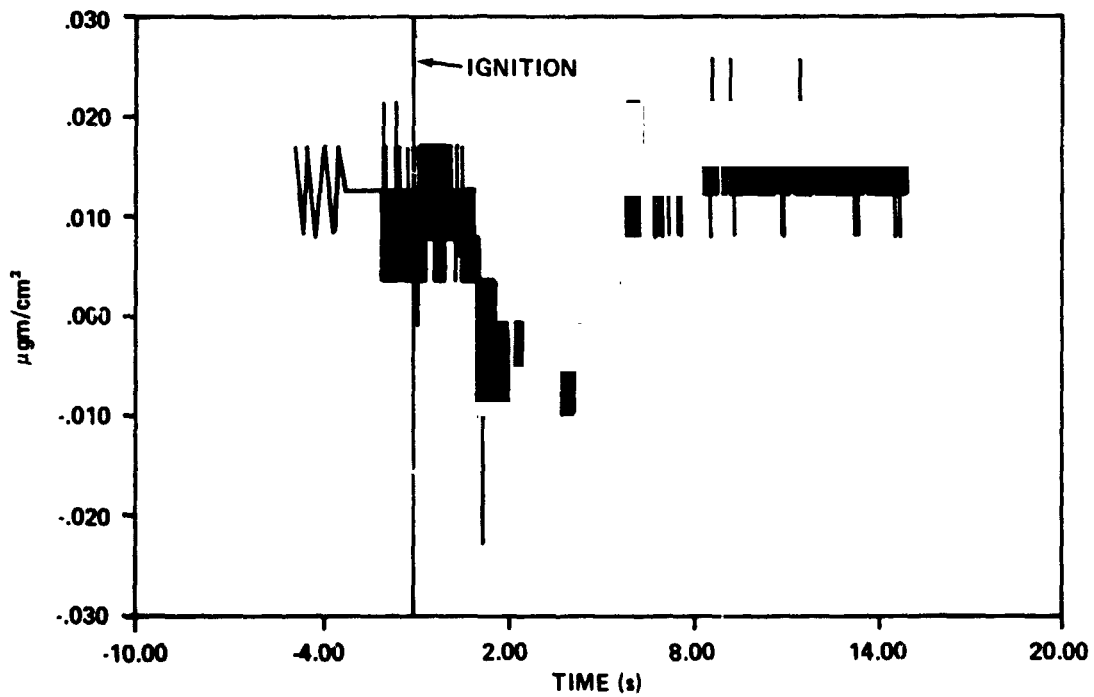


Figure I-38. Mass deposition on QCM No. 2.

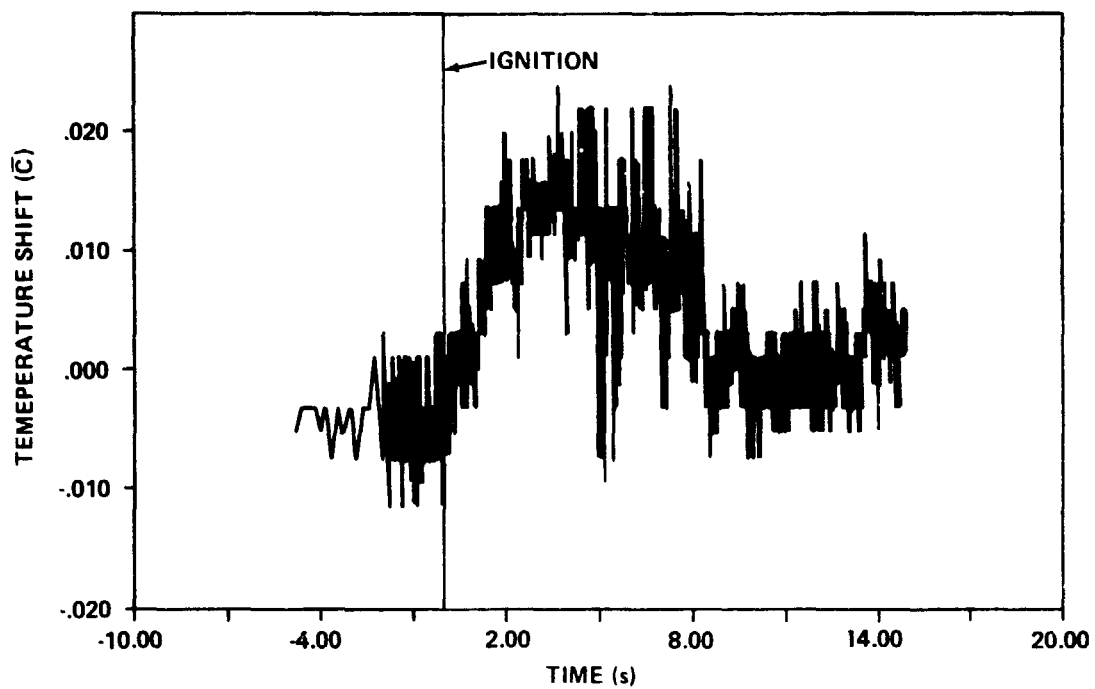


Figure I-39. Temperature shift on QCM No. 1.

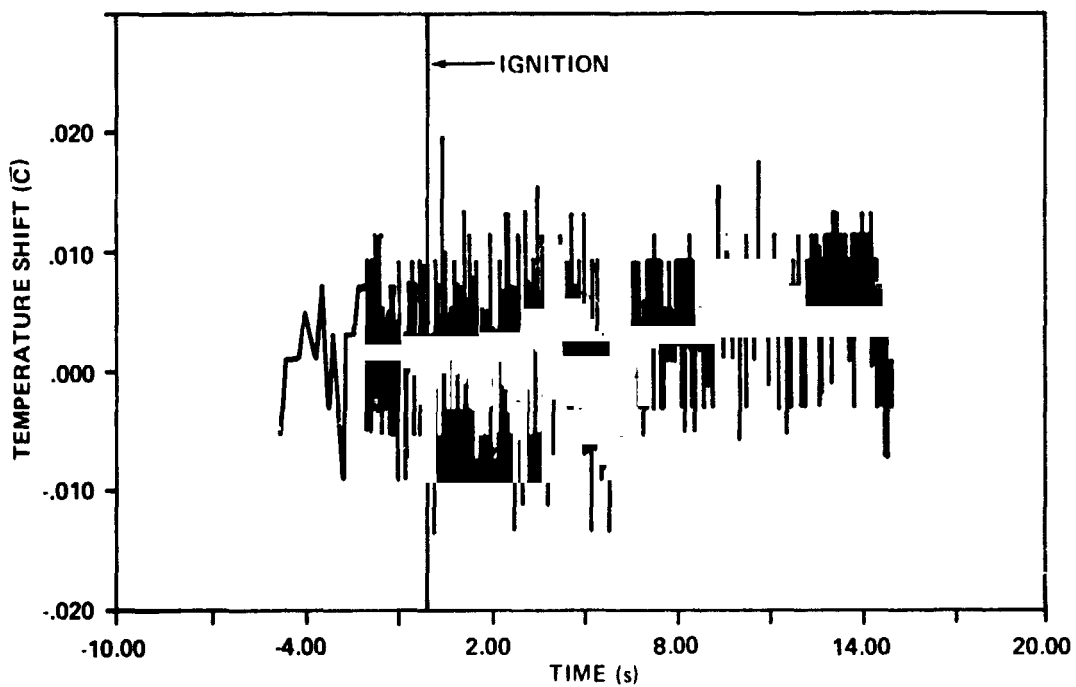


Figure I-40. Temperature shift on QCM No. 2.

Assuming that: (a) the rate of increase in temperature is directly correlated to a rate of increase in the beat frequency, (b) at any equilibrium temperature the crystals will have a characteristic beat frequency, and (c) there is a direct correlation between the temperature and the beat frequency, we can interrupt the results of the graphs to indicate an actual deposition of mass.

The deposition of mass indicated by both QCM's is between 5×10^{-9} gm/cm² and 1.58×10^{-8} gm/cm². The surfaces of both QCM's were examined by Dan Gates with a scanning electron microscope to see if there were indeed solid particulates adhering to the adhesive on the surface of the exposed QCM. Figure I-41 shows some of the solid particles observed. It will be noted that they do resemble some of the particles shown in section I. B.

It is concluded that a mass between 5×10^{-9} gm/cm² and 1.58×10^{-8} gm/cm² was ingested into the simulated bay box approximately 6 s after the ignition of the rocket motor.

3. Ultraviolet Optical Effects – Roger C. Linton and Coy W. Mattox

a. Introduction. To assess the contamination hazard of Shuttle rocket plume impingement on critical optical surfaces, two different approaches were employed. An active monitor, the transmissometer, functioned throughout the active test sequence and provided a measure of the degradation to the Shuttle windshield. Passive sample beds included various optical surfaces that were deployed throughout the J-4 chamber during tests, including a simulated Shuttle cargo bay with open vents. The measured effects of plume impingement on these optical surfaces would be expected to be applicable to optical instruments or experiments to be carried in a flight Shuttle cargo bay. Samples, including windshield materials, were deployed at various radial and height locations in the J-4 chamber during the three firings in the fall of 1973.

b. The Transmissometer. The transmissometer is a device that measures the transmittance of a rotating sample in the near ultraviolet (UV). A CsI photodiode detector is positioned to view a restricted cone of light from a Pen-Ray mercury lamp. The ratio of the recorded intensities when the sample is rotated into and out of the light beam is the sample transmittance. Normally, the transmissometer employs a narrow-band filter before the photodiode to restrict the measured wavelength to 253.6 nm (2536 Å). Using the Shuttle windshield material as a sample with its very low transmittance at this wavelength, the filter was removed and the transmissometer monitored the average of the mercury lines at 296.7 nm (2967 Å) and 312.6 nm (3126 Å). The spectral sensitivity of the photodiode precluded sensing other lines from the source lamp.



Figure I-41. Solid particles found on adhesive surface of QCM
(scanning electron microscope with 1K magnification).

ORIGINAL PAGE IS
OF POOR QUALITY

The windshield samples (cut and supplied by S. Jacobs of JSC) were approximately 15 cm long by 3 cm wide by 1 cm thick. A small hole was cut through the center of each sample for attachment to the dc motor assembly of the transmissometer that rotated the sample at variable speeds.

Figure I-42 is a photograph of the transmissometer taken at the conclusion of firing 3 at AEDC. The wires have been cut for removal of the unit from the J-4 chamber. The dusty film covering the unit is the contamination encountered in the firing. The white box on the transmissometer pallet is the light source transformer. The transformer, because of the environmental constraints of the J-4 facility, was required to be adjacent to the transmissometer and was potted with high-vacuum epoxy as shown.

The first firing of a Shuttle ullage rocket motor, November 11, 1973, was intended as a check on the performance of the rocket only. However, the transmissometer was activated on the J-4 chamber deflector plate following pump-down and throughout the test sequence. From measurements taken prior to pump-down (Fig. I-43), a relative change in transmittance of 4 percent was noted because of turbulence and subsequent settling of sediment under vacuum up to the time of firing. For some 10 s during and after the firing, the transmissometer acted erratically due either to heat generated or incident ultraviolet light from the plume. A final transmittance of 26 percent was recorded. Since the initial transmittance was 48 percent, and accounting for the prefiring 4 percent loss, a net change of 41 percent in the transmittance in the near UV was recorded.

For the second Shuttle rocket firing test, the transmissometer was again left on the deflector plate about 45 degrees radially from the rocket. Less than a 2 percent change in transmittance was noted under vacuum prior to firing. After firing the rocket, the transmittance had decreased to 27 percent. A more detailed transmittance measurement was made on this sample at MSFC, and the results are shown in Figure I-44. As in the case for the first firing, the contamination was visibly apparent as a dusty film of uniform appearance. From the appearance of the contaminant film, it is expected that the bulk loss of transparency is due more to scattering than absorption. The measurements, as taken, do not specify the mode of loss.

For the third firing the transmissometer was placed on the 6.1 m (20 ft) level catwalk at an axial distance of 8.2 m (324 in.) and at a radial distance of 6.4 m (250 in.). Two other Shuttle windshield material samples were placed on the 6.1 m (20 ft) level platform at an axial distance of 8.2 m (324 in.) and at a radial distance of 2.54 m (100 in.). These faced down toward the rocket engine to simulate direct impingement of the Shuttle windshield by these engines. The back side of each of these windshield samples, which would

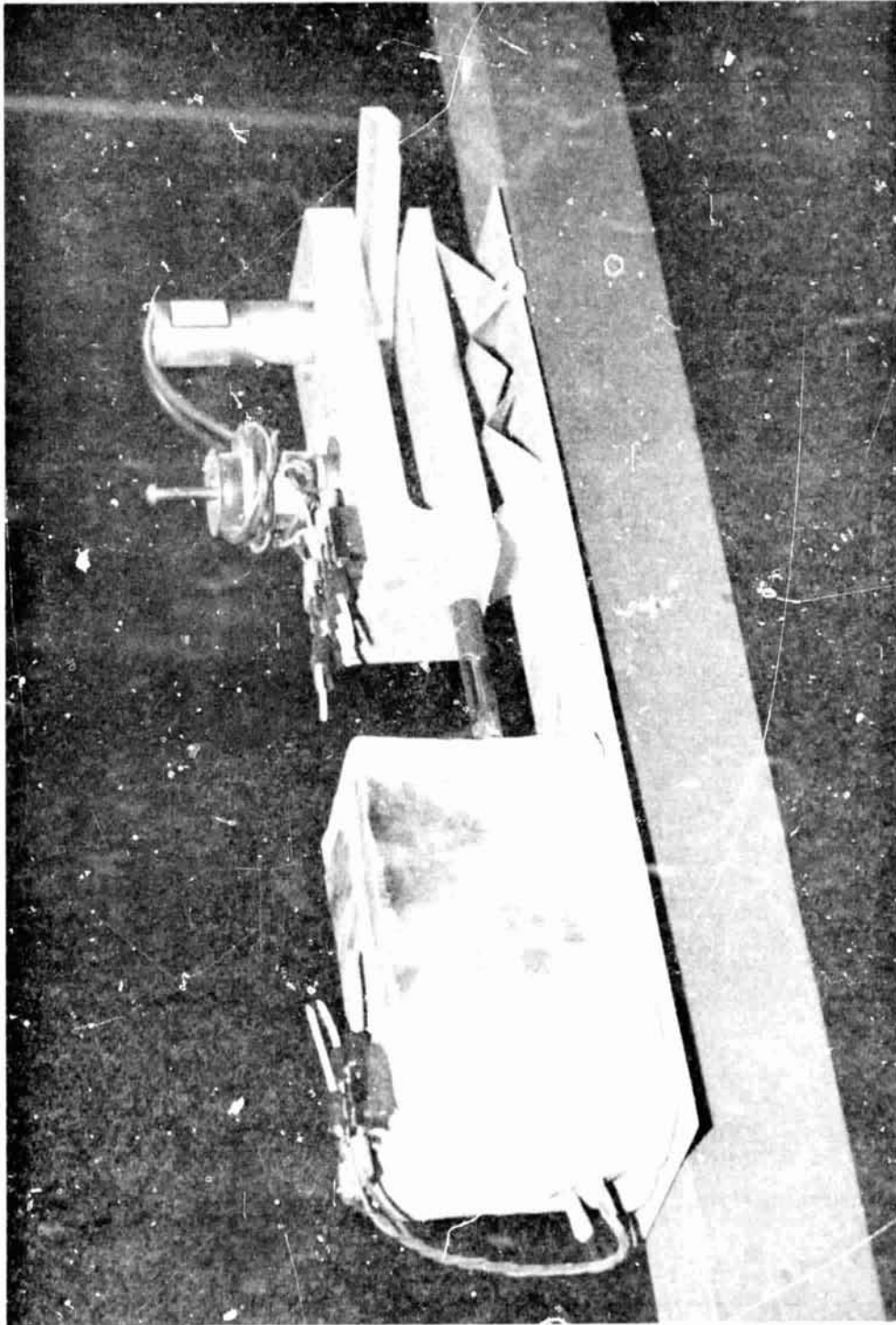


Figure I-42. Transmitter after firing 3.

ORIGINAL PAGE IS
OF POOR QUALITY

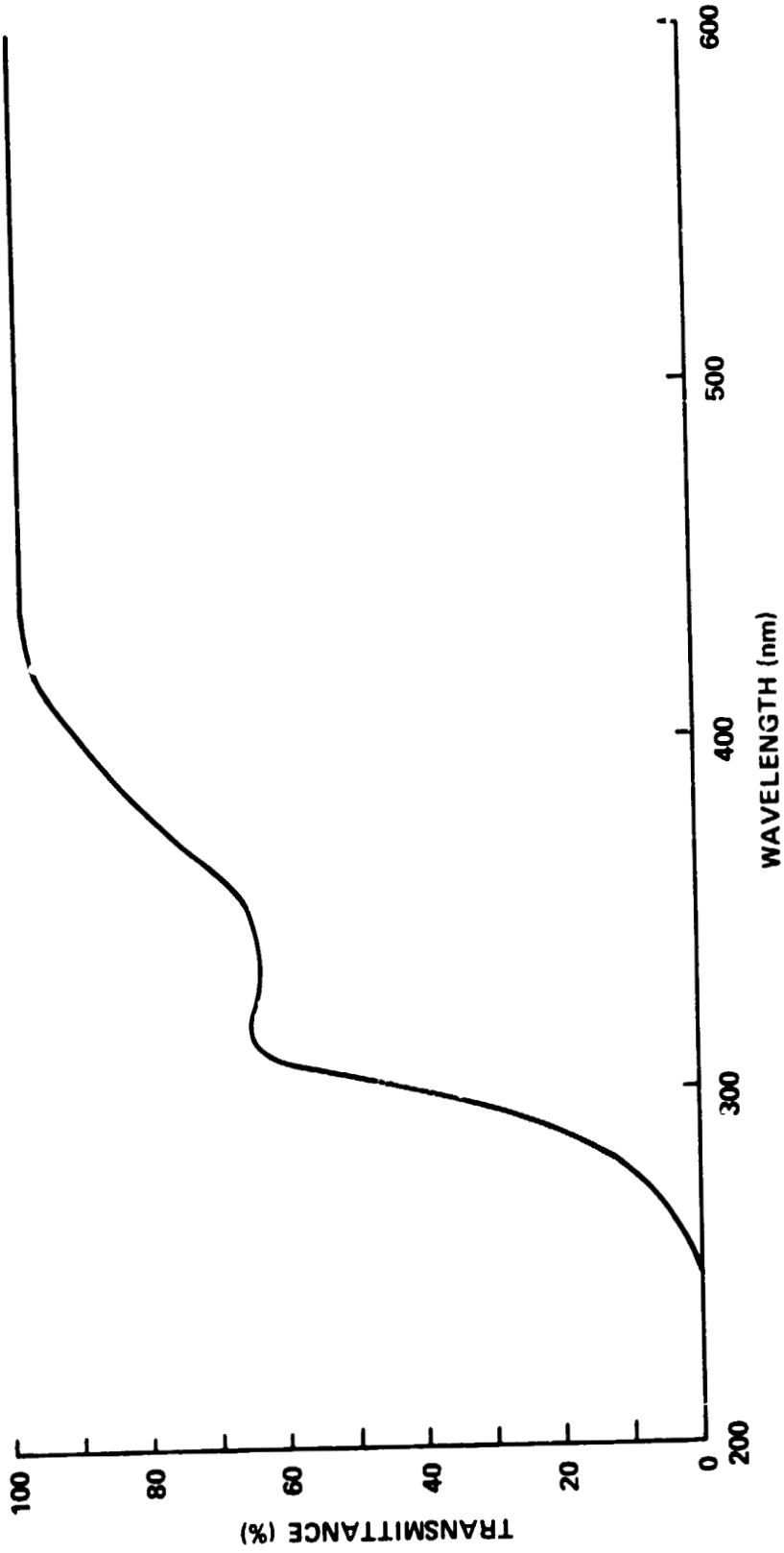


Figure I-43. Transmittance of clean Shuttle windshield.

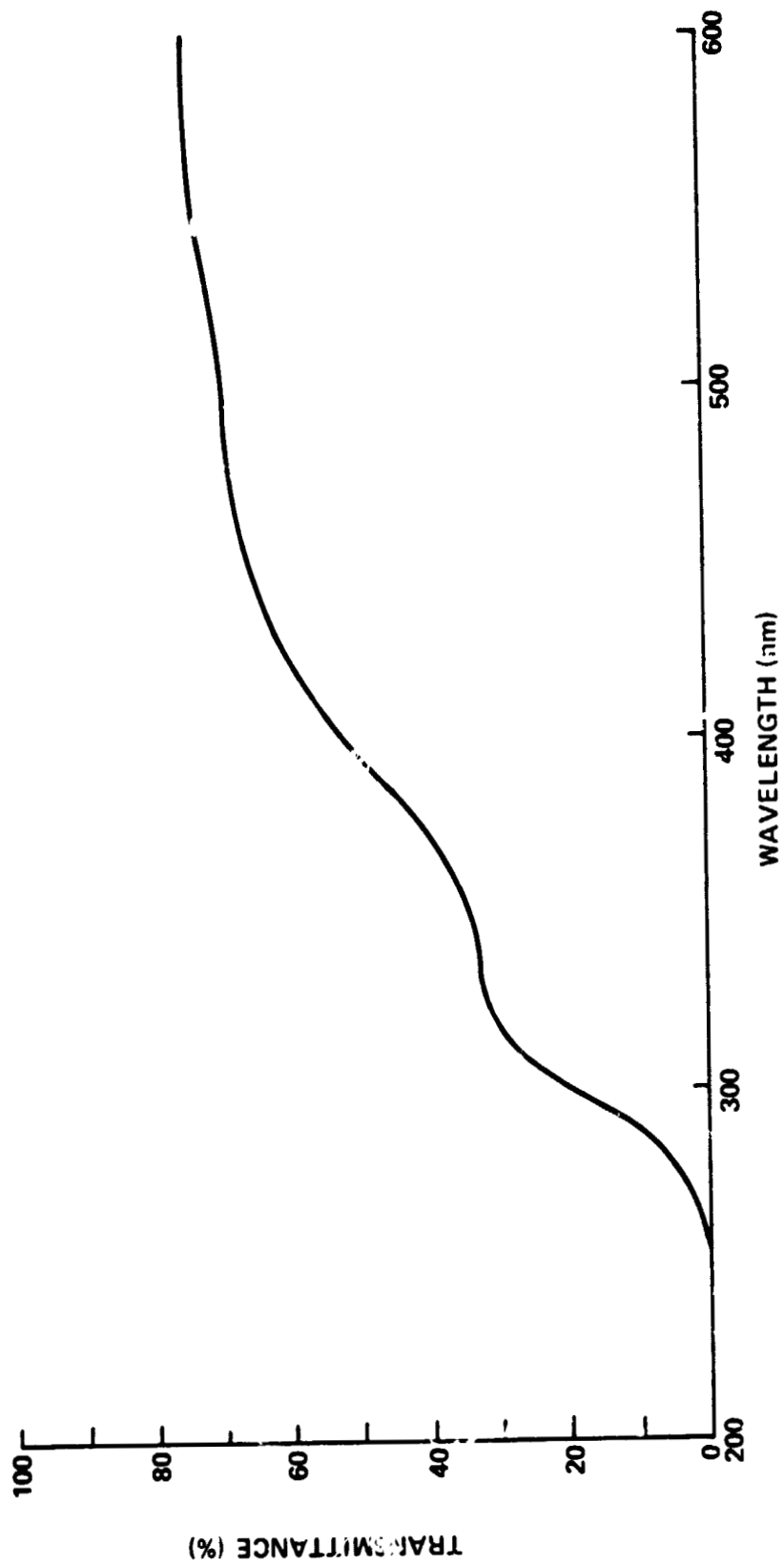


Figure I-14. Transmissometer windshield sample, firing 2, deflector plate.

correspond to the interior of the Shuttle pilot cabin, was masked to preclude deposition. Following pump-down in the J-4 chamber, the transmissometer recorded an initial 7 percent drop in transmittance of the sample in the device. However, by the time of the firing, the transmittance was back to 48 percent, the initial value. The effect of the test on the specimen was a 50 percent drop in transmittance, measured over a larger spectral region as shown in Figure I-45. Once again, the appearance of the contaminant film was dusty and milky, and it is thought that the dominant loss in transparency is a result of forward scattering by the particulates.

Both of the windshield samples left at the 2.5 m radial location were recovered and measured. The resulting damage is shown in Figure I-46. In effect, at this location, the Shuttle windshield would become opaque. The deposit, while similar to those encountered on the transmissometer samples, was mottled and somewhat darker in appearance. A view of one of these windshield samples, taken just after venting following the third firing, is shown in Figure I-47. In this photo, the rectangular sample is mounted to the base of the I-beam triangle in the center; the rocket was below and to the left.

Two general conclusions may be drawn from the transmissometer data relative to contamination effects. First, since the spectral sensitivity of the active transmissometer was in the near UV which increased its sensitivity and no serious degradation was noted prior to firing the motors, it can be assumed that the J-4 chamber was relatively "clean" for these type of tests, considering the very "weak" vacuum required and attained. Second, for the type of motors employed, and the test data of Figures I-43 through I-46, it is apparent that the Shuttle windshield would suffer greatly in loss of visible observation capability. In the case of the results of firing 3 at the 2.5 m radius, the Shuttle windshield would be useless for viewing. Because of results observed with other experiments in the tests, however, some consideration is being given to changes in the rocket propellant and further tests will show if any revised sequence is a contamination hazard.

c. The Passive UV Optical Test Beds. In various locations in the J-4 chamber and inside the simulated Shuttle cargo bay test beds containing an assortment of optical and thermal control surfaces were deployed during the three Shuttle rocket firings of 1973. One of the passive sample test beds is shown in Figure I-48. This report will discuss the effects of plume contamination on the optical surfaces.

It is to be expected that various optical instruments and experiments will be carried in the Space Shuttle cargo bay. It is further expected that many of these will be sensitive in the vacuum UV spectral region. Platinum and gold

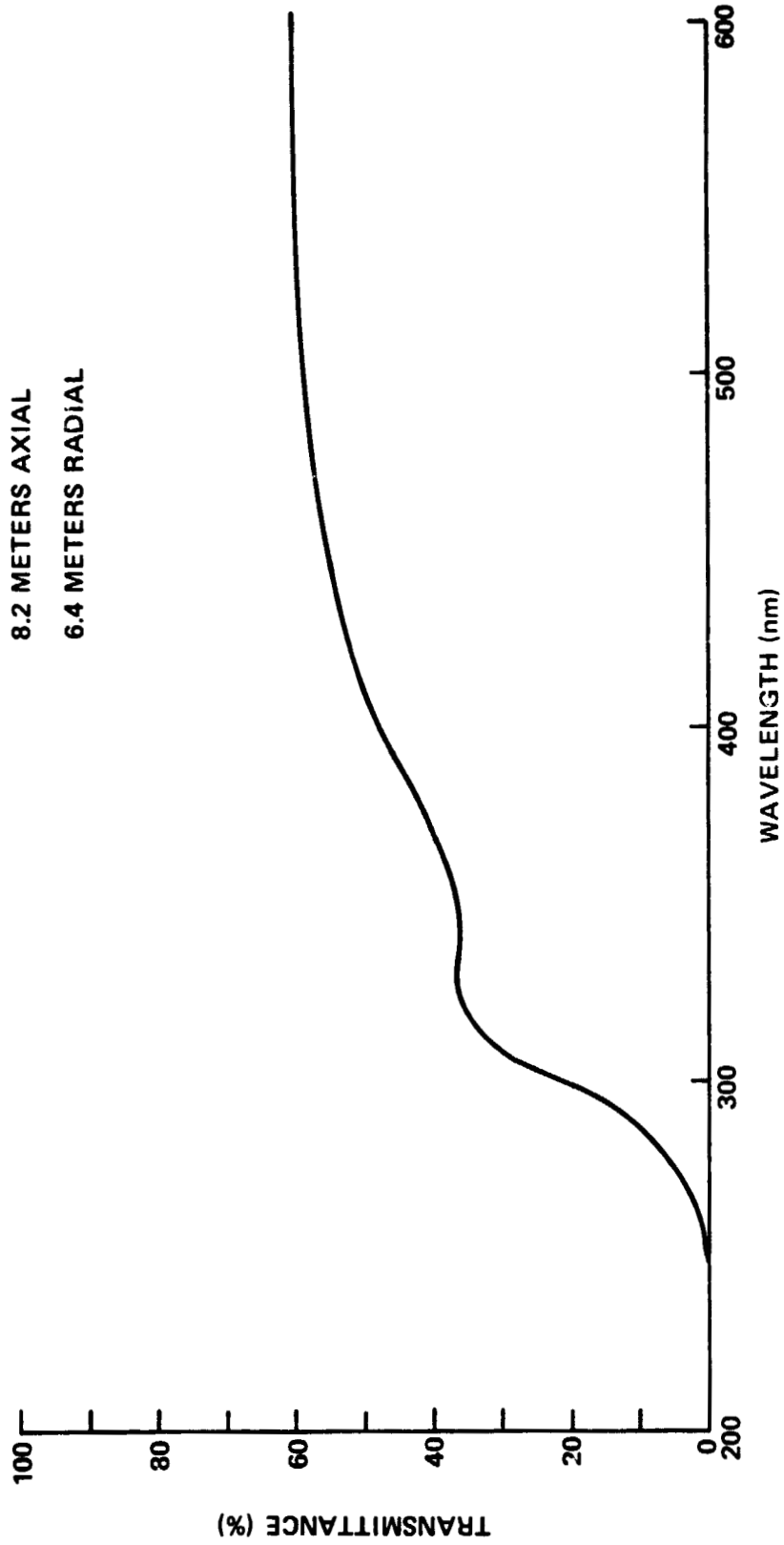


Figure I-45. Transmissometer windshield sample, firing 3.

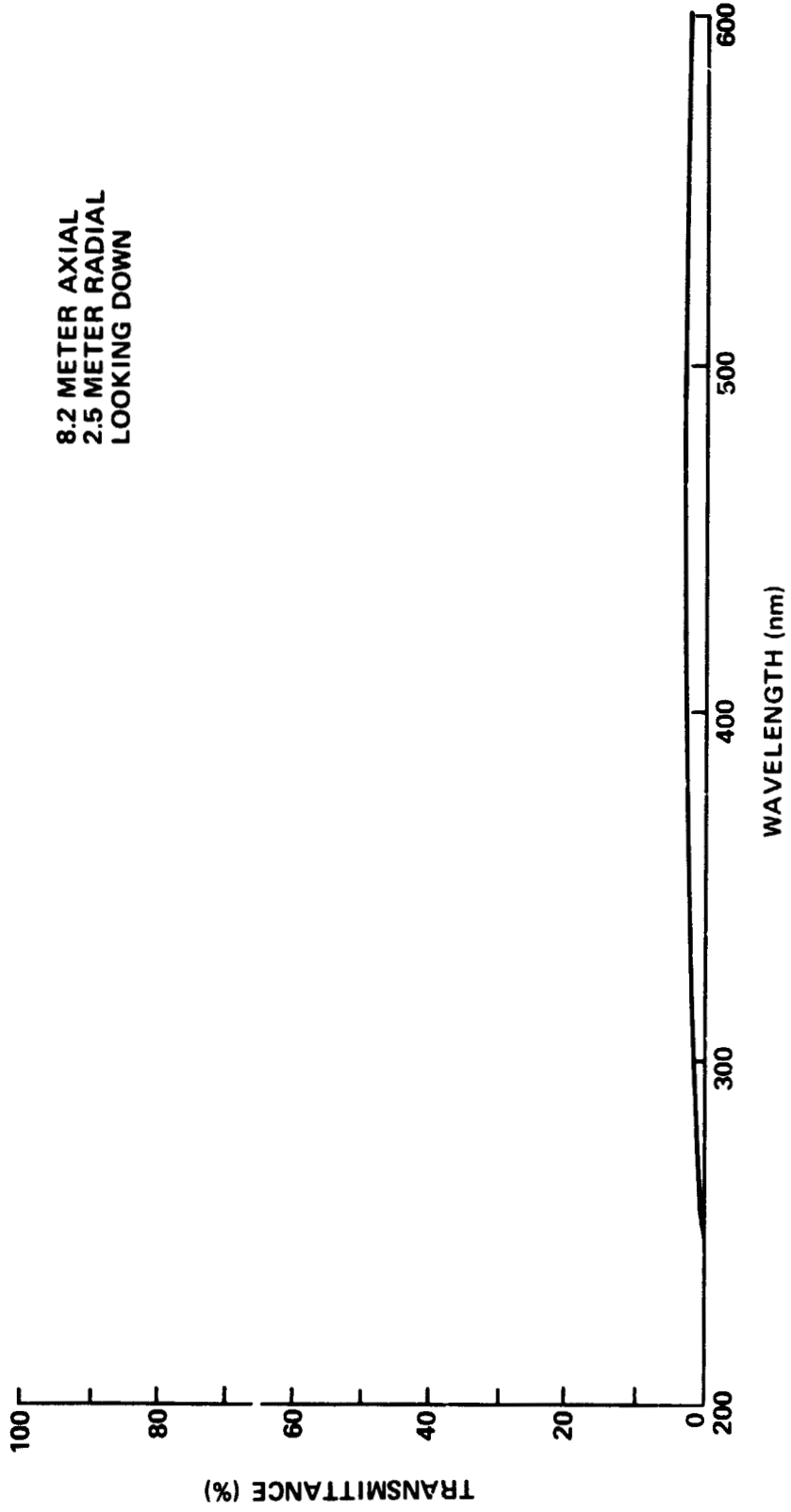


Figure I-46. Windshield sample No. 3, aluminum.

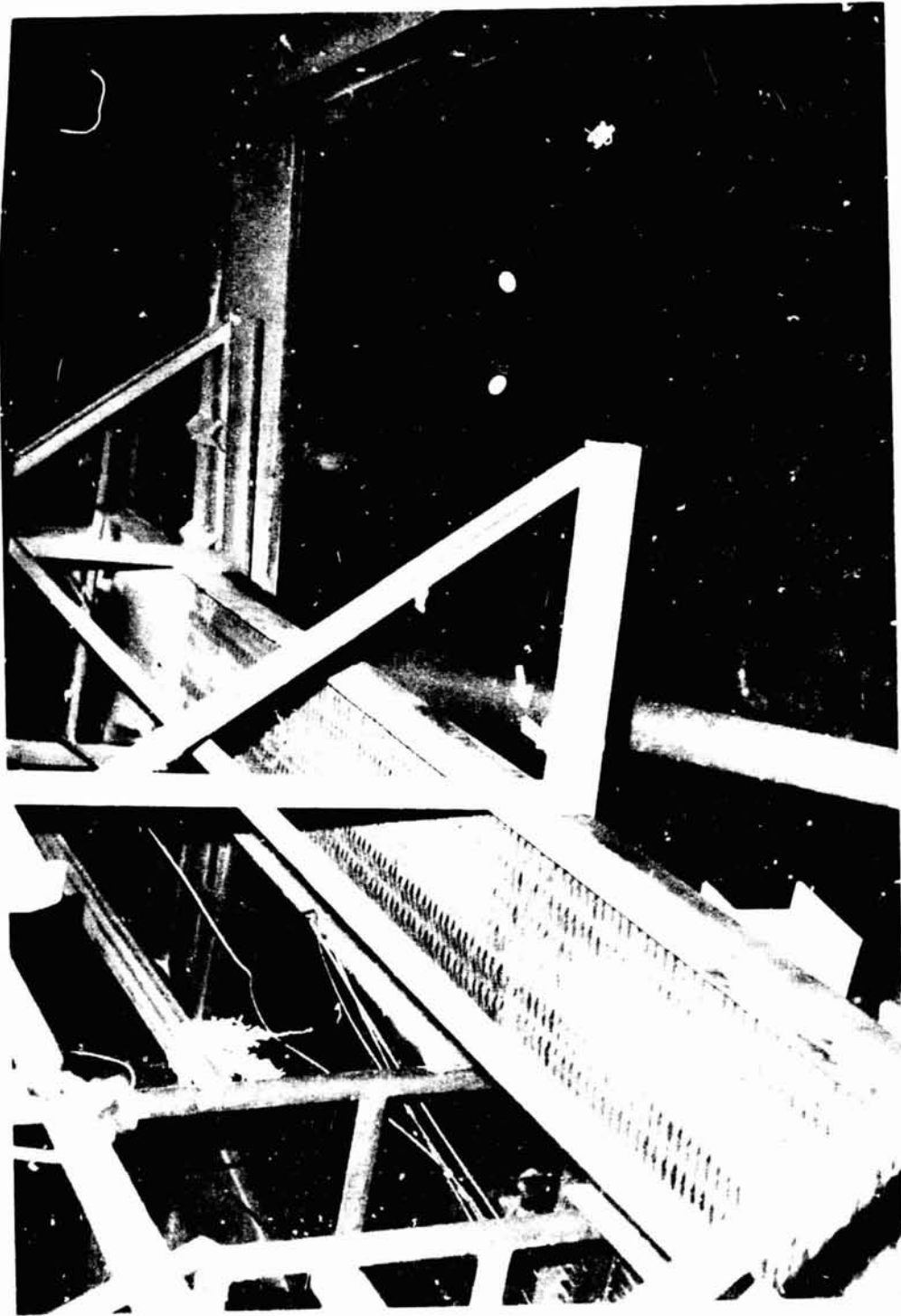


Figure I-47. Windshield sample location photographed after firing 3.

ORIGINAL PAGE IS
OF POOR QUALITY

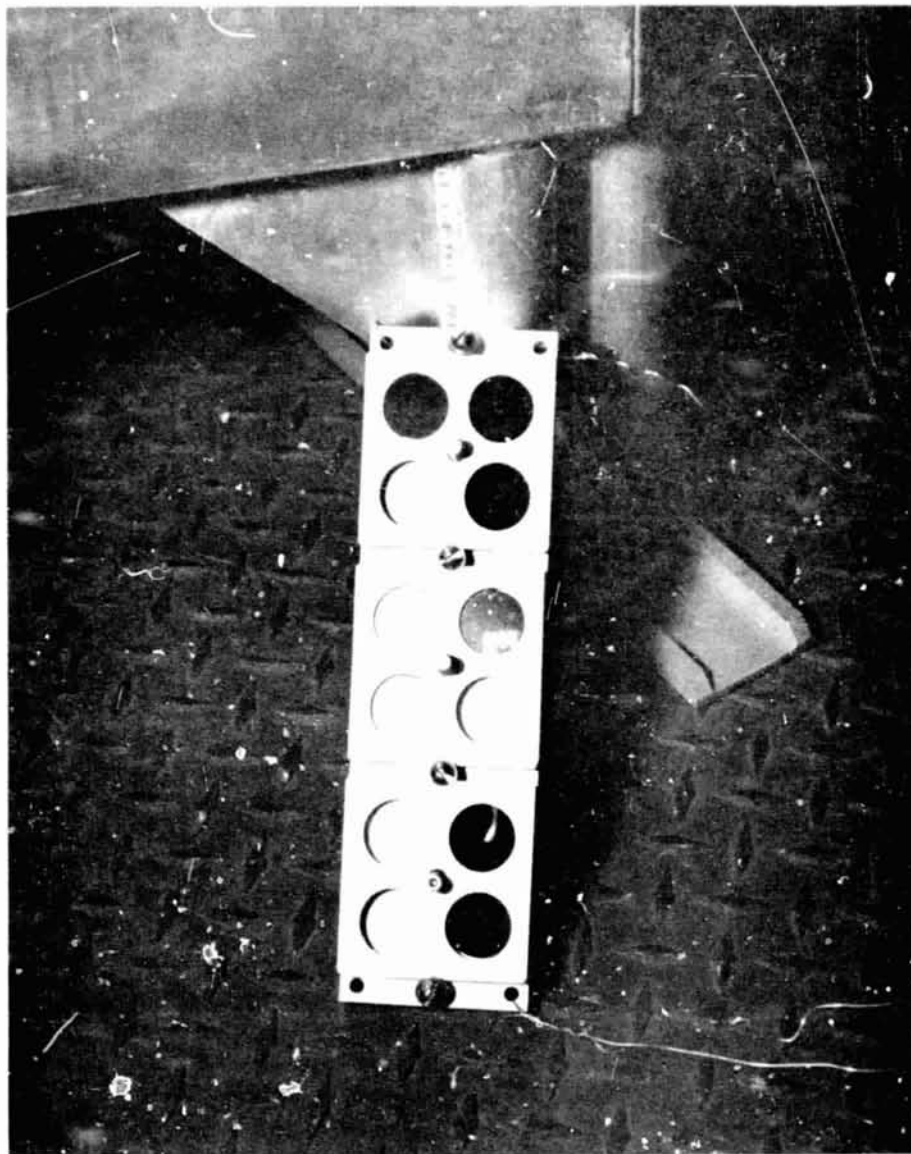


Figure I-48. Passive optical sample test bed.

are representative optical coatings that have been and will be used in space UV experiments. Platinum, gold, and osmium mirrors were placed in the passive test beds and exposed in various ways to the test environment.

The specular reflectance at near-normal incidence of all the deployed samples was first measured at MSFC. A 1 m McPherson 225 monochromator with a Hinteregger hydrogen discharge light was used with a dual-beam reflectometer to measure the reflectance in the spectral range from 100 to 200 nm, restricting the wavelength interval compatible with the useful range of the optical samples to be used. Following each test firing, the exposed test beds were returned to MSFC for remeasurement to determine the effects of plume impingement on their optical properties.

Passive test beds deployed exterior to a simulated Shuttle cargo bay contained, as mentioned, a variety of optical and thermal control surfaces. Since it is unlikely that any vacuum UV optical instrumentation would be deployed external to the cargo bay in flight to orbit, the results of measurements on these samples are not generally applicable but do give some information of a possible worst case. Basically, the reflectance changes were proportional to those of the transmissometer and windshield samples at the various locations.

The results from the passive samples located in a simulated cargo bay box will now be discussed. The construction of this box is given in section I. D. 1. One test bed, containing multiples of the platinum, gold and osmium mirrors, was recovered after each firing. The most serious damage, optically, occurred during the first firing when the cargo bay box was on the deflector plate. Observations after venting revealed a covering of sooty black particulates covering all samples inside. The optical effects, particularly in terms of scattering, would have been severe. It was revealed that the cable inlet to the cargo bay was oriented so that a direct turbulent flow was incident on the vent that would not be present in the actual Shuttle cargo bay. These data are, therefore, not included.

The box was reoriented at the same location for the second firing. The box was located -2.4 m (-96 in.) axially, which is the surface of the deflector platform, and 2.4 m (96 in.) radially for test 2. The box was located at 8.2 m (324 in.) axially and 6.4 m (250 in.) radially for test 3. The orientation of the vents with respect to the plume flow lines is described in section I. D. 1. The results for samples from the second and third firings are shown in Figures I-49 and I-50. The change in reflectance for the gold and platinum mirrors is generally less than 10 percent (this is $\Delta R/R_0$, where $\Delta R = R_0 - R$ and R_0 is the original monochromatic reflectance). The $\Delta R/R_0$ value of 10 percent was the base acceptability factor for contamination degradation allowed for the Apollo Telescope Mount vacuum ultraviolet spectrometers in preflight testing. Thus, the observed changes would seem to be acceptable. It is important to recognize, however, that the Shuttle matrix vent is much greater in extent than that employed in the simulated Shuttle cargo bay and, consequently, the damage might be greater than that predicted from these results.

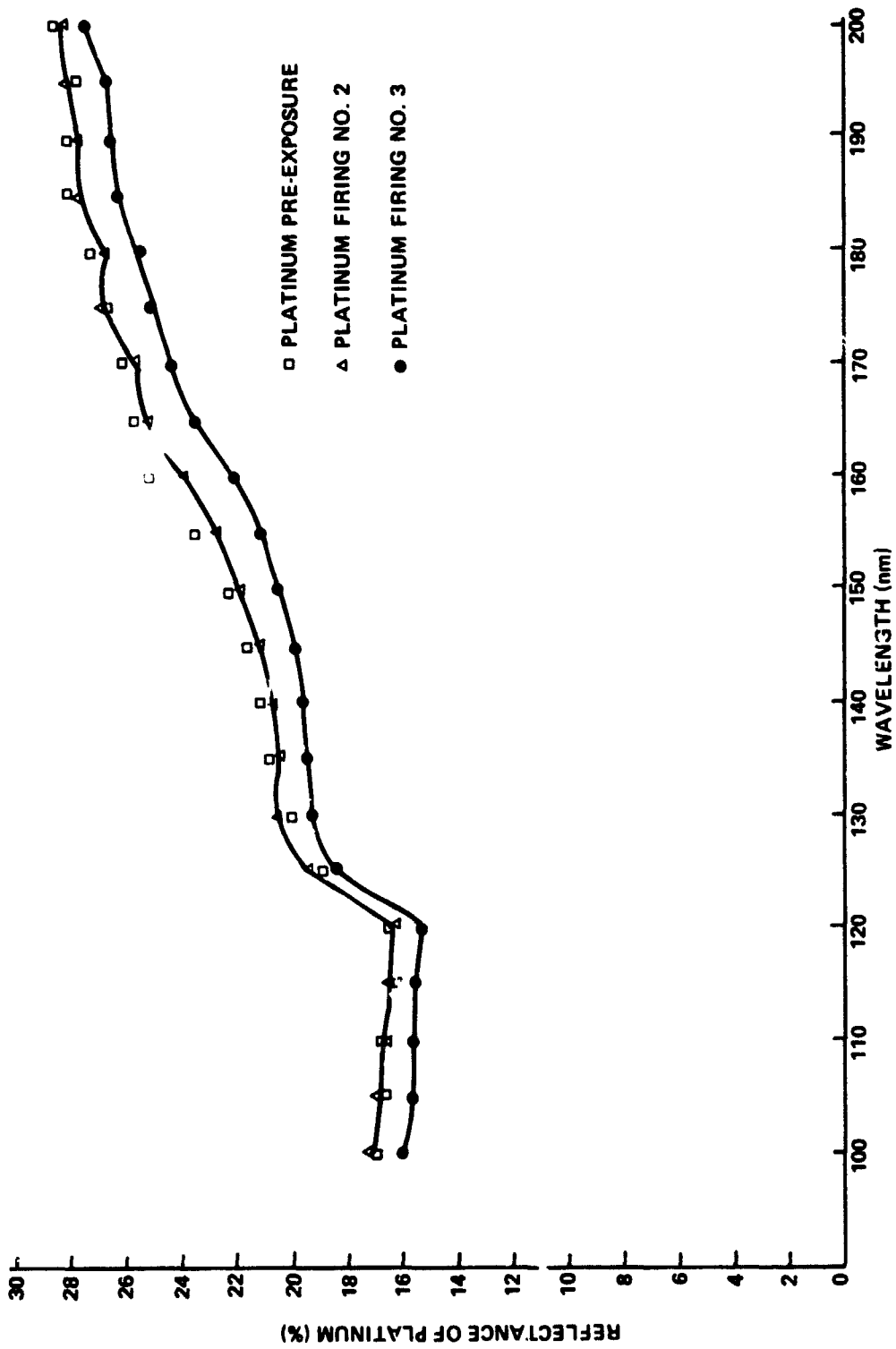


Figure I-49. Optical effects of Shuttle rocket firing tests 2 and 3 on passive platinum samples.

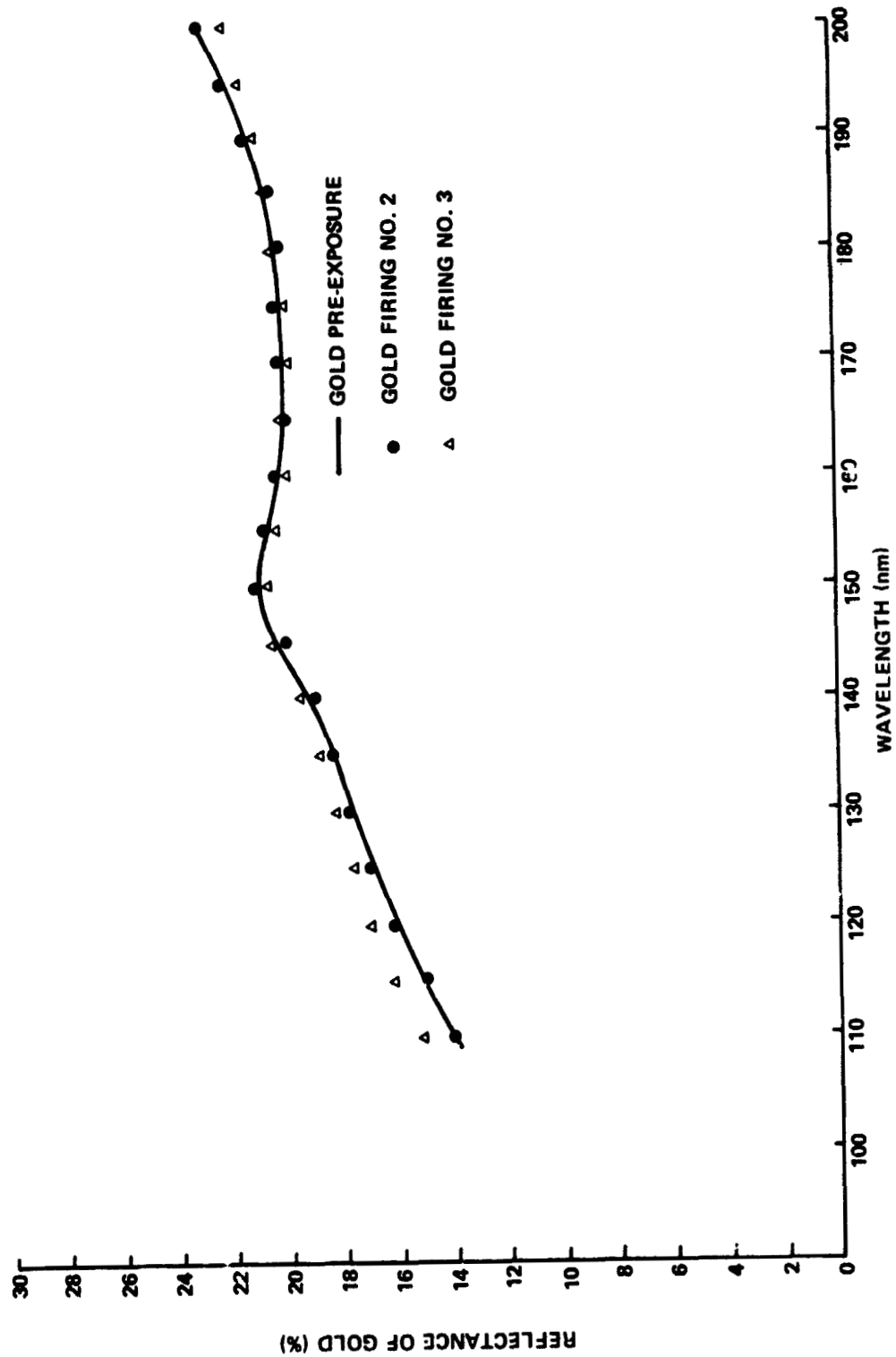


Figure I-50. Optical effects of Shuttle rocket firing tests 2 and 3 on passive gold sample.

The visible appearance of the sample after the firings confirmed the measured results to some degree. The mirrors showed some very small particulates scattered across the surface and no visible film. The data of Figures I-49 and I-50 show at some wavelengths an actual increase in reflectance. This may well be evidence of some very thin film causing constructive interference effects. In general, however, the effects are small. A more applicable measurement would be UV scattering for these types of samples, and such may be attempted in any future tests of Space Shuttle rocket engines.

4. Optical Contamination Measurements -- Near Ultraviolet/Visible/Near Infrared -- J. J. Trenkle and D. R. Wilkes

a. Introduction. Contamination of spacecraft optical surfaces can cause two serious problems. First, the optical properties of thermal control surfaces can be altered, thus changing the heat balance of the vehicle. Secondly, transmitting and reflecting optics in experimental and operational instruments can become contaminated, thus causing loss in reflectance or transmittance or, more importantly, scatter light within the system.

The heat balance of a spacecraft is extremely critical if the vehicle's thermal equilibrium is to remain within the designed boundaries. The equilibrium temperature of a spacecraft is determined by the radiative properties of the thermal control surfaces. Regardless of how heat is transferred or distributed throughout the space vehicle, when heat is "dumped" into outer space it must ultimately be emitted by the optical properties of the thermal control surfaces making up the radiators of the spacecraft. Figure I-51 represents a simplified schematic of the heat balance problem. The two major sources of heat input are the spacecraft itself and the solar electromagnetic energy. The only source of heat rejection is through the thermal control surfaces of the spacecraft. The quantity of heat a surface absorbs from the sun at a given wavelength is equal to the product of the material's absorption at that wavelength times the quantity of energy incident on the surface at that wavelength or²

$$E(\lambda) = \alpha \lambda E_s(\lambda) \quad ,$$

2. Wilkes, D. R.: A Numerical Integration to Determine Hemispheric Emittance, Solar Absorptance and Earth Infrared Absorptance From Spectral Reflectance Data. NASA IN-SSL-T-68-10, October 1968.

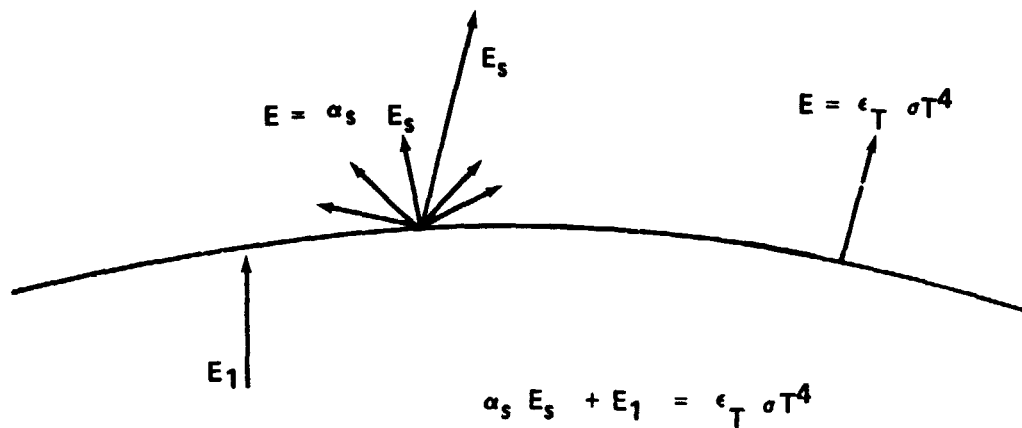


Figure I-51. Simplified heat-balance description.

where

$E(\lambda)$ = energy absorbed at wavelength λ

$\alpha \lambda$ = spectral absorptance

$E_s(\lambda)$ = solar energy at λ .

Therefore, the total energy absorbed by the surface from the sun is a summation of this equation over the solar spectrum or

$$E = \alpha_s E_s \quad ,$$

where

α_s = solar absorptance

E_s = integrated solar energy .

The efficiency with which a material will radiate heat is called the total emittance (ϵ_T). The total emittance of a surface is defined as

$$\epsilon_T = \frac{\text{Energy totally emitted by a surface at a given temperature}}{\text{Energy totally emitted by a black body at the same temperature}}$$

The amount of energy that a surface radiates is

$$E = \epsilon_T \sigma T^4$$

where

$$\sigma = 5.67 \times 10^{-8} \text{ W/m}^2 (\text{°K})^4$$

$$T = \text{temperature (°K)}$$

Equating the known heat inputs and output, the following simplified thermal balance equation results:

$$E_I + \alpha_s E_s = \epsilon_T \sigma T^4 \quad ,$$

where

$$E_I = \text{internal heat load} \quad .$$

From this equation it is apparent that the equilibrium temperature of the system is directly related to the surface radiative properties (α_s , ϵ_T). Any modification of the radiative properties because of surface contamination will alter the vehicles equilibrium temperature.

The second problem of concern is the effects of contamination on reflecting or transmitting optics. With the increasing emphasis on placing sophisticated optical instrumentation in space, this problem is of increasing

importance. If an optical surface is contaminated, the "on axis" energy may be reduced because of both absorption and radial scatter. Generally, scattered light presents more of a problem in optical systems than absorption. Energy scattered radially off the optical path may even generate selective "off-axis" peaks as a result of its interaction with the contaminated surface. The degree with which an uncontaminated surface will scatter is a function of the radiation incidence angle, the surface roughness, and the wavelength of the incident radiation. Figure I-52 represents the distribution of scattered radiation from a reflector as a function of an arbitrary angle of incidence, 20 degrees. The angle of incidence and the wavelength of incident radiation will remain constant in the following simplified discussion. Figure I-52 shows a practical representation of a good specular reflector. This reflector does generate very low intensity scatter at radial angles close to that of the primary reflection. If the surface is contaminated, the scatter distribution is altered as shown in the example. It is seen that the intensity of the primary reflection is reduced and the "wings" or radial scatter is greatly increased. If the surface is further contaminated, the intensity of the primary reflection will further be reduced and the "wings" will spread further. The degree of the surface's specular properties is reduced. A severely contaminated surface can even exhibit no specular properties and its energy distribution can closely resemble that of a diffuse scatterer shown in Figure I-52.

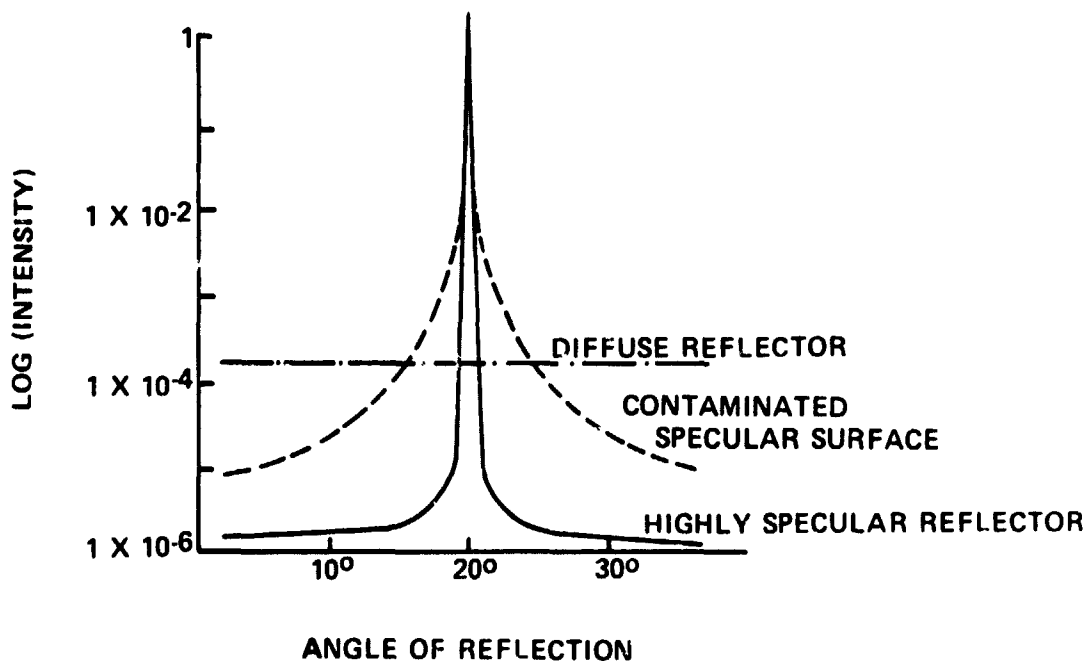


Figure I-52. Specular versus diffuse surface.

The purpose of this investigation was to expose candidate thermal control surfaces and a representative specular reflector to the S-II usage motor plume at various heights and radial distances and to examine any changes in the radiative or optical properties of the materials.

b. Optical Measurement Techniques. Direct sample absorption measurements are extremely difficult to obtain, but if the sample is assumed to be opaque, the sample absorptance (α , λ) for a given wavelength is

$$\alpha_{\lambda} = 1 - \rho_{\lambda} \quad ,$$

where ρ_{λ} is the total hemispherical reflectance for a given wavelength.

The results of these tests were obtained utilizing a Beckman DK-2A spectrophotometer with a Gier-Dunkle Instruments modified photometer attachment used to make the total hemispherical reflectance measurements over the wavelength range from 0.25 to 2.5 μ , the solar region of the spectrum. The schematic of the optical measuring system is shown in Figure I-53. The system consists of a prism type monochromator with tungsten and hydrogen lamp sources, an integrating sphere with photomultiplier and lead sulphide detectors, and ratiometric amplifiers.

A Lyons model 25B-6 emissometer was used to obtain total emittance measurements of test samples at room temperature. This instrument uses a calibrated cooled detector for measurement of total emittance. The wavelength response of the thermoelectrically cooled detector of this unit has been tailored to match, to the first order, the output of a 300° K (room temperature) black body. By calibrating the instrument output, using known references, at the high and low ends of the range, the total emittance of an unknown sample may be obtained. The references used for this test were fresh aluminum ($\epsilon_T = 0.03$)³ and a homemade ambient temperature "black hole" ($\epsilon_T = 0.98$).

c. Optical Data Test Results. S-13G, Z-93 (two zinc oxide pigmented, white paints), and silver-teflon second surface mirrors were used as representative thermal control surfaces in these tests. The 2.54 cm (1 in.) diameter samples were placed at locations in the AEDC J-4 chamber as indicated in Table I-7.

3. Arnett, G. M., Technical Coordinator: Lunar Excursion Module RCS Engine Vacuum Chamber Contamination Study. NASA TM-53859, July 1969.

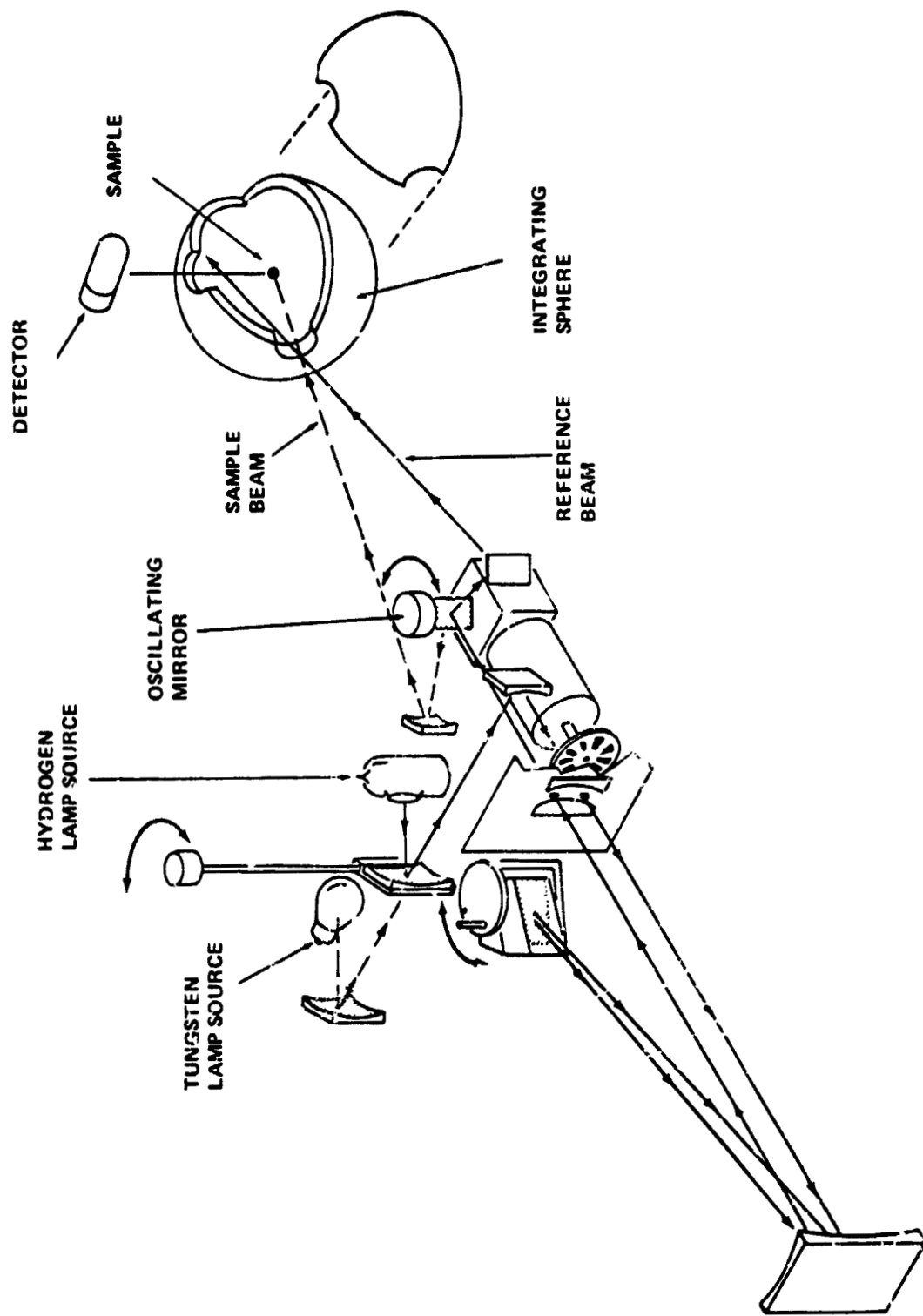


Figure I-53. Spectrophotometer schematic, Beckman : DU.

TABLE I-7. TABULATED RESULTS OF 2.54 cm (1 in.) DIAMETER SAMPLES

Sample		Before Test			After Test			Sample Location	Rocket Firing
Type	No.	α_s	ϵ_T	α_s / ϵ_T	α_s	ϵ_T	α_s / ϵ_T		
S13G	001	0.199	0.88	0.226	0.417	0.84	0.496	98.4 cm radially facing up 8.2 m level	3
S13G	002	0.202	0.88	0.230	0.208	0.84	0.248	80.7 cm radially in cargo bay box 8.2 m level (toward vents)	3
S13G	003	0.210	0.88	0.239	0.206	0.86	0.240	Cargo bay box (facing up)	2
S13G	004	0.193	0.88	0.219	0.859	0.84	1.02	39.4 cm radially facing down 8.2 m level	3
S13G	005	0.213	0.88	0.242	0.759	0.83	0.914	39.4 cm radially facing down 8.2 m level	3
Silver Teflon	1	0.082	0.75	0.109	0.115	0.72	0.160	98.4 cm radially facing up 8.2 m level	2
Silver Teflon	2	0.082	0.75	0.109	0.620	0.74	0.838	39.4 cm radially facing down 8.2 m level	3
Z93	101	0.160	0.90	0.178	0.173	0.90	0.192	In cargo bay box	2
Z93	103	0.165	0.90	0.183	0.375	0.88	0.426	39.4 cm radially facing down 8.2 m level	3
Z93	106	0.168	0.90	0.187	0.871	0.89	0.979	39.4 cm radially facing down 8.2 m level	3

TABLE I-7. (Concluded)

Sample		Before Test			After Test			Rocket Firing
		α_s	ϵ_T	α_s / ϵ_T	α_s	ϵ_T	α_s / ϵ_T	
Z93	107	0.172	0.90	0.191	0.803	0.90	0.892	3
Z93	108	0.162	0.90	0.180	0.251	0.91	0.276	

Note: α_s = solar absorptance

ϵ_T = total emittance at 300° K

The initial and final radiative properties of the thermal control surfaces are also presented. Figures I-54 through I-65 represent the reflectance as a function of the wavelength for each sample. Figures I-66 through I-70 show the plume contamination effects on platinum mirrors. The sample test locations are identified on Table I-8. The before and after 20 degree incident total hemispherical reflectance measurements are an indication of how much energy is lost because of surface contamination absorption. The scatter reflectance measurements are obtained by placing the sample normal to the beam so that the specular reflected energy exits through the integrating sphere entrance port. Any energy that is scattered, because of the surface contamination, greater than approximately 5 degrees from the normal will be collected by the integrating sphere. This scatter reflectance measurement technique does not yield scatter directional information but it does indicate losses in the specularity of a surface.

d. Conclusion. From the data presented, it can be seen that the reflectance properties of samples that faced the rocket plume were essentially destroyed. Samples that were in the plume but facing away showed considerable contamination damage but their original optical properties were not totally destroyed. The total emittance of the thermal control surfaces, however, did not significantly change in either case, which is not inconsistent since total emittance at room temperature is confined to longer wavelengths.

Measurements of samples placed in the simulated cargo bay showed minor contamination and this would need to be taken into account on a mission. The results of the samples in the simulated bay are discussed in section I. D. 3.

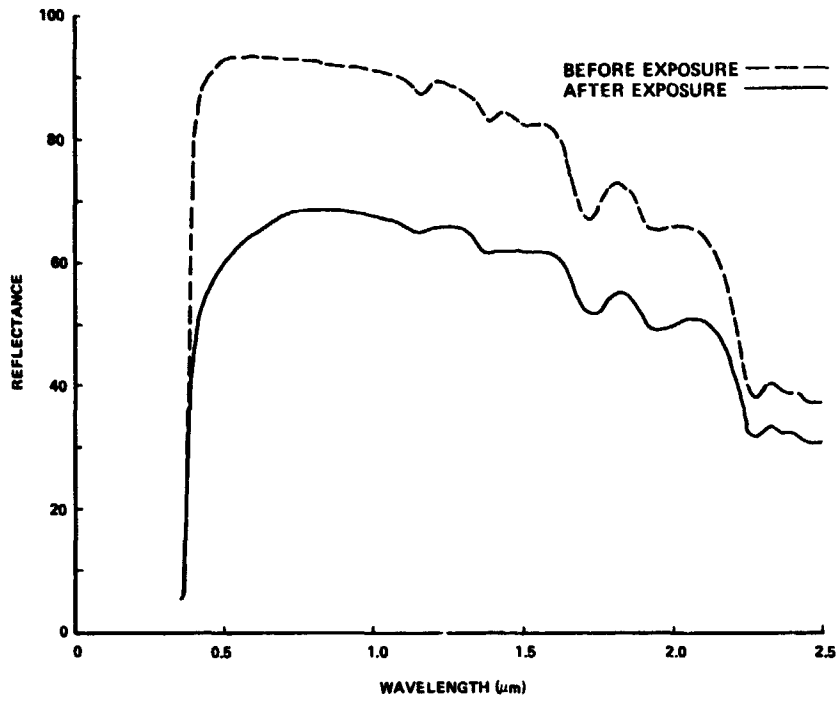


Figure I-54. S13G sample 001.

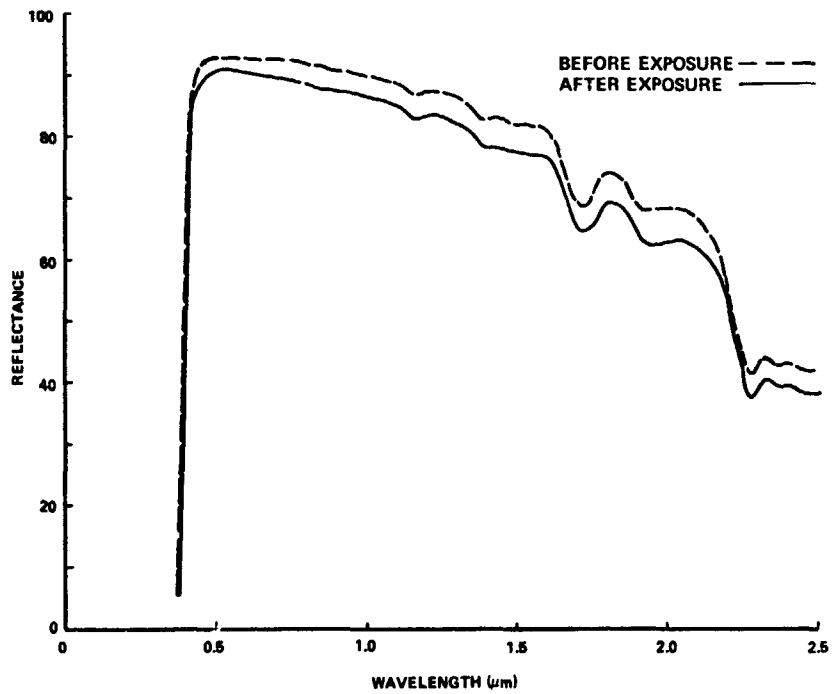


Figure I-55. S13G sample 002.

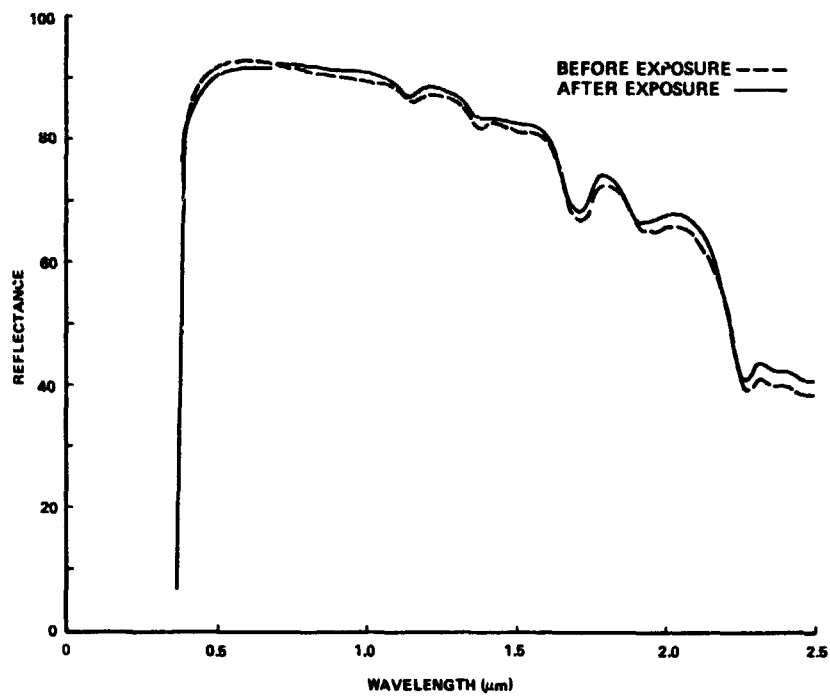


Figure I-56. S13G sample 003.

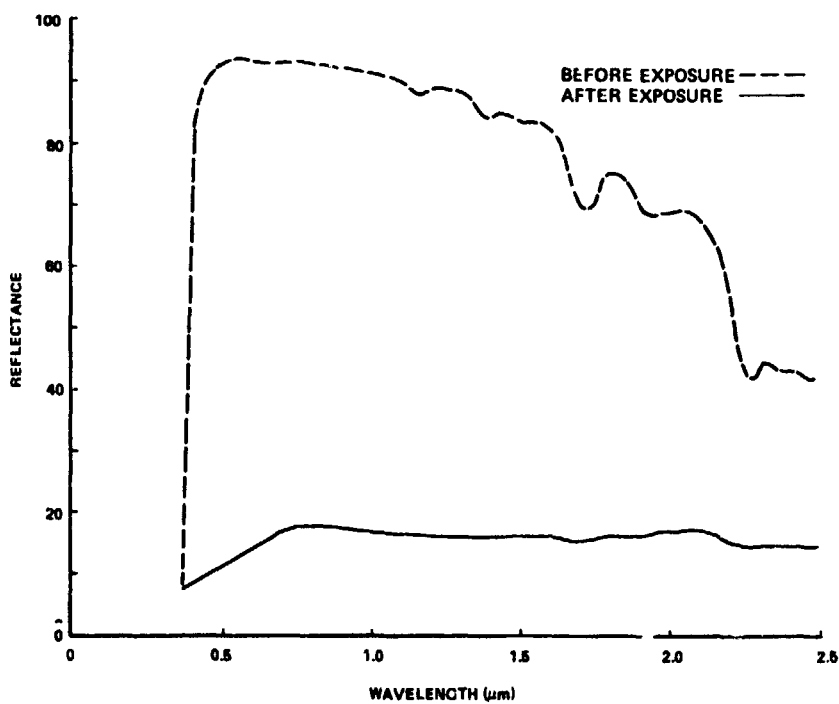


Figure I-57. S13G sample 004.

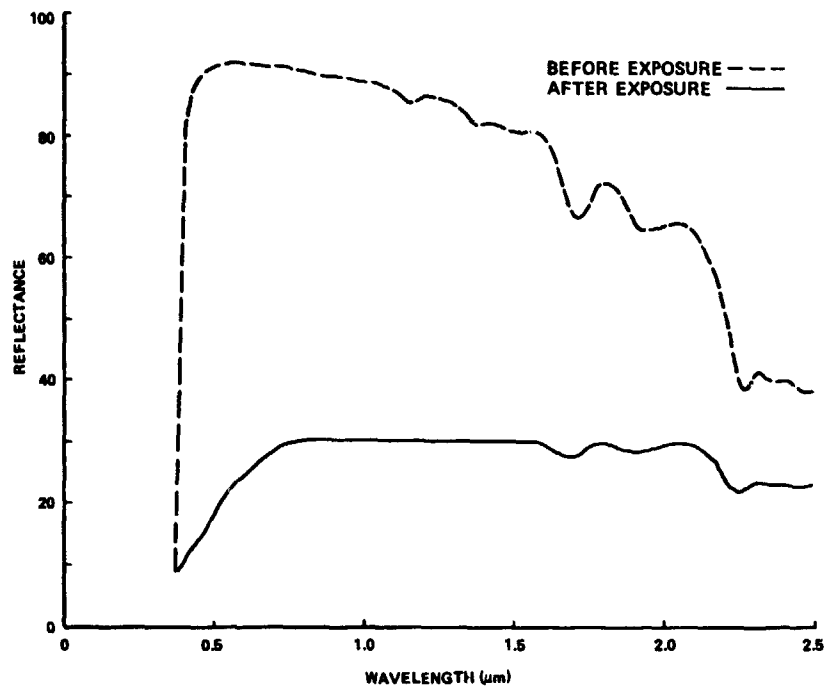


Figure I-58. S13G sample 005.

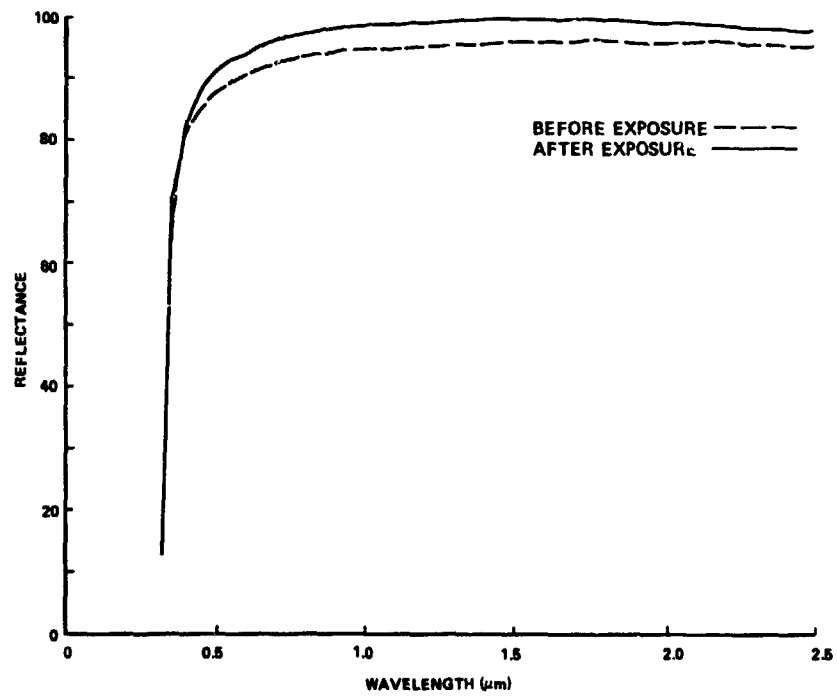


Figure I-59. Silver-teflon sample 1.

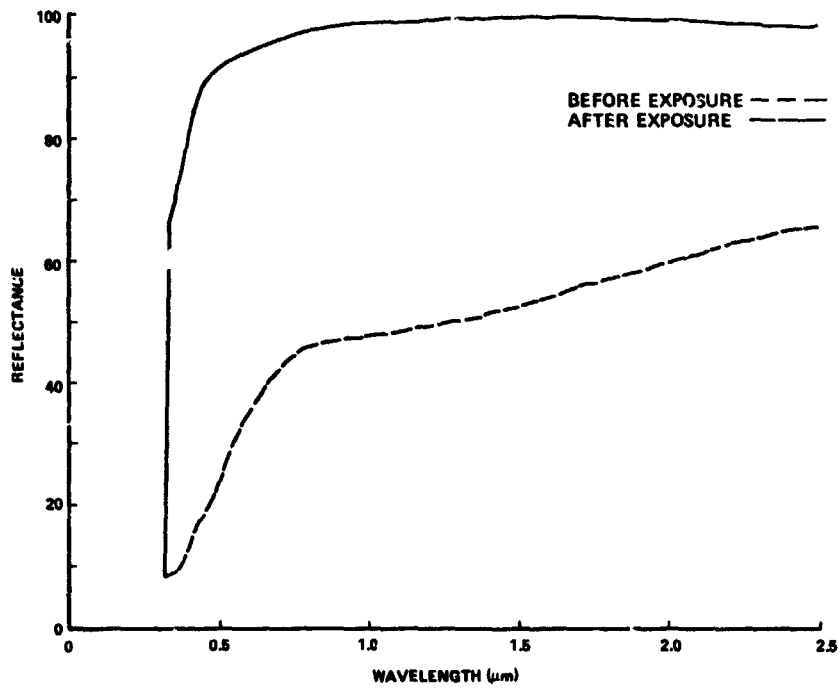


Figure I-60. Silver-teflon sample 2.

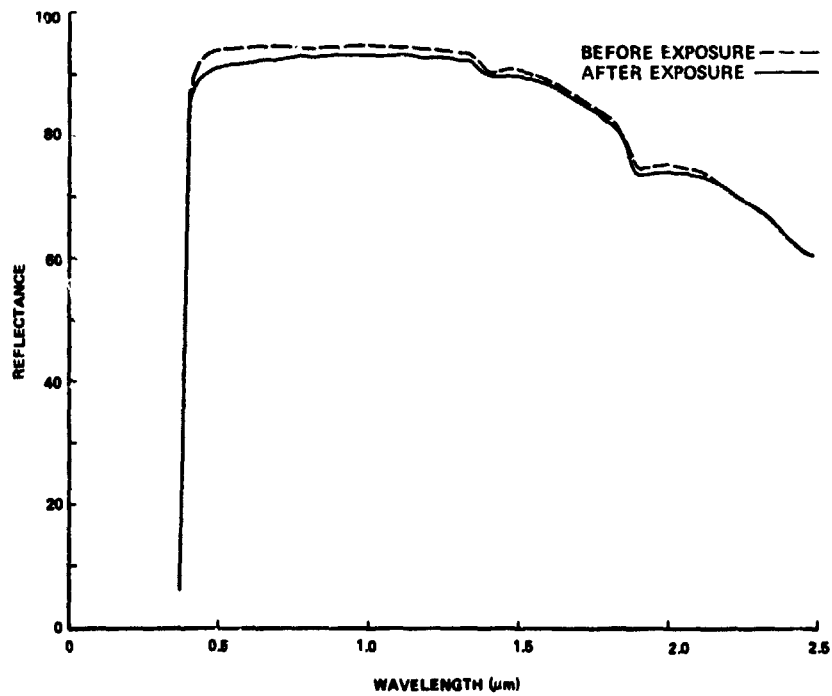


Figure I-61. Z-93 sample 101.

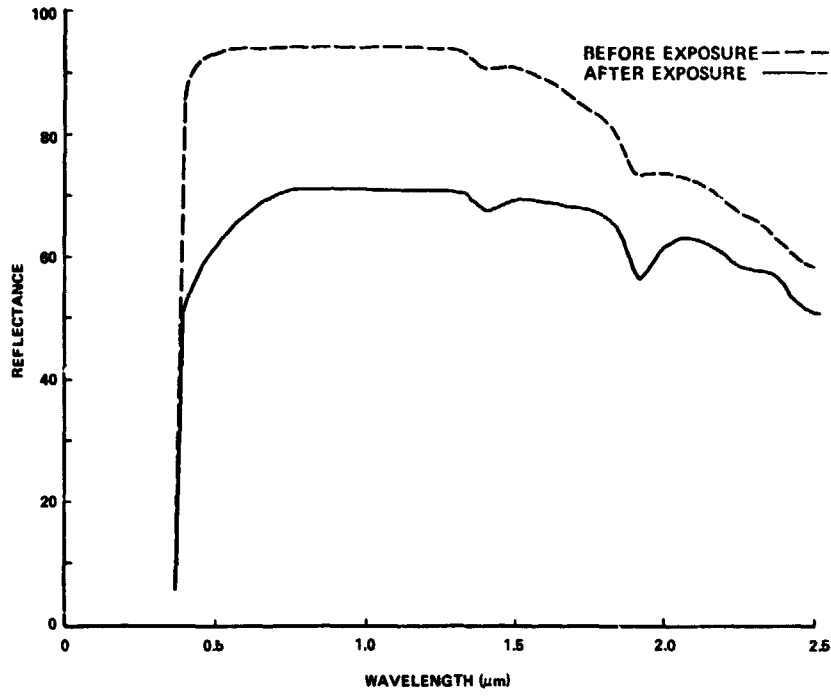


Figure I-62. Z-93 sample 103.

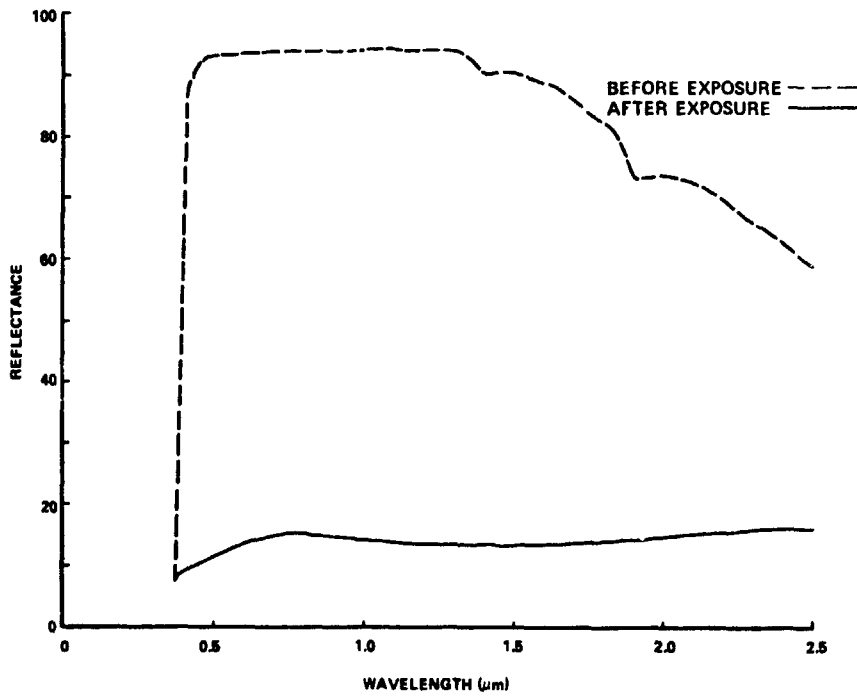


Figure I-63. Z-93 sample 106.

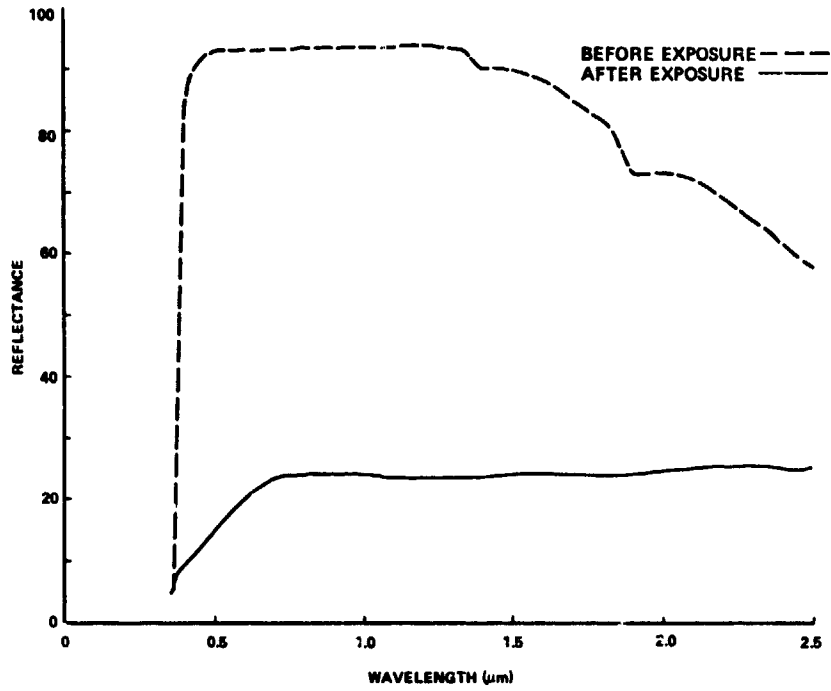


Figure I-64. Z-93 sample 107.

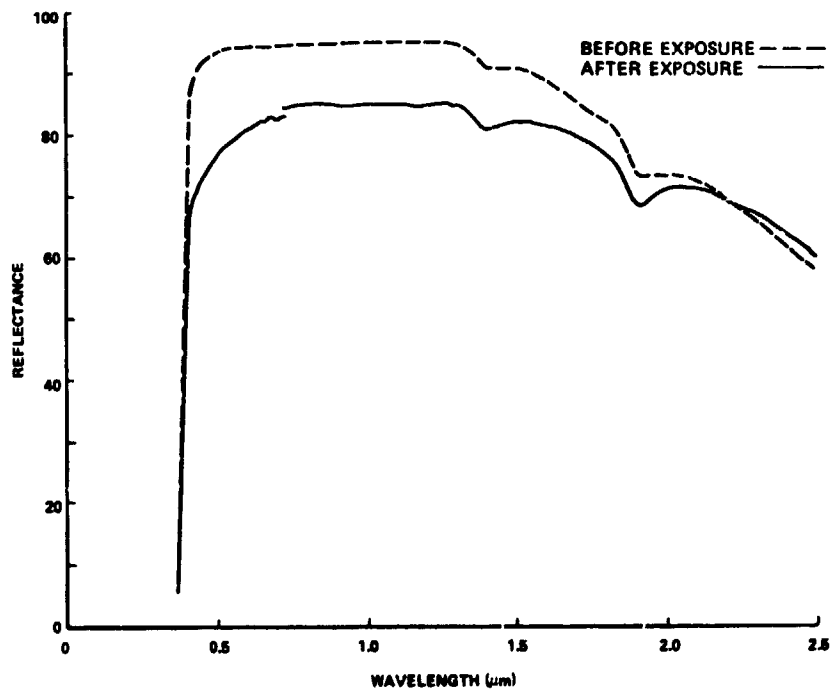


Figure I-65. Z-93 sample 108.

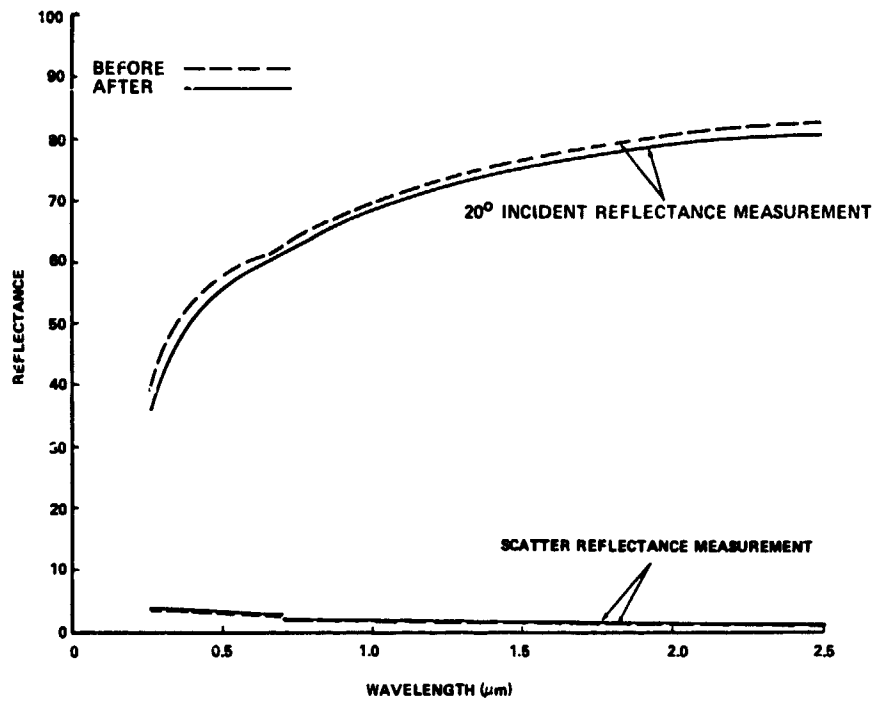


Figure I-66. Platinum mirror sample 201.

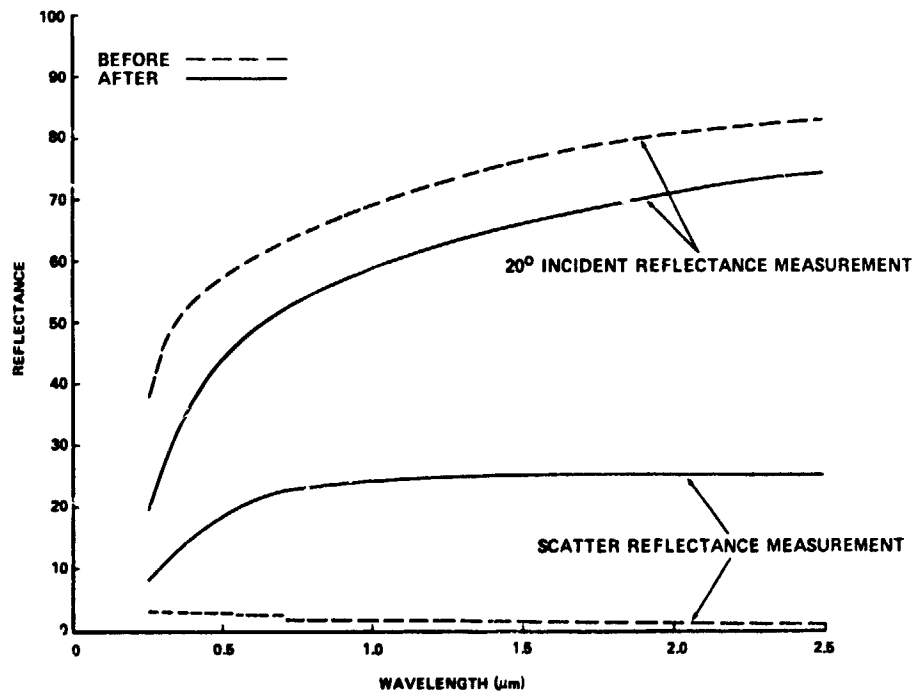


Figure I-67. Platinum mirror sample 202.

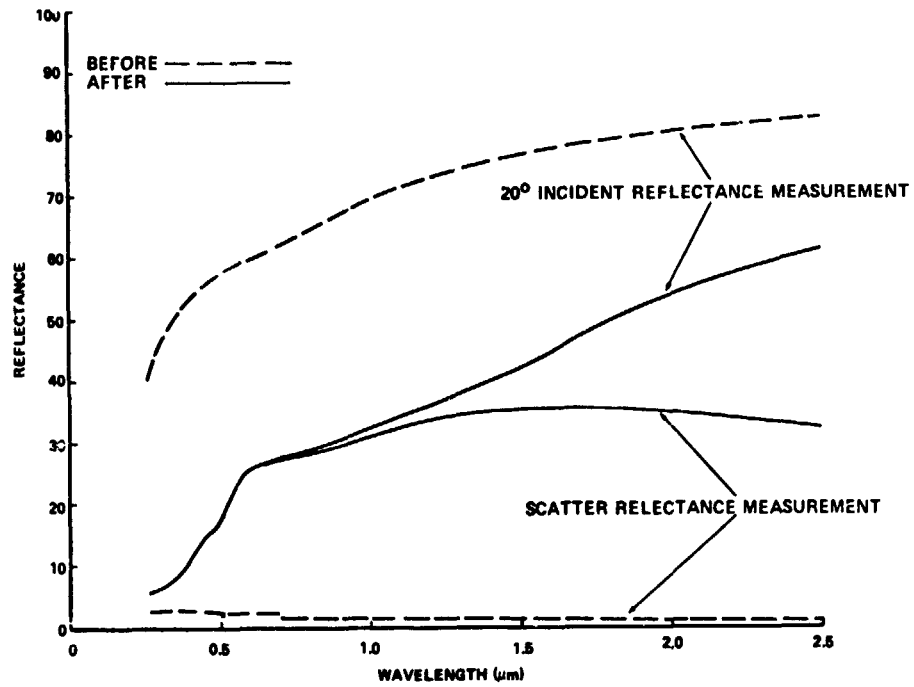


Figure I-68. Platinum mirror sample 203.

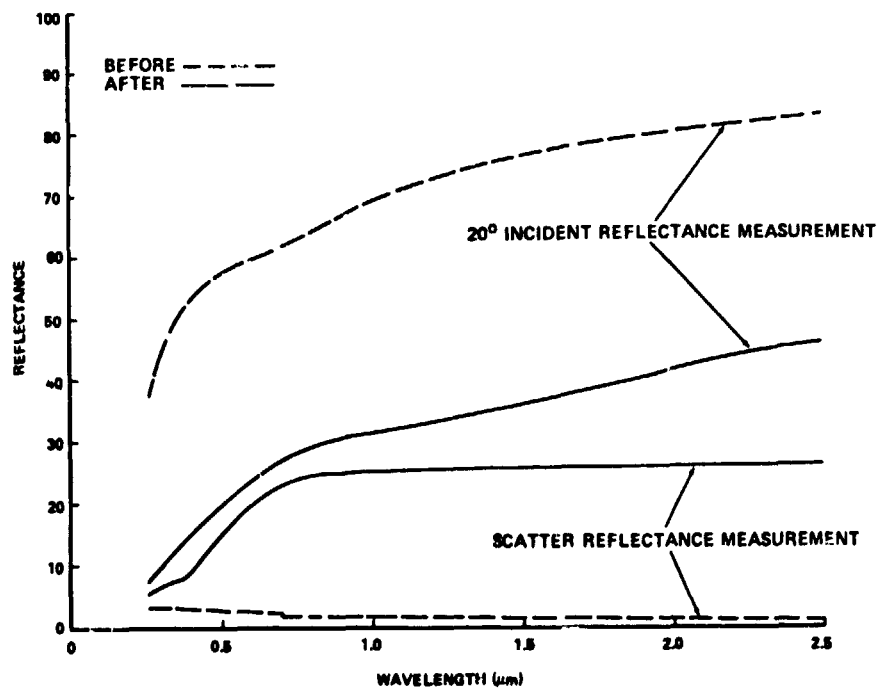


Figure I-69. Platinum mirror sample 204.

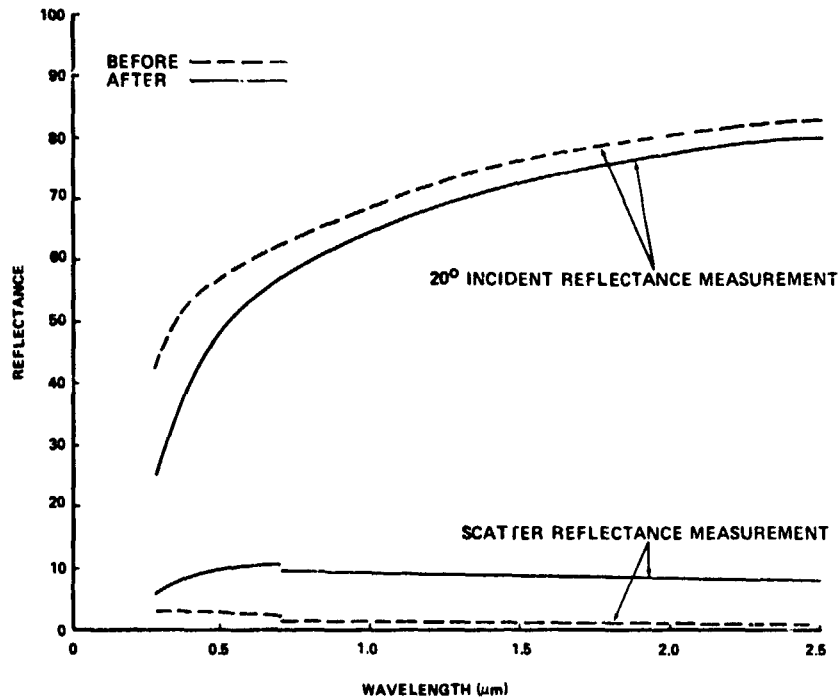


Figure I-70. Platinum mirror sample 205.

TABLE I-8. SAMPLE LOCATIONS

Sample	Sample No.	Sample Location
Platinum Mirror	201	Cargo bay box (facing up)
Platinum Mirror	202	6.35 m (250 in.) radially facing down 6.1 m (20 ft) level
Platinum Mirror	203	2.54 m (100 in.) radially facing down 6.1 m (20 ft) level
Platinum Mirror	204	2.54 m (100 in.) radially facing down 6.1 m (20 ft) level
Platinum Mirror	205	6.35 m (250 in.) radially at top of cargo bay box 6.1 m (20 ft) level facing up

N76-16171

SECTION II. THE SMALL MOTOR PLUME/MATERIAL IMPINGEMENT TEST PROGRAM AT MSFC UTILIZING NINE DIFFERENT PROPELLANT FORMULATIONS (APRIL AND MAY 1974)

A. Introduction⁴

The specific objective of this test was to evaluate the relative effects of several candidate SSRM propellant formulations and their plume impingement effects on HRSI and RCC materials.

Rockwell International had the overall responsibility for the small motor plume/material impingement test program. NASA/MSFC and NASA/JSC directed and conducted significant portions of this test program. The small motor test firings were conducted by MSFC at the MSFC test position 112 altitude test facility. Rockwell personnel were present at MSFC to monitor the test operations and analyze test results.

Nine solid propellant formulations were tested. The selected propellant matrix allowed an evaluation of propellants with and without metal additives, with and without burning rate catalyst, and low (approximately 1927° C) and high (approximately 2649° C) combustion temperatures.

Motors were fired at a simulated SRB staging altitude of 3.96 km (130 000 ft) (nominal). The altitude pressure was predicted to drop approximately 0.6 km (20 000 ft) during a motor firing. All motors were loaded with 1.8 to 2.3 kg (4 to 5 lb) of propellant and burned for approximately 2 s.

Two types of motor tests were performed:

1. Plume calibration firings — for the primary purpose of establishing physical and thermal characteristics of the exhaust plumes.
2. Material exposure firings — to determine the effects of plume impingement on samples of orbiter TPS material at several locations in the rocket plume.

The plume calibration test of a given propellant/motor type was performed in a single firing that preceded the material exposure tests. During plume calibration tests heat flux, total pressure, and solid particle size and

4. This test series conducted at MSFC was under the direction of William F. Richardson, Office of Associate Director for Engineering.

mass flux were measured at selected locations in the plume. The results were compared with analytical predictions established prior to the test. Materials to be exposed to the rocket plume were HRSI and RCC samples. HRSI was the primary material to be tested because a greater number of samples were available for the test. RCC samples were tested in selected firings where good HRSI survival characteristics have been demonstrated in a prior test with the same motor/propellant type.

Several inspection methods were employed to establish the post-test condition of the material samples. The HRSI and the RCC materials were considered to pass the SSRM plume exposure test if there was no detectable degradation of the coating.

Nine propellant formulations were tested; eight composite propellant formulations and one double base. The composite propellants were mixed and cast into test motors by the Jet Propulsion Laboratory. The double-base propellant grain was mixed and cast by the Naval Ordnance Station, Indian Head, Maryland.

The composite propellant formulations are numerically designated in Table II-1 for identification purposes. Table II-1 also shows the chemical formulation of the eight composite propellants. The double-base propellant is identified as propellant No. 9, and the chemical formulation is shown in Table II-2.⁵

A flow chart of the three experimental techniques used by SSI to support these tests is shown in Figure II-1. This chart also includes the names of the experimenters. The test firing number, date, type of firing, propellant type, position of the holographic film box, and filter data are shown in Table II-3. The axial distance from the motor nozzle to all particle collectors was 101.6 cm (40 in.) and the radial distance is designated.

The results of these experiments are detailed in the following subsections.

5. For further details of motor characteristics the reader is referred to Don Denison at Rockwell International, who has the details, or William F. Richardson at MSFC.

TABLE II-1. COMPOSITE PROPELLANT FORMULATIONS

Ingredient	Propellant Formulation Number							
	1	2	3	4	5	6	7 ^b	8
AP (wt. %)	79.00	86.00	76.5	83.9	77.7	78.50	82.00	78.00
HTPB ^a (wt. %)	21.00	14.00	21.50	14.00	20.30	20.50	-	20.50
CTPB ^a (wt. %)	-	-	-	-	-	-	12.00	-
Al (wt. %)	-	-	2.00	2.00	-	-	4.00	-
Al ₂ O ₃ (wt. %)	-	-	-	-	2.00	-	-	0.50
Fe ₂ O ₃ (wt. %)	-	-	-	0.10	-	1.00	2.00	0.50
Graphite (wt. %)	-	-	-	-	-	-	-	0.50

a. Contains cure catalyst.

b. Saturn S-II ullage propellant.

Abbreviations: AP - Ammonium Perchlorate

HTPB - Hydroxy Terminated Polybutadiene

CTPB - Carboxyl Terminated Polybutadiene

Al - Aluminum

Al₂O₃ - Aluminum Oxide

Fe₂O₃ - Ferric Oxide

TABLE II-2. DOUBLE-BASE PROPELLANT FORMULATION
(PROPELLANT NO. 9)

Ingredient	Weight (%)
Nitrocellulose (12.6% N)	60.38
Nitroglycerin	22.08
Dinitrotoluene	6.80
Dimethylphthalate	9.60
Ethyl Centralite	1.00
Carbolic I	0.14

B. Solid Particle Collection

David W. Jex

Two different techniques were used in collecting solid particles present in the solid rocket exhaust plume. Figure II-2 shows the design of the particle collector/calibration boxes. Particles enter the 0.0635 cm (0.25 in.) diameter orifice and are collected by the baffle. Four of these boxes were fabricated to permit simultaneous particle collection at each of the four radial locations in the plume. The baffle also isolated the pressure transducer tube from the entering particles.

A second particle collection technique which utilizes a screen trap is indicated in Figure II-3. Two particle collection screen devices are mounted side by side on one of the 3.81 cm (1.5 in.) diameter pipe mounting fixtures. This arrangement permits two different collector screen configurations to be used at the same radial position during a single firing. The details of a filter collector are shown in Figure II-4. The total mass collected by these two techniques is given in Tables II-4 and II-5.

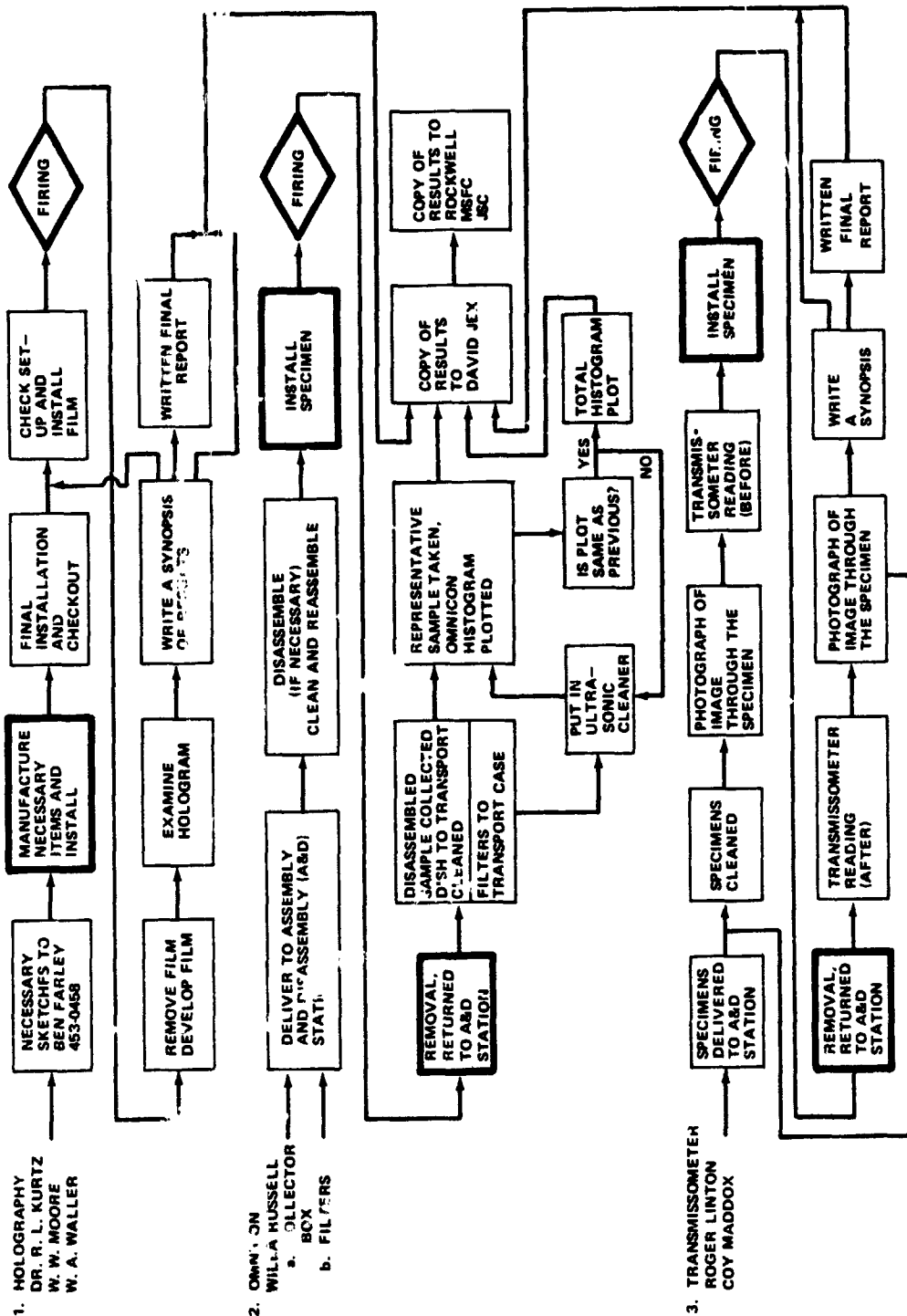


Figure II-1. Active experiments flow chart.

TABLE II-3. TEST FIRING DATA

Test Firing Number	Date of Test	Type of Firing		Propellant Type	Holograph Film Box Protector (cm)	Filters	
		Calibration	Material			S/N	Position (cm)
1	Thurs., April 18	X		7			
2	Fri., April 19		X	7			
3	Mon., April 22		X	7			
4	Tues., April 23	X		8			
5	Wed., April 24		X	8			
6	Thurs., April 25	Recal.		1	12.7		
7	Fri., April 26		X	8	12.7		
8	Mon., April 29	Recal.		1	-		
9	Tues., April 30		X	1	-		
10	Wed., May 1	X		3	58.9	001, 002	38.1
11	Wed., May 1		Ignitor Only	9	58.9	-	
12	Thurs., May 2		X	3	38.1	007, 009	38.1
13	Fri., May 3	X		2	-	-	
14	Mon., May 6		X	2	-	-	
15	Tues., May 7	X		6	38.1	-	
16	Wed., May 8		X	6	38.1	-	
17	Thurs., May 9		X	1	38.1	-	
18	Thurs., May 1		X	2	(Shutter)	-	
19	Fri., May 10	X		5	38.1	-	
20	Mon., May 13		X	5	38.1	-	

TABLE II-3. (Concluded)

Test Firing Number	Date of Test	Type of Firing		Propellant Type	Holograph Film Box Protector (cm)	Filters	
		Calibration	Material			S/N	Position (cm)
21	Mc., May 13	Holography		3	12.7	006, 010	12.7
22	Tues., May 14	X		4	38.1	003, 006	38.1
23	Tues., May 14	X		4	38.1	-	-
24		Misfire		9	38.1	-	-
25	Wed., May 15	X		5		004, 009	38.1
26	Thurs., May 16	Misfire		9	38.1	-	-
27	Thurs., May 16	X		9	38.1	-	-
28	Fri., May 17	X		-	38.1	-	-
29	Fri., May 17	X		-	38.1	-	-
30	Mon., April 21	X		3	-	-	-
31	Mon., April 21	X		6	-	-	-
32	Tues., April 22	X		9	-	-	-

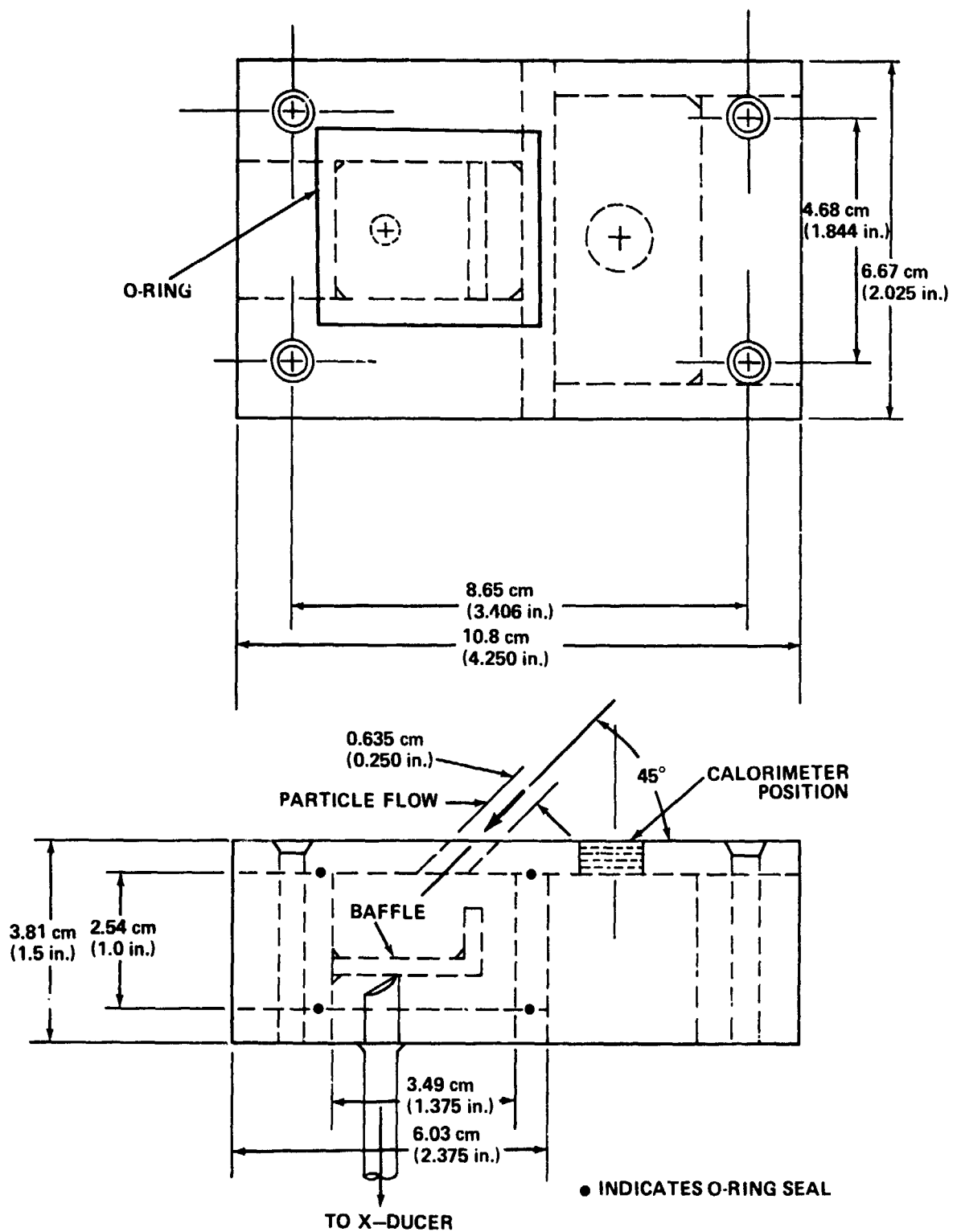


Figure II-2. Particle collector/calibration box.

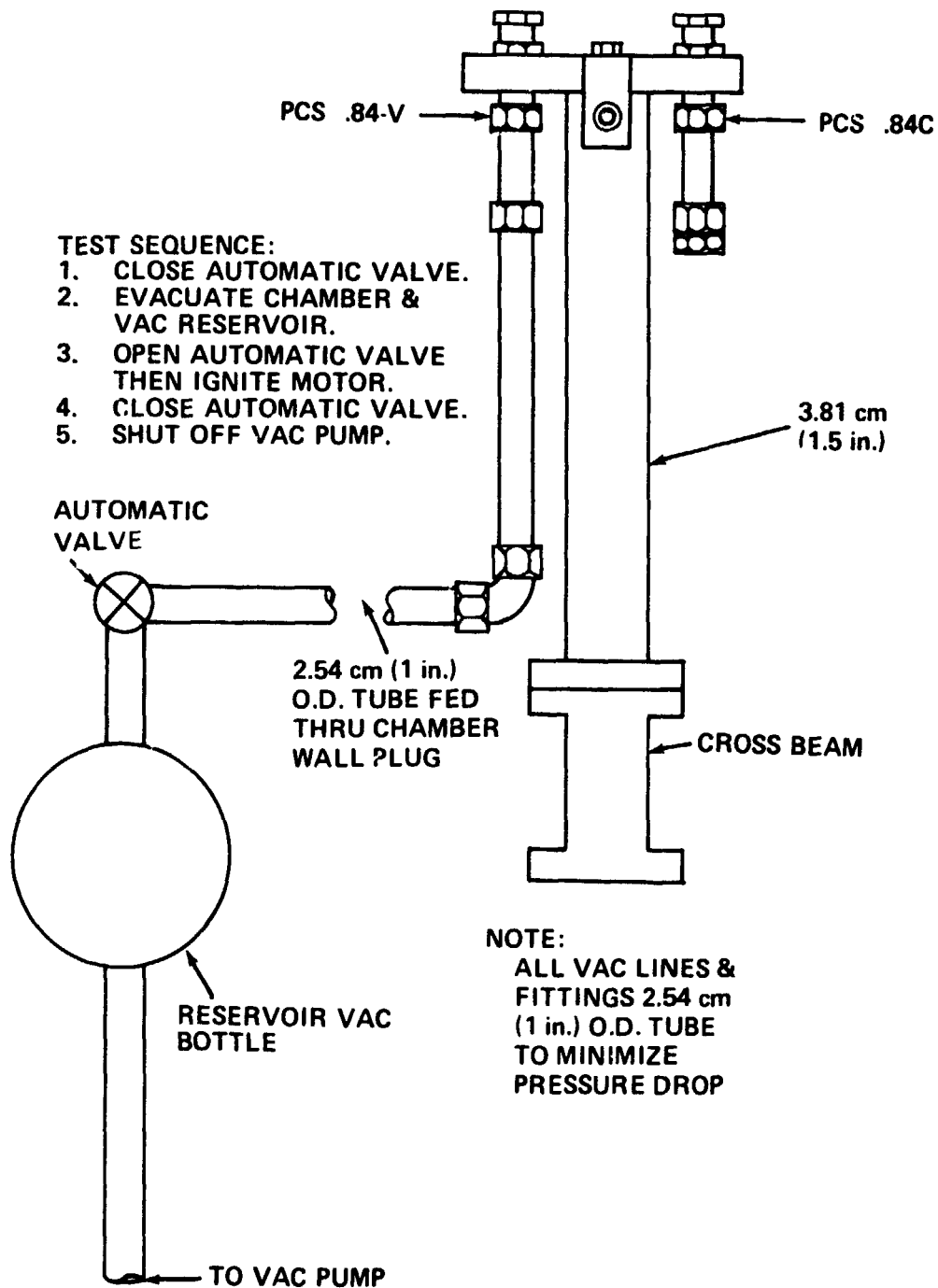


Figure II-3. Particle collection screen assembly schematic.

1. 10 μm OPENING STAINLESS STEEL WIRE MESH.
2. PROTECTION AND CONFINEMENT OF FLOW TUBING
3. INLET AND/OR OUTLET NUT

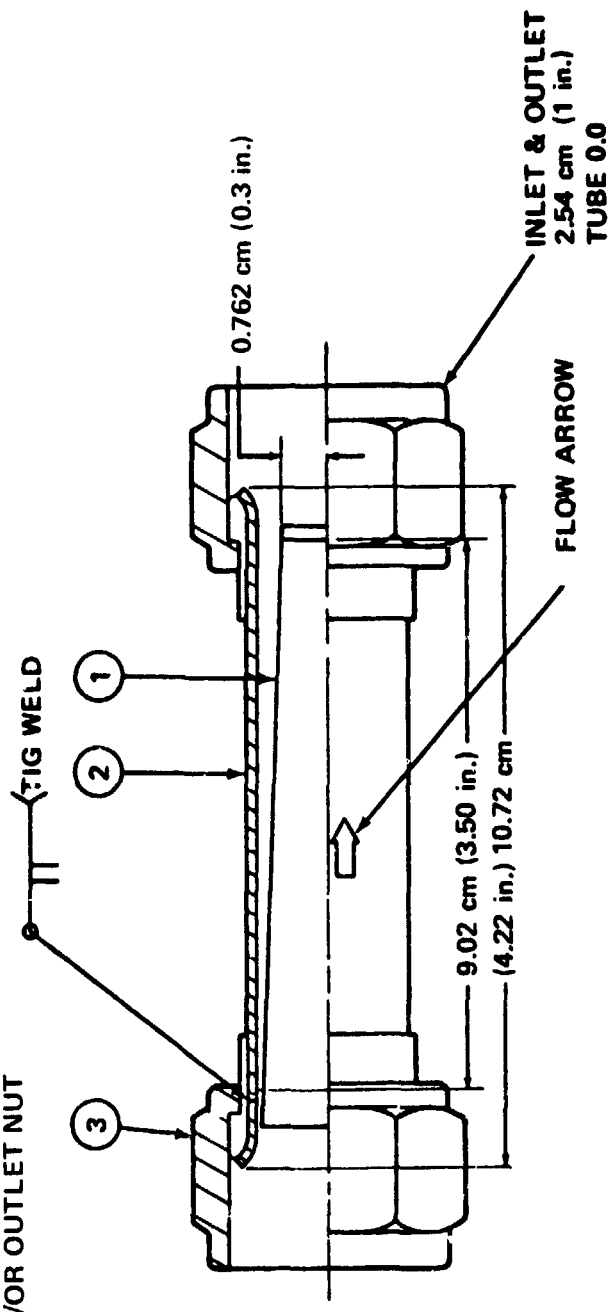


Figure II-4. Filter assembly.

TABLE II-4. WINDTEK FILTERS - TOTAL MASS COLLECTED

Test Firing No.	Propellant Formulation	Filter Weights (gm)	S/N	Position (cm)	Inlet and Exit Plug Residue (gm)
10	3	352.6278	001	38.1	18.52718
		<u>352.6134</u>			<u>18.51831</u>
		0.0144			0.00887
	3	346.2466	002	38.1	18.70191
		<u>346.2075</u>			<u>18.68417</u>
		0.0391			0.01774
12	3	346.4548	007	38.1	18.52188
		<u>346.4326</u>			<u>18.50585</u>
		0.02222			0.01603
	3	349.1396	009	38.1	18.74671
		<u>349.1275</u>			<u>18.73181</u>
		0.0121			0.01490
21	3	346.2316	006	12.7	18.88427
		<u>346.1174</u>			<u>18.87007</u>
		0.1142			0.01421
	3	348.1734	010	12.7	18.65214
		<u>348.1344</u>			<u>18.63926</u>
		0.0390			0.01288
	3	346.8400	003	38.1	18.51523
		<u>346.8097</u>			<u>18.50518</u>
		0.0103			0.01005
	3	349.2570	005	38.1	18.75631
		<u>349.2531</u>			<u>18.74589</u>
		0.0039			0.00942
23	4	346.2716	004	38.1	18.68337
		<u>346.2514</u>			<u>18.67765</u>
		0.0202			0.00572
		346.2064	008	38.1	18.60909
		<u>346.1785</u>			<u>18.60372</u>
		0.0279			0.00537

TABLE II-5. PARTICLE COLLECTION BOXES — TOTAL MASS COLLECTED

Test Firing No.	Propellant Formulation	12.7 cm (gm)	27.9 cm (gm)	38.1 cm (gm)
1	7	Petri dishes were not weighed prior to collection of residue; therefore, no total mass measurement was made.		
4	8	18.78372 <u>18.76390</u> 0.01982	18.72684 <u>18.72444</u> 0.00240	18.59805 <u>18.58762</u> 0.01043
6 Recalibration	1	18.59345 <u>18.57774</u> 0.01571	18.64412 <u>18.63269</u> 0.01143	18.47014 <u>18.46135</u> 0.00870
8 Recalibration	1	18.69593 <u>18.68139</u> 0.01354	18.32897 <u>18.31527</u> 0.01370	18.67709 <u>18.64466</u> 0.03243
10	3	18.64643 <u>18.61509</u> 0.03134	18.81229 <u>18.80117</u> 0.01112	18.50392 <u>18.48911</u> 0.01481
13	2	18.58572 <u>18.55838</u> 0.02734	18.55976 <u>18.54351</u> 0.01625	18.63887 <u>18.62372</u> 0.01515
15	6	18.52391 <u>18.50475</u> 0.01916	18.44047 <u>18.42794</u> 0.01253	18.44585 <u>18.43809</u> 0.00776
19	5	18.48964 <u>18.45140</u> 0.03824	18.86243 <u>18.84459</u> 0.01784	18.77892 <u>18.65277</u> 0.12615
22	4	18.84887 <u>18.80723</u> 0.04164	18.73097 <u>18.56481</u> 0.16526	18.53374 <u>18.66667</u> -0.13293
26	9	18.45153 <u>18.43892</u> 0.01261	18.58671 <u>18.57874</u> 0.00797	18.65713 <u>18.64663</u> 0.01050

The activities in cycling the particle collector devices from firing to firing can be separated from the actual particle analysis since the collected samples were removed from the test equipment and placed in labeled containers. The general procedure following a firing was to inspect the collector for damage, remove the sample holders, transfer the contents into appropriately labeled containers, wash the containers and other contaminated components with alcohol, dry and clean with an air jet, and reinstall the collector parts as required. If spare parts were available, as in the case of the particle collector screens, the particle removal and some of the cleanup operations were delayed until later. The collection process was generally completed within 30 minutes from the time the chamber was opened.

It should be noted that on both collection devices there was a corrosive effect which became more pronounced as the tests proceeded. It is suspected that the hydrochloric acid (HCl), which is a resulting component of solid propellant combustion, reacted with the stainless steel components of the collecting devices.

It was observed that the corrosive effect became critical to the sampling procedure after approximately 24 hours. This observation directed modifications in the collection techniques. The modifications minimized the time elapsed between firing and collection of the samples.

C. Particle Size Analysis

Willa Russell, Keith Janasak, and Dan Gates

1. Preparation of Slurries

The filters and components were delivered to the laboratory wrapped in disposable paper. Two filters were wrapped in each packet. The slurries were prepared as follows.

Each filter and components was immersed in 750 ml of pure ethyl alcohol in a 1000 ml beaker. The beaker was placed in an ultrasonic cleaner containing enough water to completely surround the beaker to the level of the alcohol. The beaker and contents were vibrated in the ultrasonic cleaner for 10 minutes. The filter and holder were removed from the solution and each set was individually wrapped in lintless paper. The alcohol solution was then heated to approximately 149° C and allowed to boil-off until only 150 to 200 ml of the solution remained. The beaker was then removed from the heating element and allowed to cool. Once cooled, the beaker was placed in an ultrasonic cleaner for approximately 30 s to cause any settled particles to regain a state of suspension, thus allowing all particles present to be transferred into a marked, capped storage bottle.

2. Preparation of Slides

Each bottled slurry was shaken vigorously to obtain a homogeneous mixture, and approximately 100 ml was drawn off using a large dropper. Of this 100 ml sample all but 5 ml was delivered to Dr. McNutt, Athens College, for analysis to determine the percentage of aluminum present. The remaining 5 ml was placed in a small beaker and stained using two drops of alidyne, a selective staining agent with a preference for aluminum oxide. The particles viewed in an unstained sample were translucent and of such low contrast with the background that boundary detection by the scanner was reduced markedly. The staining was, therefore, to aid in the determination of the edges of the individual particles. The 5 ml of solution was shaken well prior to being deposited on the surface of a clean standard microscope slide. The slide was then placed on a clean bench and allowed to dry.

These specimens and those collected in the boxes were processed through the scanning procedure.

3. Scanning Procedure

The automated transmissive light microscope scanned an area of approximately 5000 by 5000 μm at a total magnification of 400X. The software in the processing unit prevented overlapping of fields in the counting procedure. The processor counted the number of features present in the field of view having a maximum horizontal chord greater than a preset value specified by the operator. The feature counts were made using consecutively higher preset values for the horizontal chord from 0.5 μm to 100 μm in steps of 0.5 μm from 0.5 μm to 10 μm , 40 μm from 10 μm to 50 μm , and 50 μm from 50 μm to 100 μm . The processor then calculated the differences in number of features from one size setting to the next to determine the total number of features with horizontal chords in that size range. Since the maximum horizontal chord measurement is dependent on orientation of the features in the field of view and the measuring disk was placed randomly on the microscope stage, measurements were made two separate times on each slide and the resulting counts were averaged. With this procedure we hoped to minimize the orientation factor. Histograms of these averages for each filter are given. Because of the lack of phase contrast capability to aid in detection of particles on low contrast samples such as these, the lower limiting size that could be detected was 1.5 to 2 μm in diameter. All histogram plots, Figures II-5 through II-10 show the averaged size distribution above 1.5 μm or, in some cases, 2 μm . Figures II-11 through II-16 show second degree polynomial curve fits of the size distribution for each filter.

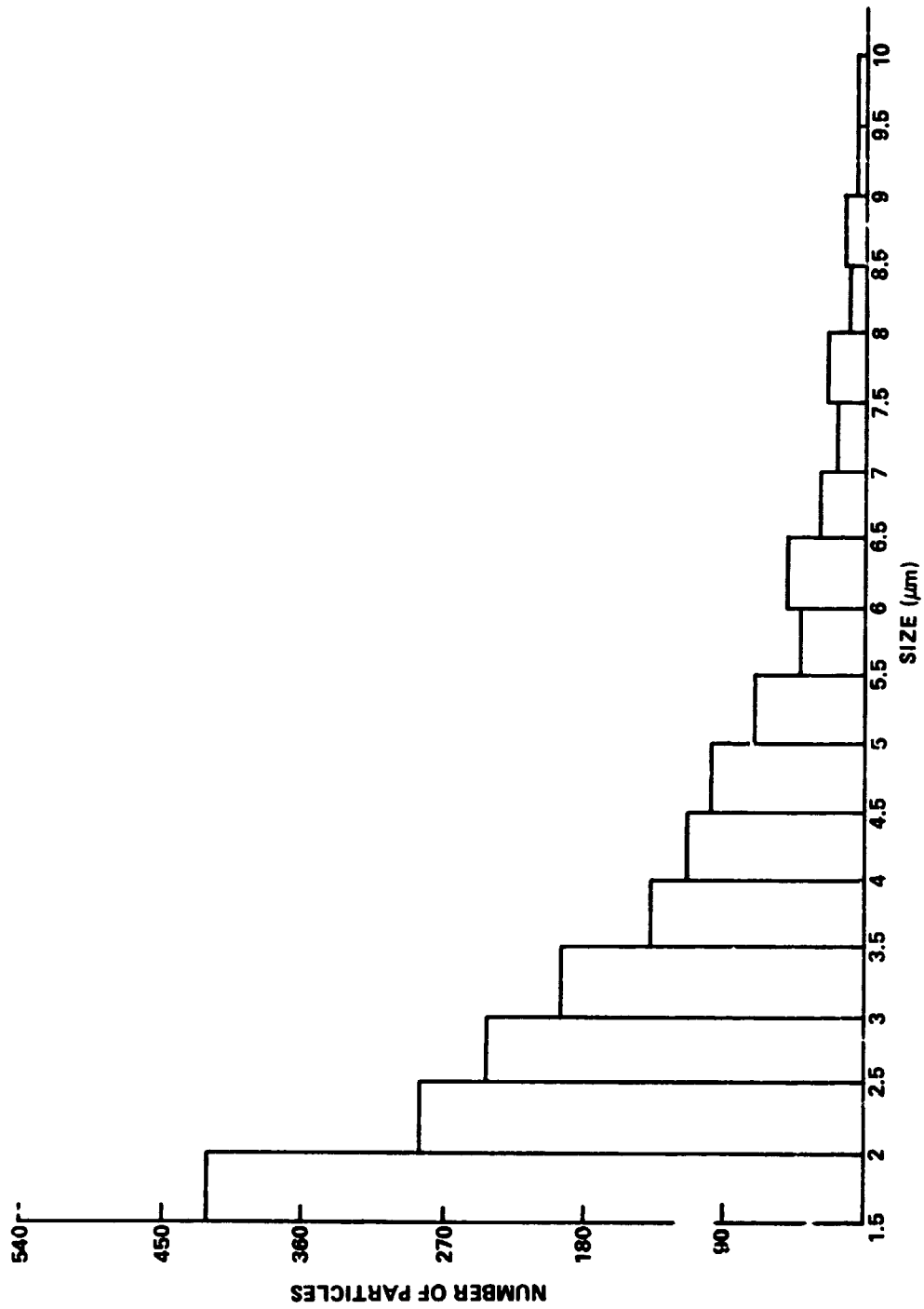


Figure II-5. Particle size distribution, filter S/N 003, propellant 3, firing 21, 38.1 cm (15 in.).

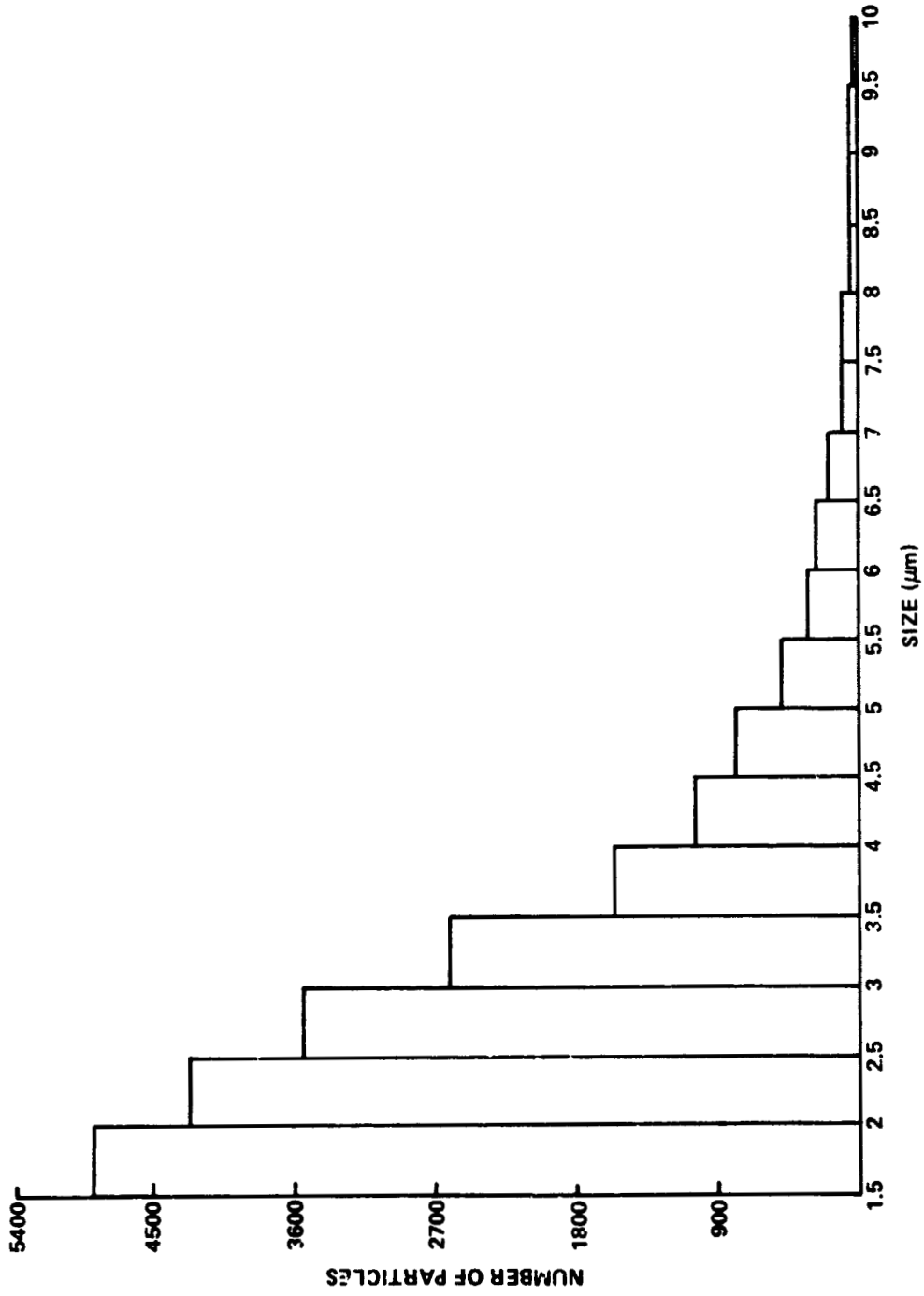


Figure II-6. Particle size distribution, filter S/N 005, propellant 3, firing 21, 38.1 cm (15 in.).

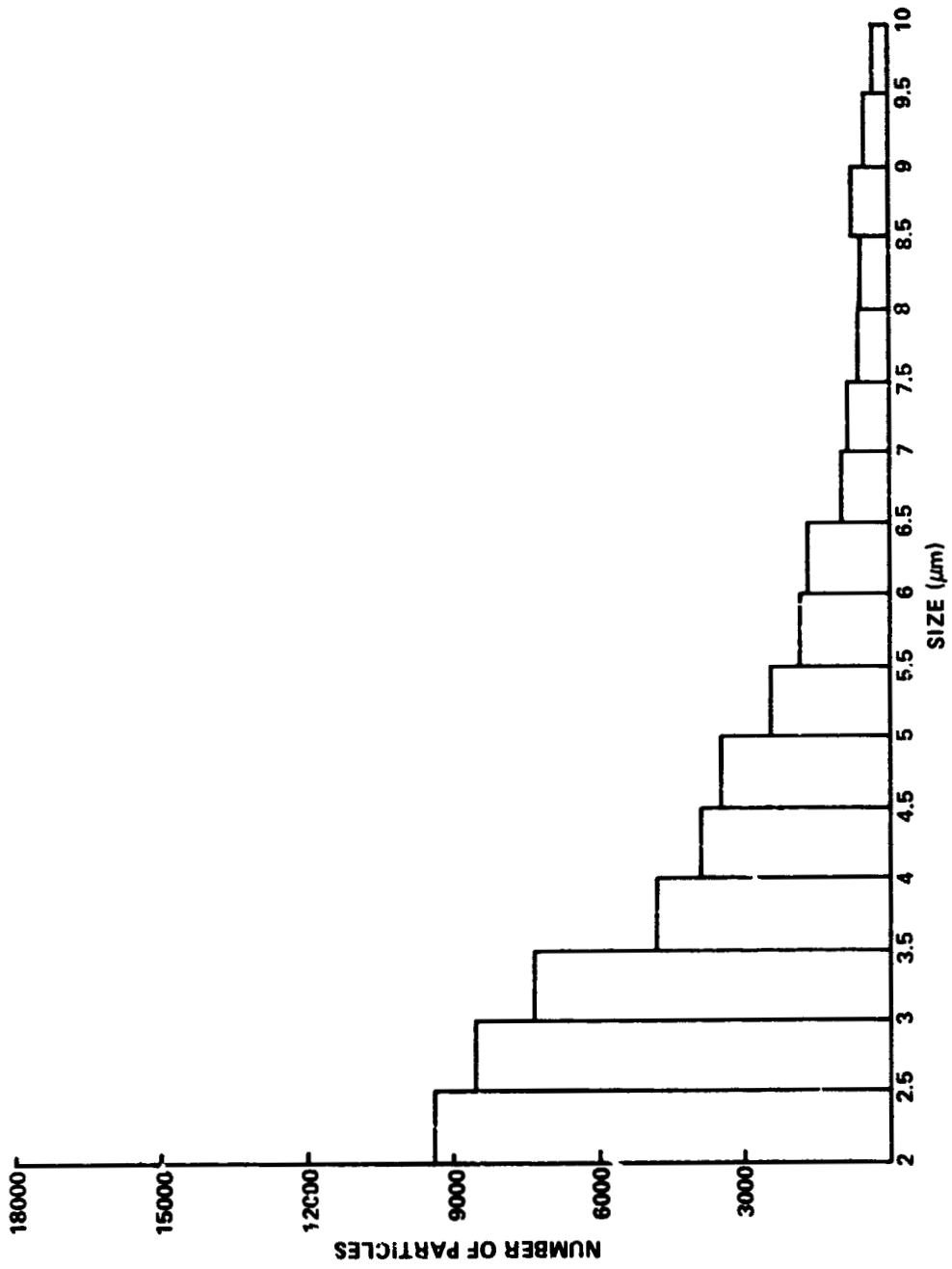


Figure II-7. Particle size distribution, filter S/N 006, propellant 3, firing 21, 12.7 cm (5 in.).

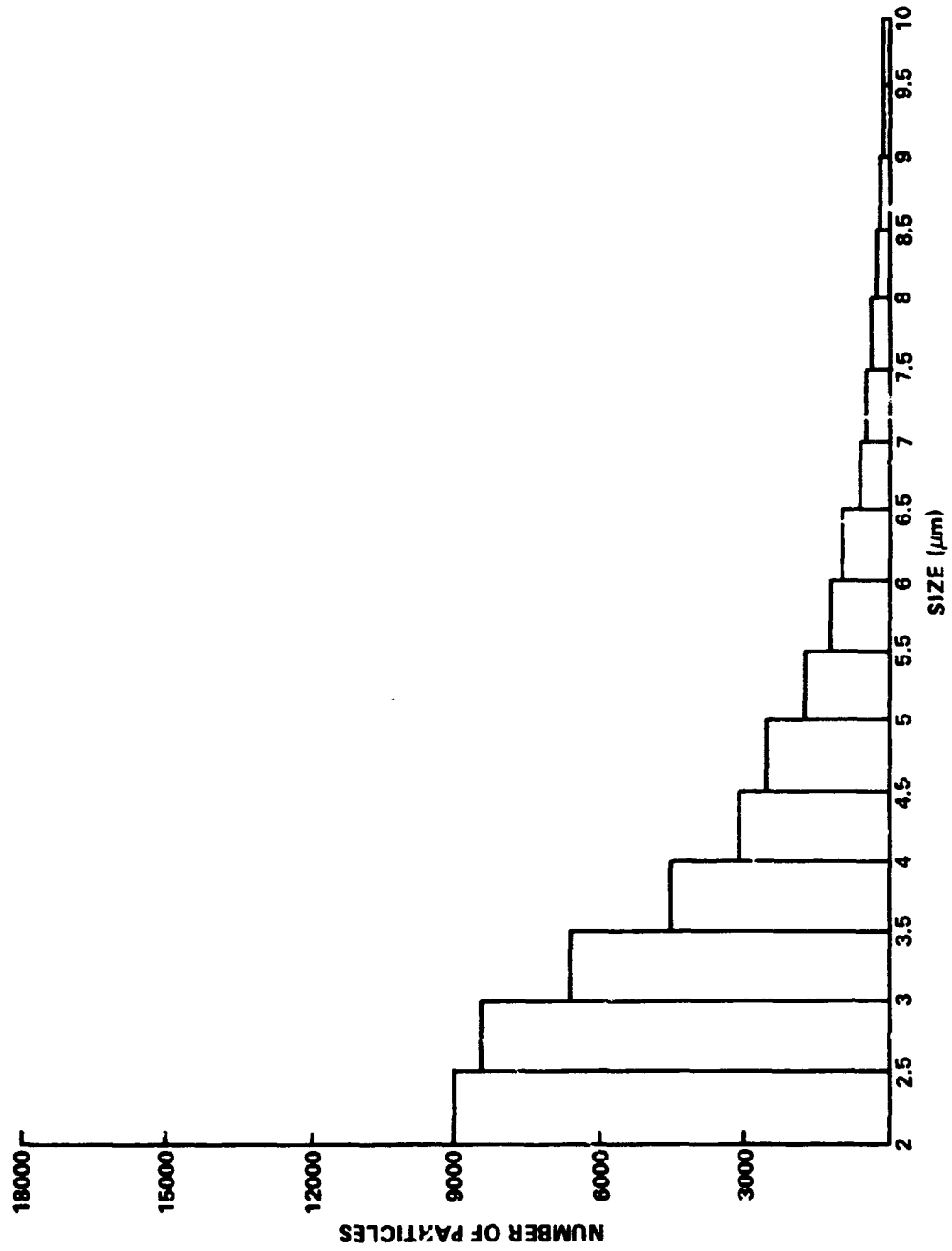


Figure II-8. Particle size distribution, filter S/N 010, proellant 3, firing 21, 12.7 cm (5 in.).

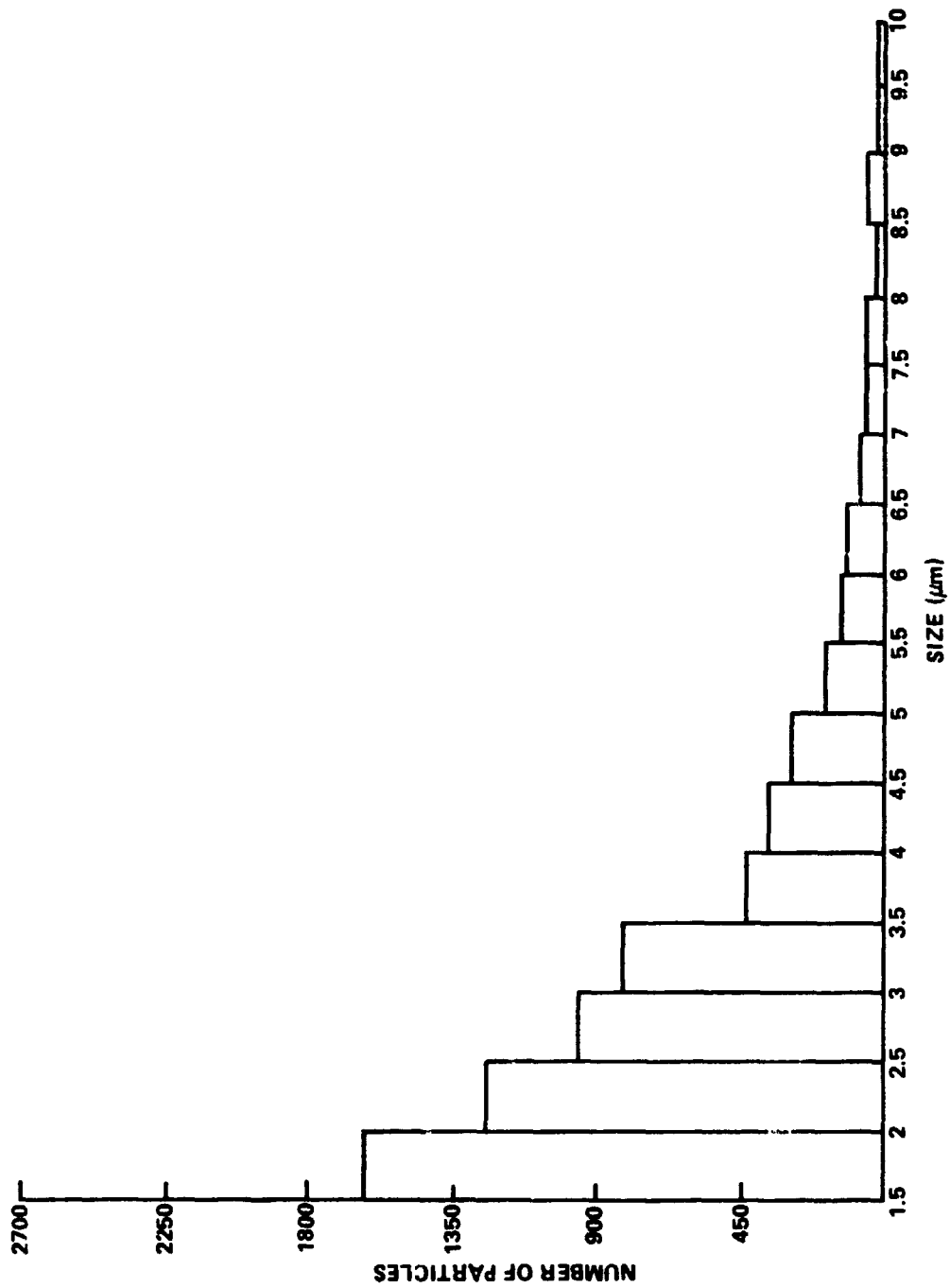


Figure II-9. Particle size distribution, filter S/N 001, propellant 3, firing 10, 38.1 cm (15 in.).

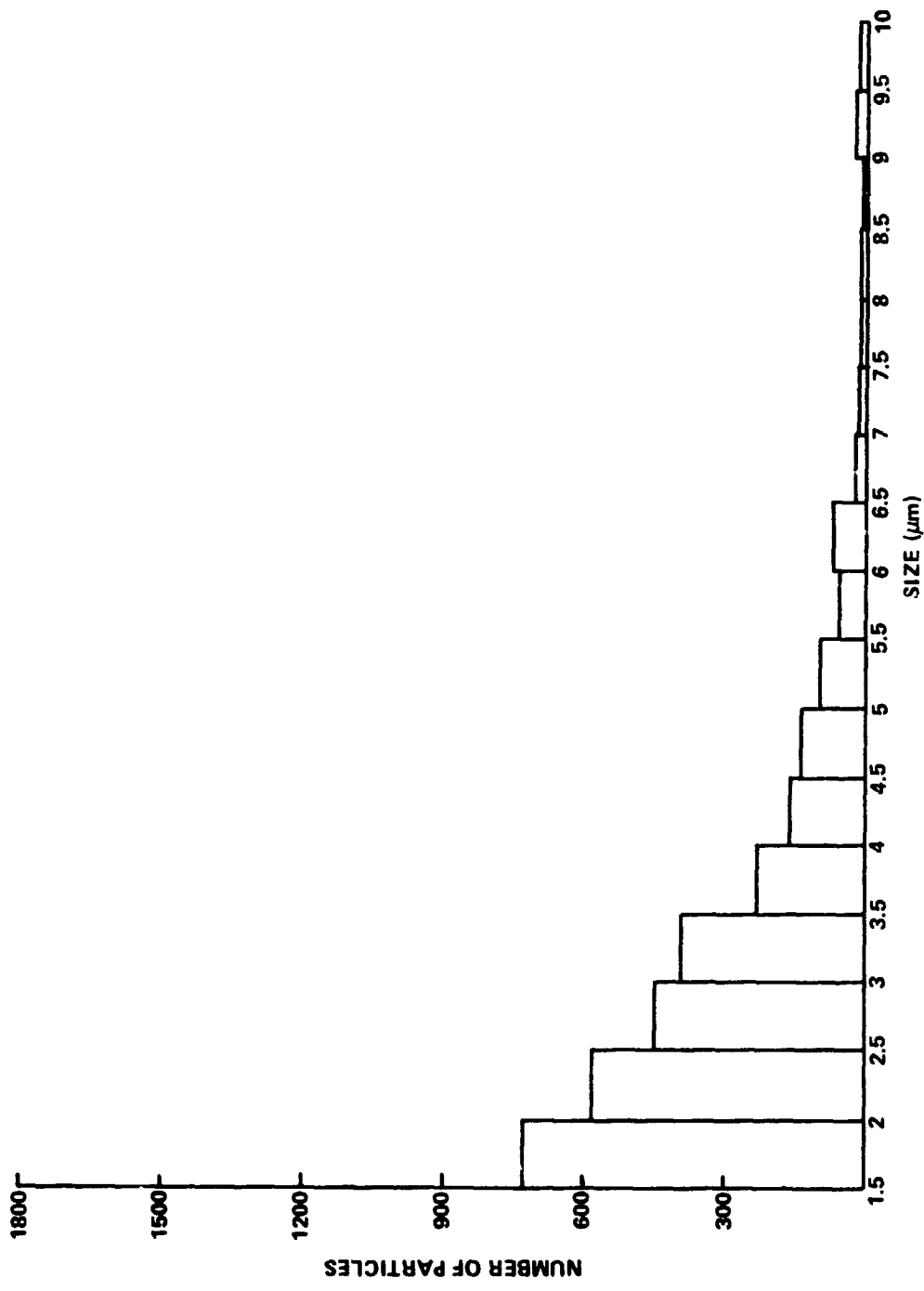


Figure II-10. Particle size distribution, filter S/N 002, propellant 3, firing 10, 38.1 cm (15 in.).

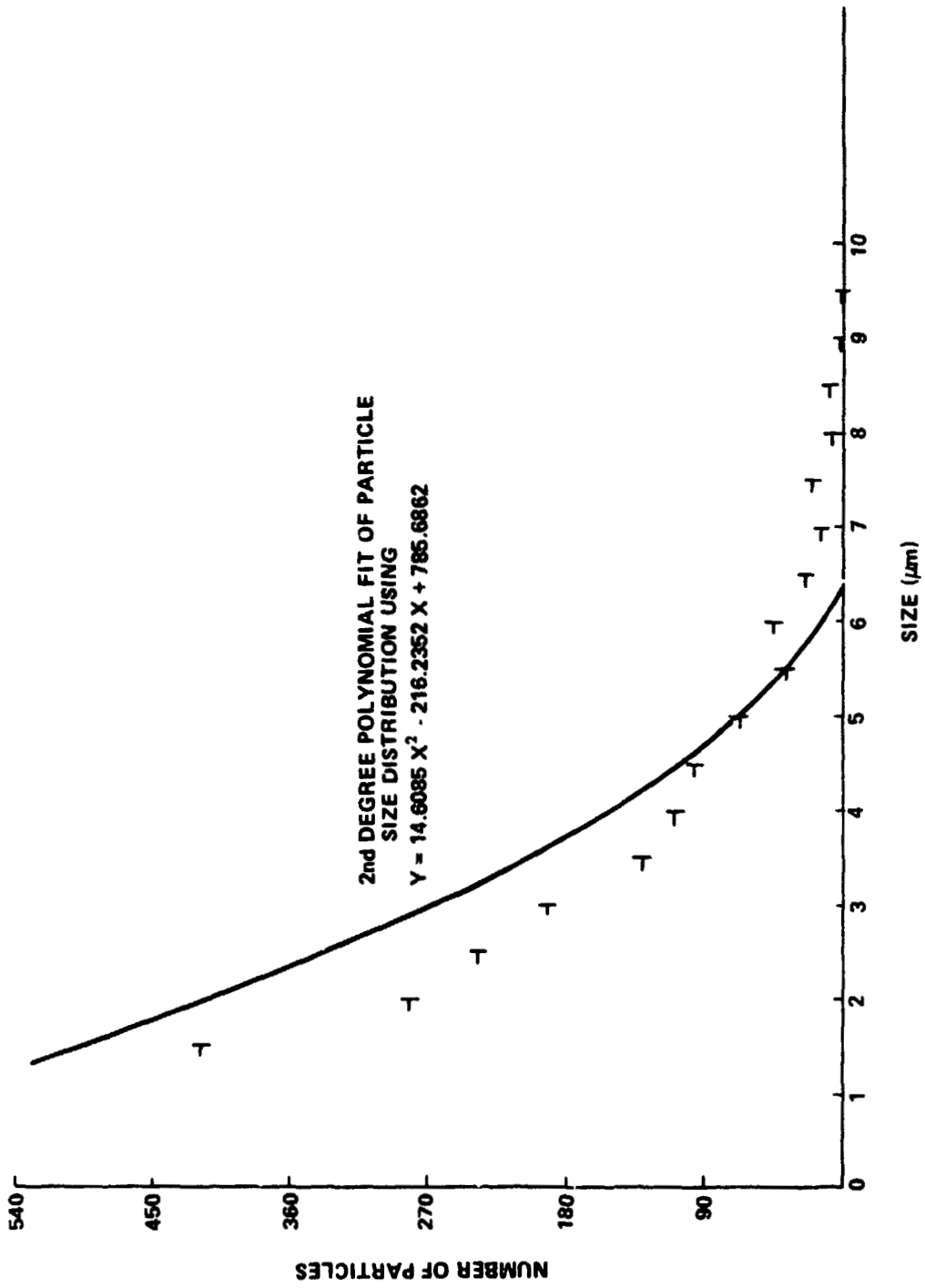


Figure II-11. Filter S/N 003, propellant 3, firing 21, 38.1 cm (15 in.).

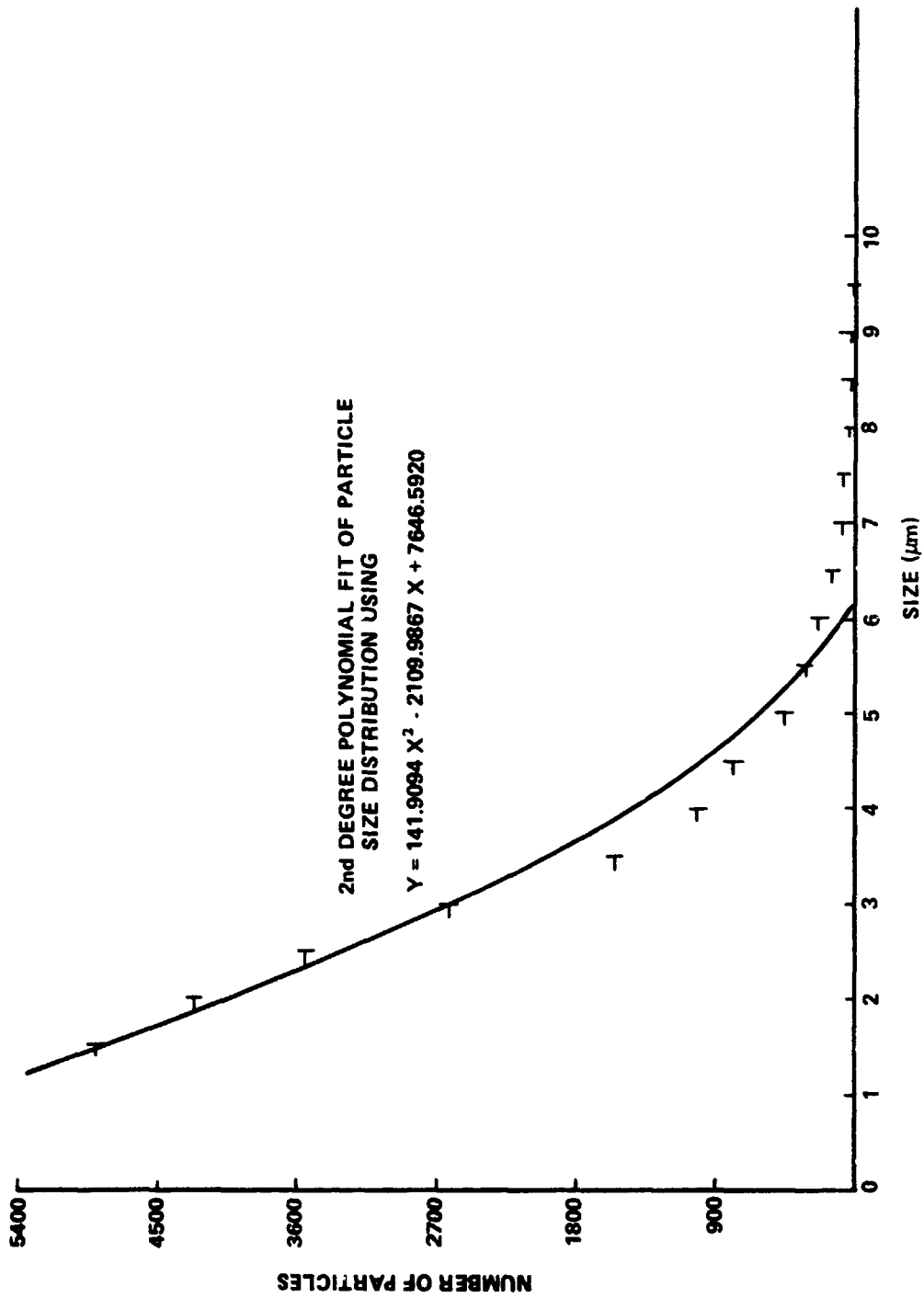


Figure II-12. Filter S/N 005, propellant 3, firing 21, 33.1 cm (15 in.).

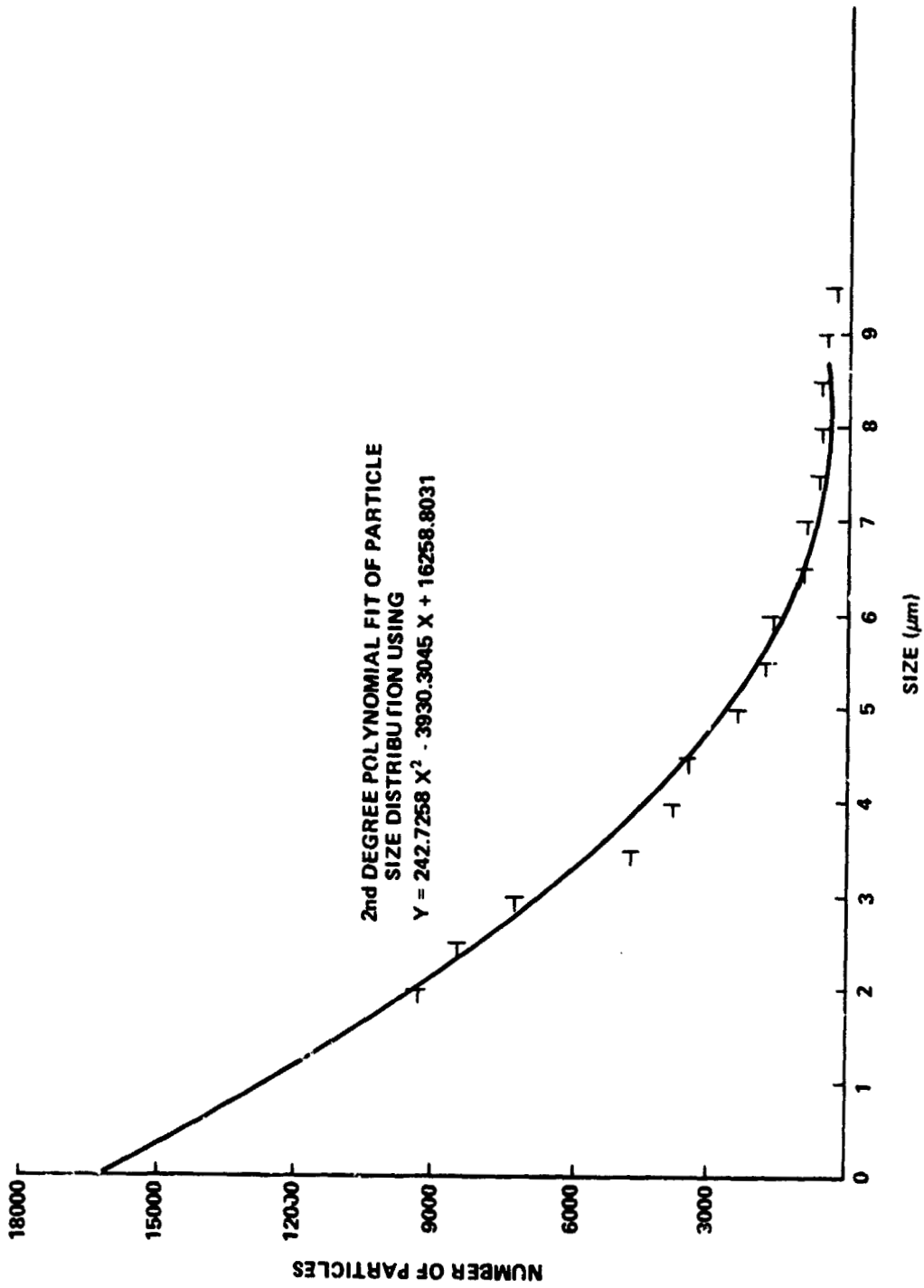


Figure II-13. Filter S/N 006, propellant 3, firing 21, 12.7 cm (5 in.).

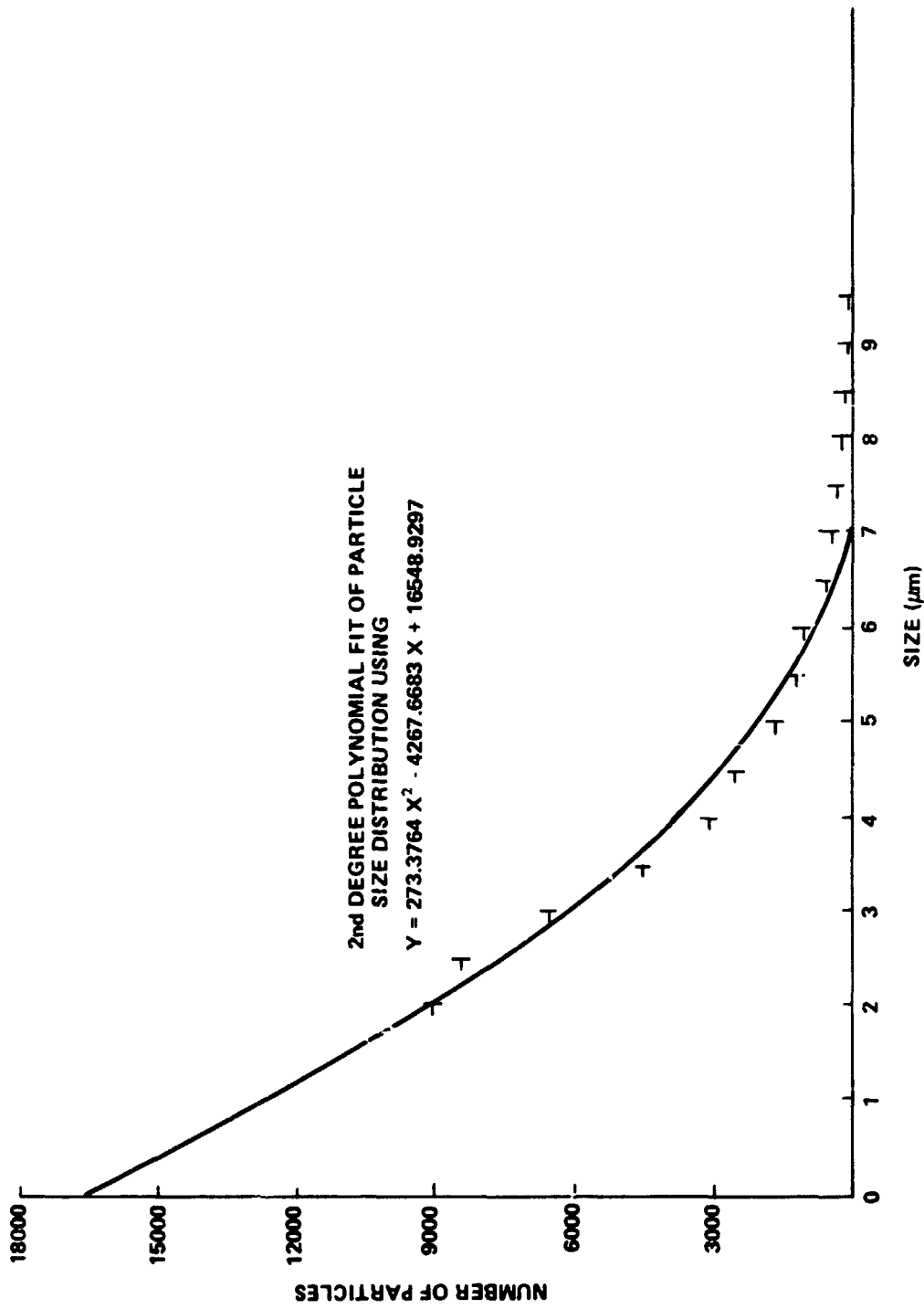


Figure II-14. Filter S/N 010, propellant 3, firing 21, 12.7 cm (5 in.).

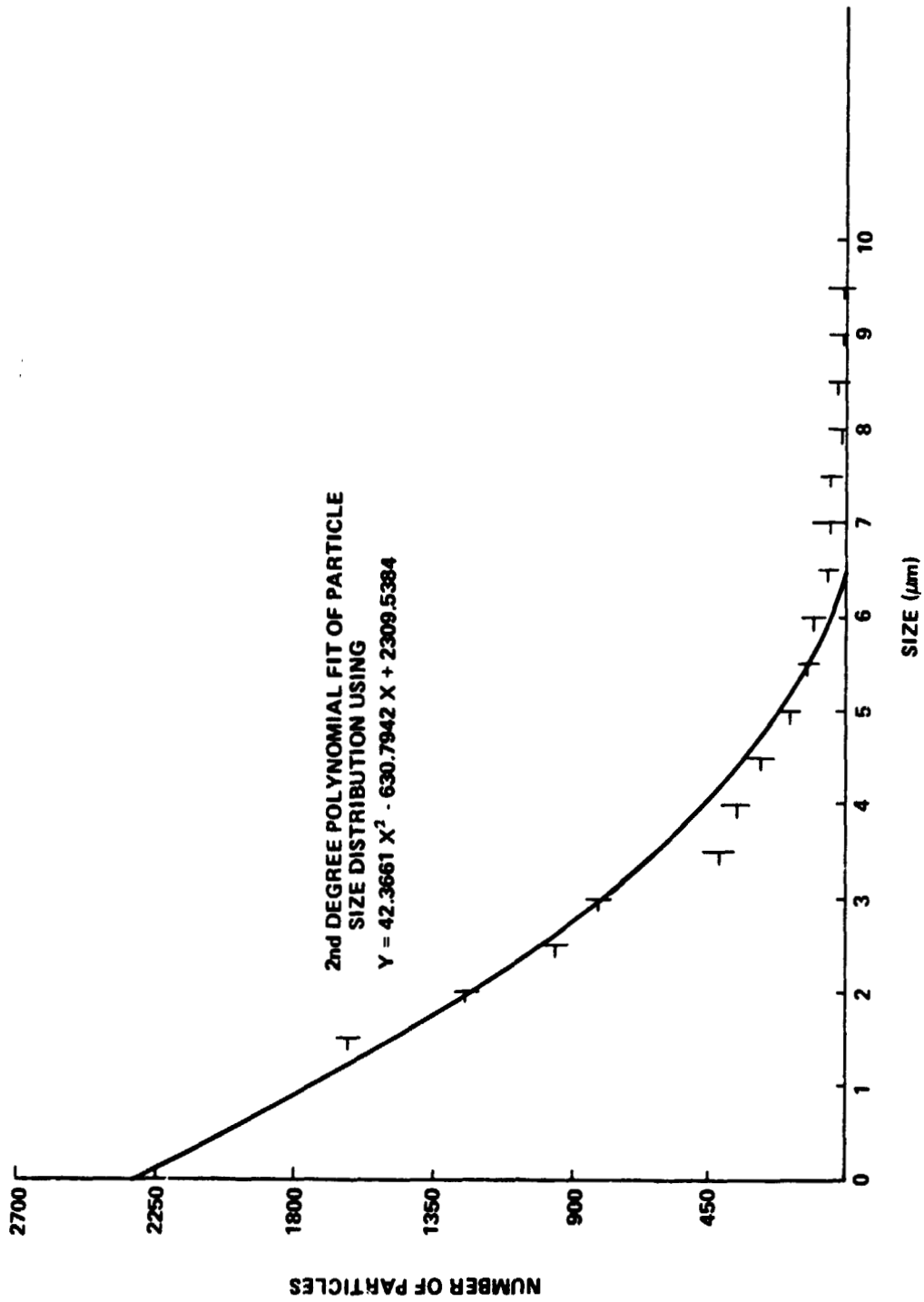


Figure II-15. Filter S/N 001, propellant 3, firing 10, 38.1 cm (15 in.).

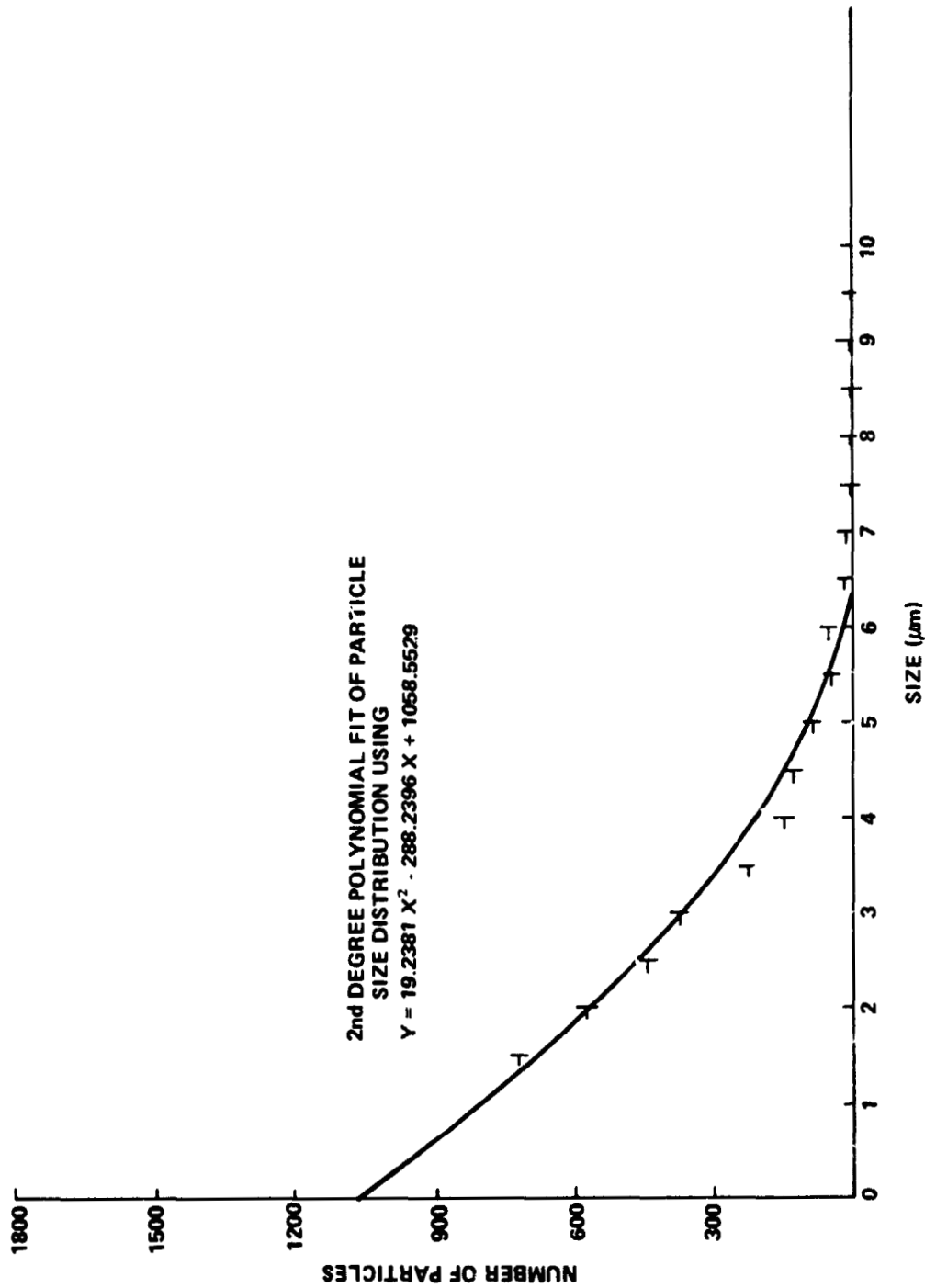


Figure II-16. Filter S/N 002, propellant 3, firing 10, 38.1 cm (15 in.).

These calculations are presented as an aid in extrapolations of the curves down to the smaller particle sizes not detectable by our electro-optical system. Using the average distributions, we calculated the percentages of particles detected in the indicated size ranges for the six filters. These results are given in Table II-6.

4. Analysis of Samples at Athens College

Six samples were delivered to Athens College as alcohol slurries. The alcohol slurries were evaporated to dryness leaving the original sample free of alcohol. These dry samples were then weighed. This weight was the basis for all percentage calculations. Two or three milliliters of concentrated sulfuric acid were added to the dry sample prior to heating it. A small amount of nitric acid was then added to the sample. The residue left after evaporation was processed for determination of aluminum. The analyses were carried out using standard colorimetric techniques, with a Delta Scientific Model 260 colorimeter. The results are summarized in Table II-7.⁶

Photographs of samples prepared on brass platforms and analyzed by Mr. Daniel Gates using a scanning electron microscope are presented in Figures II-17 through II-28. The photographs are included in this report merely to provide visual information as to the geometric characteristics of the particles and the varying populations of particles from sample to sample. Analysis of the composition of the particles was not undertaken.

An analysis to determine the percentage of iron, aluminum, and other elements was performed by Athens College in addition to the data presented in Table II-7. The results, included as a letter sent to David Jex, task team leader, were as follows:

Test	Propellant	Location (cm)	% Fe	% Al	% Weight Loss on Ignition
4	8	12.7	5.7	2.5	47
10	3	12.7	3.5	1.9	76
12	3	38.1	8.1	3.0	81
		Filter 009			
19	5	12.7	6.7	3.6	78

6. McNutt, Ronald C.: Quarterly Report, Contact NAS8-28058, June 26, 1974.

TABLE II-6. PERCENTAGE OF PARTICLES IN SELECTED SIZE RANGES FOR EACH FILTER

Particles Size (μm)	Percentage of Total Particles Counted for Each Filter							
	S/N 003	S/N 005	S/N 006	S/N 010	S/N 001	S/N 002		
1.5 to 2.0	24	24	-	-	25	25		25
2.1 to 2.5	16	21	18	22	19	20		20
2.6 to 3.0	14	17	17	21	15	15		15
3.1 to 3.5	11	13	14	16	13	13		13
4.1 to 4.5	8	8	2	11	6	8		8
4.6 to 5.0	6	5	7	8	5	5		5
5.1 to 5.5	4	2	5	4	3	3		3
5.6 to 6.0	2	2	4	3	2	2		2
6.1 to 6.5	3	1	3	2	2	2		2
6.6 to 7.0	2	0.8	2	1	1	0.7		0.7
7.1 to 7.5	0.9	0.5	2	1	0.9	0.7		0.7
7.6 to 8.0	1	0.4	1	0.8	1	0.4		0.4
8.1 to 8.5	0.6	0.2	1	0.6	0.4	0.3		0.3
8.6 to 9.0	0.7	0.2	1	0.5	0.5	0.2		0.2
9.1 to 9.5	0.3	0.2	1	0.3	0.2	0.4		0.4
9.6 to 10.0	0.3	0.1	0.7	0.2	0.3	0.1		0.1
10.0 to 50	0.7	0.5	6	1	1	0.7		0.7
50.1 to 100	0	0	0.1	0	0	0		0
Over 100	0	0	0.1	0	0	0		0

Test	Propellant	Location (cm)	% Fe	% Al	% Weight Loss on Ignition
19	5	27.9	5.5	3.1	96 96*
19	5	38.1	6.5	6.8	43

Percentages are based on the dry sample weight.

* Essentially all the material in this sample was lost on ignition. Allowance for the apparent sum of more than 100% should be made in the % weight lost column due to weighing the very small amount of residue.

TABLE II-7. PERCENTAGE OF ALUMINUM IN ROCKET EFFLUENTS

Sample S/N	Weight of Dried Sample (gm)	Weight of Aluminum (gm)	Percent of Aluminum in Dried Sample
003	0.0092	0.00004	0.43
005	0.0056	0.00033	5.89
006	0.0157	0.00151	9.62
010	0.0139	0.00152	10.94
001	0.0056	0.00039	7.01
002	0.0101	0.00049	4.88

D. Holographic Analysis of Small Motor Plumes

W. W. Moore

In general, if information on particles and particle parameters is desired from any given environment or particle field, one must resort to experimental techniques to determine particle parameters. In this test program the technique of in-line holography has been applied to the recording of plumes and the particulate distributions such that particle content and other data may be extracted. The basic concept of the equipment layout is contained in Figure II-29. A plane wave-front beam is incident on and passes through some target volume. The presence of individual particles distributed throughout this volume



Figure II-17. Filter 003, 1000X magnification.

ORIGINAL PAGE IS
OF POOR QUALITY



Figure II-18. Filter 003, 3000X magnification.



Figure II-19. Filter 005, sample A, 3000X magnification.

**ORIGINAL PAGE IS
OF POOR QUALITY**



Figure II-20. Filter 005, sample B, 1000X magnification.



Figure II-21. Filter 005, sample B, 3000X magnification.

ORIGINAL PAGE IS
OF POOR QUALITY



Figure II-22. Filter 006, 3000X magnification.



Figure II-23. Filter 010, 3000X magnification.

ORIGINAL PAGE IS
OF POOR QUALITY

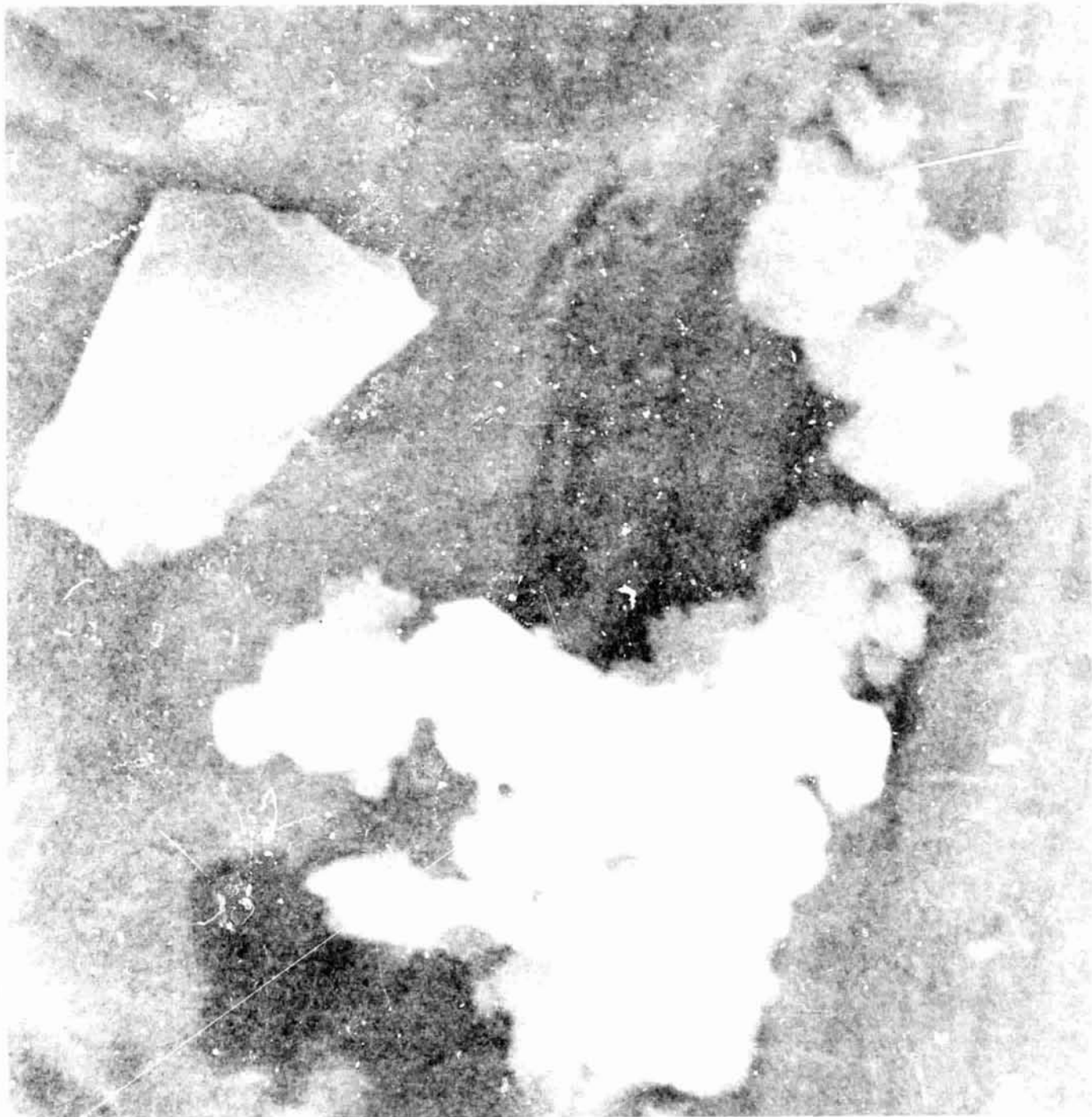


Figure II-24. Filter 010, 10 000X magnification.



Figure II-25. Filter 001, 3000X magnification.

**ORIGINAL PAGE IS
OF POOR QUALITY**



Figure II-26. Filter 002, 3000X magnification.



Figure II-27. Filter 002, 3000X magnification.

ORIGINAL PAGE IS
OF POOR QUALITY



Figure II-28. Filter 002, 1000X magnification.

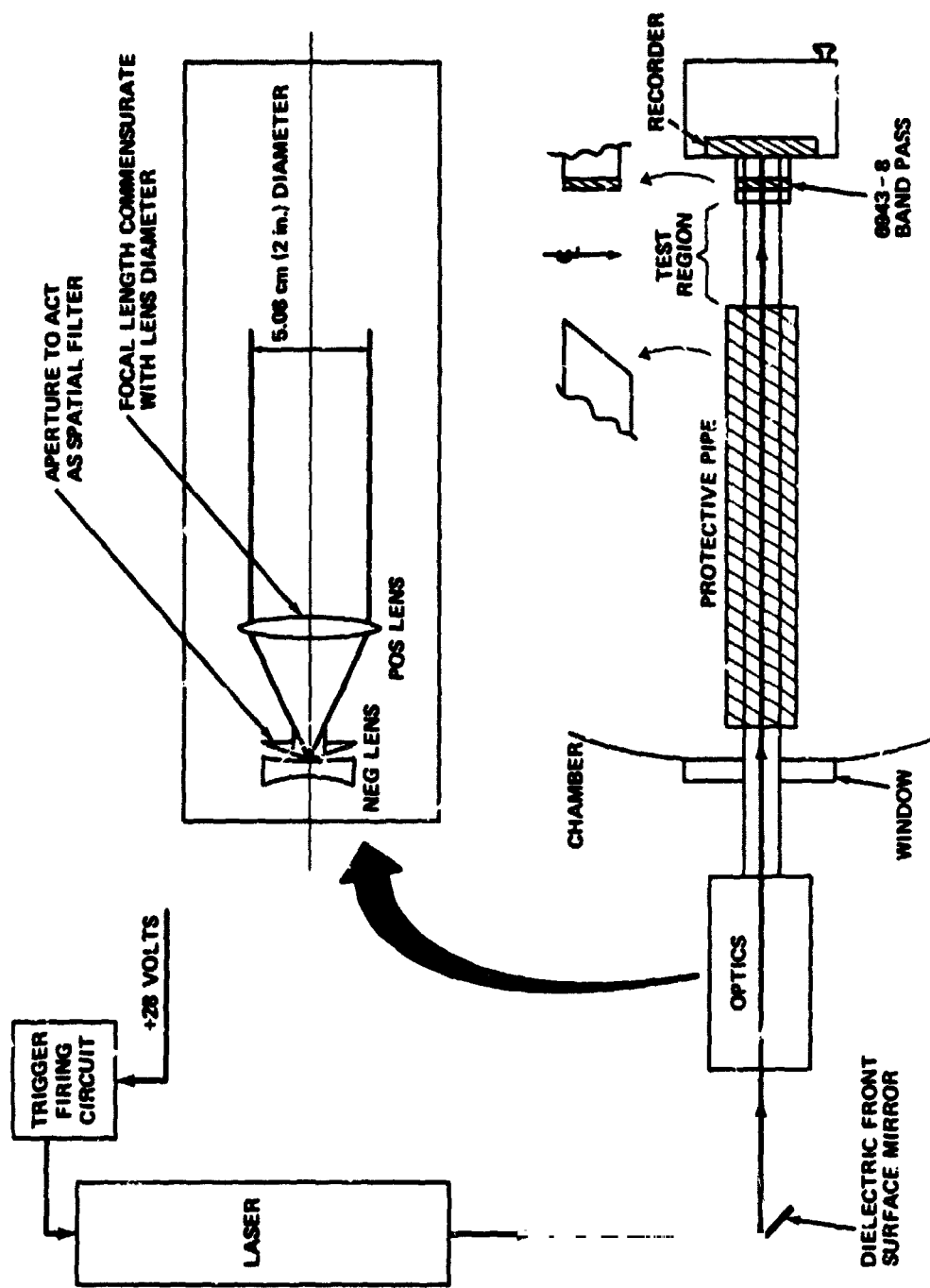


Figure II-29. In-line holographic layout.

essentially causes the plane wave to become scattered and diffracted at many points so as to produce a spherical wave as well as a plane wave. The plane wave is that part of the incident wave which passes through the target field region undisturbed. This undisturbed plane wave is then called the holographic reference beam. The spherical wave produced by the scattering and diffraction around the individual particles constitutes the holographic object beam. These two waves interfere at the film plane, and the interference pattern so recorded at the film plane provides the means for reconstructing the real image of the target field volume. An inspection of this real image provides quantitative information about the individual particles that make up the target field. The basic problem with the in-line system is that for high density fields of particles, the reference beam is excessively attenuated and the observer or detector must look directly back into the reconstructed laser source.

During the small motor plume/material improvement test program of 29 firings, a total of 21 attempts was made to record a hologram record (firings 6 through 26). The discrepancy here is a result of the holography system not being interfaced to the chamber at the start of the tests and a result of the complete operational loss of the laser source near the end because of the severe environment. Of the exposed plates, eight are considered of reasonable quality. The others are disregarded because of overexposures, underexposures, and/or optical or mechanical component failures caused by the caustic environment.

At this phase of the data reduction sequence, two holograms have been extensively examined. These are the records for firings 19 and 21 (propellant types 5 and 3, respectively). The observed particles have been primarily in the volume near the film holder and have been mostly smaller particles; i. e., 10 μm or less. No particle distribution graphs have been proposed at this time because only a small area of the holograms has been examined over the test volume images. This means the statistical sample would not be as good as necessary for comparison to other measurements. At present the data are evaluated qualitatively as consistent with the distribution obtained from the test filter samples image data analyses that were reported previously.

E. Solid Rocket Motor Contamination of Shuttle Windshield Samples

Roger Linton, David W. Jex, and Coy W. Mattox

During the small solid rocket motor firings at MSFC, April 18 through May 22, 1974, samples of the Shuttle windshield material were strategically placed in the space simulation chamber during each firing to collect plume

residuals and provide a method of estimating the optical degradation to be expected during the SRM separation phase of the actual Shuttle vehicle. After each firing, the two windshield samples deployed were removed and immediately brought to the portable transmissometer used in the earlier Shuttle rocket test at AEDC. The transmittance between 290 and 310 nm (2900 and 3100 Å) was measured. Following this, image clarity photographs were taken and the samples were taken to a more versatile facility in Space Sciences Laboratory for detailed transmittance measurements in the range of 320 to 600 nm (3200 to 6000 Å).

To establish a baseline for reference, each sample was measured in the laboratory facility and then by the portable transmissometer at the test site prior to each firing. It was, therefore, possible to determine the optical degradation for each firing by comparing the baseline to the results obtained after each test firing. This provided a relative scale for evaluating the "cleanliness" of the nine types of propellants used in these tests.

The tests included multiple firings of nine different fuel compositions and one firing of an ignitor only. The latter test (ignitor only) was run on the afternoon of May 1, 1974. The measured degradation, as indicated by the transmissometer, of -5 percent⁷ is considered to be a measure of the background and must be considered in evaluating all data. A composite of all the transmissometer data collected, with the corresponding firing history, is contained in Tables II-8 and II-9. Even a cursory glance at Table II-9 reveals problems in interpreting the data. For example, the degradation measured for the two orientations of the Shuttle windshield samples in firings 1 and 2, both for rocket type 7, are fairly similar, while that of firing 3 for the same type rocket is markedly reduced. The extended transmittance measurements from 320 to 600 nm (3200 to 6000 Å) and the before and after image clarity photographs confirm the validity of the transmissometer data. It is possible that the differences in optical degradation are related to the venting of the simulation chamber. Venting was accomplished by bleeding outside air into the chamber after the firing. This outside air was subject to the prevailing humidity, and this, together with the observable clouds of vapors in the chamber as a result of the firing, could cause a difference in the condensation of the plume residue on windshield samples.

7. This is $\Delta T/T_0$, where $\Delta T = T - T_0$; T being the transmittance after exposure, and T_0 being the transmittance before exposure to the plume. (The negative sign on all measurements implies a decrease in transmittance.)

TABLE II-8. TEST FIRING HISTORY AND CORRESPONDING TRANSMISSOMETER DATA (NEGATIVE SIGN INDICATES A LOSS IN TRANSMISSION OF SAMPLE)

Date	Firing No.	Propellant	$\Delta T/T_o$ for Orientation A (Up) (%)	$\Delta T/T_o$ for Orientation B (Out) (%)
4/18/74	1	7	No Sample	-37
4/19/74	2	7	-38	-24
4/22/74	3	7	-18	- 8
4/23/74	4	8	-18	- 8
4/24/74	5	8	- 8	- 6
4/25/74	6	1	- 7	0
4/26/74	7	8	No Sample	No Sample
4/29/74	8	1	- 5	- 6
4/30/74	9	1	-22	-18
5/1/74 a. m.	10	3	-21	-10
5/1/74 p. m.	11	Ignitor Only	- 5	- 5
5/2/74	12	3	- 2	-10
5/3/74	13	2	- 8	-16
5/6/74	14	2	0	0
5/7/74	15	6	No Sample	No Sample
5/8/74	16	6	- 6	0
5/9/74 a. m.	17	1	-15	-14
5/9/74 p. m.	18	2	0	0
5/10/74	19	5	-18	-19
5/13/74 a. m.	20	5	-21	-14
5/13/74 p. m.	21	5	-16	- 3
5/14/74 a. m.	22	4	-16	-16
5/14/74 p. m.	23	4	-16	- 9
5/15/74 a. m.	24	9	No Ignition of Propellant	
5/15/74 p. m.	25	9	-15	-18
5/16/74 a. m.	26	9	No Ignition of Propellant	
5/16/74 p. m.	27	9	-17	-15
5/17/74 a. m.	28	2	- 1	- 1
5/17/74 p. m.	29	4	-21	-10
5/21/74 a. m.	30	3	Samples left to	
5/24/74 p. m.	31	6	-37 accumulate residue over 2 firings	-19
5/22/74	32	9	-14	-16

**TABLE II-9. TRANSMISSOMETER RESULTS OF SHUTTLE
WINDSHIELD SAMPLES (PERCENT TRANSMISSION
LOSS ($\Delta T/T_0$) BETWEEN 290 AND 310 nm (2900 AND
3100 Å) FOR EACH PROPELLANT TYPE)**

Propellant Type	T/T ₀ for Orientation A (Up) From Table 1 (%)	T/T ₀ for Orientation B (Out) From Table 1 (%)	Number of Independent Tests
1	-7, -5, -22, -15	0, -6, -18, -14	4
2	-1, 0, 0, -8	-1, 0, 0, -16	4
3	-2, -21	-10, -10	2
4	-21, -16, -16	-10, -16, -9	3
5	-16, -18, -21	-3, -19, -14	3
6	-6	0	1
7	-38, -18	-37, -24, -8	3
8	-18, -8	-8, -6	2
9	-15, -17, -14	-18, -15, -16	3
Ignitor Only	-5	-5	1
Accumulation of 3 and 6	-37	-19	-

The data in Table II-10 show the rank order of the propellants, from the one giving the least transmission loss to the one giving the most transmission loss. The rank order was assigned by a modified Wilcoxon test: (1) sum the percent loss for each propellant at each of the two orientations A (up) and B (out); (2) obtain an average by dividing the number of figures summed; (3) assign a rank order to each propellant based on these "averaged" transmission losses for each orientation; (4) obtain a "total averaged" loss by summing both orientation losses together and dividing by the total number of figures summed; (5) assign a rank order based on this "total averaged" loss for each propellant; (6) sum the rank orders resulting from (3) and (5) above; and (7) order the propellants according to the sum of the rank orders.

TABLE II-10. PROPELLANTS ORDERED FROM LEAST TRANSMISSION LOSS TO MOST TRANSMISSION LOSS

Propellant Type	Number of Independent Tests with Samples (n)	Orientation A		Orientation B		Orientation A + Orientation B		Ingredient (% by Weight)								
		Average % Loss $\left[\frac{\sum_{i=1}^n (\Delta T/T_i)}{n} \right]$	Rank Order	Average % Loss $\left[\frac{\sum_{i=1}^n (\Delta T/T_i)}{n} \right]$	Rank Order	Total Average % Loss In $\left[\frac{\sum_{i=1}^{27} (\Delta T/T_i)}{27} \right]$	Rank Order	Sum of Rank Orders	AP ^b	HTPB ^b	CTPB ^b	Al ^b	Al ₂ O ₃ ^b	Fe ₂ O ₃ ^b	C ^b	
6 ^a	1	-6.0	2	0	1	-3.0	1	4	78.5	39.5	-	-	-	-	1.0	-
2	4	-2.3	1	-4.3	2	-3.3	2	6	86.0	14.0	-	-	-	-	-	-
8	2	-13.0	5	-7.0	3	-10.0	3	11	78.0	20.5	-	-	0.5	0.5	0.5	-
3	2	-11.5	3	-10.0	5	-10.8	4	12	76.5	21.5	-	2.0	-	-	-	-
1	4	-12.3	4	-9.5	4	-10.9	5	13	79.0	21.0	-	-	-	-	-	-
4	3	-17.7	7	-11.7	6	-14.7	6	19	83.9	14.0	-	2.0	-	0.1	-	-
5	3	-18.3	8	-12.0	7	-15.2	7	22	77.7	20.3	-	-	-	2.0	-	-
9	3	-15.3	6	-16.3	8	-15.8	8	22	7	7	7	7	7	7	7	7
7	3	-28.0	9	-23.0	9	-25.5	9	27	82.0	-	12.0	4.0	-	-	2.0	-

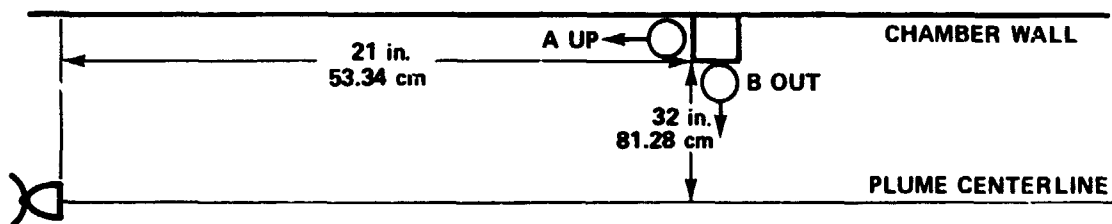
a. Propellant 6 had samples in only one test as opposed to samples in 4 independent tests for ingredient 2. It is therefore recommended that the data from this test (6) be considered with extreme care.

b. AP = Ammonium Perchlorate
 HTPB = Hydroxy-Terminated Polybutadiene
 CTPB = Carbonyl-Terminated Polybutadiene
 Al = Aluminum

Al₂O₃ = Aluminum Oxide
 Fe₂O₃ = Ferric Oxide
 C = Graphite

From Table II-10 it is possible to draw some conclusions of the expected windshield transmission loss of one type propellant relative to the other types. In examination of Table II-10 ammonium perchlorate would not appear to be a significant source of contamination as both the "cleanest" and "dirtiest" (types 2 and 7) engines had high percent weight compositions of this compound and the others follow no particular pattern. For NTPB a similar conclusion holds. For CTPB, only propellant 7 contained any and it degraded windshield samples the most, but the absence of CTPB in the other propellants precludes any comparative conclusion. Except for type 1, it appears that increasing percent weight concentrations of aluminum and/or Al_2O_3 are a significant factor in degradation. Results for Fe_2O_3 are inconclusive. Finally, the presence of graphite that was only in propellant 8 would not appear to be significant.

The transmittance of each windshield sample was measured before and after exposure using a 1 m normal incidence monochrometer with a tungsten light source. The results are generally a uniform degradation after exposure to the plume throughout the measured spectral range. For propellant 7, however, the curves are more structured as shown in Figure II-30 (curves labeled "out" and "up" refer to the orientation of the normal from the sample mounted in the chamber to the centerline of the plume as diagrammed below). The date (month/day) refers to the particular firing.



Figures II-31 and II-32 are representative; the degradation was in general not spectrally dependent. This would, of course, leave open the question of to what degree the degradation observed is from absorption or scattering. The filmy nature of the contamination films would seem to indicate that the major loss is absorption.

Photographs of each windshield sample were taken before and after each firing to provide a qualitative assessment of image clarity with contamination. Analyses of these photographs aided the interpretation of the qualitative transmission loss data. To evaluate the true significance of the reported transmission loss, the photographs of Figure II-33 are shown for a sample exposed

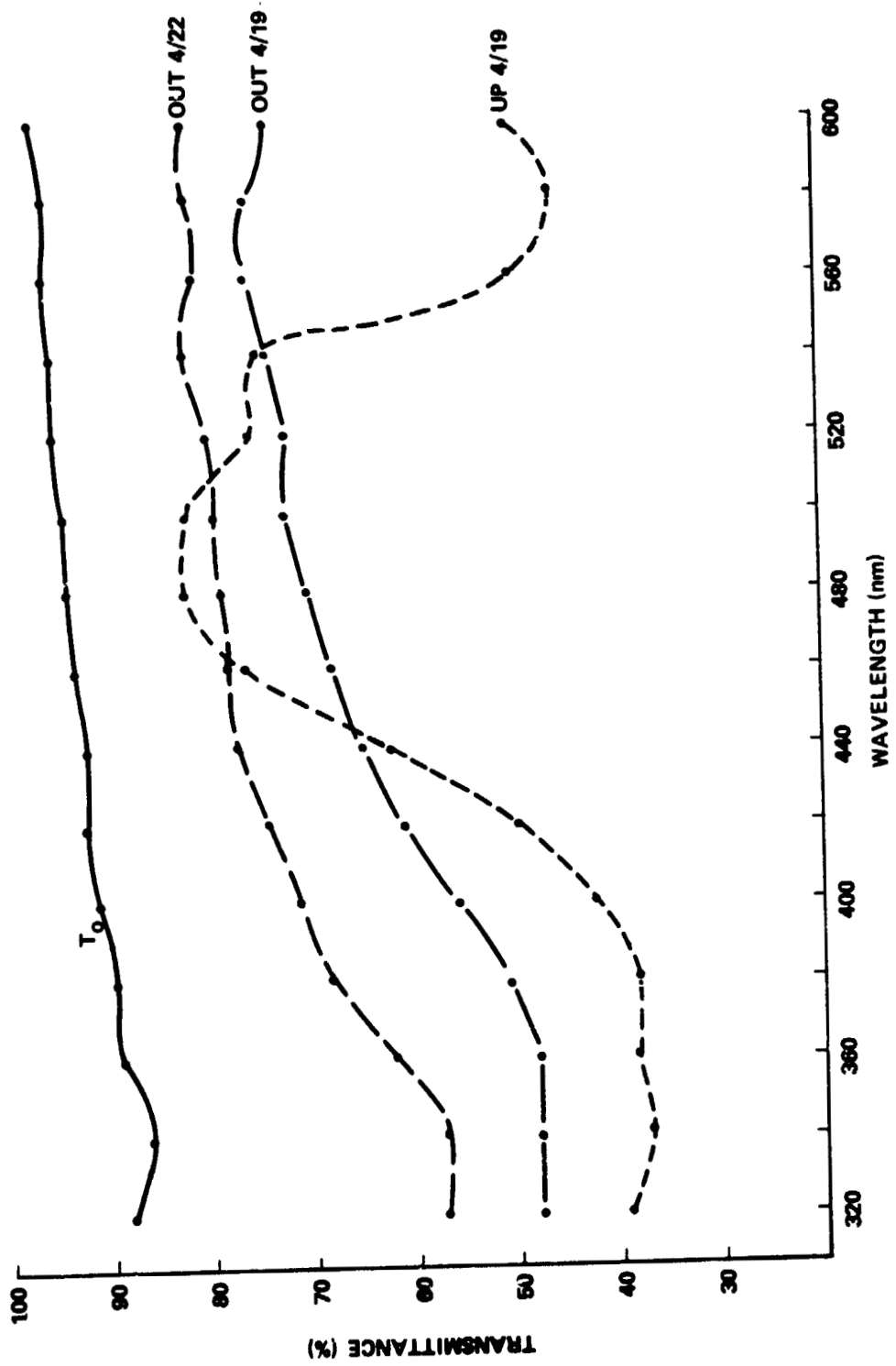


Figure II-30. Transmittance loss for propellant type 7.

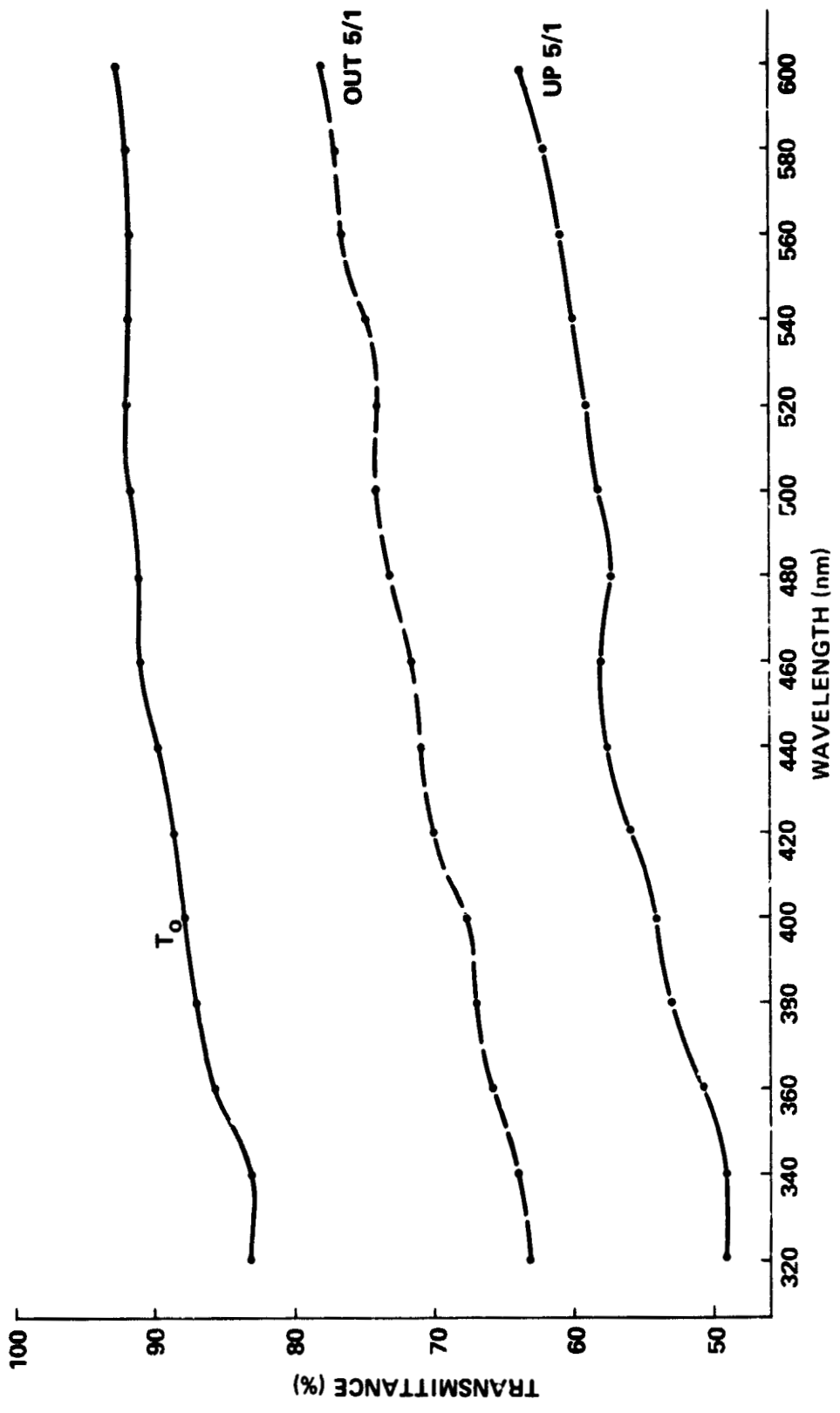


Figure II-31. Transmittance loss for propellant type 3.

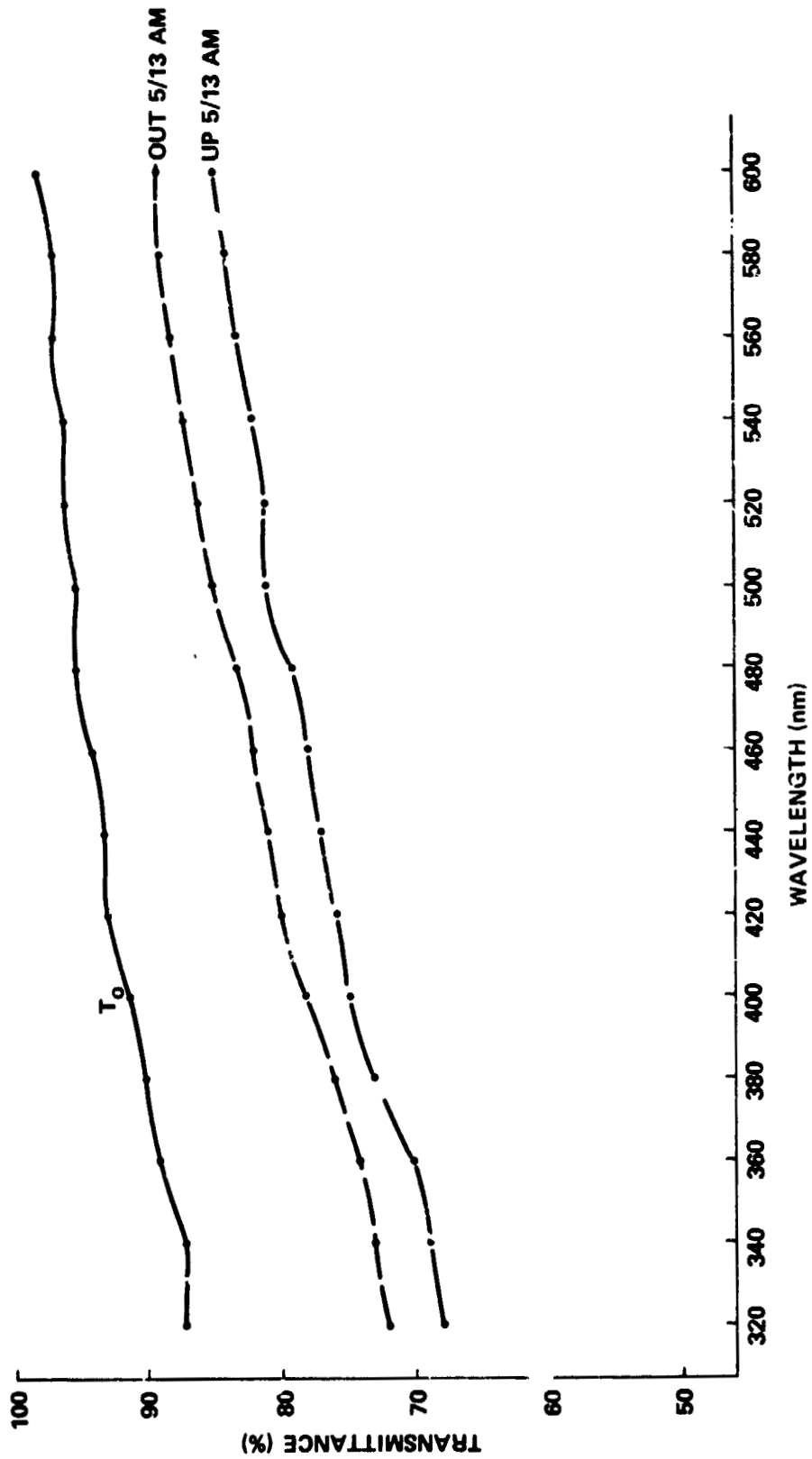


Figure II-32. Transmittance loss for propellant type 5.

ORIGINAL PAGE IS
OF POOR QUALITY

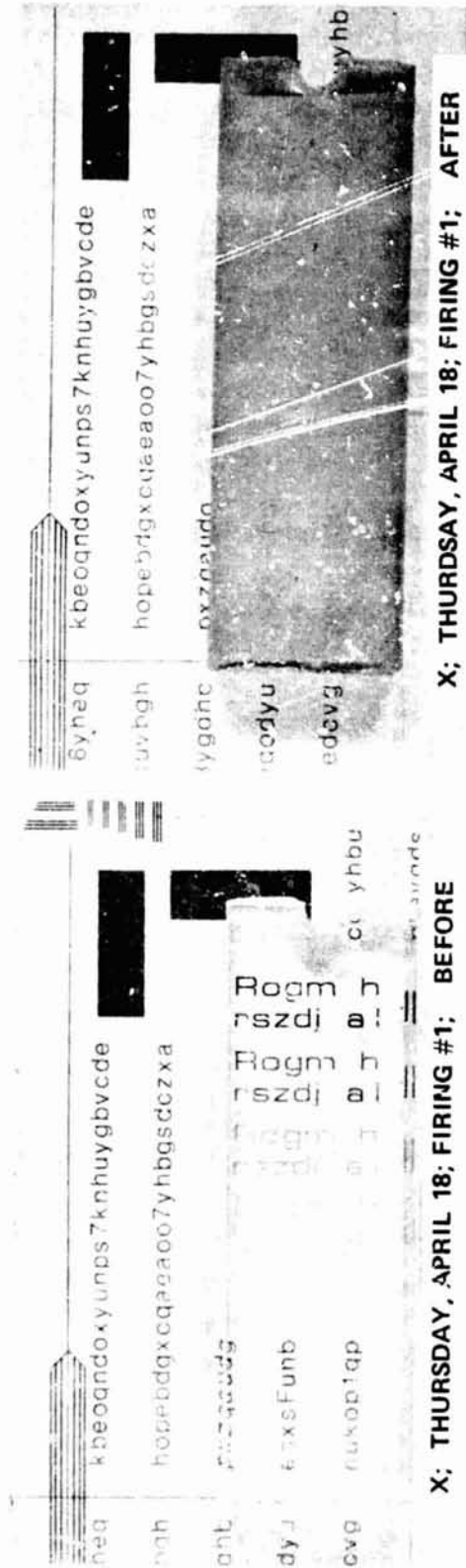


Figure II-33. Image clarity photographs (propellant 7, April 13, 1974, test firing 1).

to the plume from propellant formulation 7. The transmissometer (results of test 1) indicated that the transmittance of this sample dropped from 62 to 39 percent ($\Delta P/R = 37$ percent). There is a marked loss of visual "imaging" in the exposed sample. Since the average loss of transmittance for samples exposed to the various rockets was on the order of -15 percent, then the significance of all these photographs may be illustrated by Figure II-34. These photographs are for samples in firing 4 (4/23/74); the $\Delta T/T$ value reported is -18 percent. Besides a basic darkening in the after photo, there is a discernible loss of image clarity for the fainter characters to the left of the "after" photo. For $\Delta T/T$ values less than 10 percent, the image clarity in the exposed samples is best studied in the original photographs. Figure II-35 shows typical effects for a sample exposed to propellant 3 in firing 12 (5/2/74). Image clarity is reduced basically, in this case, by absorption; the film itself is not visibly apparent. Figure II-36 shows the transmittance of the clean Shuttle windshield samples from 200 to 300 nm (2000 to 6000 Å). Photographs of all samples from all tests are on file for future reference.

ORIGINAL PAGE IS
OF POOR QUALITY



Figure II-34. Image clarity photographs (propellant 8, April 23, 1974, test firing 4).

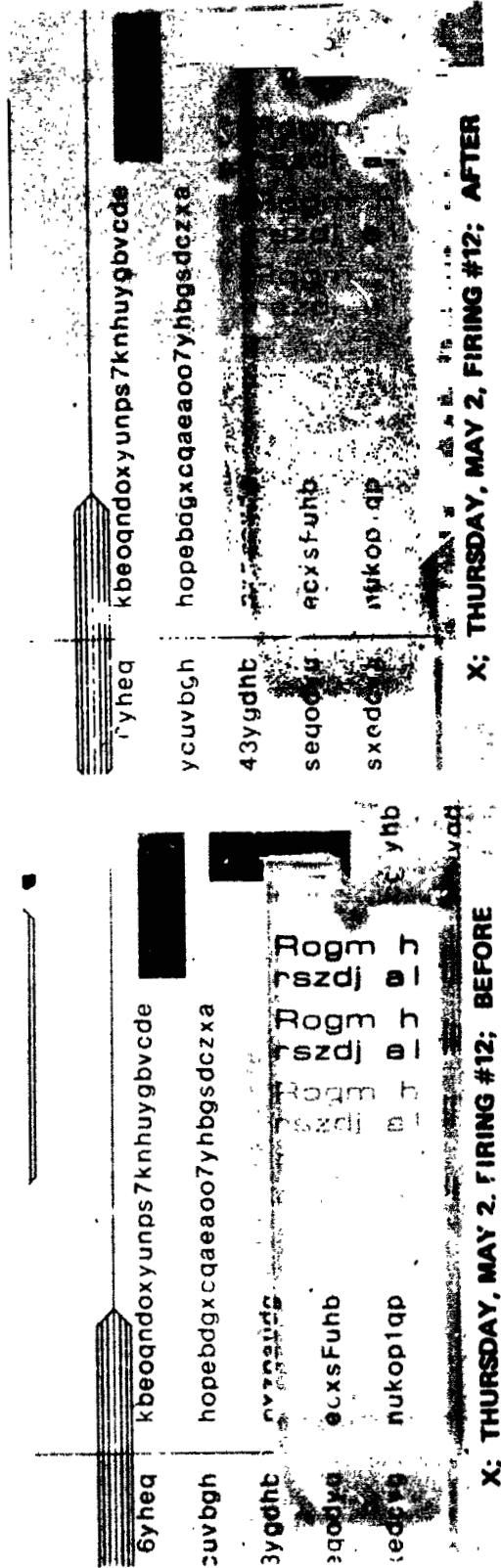


Figure II-35. Image clarity photographs (propellant 3, May 1, 1974, test firing 12).

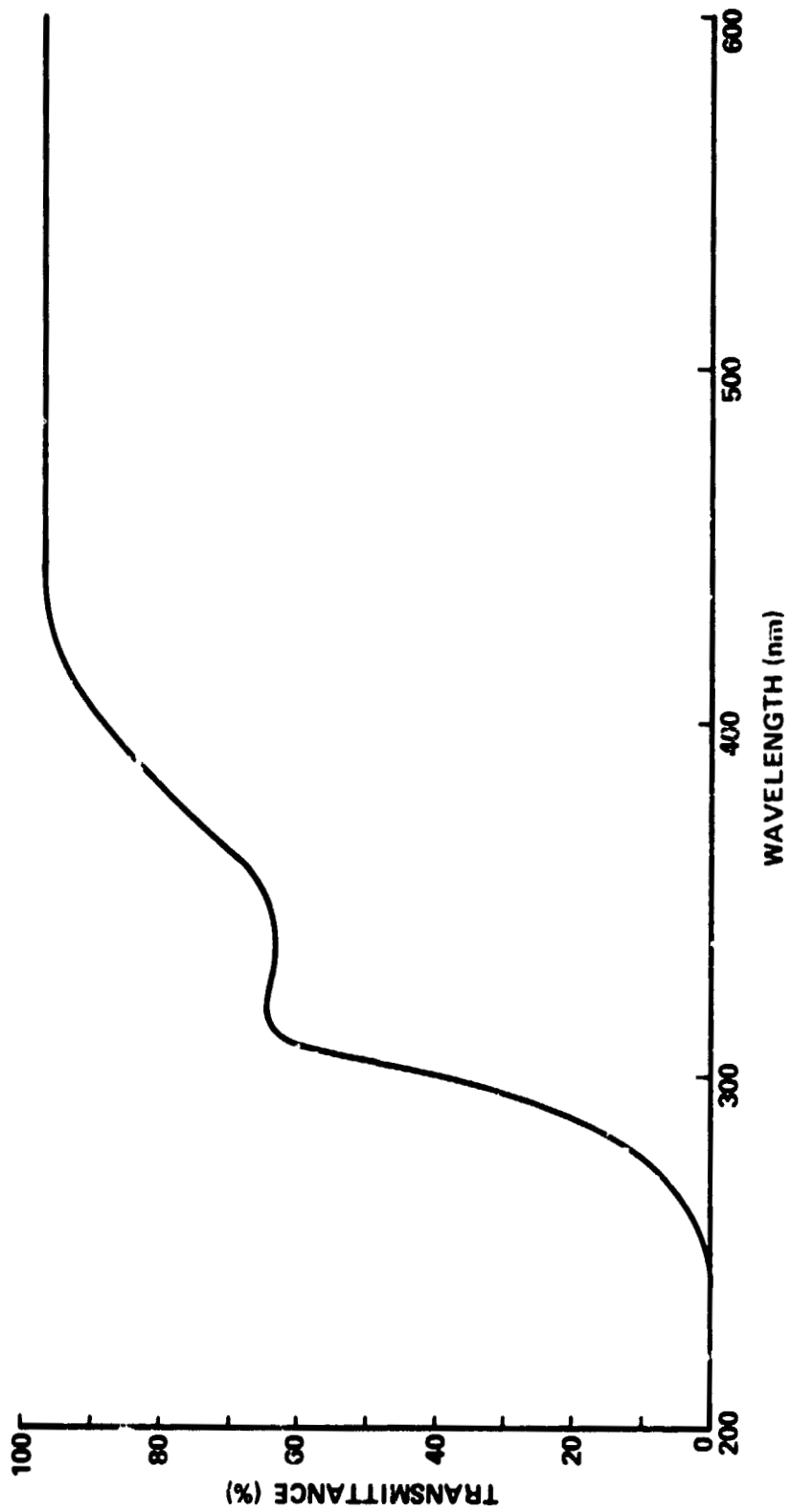


Figure II-36. Transmittance of clean Shuttle windshield samples.

N76-16172

SECTION III. THE LARGE MOTOR PLUME/MATERIAL
IMPINGEMENT TEST PROGRAM AT AEDC UTILIZING
THE FOUR SELECTED PROPELLANTS FROM THE
SMALL MOTOR TESTS AT MSFC (JULY,
AUGUST, AND SEPTEMBER 1974)

A. Introduction

This series of tests at AEDC was under the direction of MSFC program director William F. Richardson and Gerald Smith, both of the Office of Associate Director for Engineering.

In the small motor plume/material impingement test at MSFC, nine propellant formulations were used. Four of these formulations were chosen for further testing at AEDC. They are detailed in Table III-1. Also included are the components of the ignitor used with each motor firing.

This test series was conducted to support an evaluation of the feasibility of SSRM's for SRB separation and the acceptability of various SSRM orientations.

The test objectives were:

1. Determine the vulnerability of Orbiter and ET materials located at various positions within exhaust plumes from test SSRM's using four different propellant formulations.
2. Determine the effect on TPS materials from a single SSRM plume and dual SSRM plumes.
3. Define test SSRM plume environment at material specimen locations.

The test was a coordinated effort between NASA/MSFC, NASA/JSC, Rockwell International, and AEDC.

The tests were conducted in the AEDC J-4 high altitude test facility at pressure conditions simulating the nominal SRB staging altitude of 4.3 km (140 000 ft). The rocket motors were installed at the test cell deflector plate with the nozzles exhausting upward. Plume impingement targets were located at two axial locations, 3.4 m and 6.2 m (134 and 246 in.) above the nozzle exit, as shown in Figure III-1. The impingement targets, consisting of material specimens, calibration plates, calorimeter probes, and particle collectors,

TABLE III-1. PROPELLANT FORMULATIONS FOR TESTS

Ingredient	Propellant Formulation Number				Ignitor
	1	3	6	8	
AP (Weight %)	79.0	76.5	78.5	78.0	Melimine Glass Liner: Silicone Dioxide 54% Calcium Oxide } 20% Magnesium Oxide } Aluminum Oxide 14% Boron Oxide 10% Sodium Oxide } 4% Potassium Oxide }
Binder (Weight %) HTPB } IPDI } Alroperse }	{ 18.80 } 1.38 } 0.32 }	{ 19.63 } 1.43 } 0.34 }	{ 18.80 } 1.38 } 0.32 }	{ 18.80 } 1.38 } 0.32 }	
Thermax (Weight %)	0.50	-	-	-	
Al (Weight %)	-	2.0	-	-	(This Totals : 02% Because of Rounding Off of Percentages.)
Fe ₂ O ₃ (Weight %)	-	0.1	1.0	0.5	
Al ₂ O ₃ (Weight %)	-	-	-	0.5	
Graphite (Flake Grade) (Weight %)	-	-	-	0.5	<u>Propellant:</u> Boron-Potassium Nitrate

Abbreviations/Function

- AP - Ammonium Perchlorate
- HTPB - Hydroxyl Terminated Polybutadiene
- IPDI - Isophorone Diisocyanate
- Alroperse - Bonding and Wetting Agent
- Thermax - Carbon Black (a burning stabilizer)
- Al - Aluminum
- Al₂O₃ - Aluminum Oxide
- Fe₂O₃ - Ferric Oxide

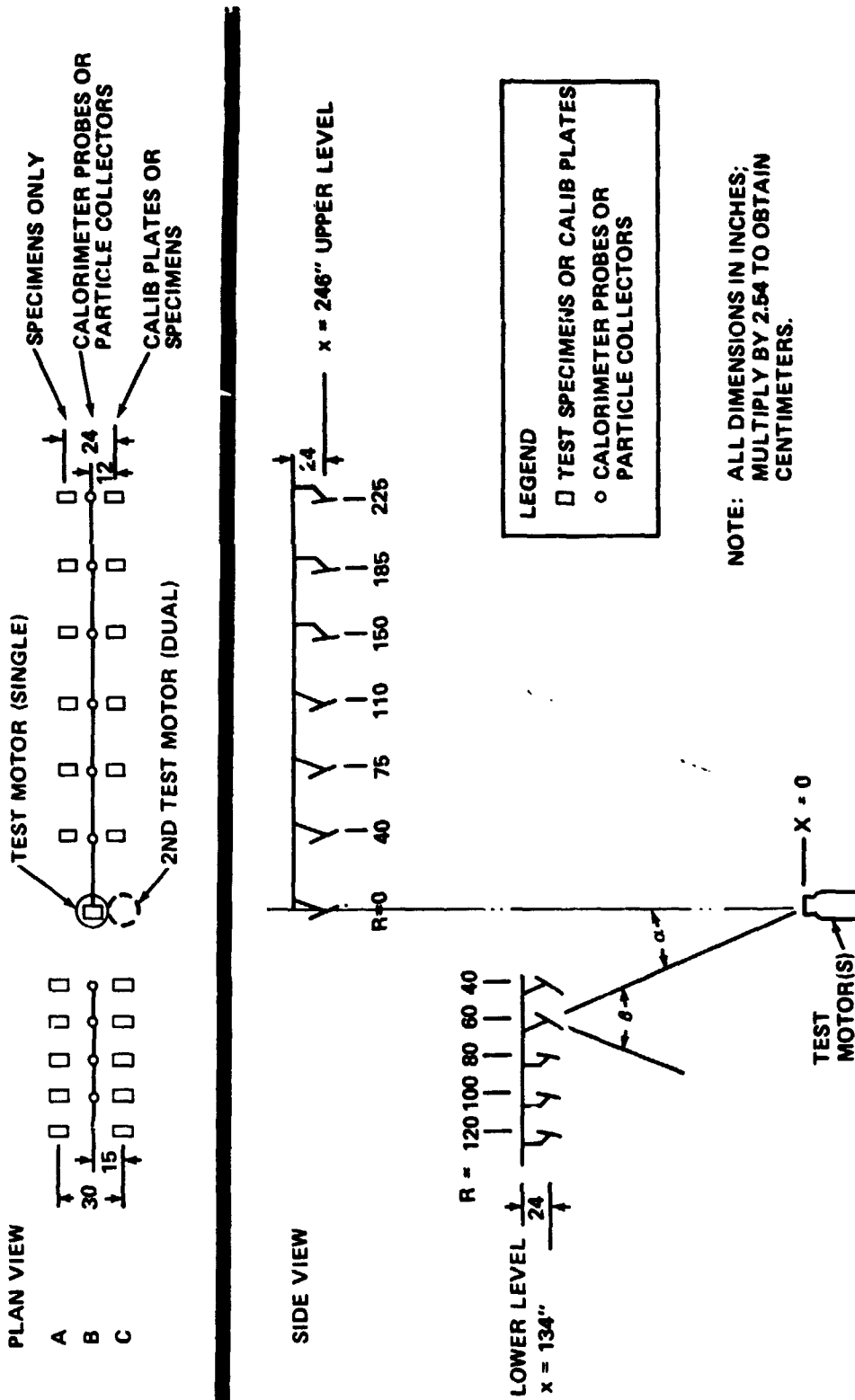


Figure III-1. Large motor impingement test arrangement.

were attached to individual brackets that bolt to a horizontal I-beam structure. The bracket identification for the various target locations are specified in Figure III-1.

For further details concerning the tests, the reader is referred to William F. Richardson, EE01, NASA/MSFC, and Don Dennison, Rockwell International, or Rockwell International document SD 74-SH-0232.

B. Solid Particle Collection Technique

David W. Jex and Joe C. Birdsong

Solid particle collection was made using a particle collector screen (PCS) filter system. The filter is detailed in Figure III-2. The screen of the filter (item 1 in Figure III-2) was a stainless steel wire mesh with $10\ \mu\text{m}$ openings. The flow of gases and particles was in the direction of the flow arrow in the figure.

The entire particle collector screen filter assembly is shown in Figure III-3. The bracket oriented the assembly and protected the system components from direct plume impingement. It also helped create a partial vacuum at the exit end of the assembly to aid the flow through the system. The elbow was used to make the filter as horizontal as possible to keep collected material from dropping out of the system when the positive pressure from the plume ceased. The 3.81 cm (1.5 in.) pipe oriented the assembly such that a solid particle traveling in a straight line from the nozzle would enter the assembly normal to the sampling orifice. This system was devised and adapted by Jack Frye of Rockwell International.

The procedure was to weigh each component of a PCS, assemble the PCS and install it just prior to the closing of the chamber. Immediately after the test, each PCS was removed and disassembled. Each component was weighed again and then placed in a 1000 ml flask. The flask was filled with ethyl alcohol to the 800 ml level which covered all the components. The flask was then placed in an ultrasonic cleaner and vibrated for 30 min. The components were removed and the excess alcohol allowed to evaporate from each piece. They were then weighed again. The mass difference before and after the test at the identified locations is given in Table III-2. Plots of the mass data are given in Figures III-4 and III-5.

The flask containing the alcohol and particles collected from the assembly components was boiled at 65.6°C (150°F) until 200 to 150 ml remained. The solution was then transferred to containers for transportation.

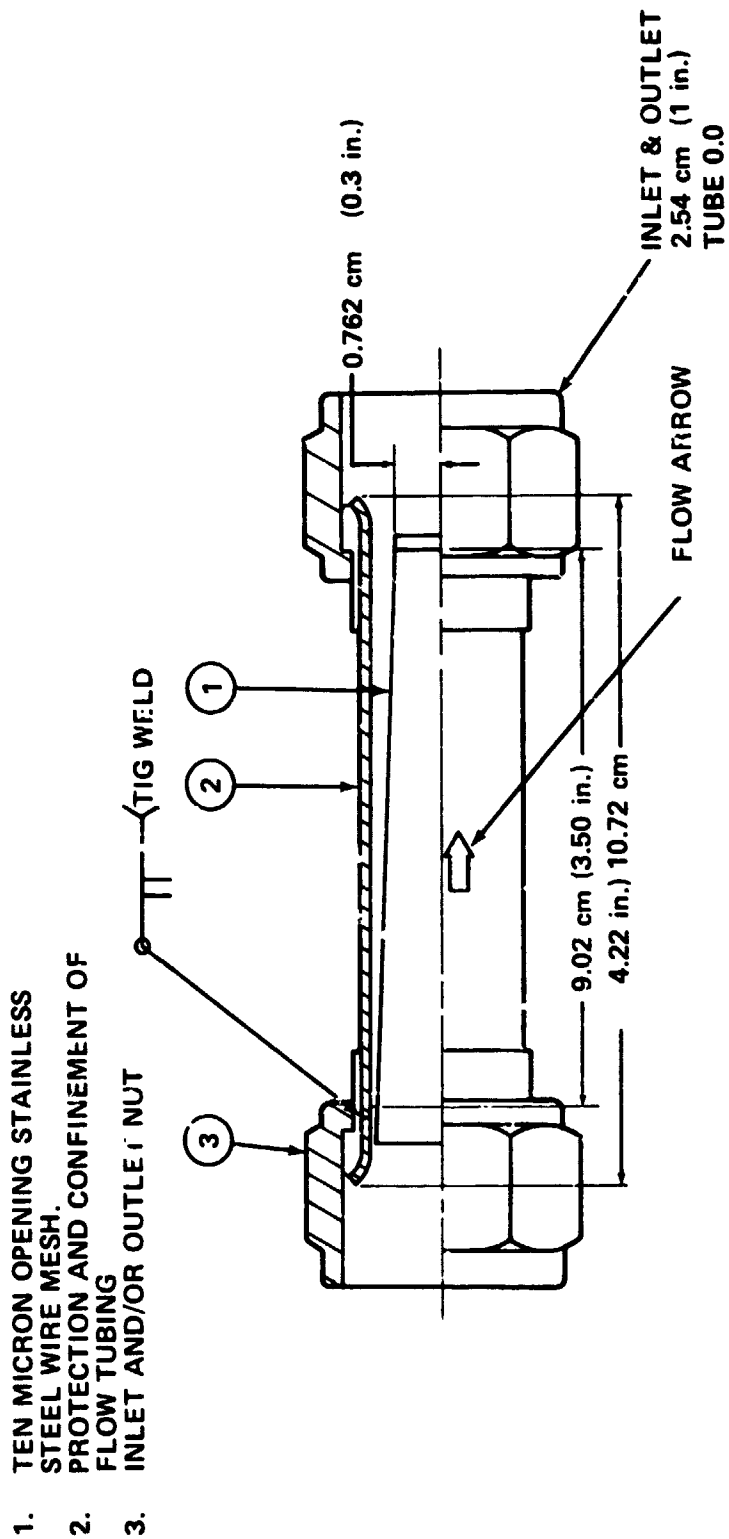


Figure III-2. Filter assembly.

UPPER BEAM INSTALLATION

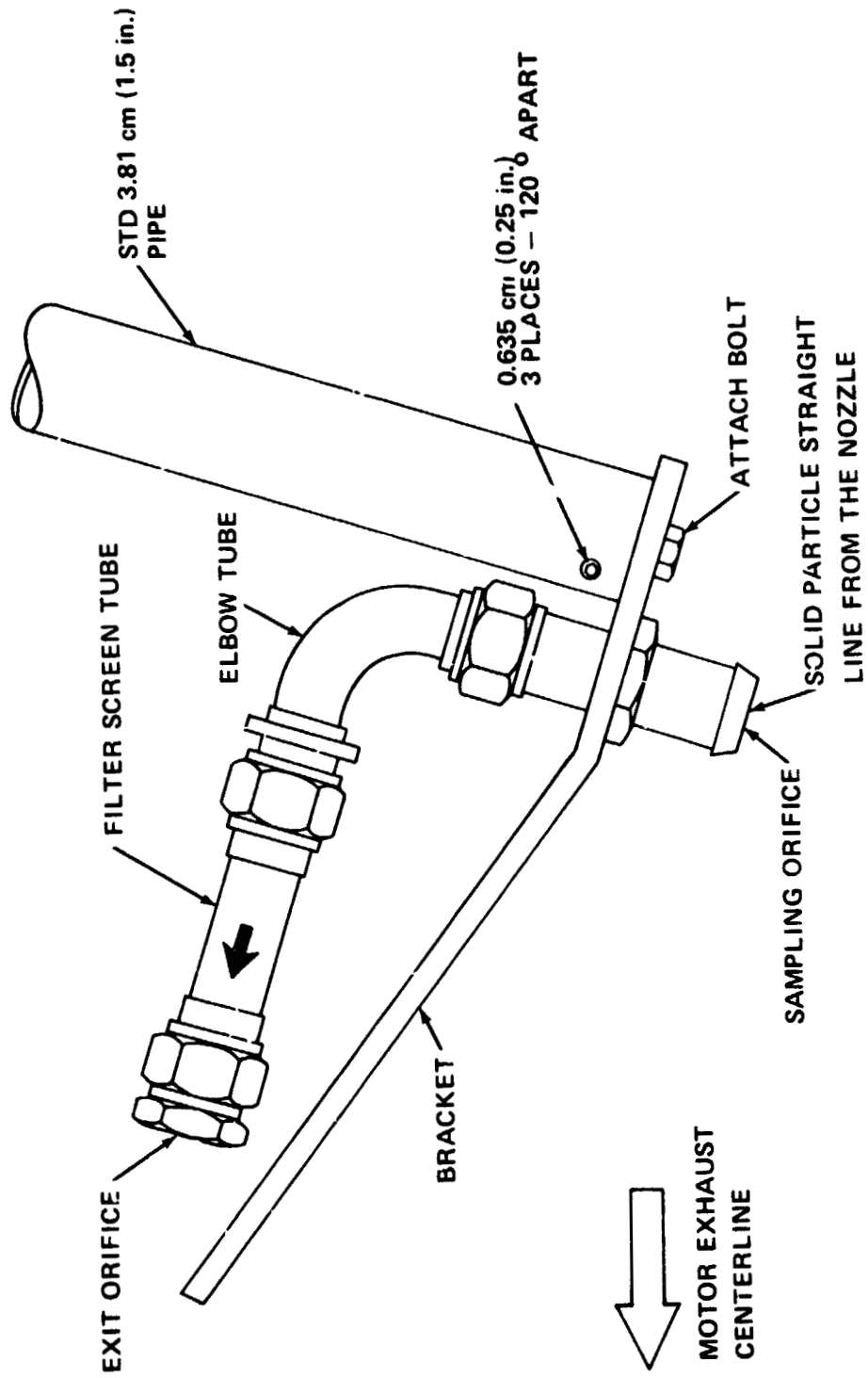


Figure III-3. Particle collector screen unit installed.

TABLE III-2. MASS COLLECTED BY PARTICLE COLLECTOR SYSTEM COMPONENTS

Test Number	1	2	3	4	5	6	7
Date	July 23	July 25	Aug. 2	Aug. 6	Aug. 8	Aug. 9	Sept. 25
Motor Type	3-single	3-dual	6-single	6-dual	1-dual	3-single	6-dual
1 Mass Collected by Entrance Orifice (in grams)							
Upper Level	0						0.0190
	40b						0.0195
	75b						0.0167
	110b						0.0135
	150						0.0017
	185						-0.0006
	225						-0.0003
Lower Level	40						0.0000
	60						0.0277
	80						0.0239
	100						0.0295
							0.0118
2 Mass Collected by Elbows (in grams)							
Upper Level	0						0.0097
	40						0.0122
	75	0.0256	0.0417	0.0157	0.0258	0.0137	0.0185
	110			0.0052	0.0292	0.0151	0.0253
	150	0.0035	0.0013	0.0225	0.0027	0.0027	0.0037
	185	0.0028	0.0036	0.0020	0.0029	0.0026	0.0031
	225	0.0034	0.0011				0.0025

Behind the Beam

TABLE III-2. (Concluded)

Test Number	1	2	3	4	5	6	7
Date	July 23	July 25	Aug. 2	Aug. 6	Aug. 8	Aug. 9	Sept. 25
Motor Type	3-single	3-dual	6-single	6-dual	1-dual	3-single	6-dual
2 Mass Collected by Elbows (in grams): (Concluded)							
Lower Level			0.185	0.0215	Behind the Beam		0.0000
60	0.0138	0.0748					0.0264
80	0.0043	0.0309	0.0027	0.0114	0.0223		0.0218
100							0.0284
							0.0159
3 Mass Collected by Filters (in grams)							
Upper Level							0.0496
40	0.0745	0.0615	0.0517	0.0309	0.0331		0.0118
75			0.0202	0.0573	0.0713	0.0122	0.0538
110	0.0041	0.0103		0.0065	0.0090		0.0300
150	0.0022	0.0132	0.0031	0.0073	0.0044		-0.0013
185	0.0124	0.0023					0.0352
225							0.0000
							0.0006
Lower Level			0.0370	0.0248	Behind the Beam		0.0165
40							0.0216
60	0.0262	0.0929					0.0248
80	0.0163	0.0755	0.0066	0.0424	0.0180		0.0220
100							

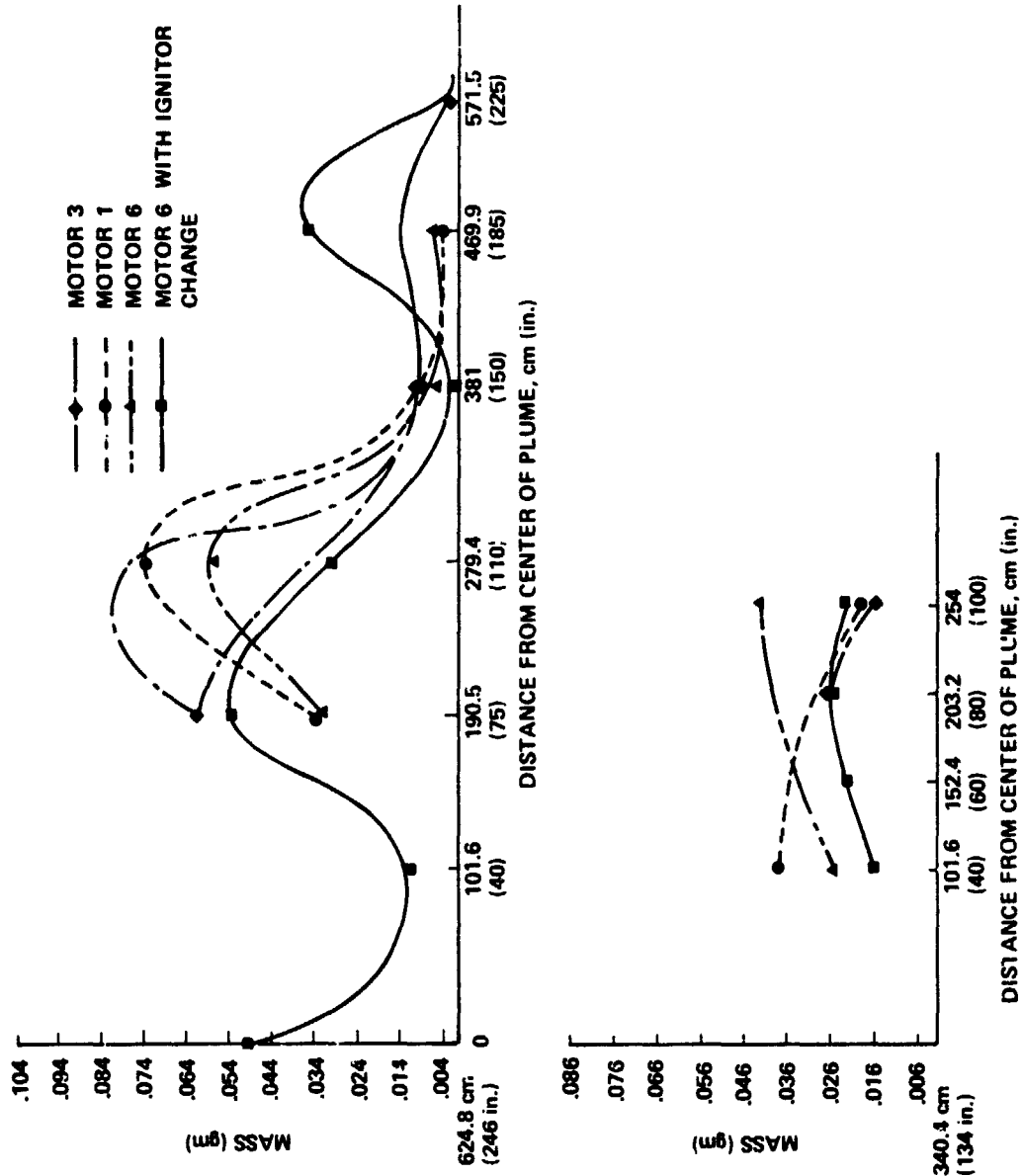


Figure III-4. Dual motor firings — mass collected by filters.

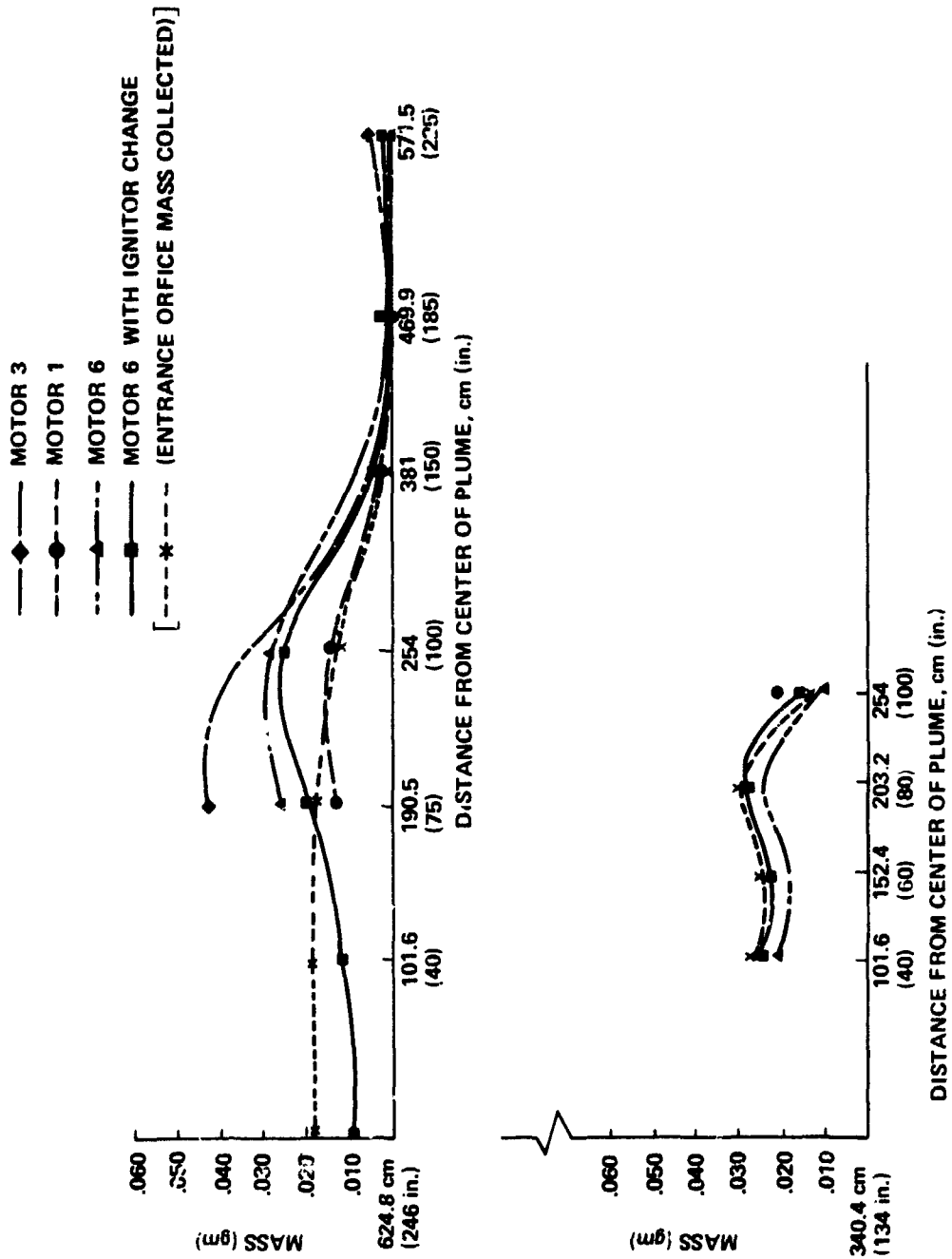


Figure III-5. Dual motor firings — mass collected by elbows.

Several things were done with the collected solutions: (1) a size distribution of the solid particles in each solution was plotted similar to the procedure outlined for the MSFC tests (Section II); (2) half of each solution was given to Marshall King (EH34) for analysis; (3) six specimens of selected solutions were sent to Walter C. McCrone for analysis using x-ray diffraction and electron microprobe techniques; (4) several selected specimens were sent to David Nichols and Dan Gates for electron microscope photographs and electron probe analysis; (5) selected specimens were sent to Athens College for wet chemistry analysis. The results from each of these tests are presented in Subsections C and D which follow, with the exception of data obtained by Marshall King. The data obtained by Mr. King can be obtained and discussed with him.

C. Particle Size Distribution

Willa Russell and David Jex

Solid Rocket Motor Plume Impingement Tests were conducted at AEDC during July, August, and September of 1974. The tests were to assess the damage of plume impingement on Shuttle thermal protective surfaces (TPS). To assist in this effort the sizes of collected particles in the plume flow were measured.

There are two possible levels for particle collection: (1) upper level [axial distance 624.8 cm (246 in.)] and (2) lower level [axial distance 340.4 cm (134 in.)]. The axial distance is the distance from the rocket motor nozzle to the position of the location holders. The maximum number of locations for collecting samples is seven for the upper level and four for the lower level. This is illustrated in Figure III-6.

Samples were not taken at all possible locations on each firing. Therefore, to identify which locations were sampled on the given test firing. The level identifier in the upper right hand of Figure III-6 is used and a circle placed at each location sampled on the designated test firing. The width of the identifier corresponds to the width of the bar in the graphs. The narrower the width of the bar, the closer it is radially to the centerline of the plume.

There are locations on the upper level that are on or close to a straight line drawn from the rocket nozzle through locations on the lower level. For solid particle trajectories, locations that meet this criteria should be comparable in particle size distributions, if size and distribution are not a function of axial distance. Those locations considered comparable would be:

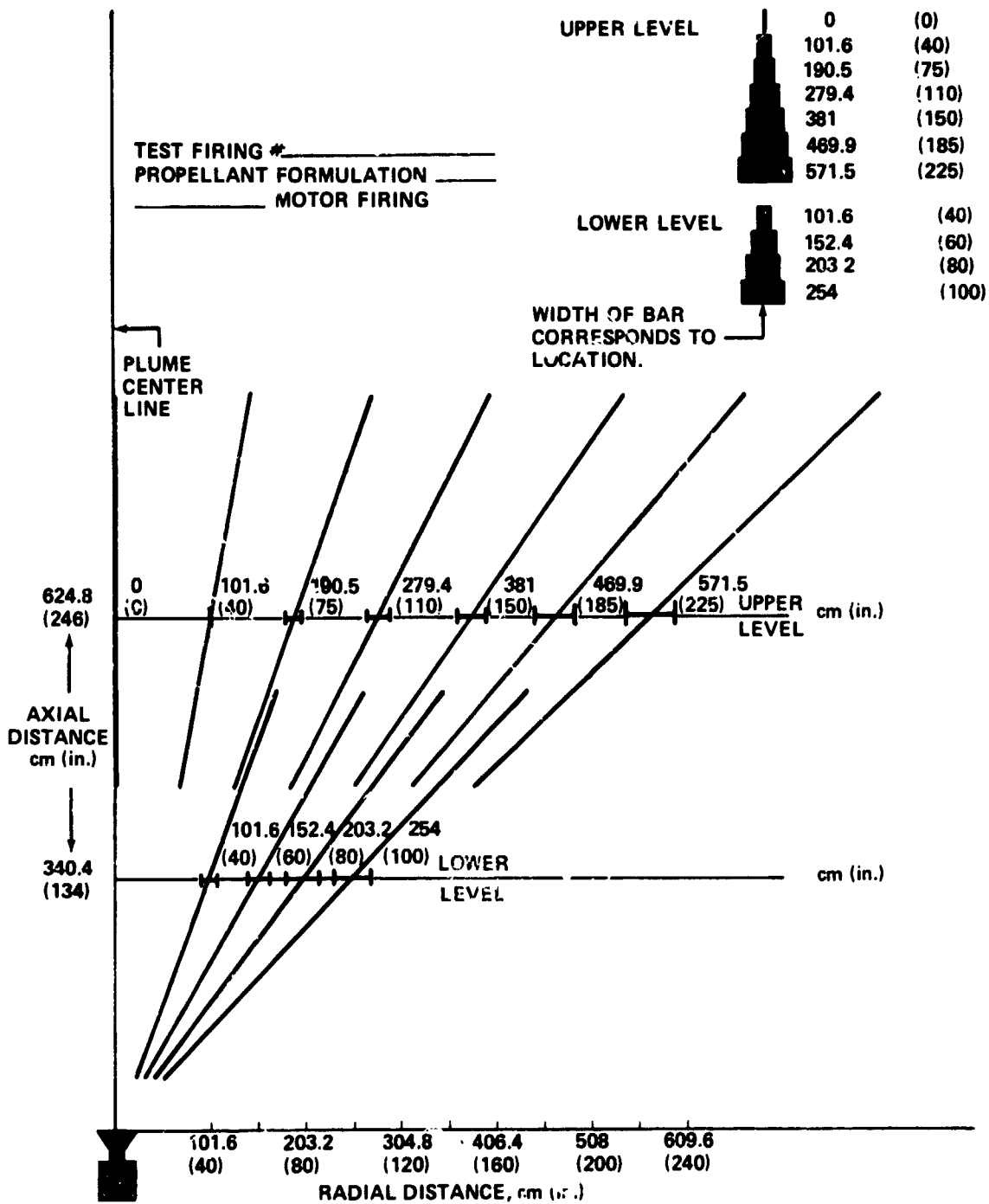


Figure III-6. Particle size sampling locations.

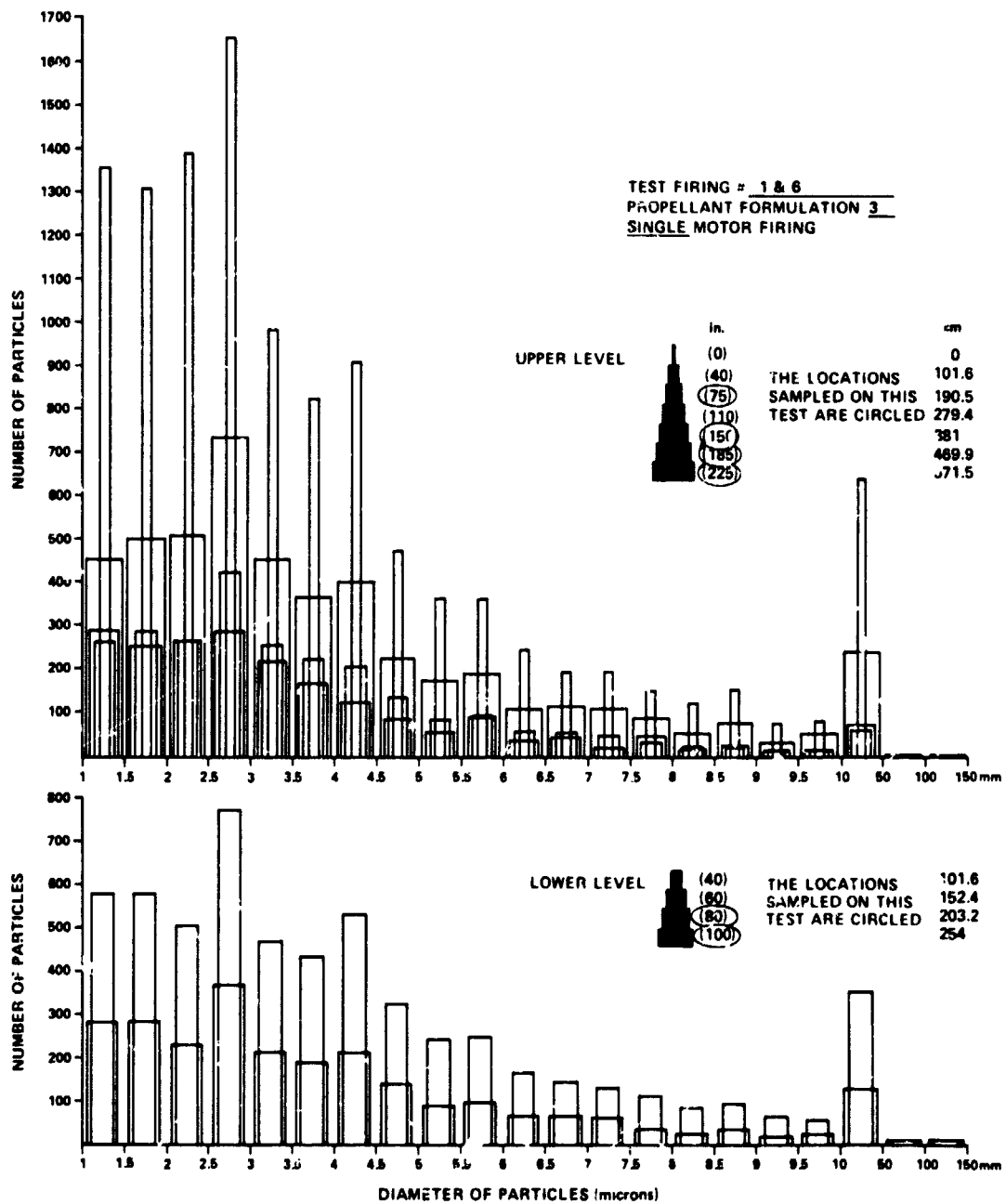


Figure III-6. (Continued).

TEST FIRING # 2
 PROPELLANT FORMULATION 3
 DUAL MOTOR FIRING

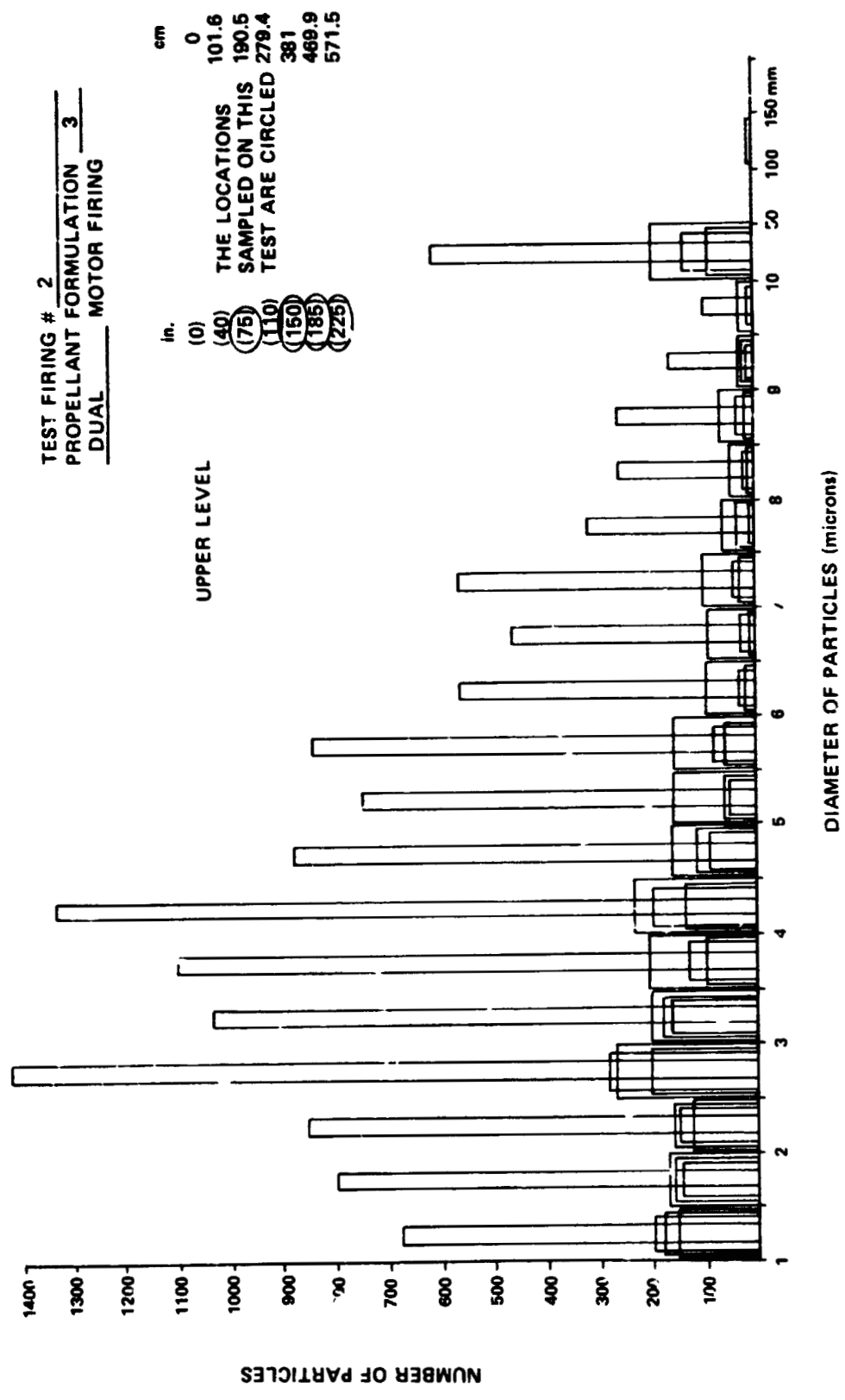


Figure III-6. (Continued).

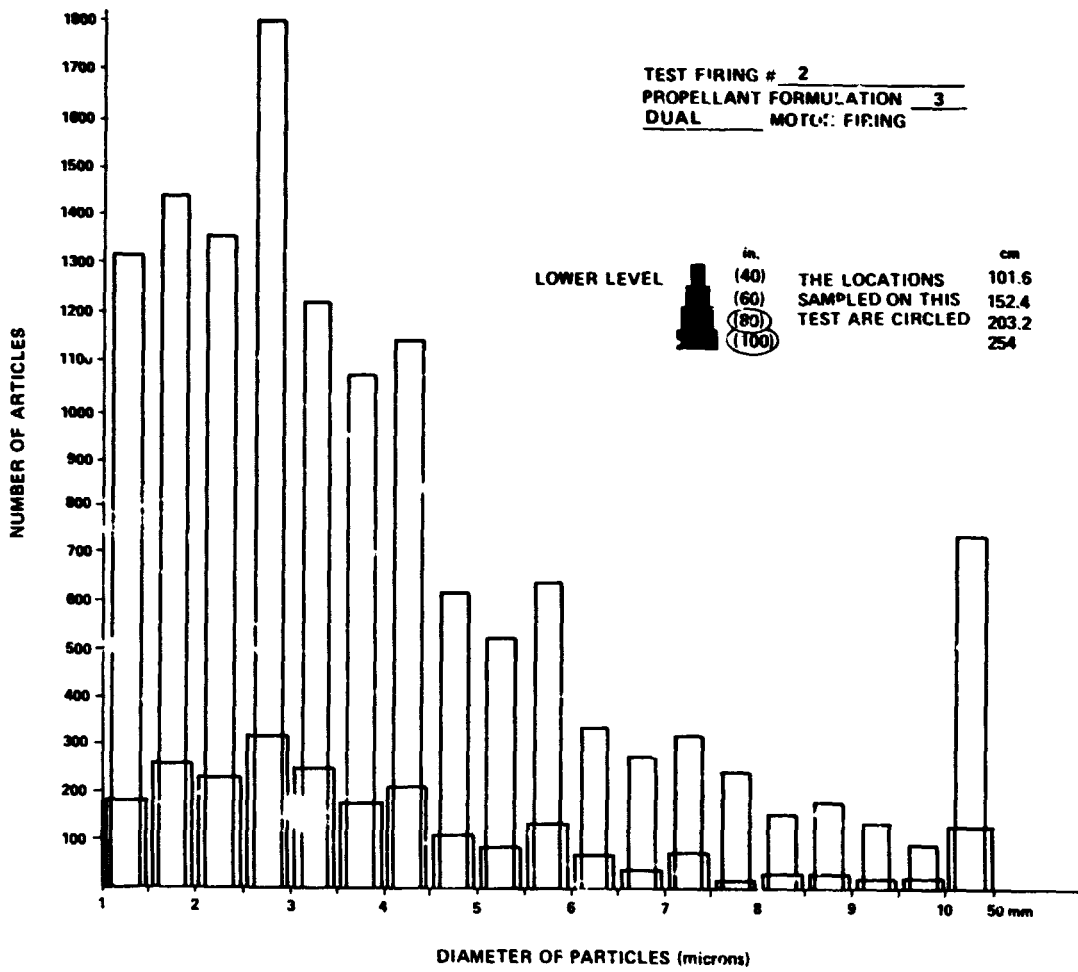


Figure III-6. (Continued).

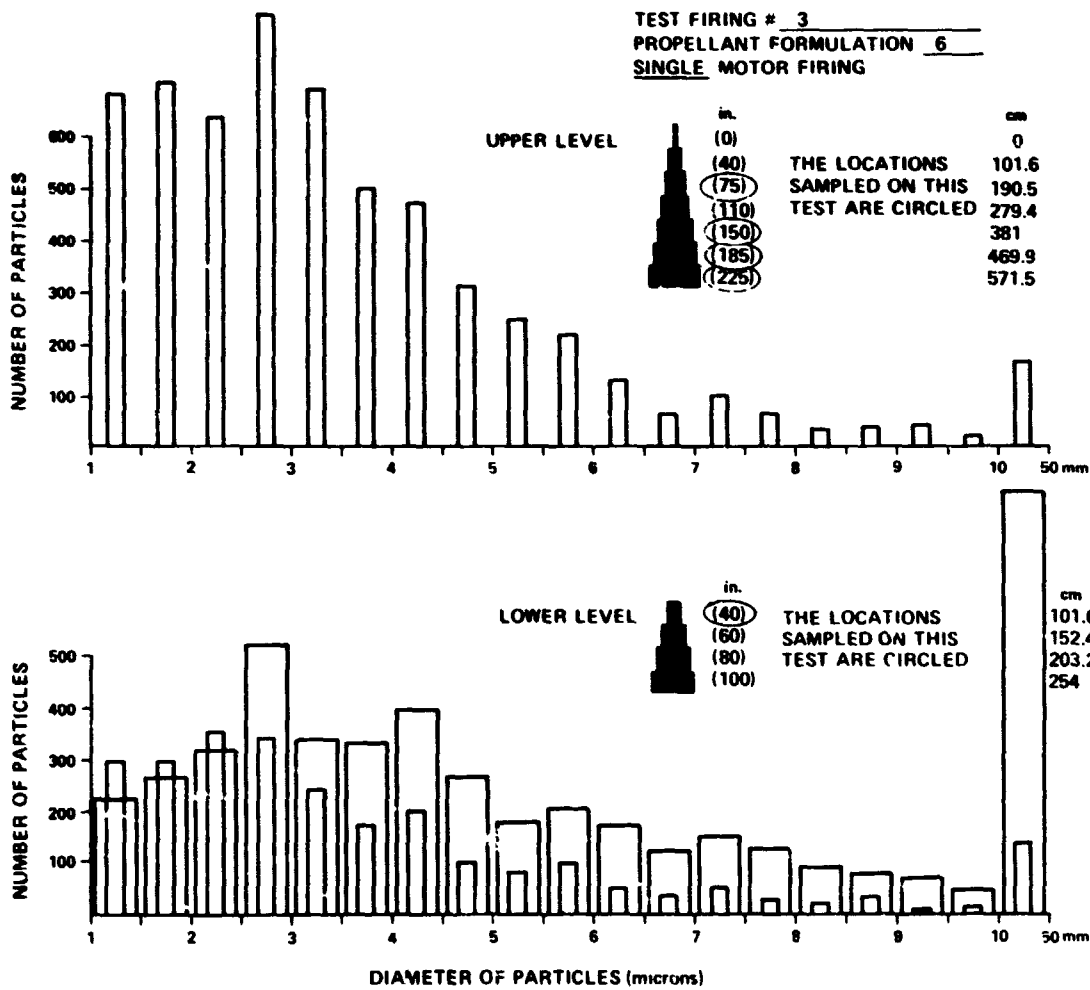


Figure III-6. (Continued).

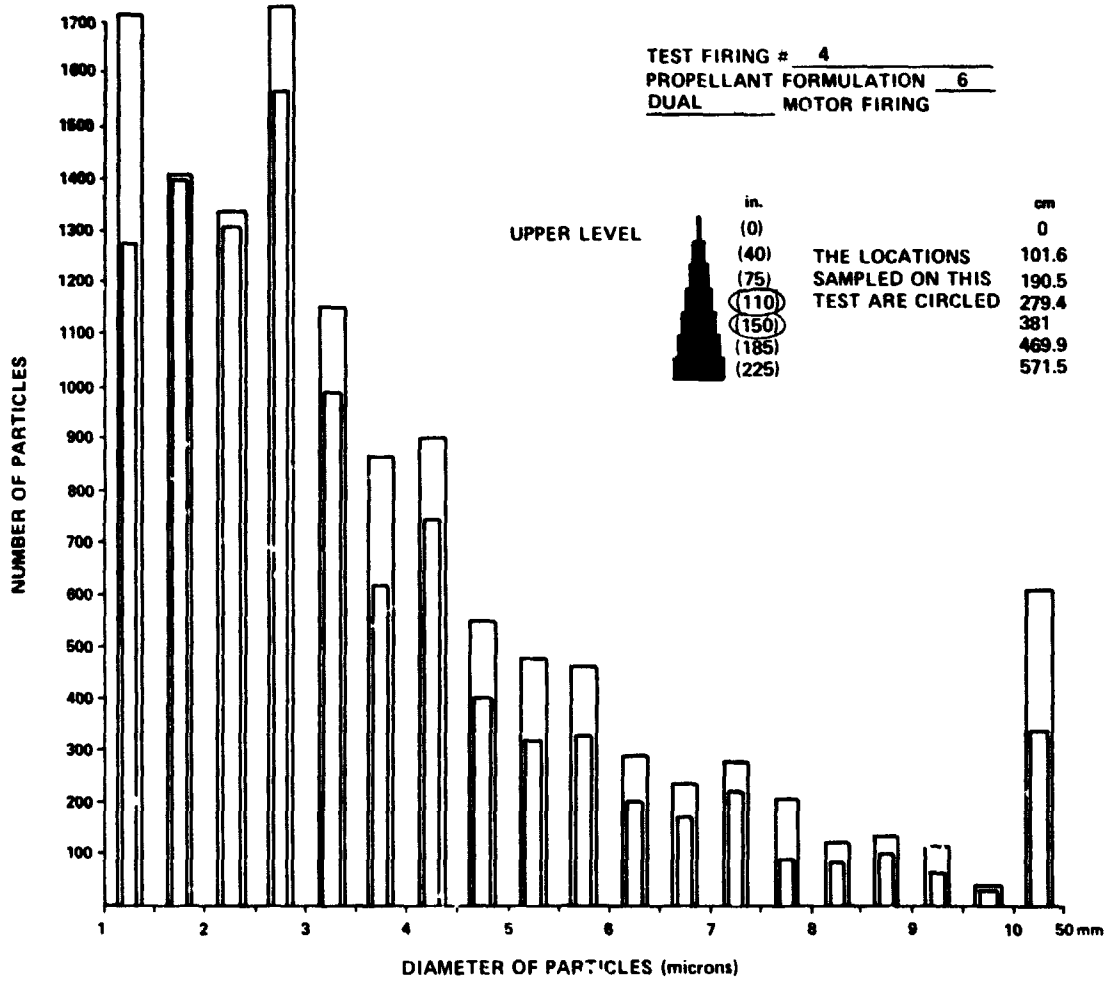


Figure III-6. (Continued).

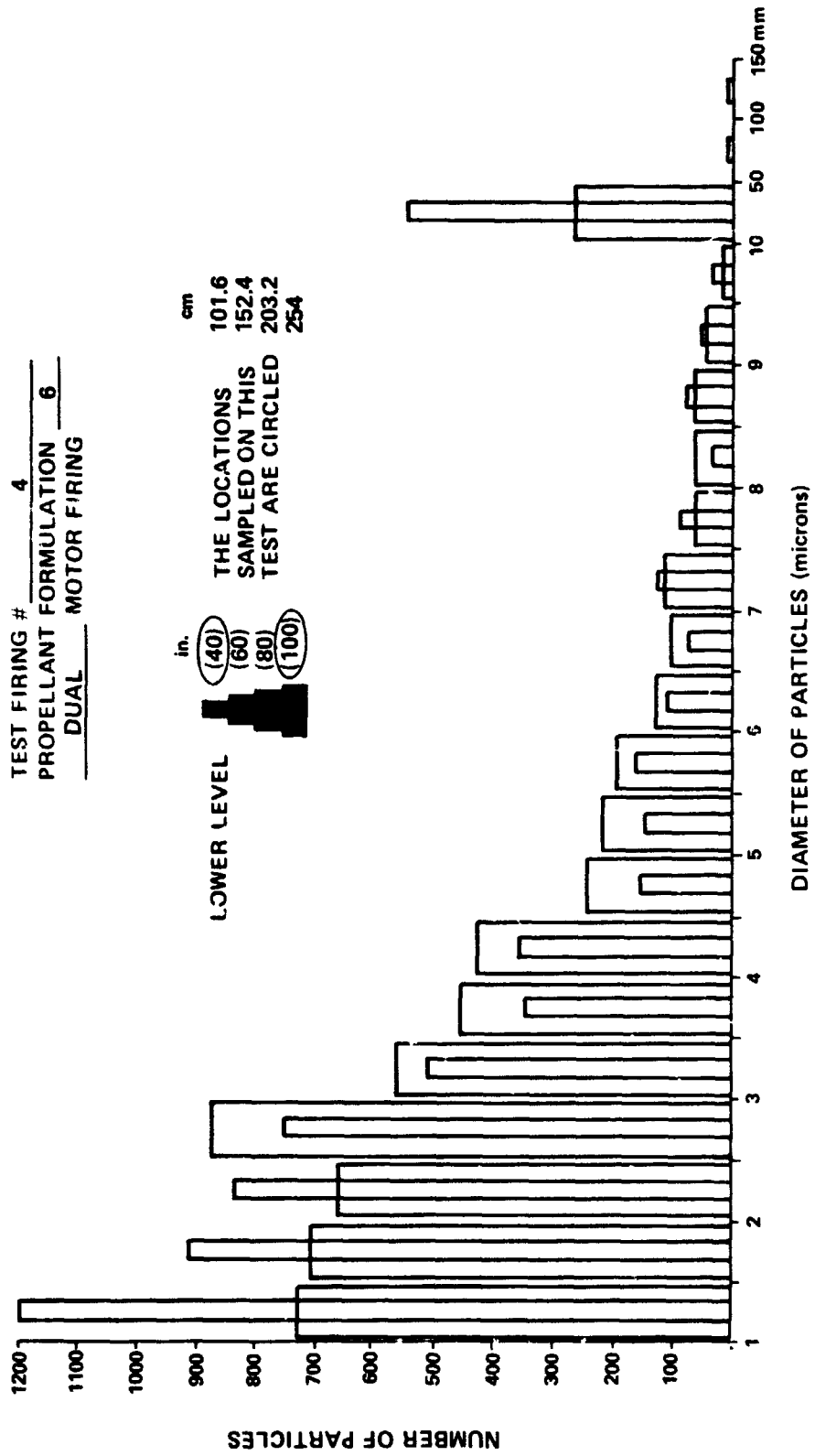


Figure III-6. (Continued).

TEST FIRING # 5
 PROPELLANT FORMULATION 1
 DUAL MOTOR FIRING

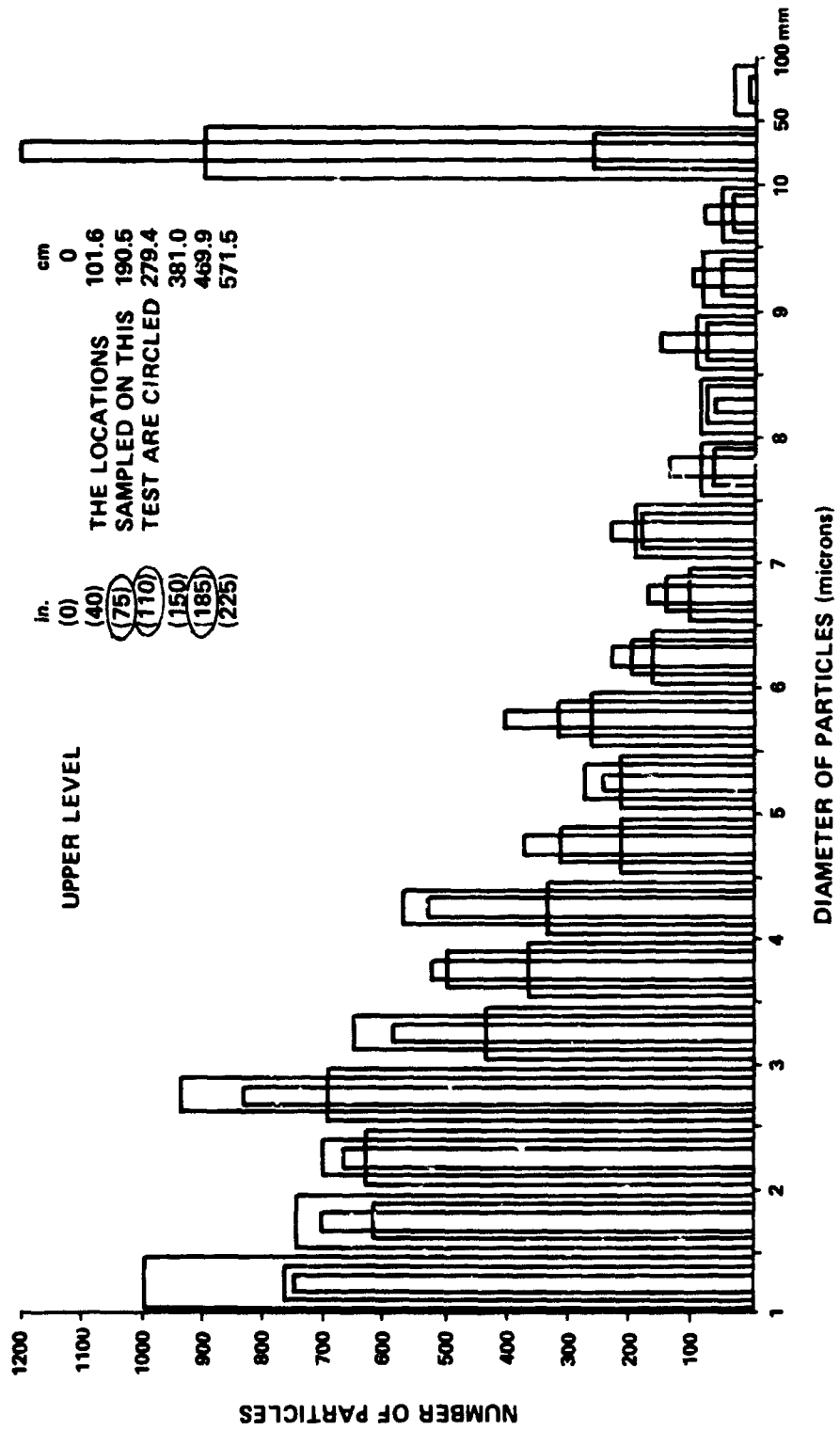


Figure III-6. (Continued).

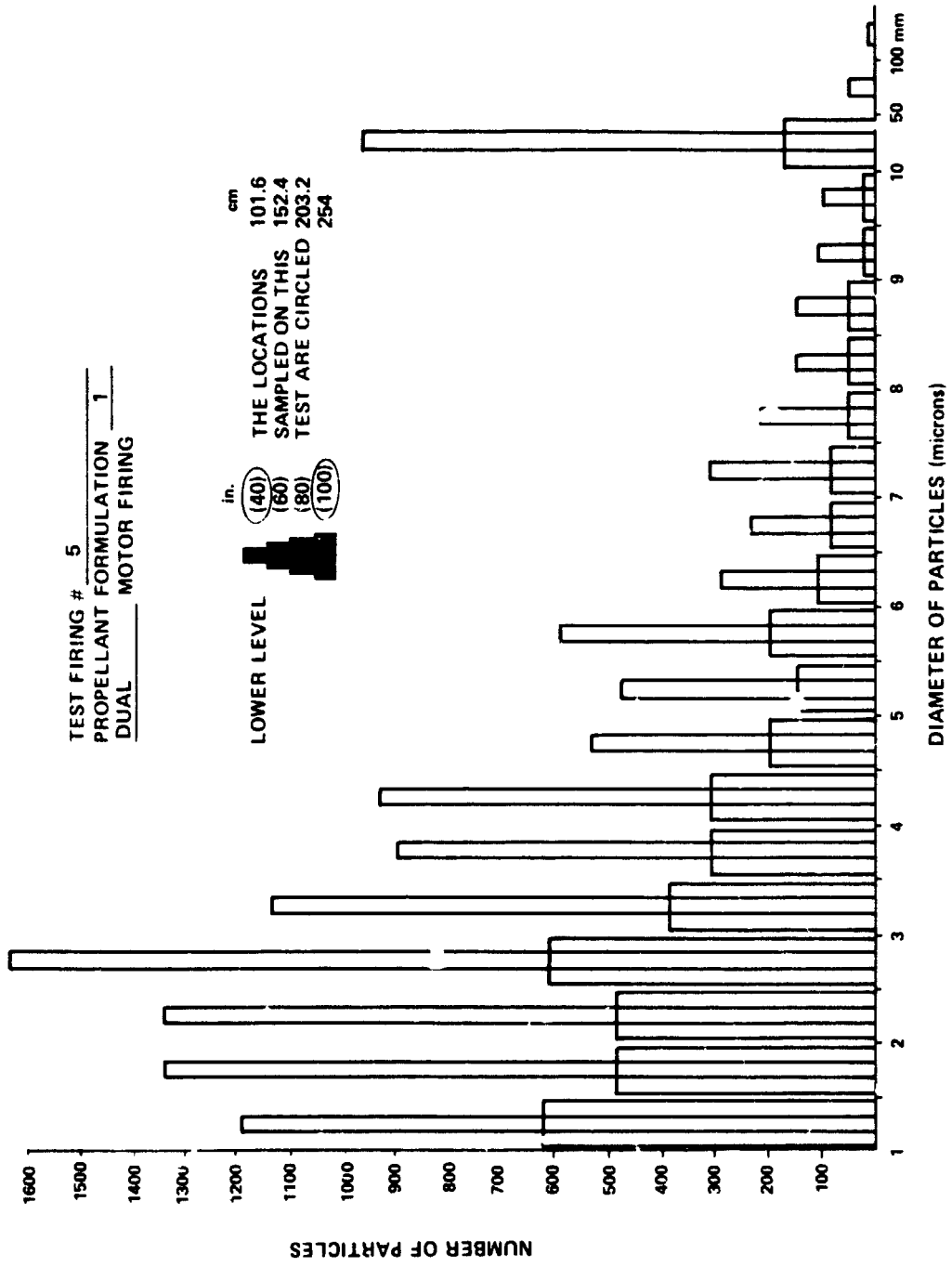


Figure III-6. (Continued).

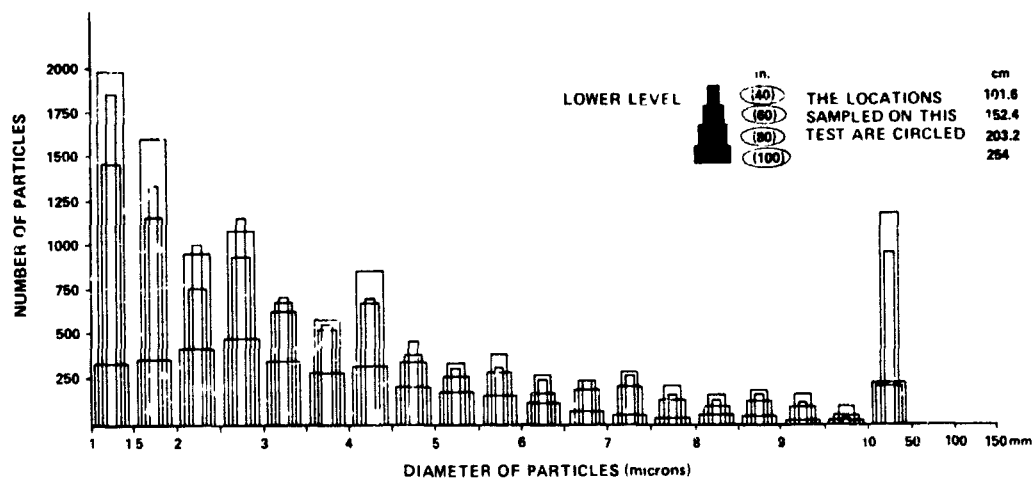
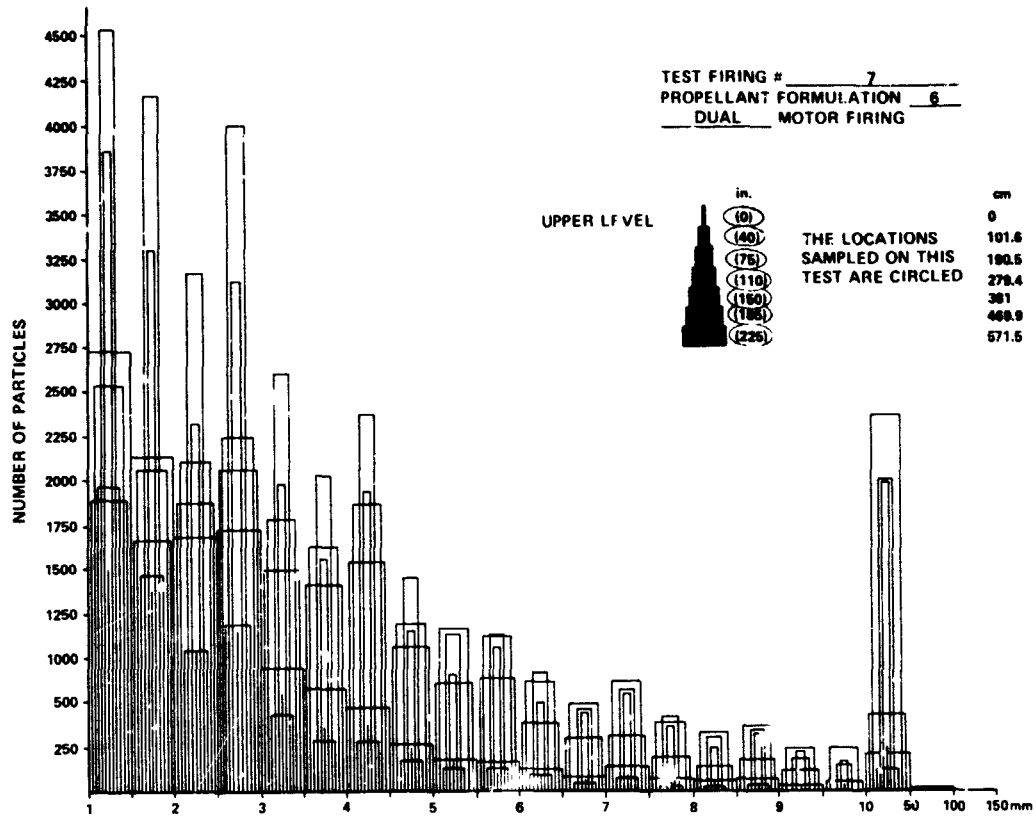


Figure III-6. (Concluded).

Lower Level Locations, cm (in.) compare to Upper Level Locations, cm (in.)

101.6 (40)	190.5 (75)
152.4 (60)	279.4 (110)
203.2 (80)	381 (150)
254 (100)	469.9 (185)

Included in Figure III-6 are data which identify which propellant was used and whether it was a single or dual motor firing for the specified test firing.

There were seven firings in all. Data from firing 6 is included in the graph for firing 1 since they were the same propellant type and also both were single motor firings.

The size range and number of particles for each location sampled was done by Willa Russell using the Bausch and Lomb OMNICON system in the Optics and Electro-Optics Branch of Space Sciences Laboratory. The system counted the number of particles with a diameter between two limits. The total number of particles counted were from a 2 cm by 2 cm area of the prepared specimen. Specimens for each location sampled were prepared identically, and the method is described in Section II, under particle size analysis.

The limits were set at 0.5 μm intervals from 1 (which is the lower limit of confidence in accuracy for this particular setup) to 10 μm . For example, the number of particles whose diameter is greater than 1 μm but less than or equal to 1.5 μm are represented by one bar height. Therefore, the number of particles (N), $1.0 < N_1 < 1.5$; $1.5 < N_2 < 2.0$; $2.0 < N_3 < 2.5$; $2.5 < N_4 < 3.0$; etc., are the heights of the bars in the bar graphs.

After the 10 μm level was reached, the number of particles whose diameter is greater than 10 but less than or equal to 50 was accumulated. Then the number greater than 50 but less than or equal to 100 was the terminating count.

The ordinate (number of particles) on the bar graph for firing 7 is 250 particles per division, as compared to 100 particles per division for firings 1 through 6.

D. Particle Compositional Analysis

As stated in Section IIIB, there were three techniques employed to determine the composition of the collected particles:

1. X-ray diffraction.
2. Electron microscope and microprobe techniques.
3. Wet chemistry.

The results of each of these investigations are presented in the same format as that in which the data were supplied by the specific investigator. The first investigation (x-ray diffraction) was by Walter C. McCrone Associates (Mr. Howard Humecki); the second investigation (electron microscope and microprobe) was by MSFC-ASTR (David Nicolas) and MSFC-SSL (Dan Gates); and the third investigation (wet chemistry) was by Athens College (Ron McNutt).

Each of these investigators received sample specimens from the test firings. The resulting information reported by the investigators is summarized in Table III-3.

1. Particle Compositional Analysis - Walter C. McCrone Associates

On September 6, 1974, six sample specimens of particulate matter from the SRM plume were received from the Marshall Space Flight Center. These samples were evaluated and it was determined that they consist largely of magnetite (Fe_3O_4) and varying amounts of quartz and hematite. Aluminum, calcium, chlorine, chromium, potassium, manganese, phosphorus, sulfur and titanium were found in some samples, but their molecular structure could not be determined.

a. Analytical Procedures. Samples were examined microscopically prior to analysis. In addition each sample was analyzed by x-ray diffraction and electron microprobe. The microprobe supplied information regarding elemental composition, and x-ray diffraction defined molecular structure. For example: sample 1 was found to contain 12 to 17 percent by weight of iron, by electron microprobe, but it could not be determined if the iron was present in the elemental form or in combination such as an iron silicate. X-ray diffraction of the same sample showed that the iron was largely magnetite (Fe_3O_4).

TABLE III-3. SUMMARY OF COMPOSITIONAL ANALYSIS USING X-RAY DIFFRACTION,
ELECTRON MICROPROBE AND WET CHEMISTRY

Test Firing #	Walter C. McCrone, Inc. ^c						Athens College						MSFC		
	X-Ray Diffraction and Electron Microprobe						Wet Chemistry						Electron Microprobe		
	5		4		3		5		4		3		5	7	2
Propellant Type ^a	ID		6D		6S		ID		6D		6S		ID	6D	3D
Sample Location ^b	UL75	LL40	LL40	UL110	UL110	UL75	UL75	UL75	LL40	UL110	UL110	UL75	UL185	LL40	LL80
Al	1.5	0.75	-	0.75	1.5	-	3.2	2.6	5.5	1.0	7.0	21.4	27.8	32.0	15.3
Si	2.5	3.5	0.25	1.5	3.0	13.0	-	-	-	-	-	-	5.0	4.2	10.3
P	2.5	1.5	0.75	2.5	-	-	-	-	3.7	1.6	-	-	0.4	0.9	0.1
S	-	1.5	-	-	-	-	-	-	0.4	1.5	0.4	-	0.4	1.5	0.4
Cl	5.5	4.0	0.25	-	-	-	-	-	1.0	0.3	0.6	-	1.0	0.3	0.6
K	1.5	-	-	1.5	-	-	-	-	1.4	-	1.2	-	1.4	-	1.2
Ca	-	-	-	-	0.3	4.0	-	-	4.3	4.9	0.7	-	4.3	4.9	0.7
Cr	6.5	7.5	0.75	6.5	-	-	-	-	1.4	1.0	1.0	-	1.4	1.0	1.0
Mn	-	-	-	1.6	-	-	-	-	17.3	14.5	31.6	71.4	51.3	47.7	65.9
Fe	42.5	40.0	5/	35	50	15.5	12.7	6.3	17.3	14.5	31.6	71.4	51.3	47.7	65.9
Ni	-	-	-	-	-	-	-	-	0.9	0.1	0.3	-	0.9	0.1	0.3
Cu	-	-	0.35	-	-	-	49	56	28	16	5	7	0.5	0.5	0.3
Burned on Ignition															

NOTE: All numbers are percentage by weight.

a. Propellant type: The numerical designation corresponding to Table III-1 will be followed by a D (dual) or S (single) describing the number of motors with that propellant type first.

b. Sample Location: Upper Level - UL Lower Level - LL

c. The midpoint was used for the percentages of Walter C. McCrone data.

Every effort was made to prepare homogeneous samples representative of the entire specimen, although this proved difficult with specimens 1 and 5 due to the small sample available.

b. Analytical Results. Test results are presented in Table III-4. Microscopically, 1 and 2 are similar. Each contained many magnetic particles 20 to 40 μm in size. Sample 2 contained some as large as 80 μm . Many small particles less than 2 μm were present although on a mass basis the large ones represent the greatest portion. Since none of the particles were spherical it can be safely said that they never reached their melting temperature of approximately 65.6° C (1540° F).

Samples 3 and 4 consisted of 1 to 2 μm particles mostly gray-black in color but several orange-brown.

Sample 5 is mostly gray-black and similar to sample 2. They are magnetic also.

Sample 6 is largely orange-brown in reflected light and it was suspected they consisted of hematite. However in transmitted light they were entirely opaque and at least partly magnetic.

c. Discussion. The thermal protective surfaces (TPS) of the shuttle vehicle were damaged after separation. On ignition, the plume of the SRM impinges on these surfaces and it is suspected the erosion is the result of the action of gaseous and/or particular components of this plume.

Particles collected during test runs were examined by light microscopy and analyzed by electron microprobe and x-ray diffraction. In all tests, the major element found was iron. The iron was largely in the form of gray-black magnetite (Fe_3O_4) even in those cases where the sample appeared orange. Microscopical examination reveals the centers are gray but have a surface coating of orange, which is due to hematite (Fe_2O_3). Hematite is rapidly and quantitatively reduced to magnetite at high temperatures in the presence of reducing agents. It is clear that hematite present in the fuel was completely reduced to magnetite during combustion, then, when the reducing atmosphere was no longer present, the outer surfaces oxidized to hematite again.

Both hematite and magnetite melt between 1500 and 1600° C. The shape of these particles indicates they were never exposed to these high temperatures.

TABLE III-4. COMPOSITION OF EXHAUST PARTICLES

Sample	Elemental Composition by Weight ^a											Molecular Composition ^b					
	Al	Ca	Cl	Cr	Cu	Fe	K	Mn	P	S	Si		Ti				
Test 3 Motor 6S																	Iron is mostly as magnetite and silicon, partly as α -silica. Others unknown.
UL75		3-5	-	-	-	12-17	-	-	-	-	10-16	-	-	-	-	-	
UL110		0.2-0.4	-	-	-	15-55	-	-	-	-	2-4	-	-	-	-	-	Mostly magnetite
Test 5 Motor 1D																	Poor XRD data but, from appearance, at least some iron is magnetite.
UL75		-	4-7	5-8	-	35-70	1-2	-	2-3	-	2-3	1-2	-	-	-	-	
LL40		-	3-5	6-8	-	35-75	-	-	1-2	1-2	3-4	-	-	-	-	-	Mostly magnetite, but a fraction is oxidized to hematite. Silicon is as α -silica. Others unknown.
Test 4 Motor 6D																	Mixture of hematite and magnetite.
LL40		-	0.1-0.4	0.5-1	0.2-0.5	40-60	-	-	0.5-1	-	0.1-0.4	-	-	-	-	-	
UL110		-	-	5-8	-	30-40	1-2	1-2	2-3	-	1-2	-	-	-	-	-	Poor XRD data but a substantial part is magnetite.

a. From electron microprobe data.

b. From X-ray diffraction data and light microscopy.

The high silicon, calcium, and aluminum in sample 1 suggests a high level of material from the ignitor liner. The magnetic character of this sample, as well as the overall gray appearance, indicate exposure to a strong reducing atmosphere.

Sample 2 is similar in appearance to 1, but contains very little ignitor related substances.

Samples 3 and 4 are almost identical: both consist mainly of small ($\sim 2 \mu\text{m}$) particles of magnetite. The high level of chlorine (3 to 7 percent) indicates solid chlorides. We do not know where the chromium phosphorus, titanium or sulfur are coming from. Organo-phosphates are commonly used as plasticizers which suggests propellant binder as the source of phosphorus. The high level of chromium in both 3 and 4 indicates the presence of some component not previously mentioned. It would appear that a chromium or iron-chrome component is exposed to the plume (possibly paint with a titanium pigment). There is no evidence of metallic flakes; therefore, these erosion products (if they are erosion products) are oxidized.

Sample 5 resembles 2 both in composition and appearance. It is largely magnetite with small amounts of the elements found in 3 and 4.

Sample 6 is mostly iron oxides, but the proportion of hematite is greater than in the other samples. It resembles samples 3 and 4 in elemental composition except that chlorine is absent.

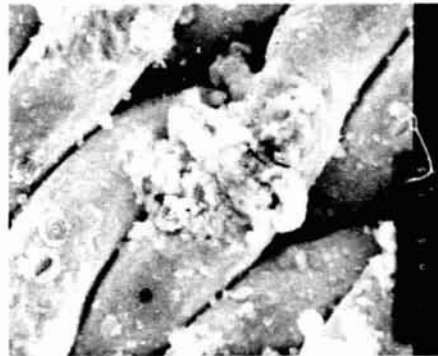
2. Electron Microscope and Microprobe Techniques - MSFC

A portion of the filter mesh from filter 26 was removed after test firing 4 and it was examined under an electron microscope. Several features were found. Figures III-7 and III-8 show some typical examples of the front (surface directly exposed to the flow) and the back of this piece of stainless steel mesh. The front surface exhibited small individual particles, clusters of particles, and areas that look like dried-up mud lakes.

Some interesting observations concerning each of these features on the front surface were that the small individual particles are generally not spherical or elliptical, indicating that they were not totally molten at any time. However, they are smooth on the outer surfaces, and several adhering to the mesh show signs of "puddling" at the interface between particle and mesh. This indicates they have been subjected to high heating and at least the outside layer was molten at the time the particle came in contact with the mesh strands.



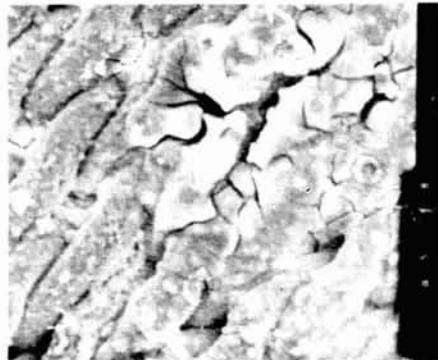
LARGE ANGLE VIEW



CLUSTERS OF PARTICLES



SMALL INDIVIDUAL PARTICLES

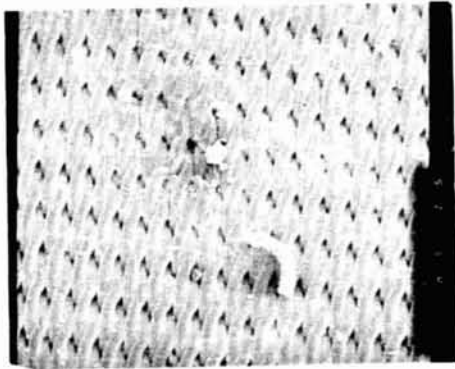


AREAS THAT LOOK LIKE DRIED UP MUD IN SIZES

Figure III-7. Features on the front surface of a portion of filter 26 mesh.

C.3

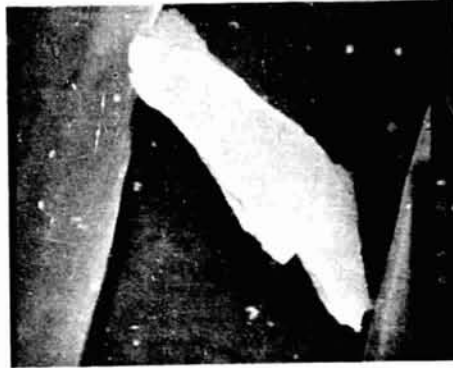
ORIGINAL PAGE IS
POOR QUALITY



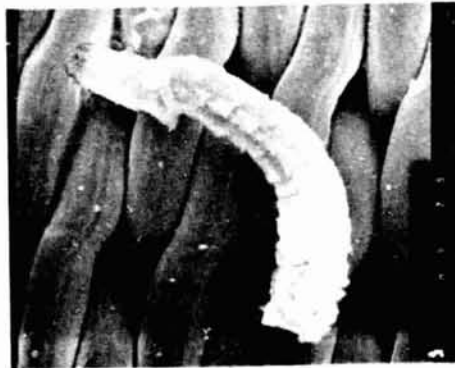
LARGE ANGLE VIEW



SMOOTHED PARTICLES



UNSMOOTHED PARTICLES



EXTRUSIONS

Figure III-8. Features on the back surface of a portion of filter 26 mesh.

The clusters of particles support the above observation that the outside layer of the particles was molten when contact was made. However, it does not reveal whether this occurred as a building process on the mesh at that location over a period of time or if the clusters were formed earlier in the flow and contacted the mesh as a cluster.

Examination of the features resembling dried-up mud lakes evidence that the material is a coating on the mesh and not a deterioration of the mesh material due to some reaction with another substance. It was also found that the long extrusions found on the back side were physically located opposite these dried-up mud lake features. This suggests that the substance was molten and collected during the actual motor firing when positive pressure could be exerted to cause the extrusions to be formed.

Small individual particles wedged in the mesh on the back surface were similar to those on the front surface with the exception that some irregular, unsmoothed particles were found that were not evidenced on the front surface.

As described in Section IIIB (solid particle collection technique) the filters and associated components were "rinsed" in ethyl alcohol and the residue collected. A sample of dual motor firings using propellants 1, 3, and 6 were analyzed by microprobe techniques (David Nicolas, MSFC-ASTR). Photographs of the area examined are shown in Figure III-9. Area 1 is a sample from firing 5, propellant 1; area 2 is a sample from firing 7, propellant 6; and area 3 is a sample from firing 2, propellant 3.

The results are shown in Table III-5.

3. Wet Chemistry — Athens College

The samples were examined using the same technique described in Section IC entitled "chemical analysis of solid rocket effluents" by Ronald McNutt dated January 24, 1974. The results are given in Table III-6.

E. Effects on Shuttle Windshields

The data accompanying this report provide a means of assessing the loss of visual opportunity through the Space Shuttle windshield due to deposition of plume deposits of the booster separation rockets. These data were obtained as a result of the deployment of passive and active windshield transmittance monitors in the J-4 chamber during the firing of SRM's. Propellant formulations 1, 3, and 6 are considered here.



TEST FIRING 5
 PROPELLANT 1 - DUAL
 LOCATION: UPPER LEVEL 185



TEST FIRING 7
 PROPELLANT 6 - DUAL
 LOCATION: LOWER LEVEL 40



TEST FIRING 2
 PROPELLANT 3 - DUAL
 LOCATION: LOWER LEVEL 80

Figure III-9. Photographs of areas examined by electron microprobe (David Nicolas, MSFC-ASTR).

TABLE III-5. ELECTRON MICROPROBE ANALYSIS OF
SOLID ROCKET MOTOR EFFLUENTS

Element	Area 1 Test Firing 5 Propellant 1-Dual Upper Level 185 (%)	Area 2 Test Firing 7 Propellant 6-Dual Lower Level 40 (%)	Area 3 Test Firing 2 Propellant 3-Dual Lower Level 80 (%)
Fe(L)	0.3	0.4	0.3
Cu(L)	0.5	0.5	0.3
Ga(L)	0.8	0.8	0.5
Al	27.8	32.0	15.3
Si	5.0	4.2	10.3
P	3.7	1.6	-
S	0.4	0.9	0.1
Cl	0.4	4.5	0.4
K	1.0	0.3	0.6
Ca(α)	1.4	-	1.2
Cr	4.3	4.9	0.7
Mn	1.4	1.0	1.0
Gd(L)	1.0	1.0	1.1
Fe(α)	44.6	41.5	57.0
Fe(β)	6.4	5.8	8.6
Ni	0.9	0.1	0.3

TABLE III-6. ANALYSIS OF ROCKET EFFLUENTS

	Sample	Dry Sample Weight (gm)	Sample Weight (gm) After Ignition	Percent Weight Loss on Ignition	Percent Iron Colorimetrically	Percent Aluminum Colorimetrically
Test 3 Motor 6S	UL75	0.0014	0.0013	7	71.4	21.4
	UL110	0.0019	0.0018	5	31.6	7.9
Test 5 Motor 1D	UL75	0.0063	0.0032	49	12.7	3.2
	LL40	0.0062	0.0027	56	6.3	2.6
Test 4 Motor 6D	LL40	0.0110	0.0079	28	17.3	5.5
	UL110	0.0297	0.0248	16	14.5	1.0

DOCUMENT IS UNCLASSIFIED DATE 07-11-2013 BY 60322 UCBAW/SJS

The passive samples were cuts of an actual windshield, each 2.54×5.08 cm (1×2 in.), and were deployed in various orientations in the J-4 facility to delineate the effects of recirculation from direct impingement. The optical data reported here correspond to one orientation deemed representative for the actual Shuttle configuration (Fig. III-10). Thus at least the relative merits of various propellant and igniter formulations may be assessed.

It is likely that the spectral range of transmitted light required for astronaut use of the windshield will be limited to the visible wavelengths 400 to 700 nm (4000 to 7000 Å). To evaluate the effects of plume deposition, however, the data are obtained through the near ultraviolet [300 nm (3000 Å)]. The transmission loss at these wavelengths is generally greater than in the visible range, leading to greater sensitivity in monitoring relative effects of different type propellants. To separate the effects of J-4 chamber cleanliness and recirculation unlikely to occur on the in-flight Shuttle, an active transmission monitor, the Transmissometer, was also deployed in these tests. It monitors the transmittance on a real-time basis of a windshield sample in the spectral range 290 to 300 nm (2900 to 3000 Å).

The results of the usage of the Transmissometer in all these tests may be summarized very briefly. There is very little (less than 5 percent loss in windshield transmittance prior to the rocket firing. At these wavelengths and at these simulated altitudes, the grimy nature of the J-4 chamber has very little effect on windshield viewing capability. After firing there is a consistent secondary loss of windshield transmittance of generally 15 percent relative, which is most likely due to recirculation in the chamber. This would not be a factor in space and thus the transmittance losses presented here exceed in magnitude the losses to be expected by about 15 percent. In other words, a 50 percent loss is probably only a 40 to 42 percent loss.

Knowing the spectral transmittance loss is a helpful criterion for evaluating effects of plume impingement, but it is not the whole picture. If the plume deposits were homogeneous thin film contaminants, which they are not, the resultant effect would be darkening of the Shuttle windshield. However, the AEDC tests have shown the windshield deposits to include film deposition, surface corrosion, and inclusion of particulates (some macroscopic). The latter two deposition properties lead to light scattering which is best evaluated by means of more sophisticated optical measurements (e.g., O. T. F.) than were allowable within the constraints of this program. As a compromise, photographs of the windshield samples before and after the rocket firing tests were taken to help illustrate effects such as loss of resolution and image clarity loss.

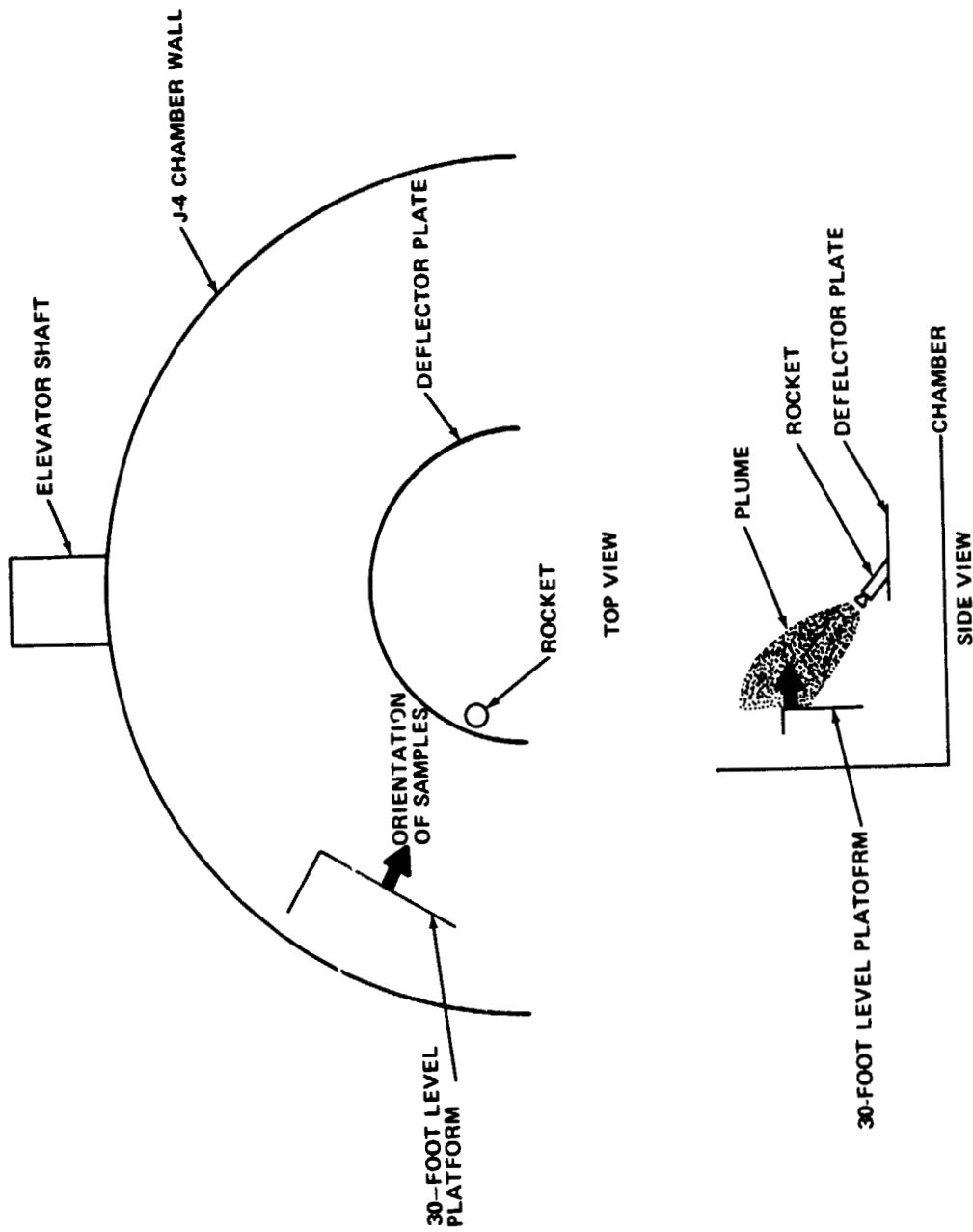


Figure III-10. Orientation for optical data.

Figure III-11 shows the spectral transmission of a clean shuttle windshield, showing the rapid loss toward shorter wavelengths.

The transmission losses of windshield samples after exposure to firings of propellant types 1, 3, and 6 are shown in Figures III-12, III-13, and III-14. What is shown here is the percent loss in transmission ($\Delta T/T$) as a function of wavelength, where $\Delta T/T = [(T - T_0)/T_0] \times 100$, T_0 being the original transmittance.

Some contradictory results seem apparent in these data which are presented with a confidence or accuracy of better than 5 percent relative. By overlapping these three figures as view-graphs, it shows the least damage to the Shuttle windshields by single firings of propellant types 1 and 6, while the most damage is caused by dual (by implication, multiple) firings of the same type. In all cases, as expected, the transmission loss is greater at the shorter wavelengths. On the Shuttle, the astronauts may encounter a 50 percent loss in light level or transmission due to firings of the separation motors. Whether the damage will continue to increase with firings of more than two motors at once is not known. The present evidence indicates that the form of the contaminant indicated by the shape of the curves remains similar while the magnitude or thickness increases.

As mentioned previously, the loss of transmission is only one feature of the effects of plume contamination. The decrease in quality of viewing as evidenced by photographs is another indicator. The taking and evaluation of these photographs has been a learning process, and it was only for the fast firing (dual 1) that it was shown that oblique viewing gave a better view of the effects of the contaminant and corresponds to the limitations of peripheral viewing by the astronauts.

Figure III-15 is a view of the sample end of the transmissometer after the firing on September 24, 1974 (dual 1) over a test grid, indicating the filmy, cloudy nature of the deposition and its effect on viewing. A clean Shuttle windshield would be evidenced only by the borders of the wedge-shaped sample in view.

From the same firing, the passive samples provide additional qualitative inferences. Figure III-16 shows a passive sample prior to the firing, while Figure III-17 shows the same sample after the dual 1 firing. The difference is an obvious darkening with some loss of clarity. This sample was then tilted to allow oblique incidence photography and the results are shown in Figures III-18 and III-19. In Figure III-18 the test grid lines labeled 10 (10 lines/cm) are no longer separable (45 degree view), while in Figure III-19 (sample at 80 degrees) the resolution is even worse.

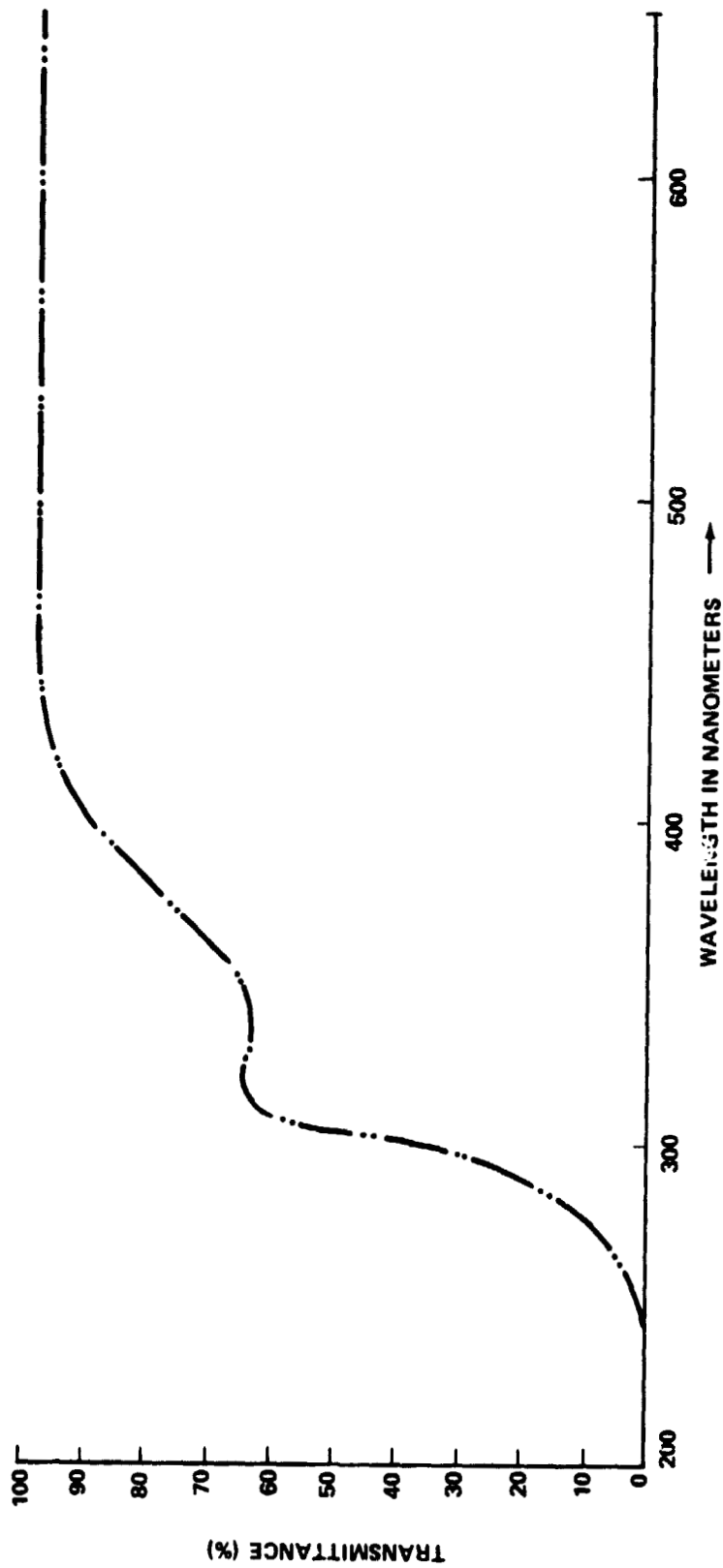


Figure III-11. Transmittance of clean shuttle windshield.

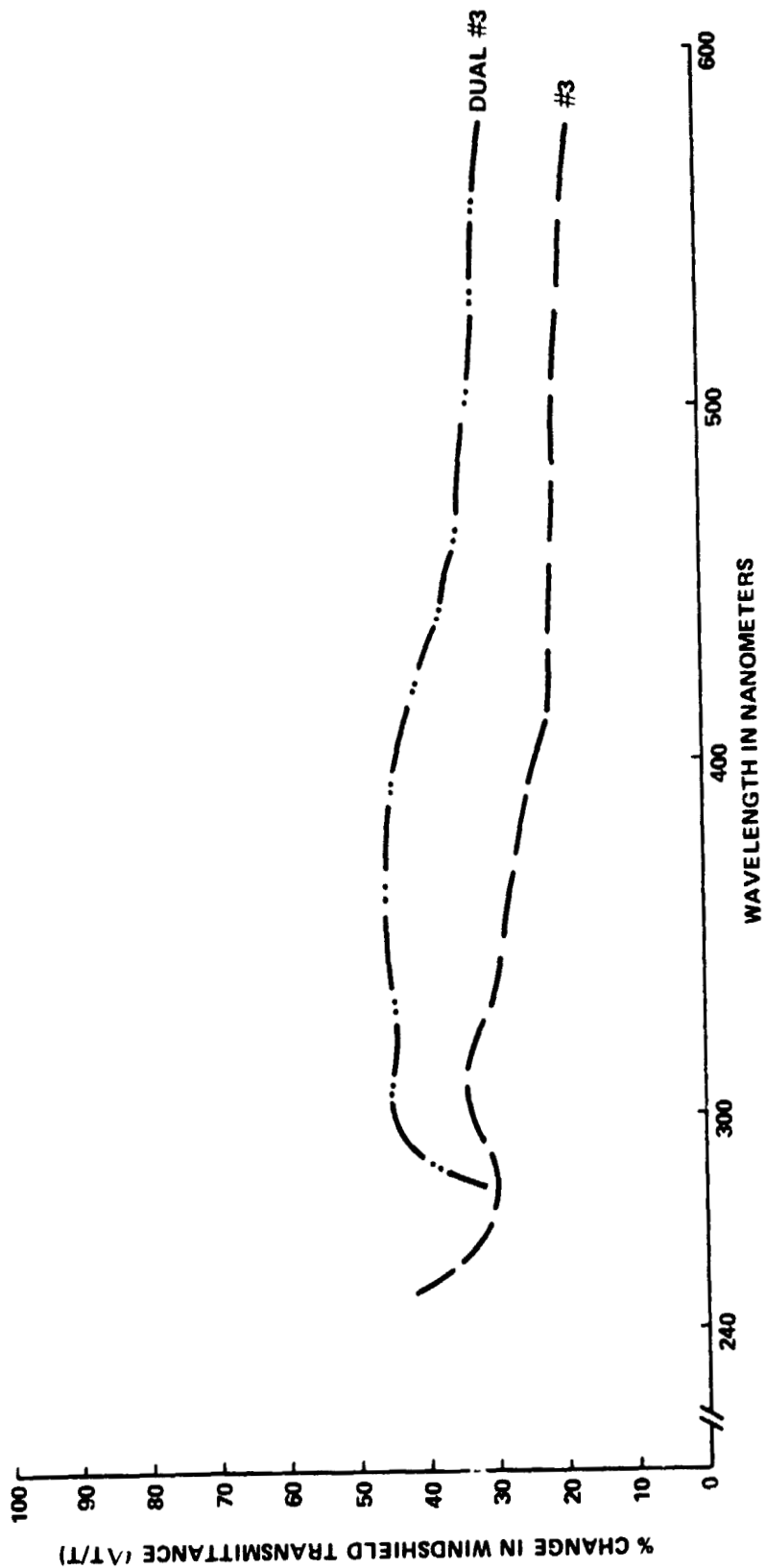


Figure III-12. Shuttle windshield contamination.

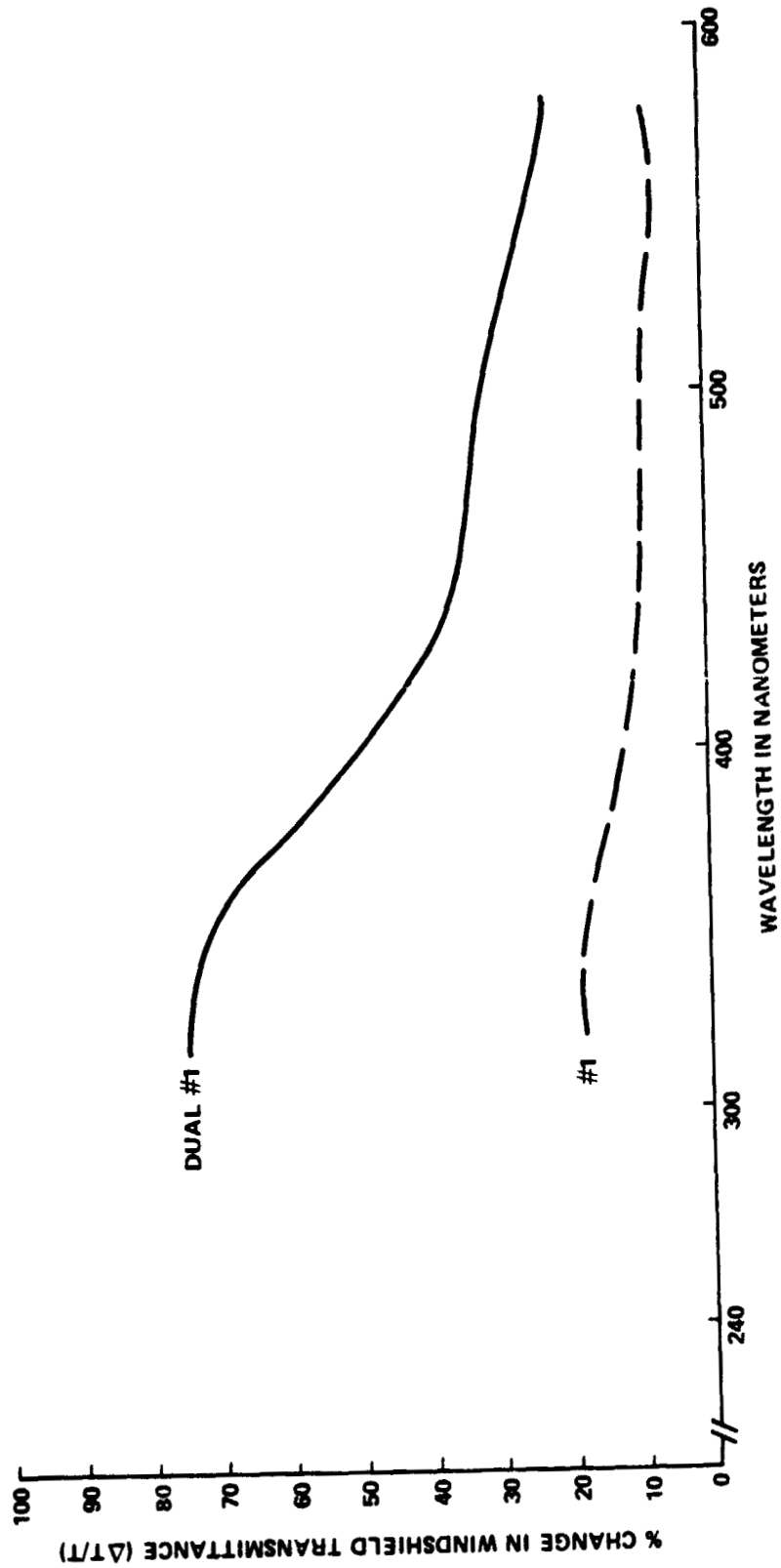


Figure III-13. Shuttle windshield effects of AEDC rocket firings, dual 1.

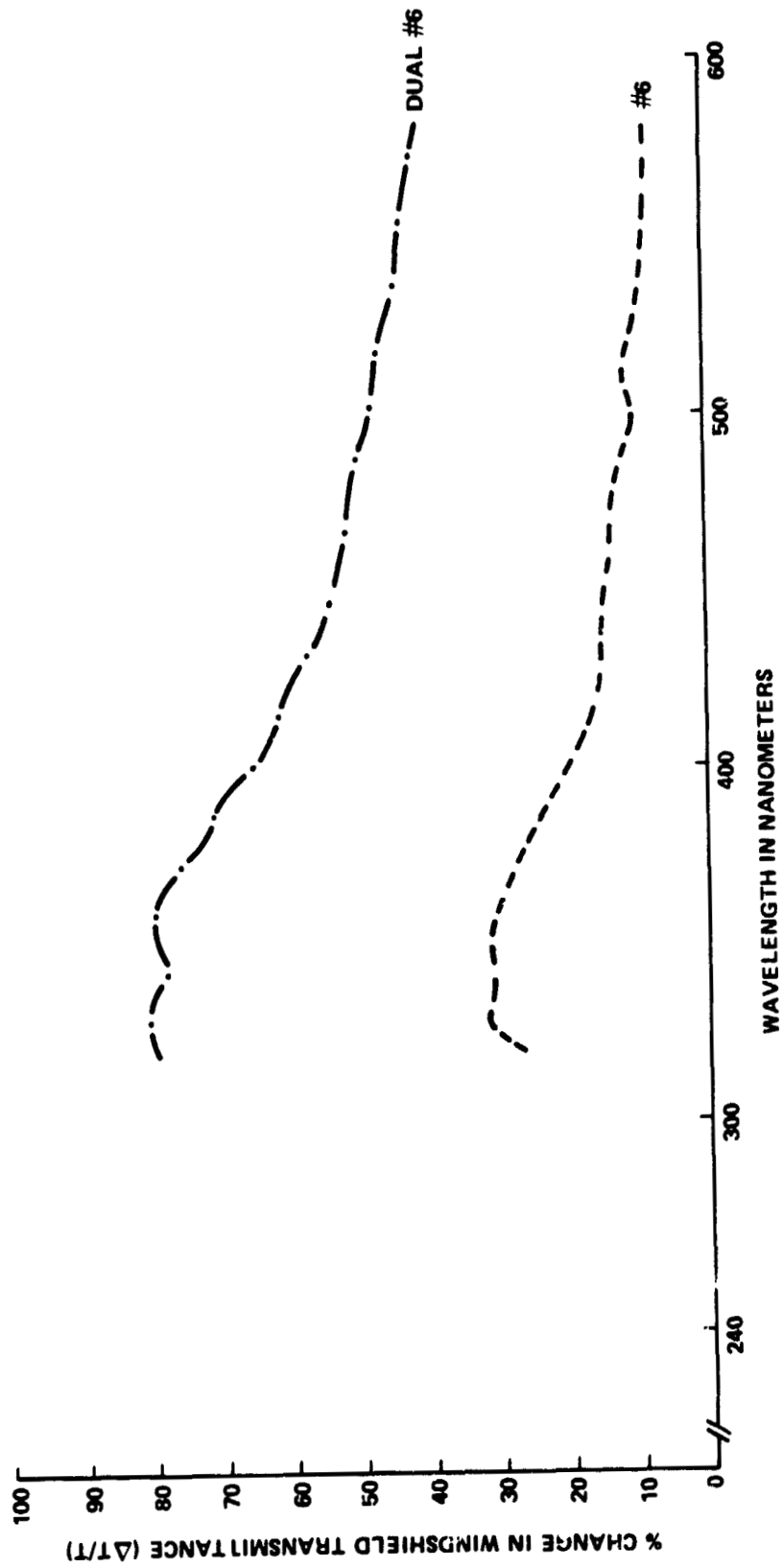


Figure III-14. Shuttle windshield effects of AEDC rocket firings, dual 6.

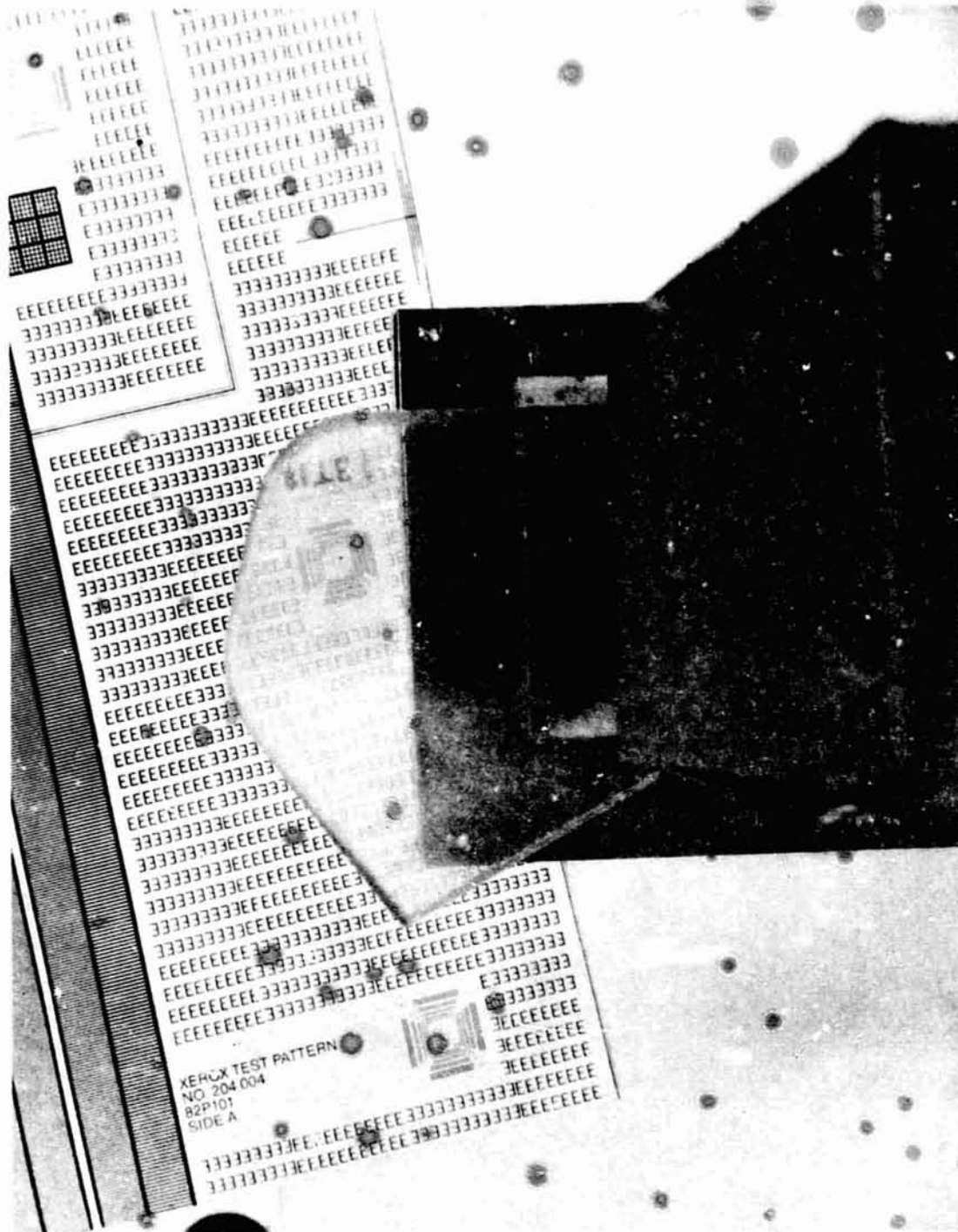


Figure III-15. Sample end of transmissometer after firing on September 24, 1974.

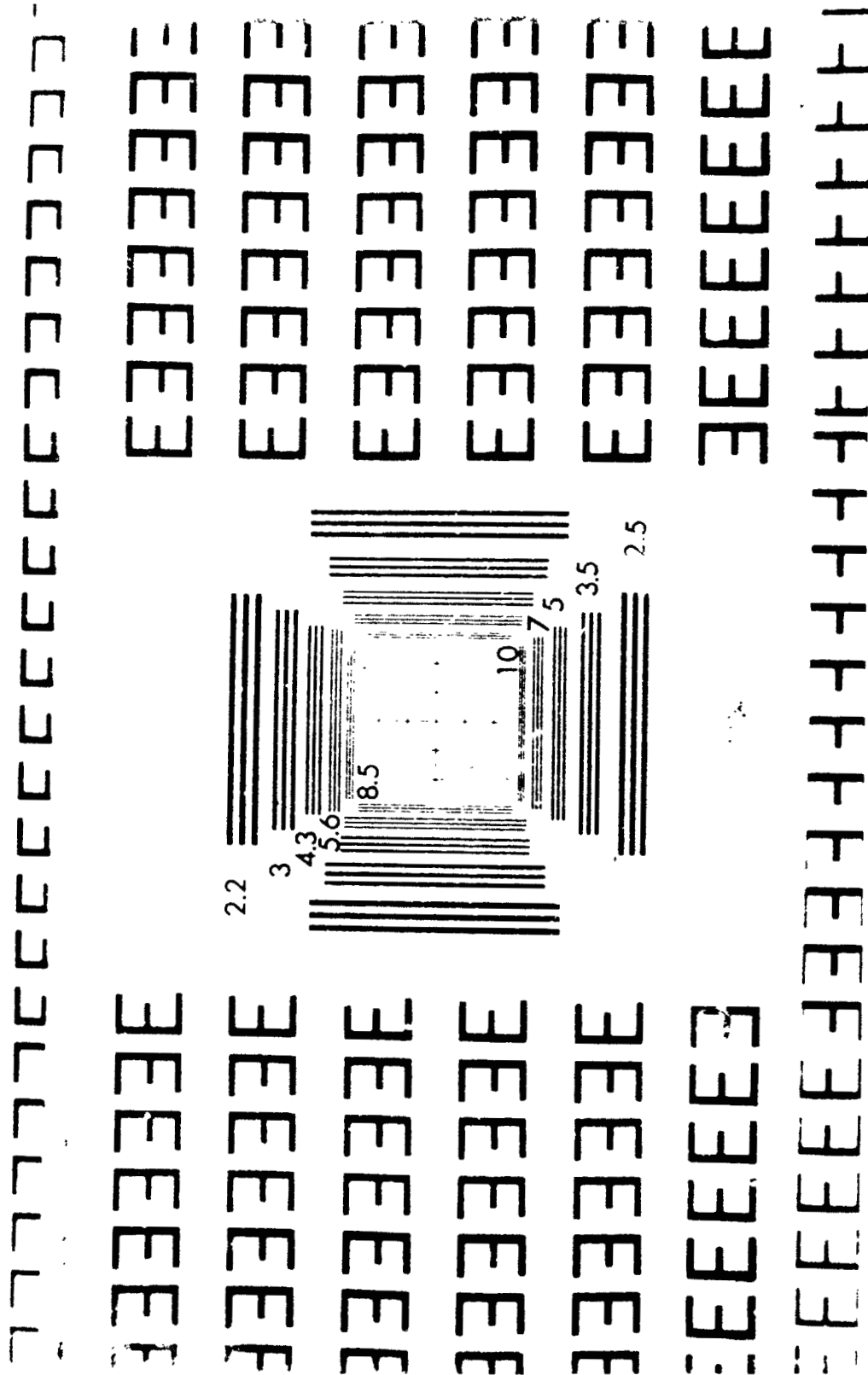


Figure III-16. Passive sample prior to firing.

ORIGINAL PAGE IS
OF POOR QUALITY

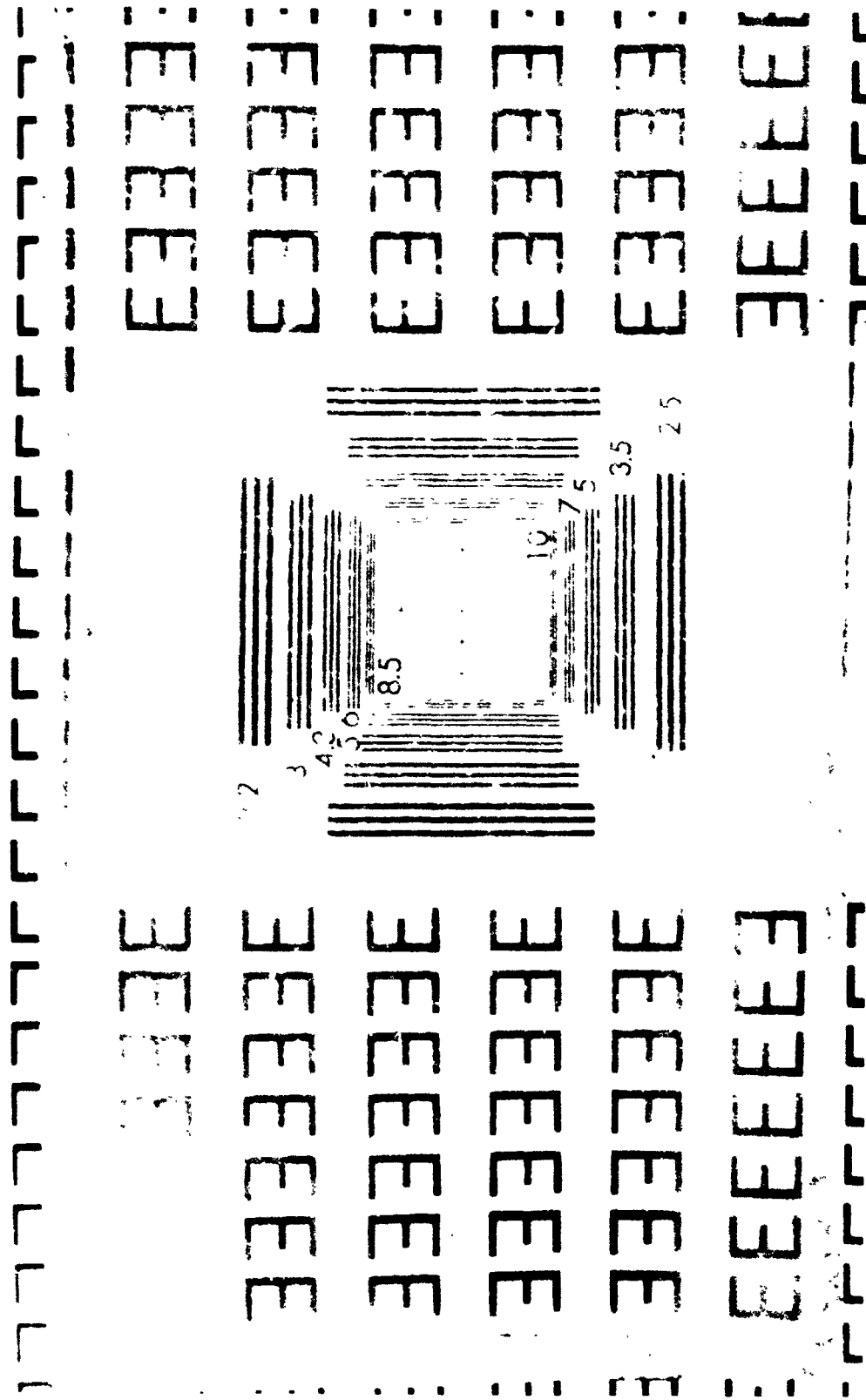
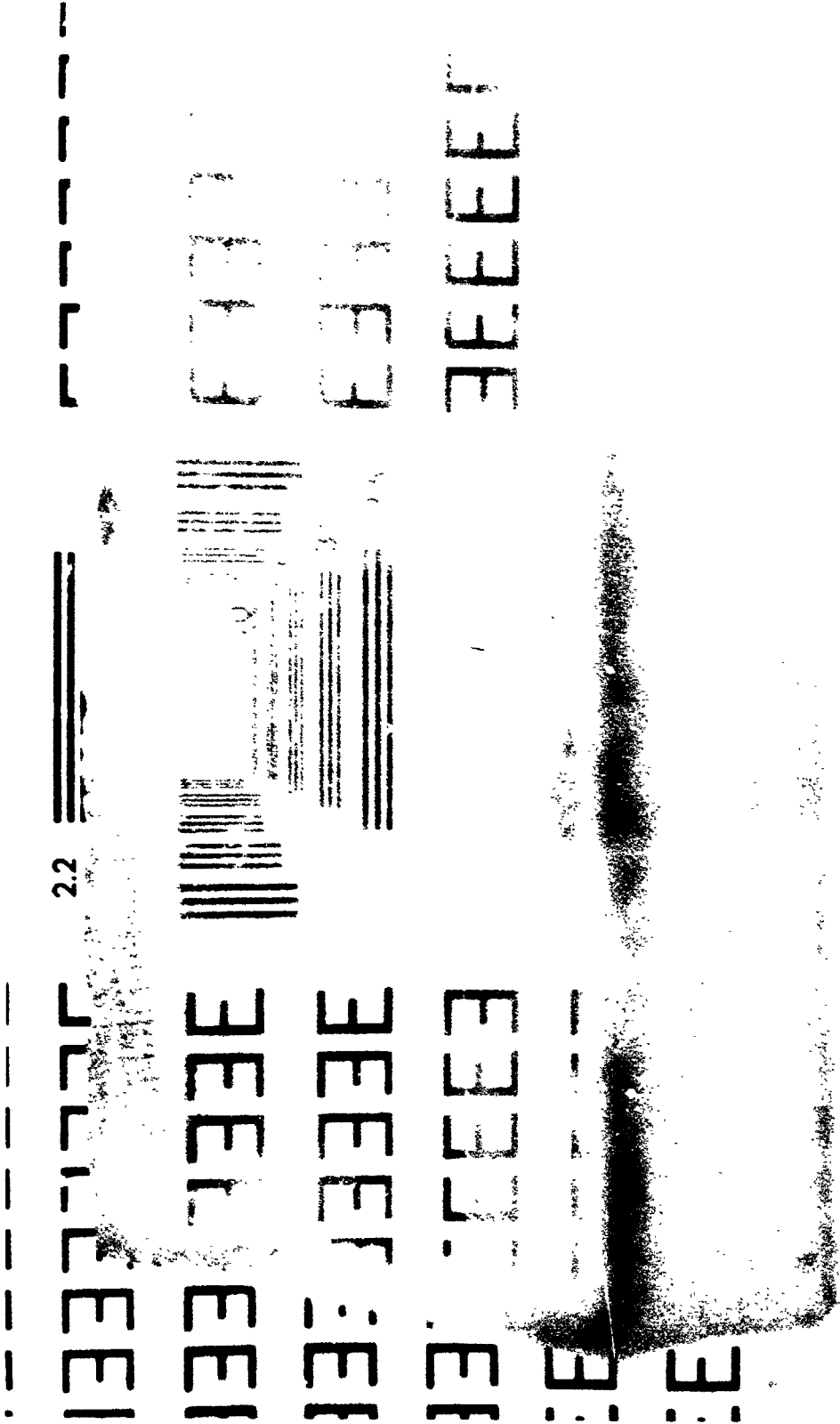


Figure III-17. Sample shown in Figure III-16 after dual 1 firing.



ORIGINAL PAGE IS
OF POOR QUALITY

Figure III-18. Sample used in Figure III-17 photographed at 45 degree angle.



Figure III-19. Sample used in Figure III-17 photographed at 80 degree angle.

Figures III-20 and III-21 show before and after firing of a single 6. Figure III-21 is blotched from mishandling of the negative, but the darkening and muddling of the image is apparent.

Figure III-22 shows results from a dual 6 firing. A dual 6 firing was shown previously to lead to the most loss in transmission. Close examination of this photograph will reveal considerable masking of the grid, although oblique photos would have shown more clearly the extent of the damage. The dark smudges (3) in the center came from the firing and are gummy in texture.

Figure III-23 shows results for type 3 propellant. Figure III-24 shows results for a dual 3 firing. Figure III-25 shows results for a dual 3 firing for a sample oriented 90 degrees down from the location of the other samples; the result is near total opacity. Figure III-25 shows only the worst that can happen and is not representative of damage to be expected on the Space Shuttle.

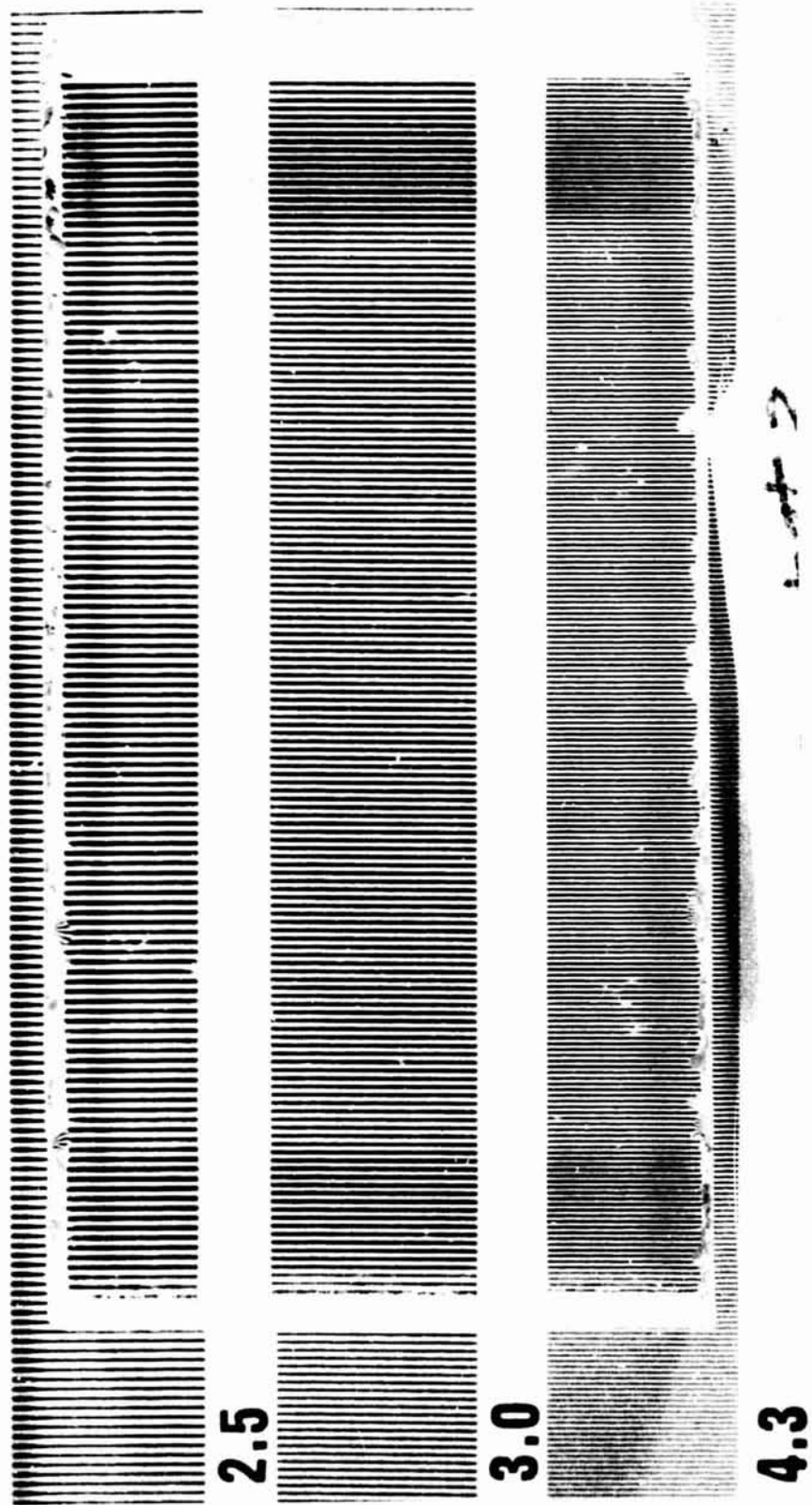


Figure III-20. Sample before firing of single 6.

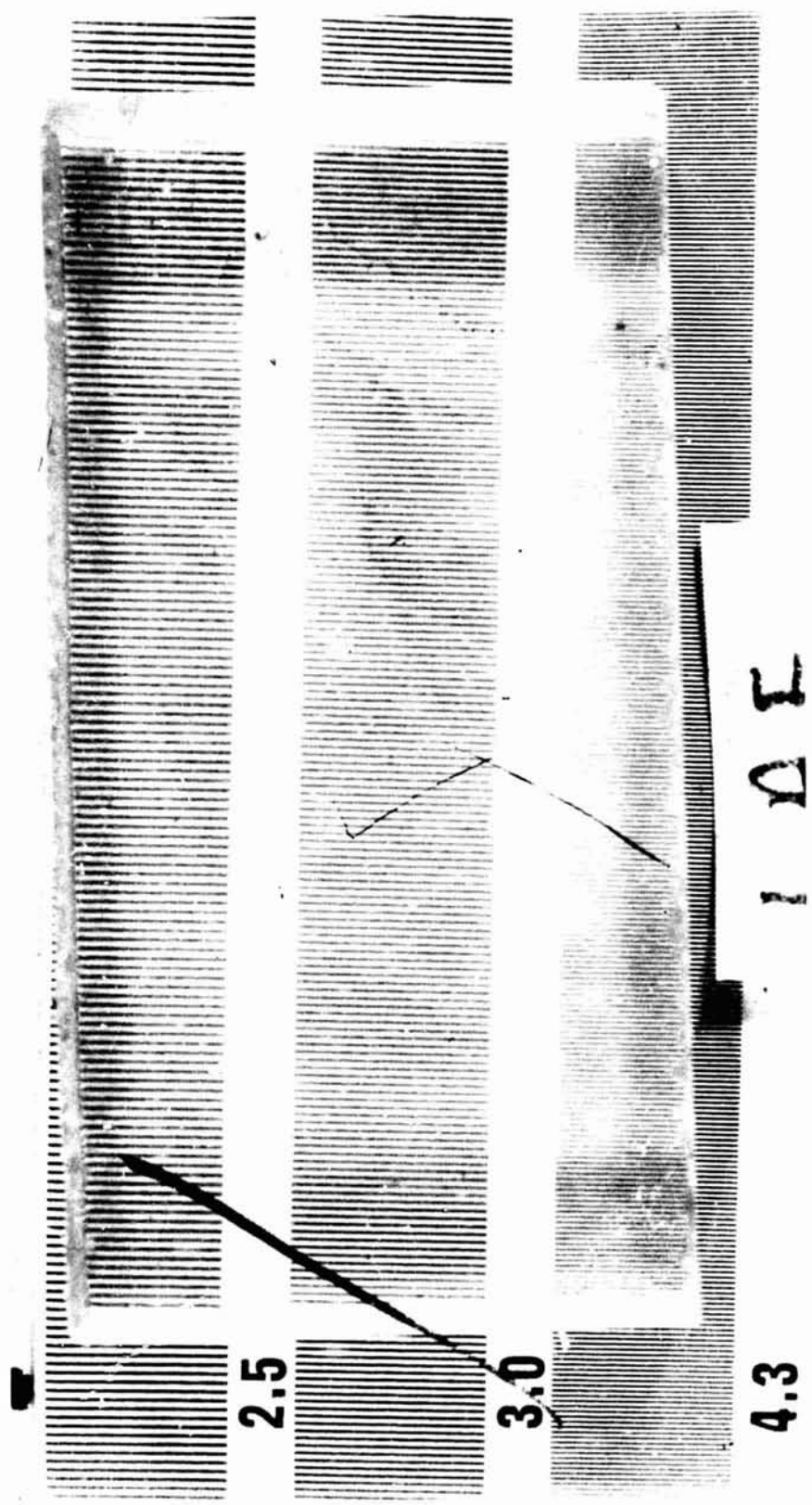


Figure III-21. Sample after firing of single 6.

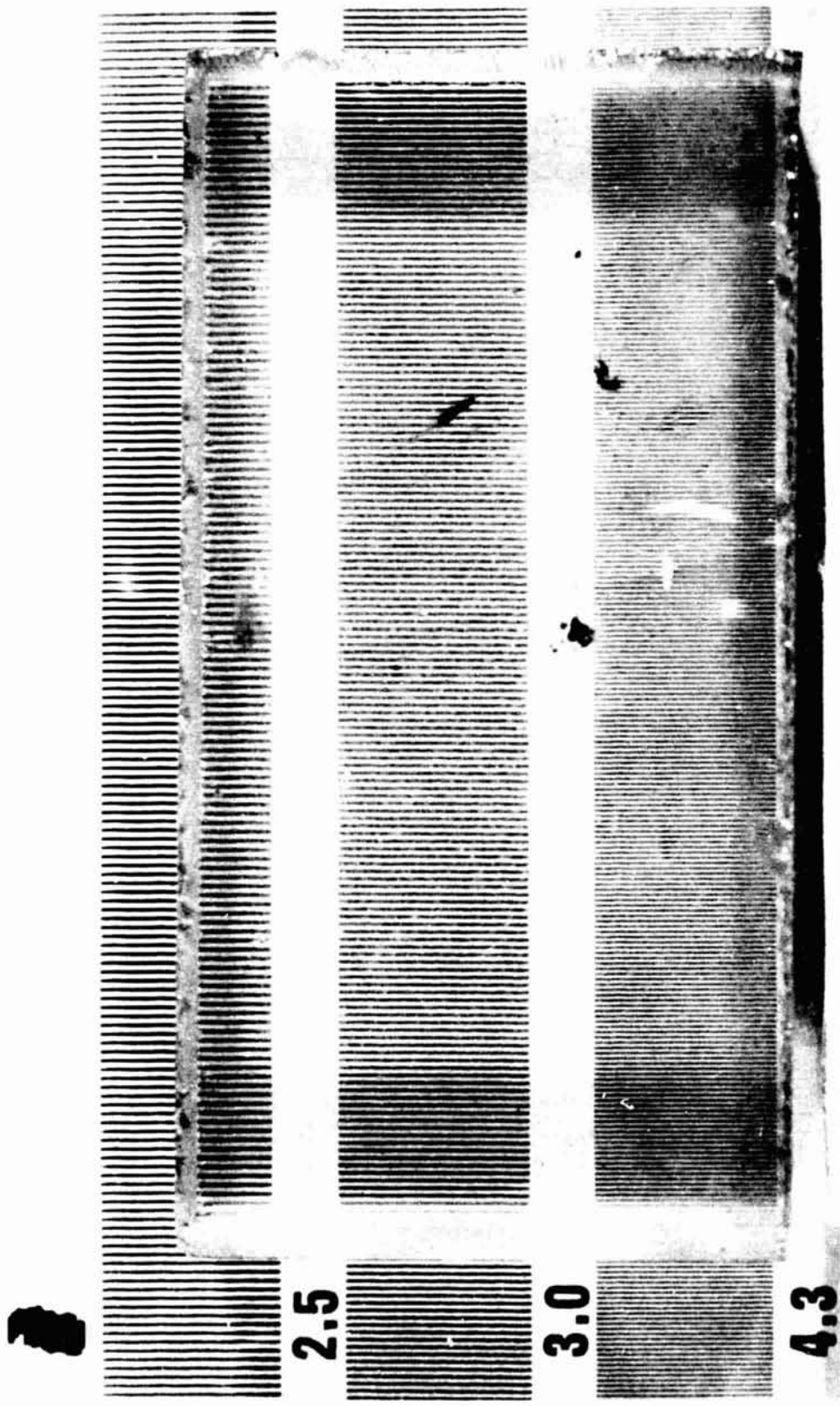


Figure III-22. Sample after dual 6 firing.

ORIGINAL PAGE IS
OF POOR QUALITY

ORIGINAL PAGE IS
OF POOR QUALITY



		nc
n m	n m	nt
if m	if m	
alln	alln	

Figure III-23. Sample using type 3 propellant.

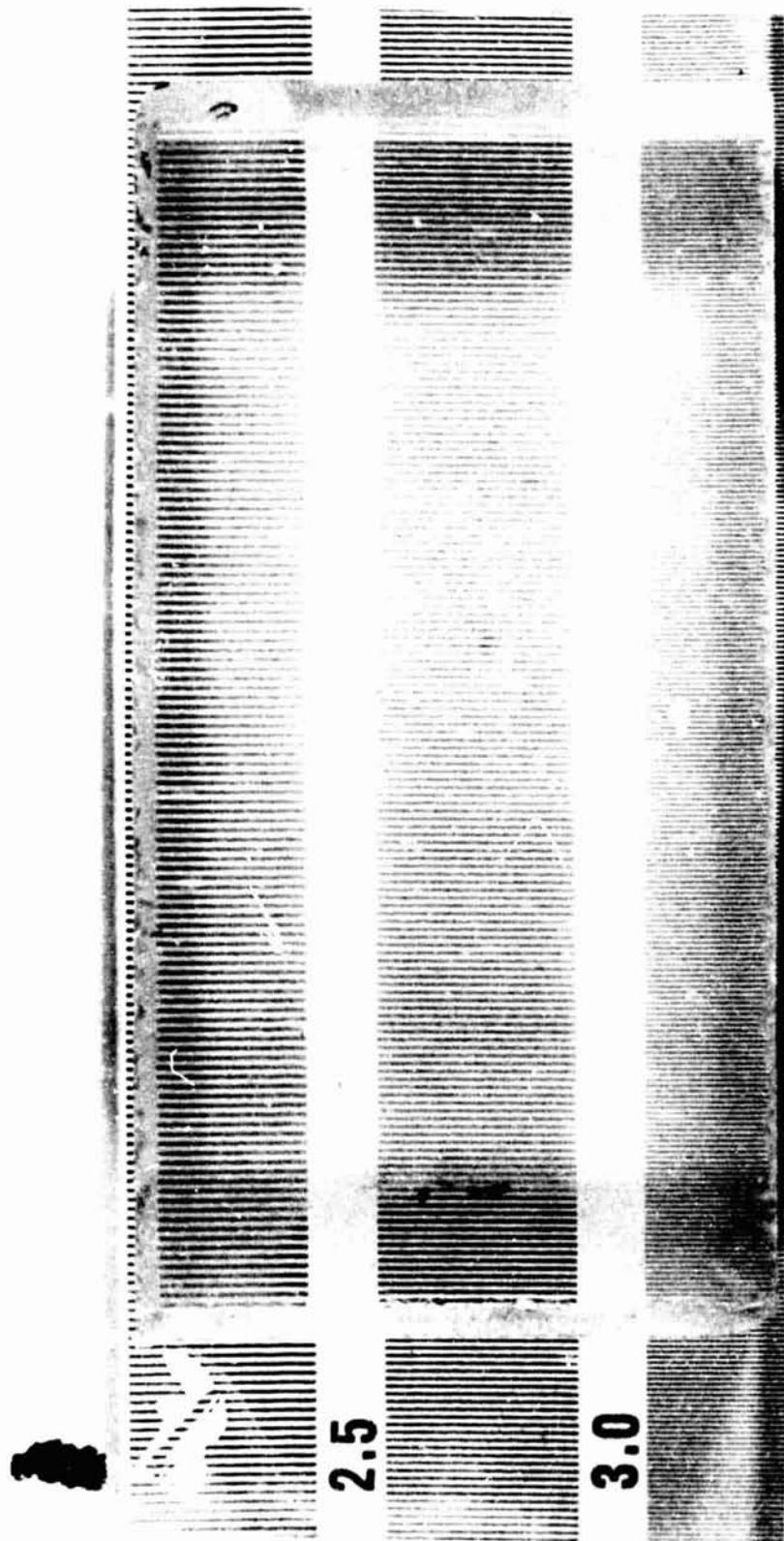


Figure III-24. Sample after dual 3 firing.

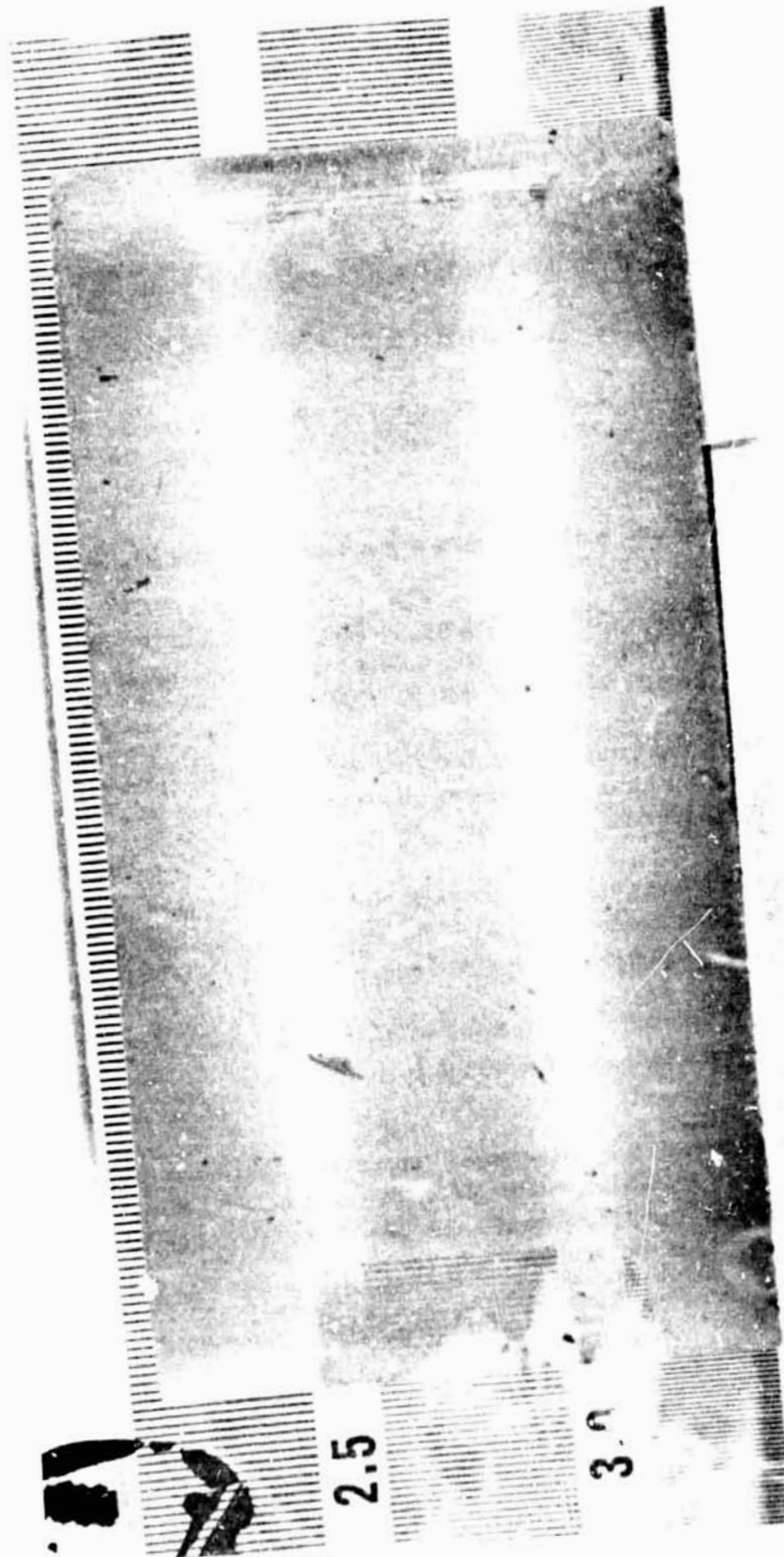


Figure III-25. Sample after dual 3 firing oriented -90 degrees.

APPENDIX

DEFINITION OF ACRONYMS

ET — the external tank associated with the Shuttle launch vehicle.

SRB — solid rocket boosters used for the Shuttle launch vehicle.

SSRM — separation solid rocket motors used to separate the solid rocket boosters from the orbiter-external tank system after the boosters are no longer in service.

TPS — thermal protective surfaces used to protect the entire Shuttle system.

HRSI — high temperature reusable surface insulation: a coating to be used on the Space Shuttle orbiter where maximum local temperatures range from 650 to 2300° F.

LRSI — low temperature reusable surface insulation: a coating to be used on the orbiter where maximum local temperatures are below 650° F.

RCC — reinforced carbon-carbon: a material to be used where local temperatures exceed 2300° F, specifically on the nose and leading edge of the wings of the orbiter.

SOFI — spray-on foam insulation: an insulating material used on the exterior and interior of the external tank.

SSME — Space Shuttle main engine: the sample that bore this designation was an insulating material made from woven stainless steel strands and proposed for use near the nozzles of the main engines of the orbiter.

SLA — an ablative silicone material proposed for use on the interior and exterior of the external tank.

APPROVAL

THE EFFECTS OF SOLID ROCKET MOTOR EFFLUENTS ON
SELECTED SURFACES AND SOLID PARTICLE SIZE,
DISTRIBUTION, AND COMPOSITION FOR SIMULATED
SHUTTLE BOOSTER SEPARATION MOTORS

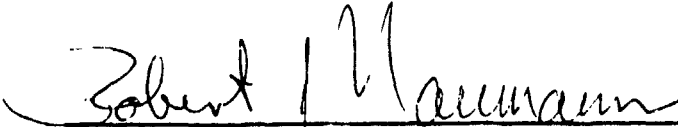
By David W. Jex, Roger C. Linton, Willa M. Russell,
John J. Trenkle, and Donald R. Wilkes

The information in this report has been reviewed for security classification. Review of any information concerning Department of Defense or Atomic Energy Commission programs has been made by the MSFC Security Classification Officer. This report, in its entirety, has been determined to be unclassified.

This document has also been reviewed and approved for technical accuracy.



ROGER L. KROES
Chief, Surface Sciences Branch



ROBERT J. NAUMANN
Chief, Physics and Instrumentation Division



CHARLES A. LUNDQUIST
Director, Space Sciences Laboratory